THE PROCEEDINGS OF THE PHYSICAL SOCIETY

Section A

VOL. 63, PART 9 1 September 1950 No. 369 A

On the Theory of Diffraction

BY W. FRANZ
University of Münster

Communicated by D. Gabor; MS. received 28th November 1949

ABSTRACT. A new method is described for calculating the diffraction of an acoustical or electromagnetic wave by successive approximations. Kirchhoff's theory is a special case of the first step in the new method, which, unlike Kirchhoff's, is not restricted to black screens, and applies to long waves as well as short ones.

---

§ 1. BASIC IDEAS

THE diffraction theory of Kirchhoff is, though very useful, not entirely satisfactory in its theoretical foundations. The main defect is that there exists no higher approximation, thus it is not possible to estimate or to amend the errors. Moreover it applies only for diffraction by a black screen, while diffraction by an object of arbitrary reflectivity is also of great interest. The deficiencies and difficulties of the Kirchhoff theory can be avoided by a new conception of the fundamental ideas, resulting in a consistent method of successive approximation to be described below.

Let us take as zero order approximation a primary wave u_0, satisfying the wave equation for empty space, ignoring all diffracting objects. The next step is to take account of these neglected objects, and this may be done in a purely experimental way by some plausible modifications of u_0. We may, for example, cancel u_0 in the geometrical shadow of an object, and add a reflected wave roughly according to geometrical optics. The resulting modified function u_0' now, of course, contradicts the wave equation in some parts of space, for instance, at the boundaries of the geometrical shadow. Thus we have next to restore the wave equation by adding a first order correction δu_1 in order to adapt the first order function $u_1 = u_0' + \delta u_1$ to the wave equation, which determines δu_1 unambiguously if only outgoing waves are taken into account. Now again δu_1 is calculated without regard to diffracting objects, therefore u_1 has to be modified yielding u_1', which again violates the wave equation and therefore demands a second order correction δu_2, and so on. The whole procedure consists, as we see, of two kinds of steps: 'intermediate steps' $u_\nu \rightarrow u_\nu'$ taking into account the influence of diffracting objects, and 'principal steps' $u_\nu' \rightarrow u_{\nu+1}$, adapting u to the wave equation. The first order of this method applied to a black screen yields Kirchhoff's theory.

§ 2. PRINCIPAL STEPS OF APPROXIMATION

Consider an acoustical wave u, satisfying

$$\left(\Delta - \frac{1}{c^2}\frac{\partial^2}{\partial t^2}\right) u = 0 \qquad \ldots\ldots(1)$$

or an electromagnetic wave, given by the electrical field strength **E** and magnetic intensity **H**, which satisfy Maxwell's equations

$$\begin{aligned} \operatorname{curl}\mathbf{H} &= \epsilon\frac{\partial \mathbf{E}}{\partial t}\,; & \operatorname{div}\mathbf{E} &= 0\,; \\ \operatorname{curl}\mathbf{E} &= -\mu\frac{\partial \mathbf{H}}{\partial t}\,; & \operatorname{div}\mathbf{H} &= 0\,; \end{aligned} \qquad \left(\epsilon\mu = \frac{1}{c^2}\right) \qquad \ldots\ldots(1\,a)$$

To perform the $(\nu+1)$th step of our approximation, we start from the modified function of the νth approximation u_ν', $\mathbf{E}_\nu'$, $\mathbf{H}_\nu'$. The corrections $\delta u_{\nu+1}$, $\delta\mathbf{E}_{\nu+1}$, $\delta\mathbf{H}_{\nu+1}$ must satisfy the inhomogeneous equations

$$\left(\Delta - \frac{1}{c^2}\frac{\partial^2}{\partial t^2}\right)\delta u_{\nu+1} = -\bar{\rho}_\nu, \qquad \ldots\ldots(2)$$

$$\left.\begin{aligned} \operatorname{curl}\delta\mathbf{H}_{\nu+1} = \epsilon\frac{\partial}{\partial t}\delta\mathbf{E}_{\nu+1} &= \mathbf{j}_\nu\,; & \epsilon\operatorname{div}\delta\mathbf{E}_{\nu+1} &= \rho_\nu\,; \\ \operatorname{curl}\delta\mathbf{E}_{\nu+1} + \mu\frac{\partial}{\partial t}\delta\mathbf{H}_{\nu+1} &= -\mathbf{j}_\nu{}^*\,; & \mu\operatorname{div}\delta\mathbf{H}_{\nu+1} &= \rho_\nu{}^*. \end{aligned}\right\} \qquad \ldots\ldots(2\,a)$$

Here the right-hand sides

$$\bar{\rho}_\nu = \Delta u_\nu' - \frac{1}{c^2}\frac{\partial^2 u_\nu'}{\partial t^2}, \qquad \ldots\ldots(3)$$

$$\left.\begin{aligned} \mathbf{j}_\nu &= -\operatorname{curl}\mathbf{H}_\nu' + \epsilon\frac{\partial \mathbf{E}_\nu'}{\partial t}\,; & \rho_\nu &= -\epsilon\operatorname{div}\mathbf{E}_\nu'\,; \\ \mathbf{j}_\nu{}^* &= \operatorname{curl}\mathbf{E}_\nu' + \mu\frac{\partial \mathbf{H}_\nu'}{\partial t}\,; & \rho_\nu{}^* &= -\mu\operatorname{div}\mathbf{H}_\nu' \end{aligned}\right\} \qquad \ldots\ldots(3\,a)$$

play the part of fictitious sources of radiation; in the electromagnetic case they represent electric and magnetic charges and currents. The solution of equations (2) and (2 *a*) is well known; if we mark the coordinates of the observer by a suffix P, the coordinates of the radiating point by a suffix J, we have

$$\delta u^{(\mathrm{P})}_{\nu+1} = \frac{1}{4\pi}\int\frac{[\bar{\rho}_\nu(\mathrm{J})]}{r_{\mathrm{PJ}}}\,d\tau_{\mathrm{J}}, \qquad \ldots\ldots(4)$$

$$\left.\begin{aligned} \delta\mathbf{E}^{(\mathrm{P})}_{\nu+1} &= -\frac{1}{4\pi}\operatorname{curl}_{\mathrm{P}}\int\frac{[\mathbf{j}^*(\mathrm{J})]}{r_{\mathrm{PJ}}}\,d\tau_{\mathrm{J}} - \frac{\mu}{4\pi}\frac{\partial}{\partial t}\int\frac{[\mathbf{j}(\mathrm{J})]}{r_{\mathrm{PJ}}}\,d\tau_{\mathrm{J}} - \frac{1}{4\pi\epsilon}\operatorname{\mathbf{grad}}_{\mathrm{P}}\int\frac{[\rho(\mathrm{J})]}{r_{\mathrm{PJ}}}\,d\tau_{\mathrm{J}} \\ \delta\mathbf{H}^{(\mathrm{P})}_{\nu+1} &= \frac{1}{4\pi}\operatorname{curl}_{\mathrm{P}}\int\frac{[\mathbf{j}(\mathrm{J})]}{r_{\mathrm{PJ}}}\,d\tau_{\mathrm{J}} - \frac{\epsilon}{4\pi}\frac{\partial}{\partial t}\int\frac{[\mathbf{j}^*(\mathrm{J})]}{r_{\mathrm{PJ}}}\,d\tau_{\mathrm{J}} - \frac{1}{4\pi\mu}\operatorname{grad}_{\mathrm{P}}\int\frac{[\rho^*(\mathrm{J})]}{r_{\mathrm{PJ}}}\,d\tau_{\mathrm{J}}. \end{aligned}\right\}$$

$$\ldots\ldots(4\,a)$$

The squared brackets indicate retardation, meaning that within the brackets the time t has to be replaced by $t - r_{\mathrm{PJ}}/c$. r_{PJ} is the distance between P and J, and $d\tau_{\mathrm{J}}$ the differential of space.

§ 3. INTERMEDIATE STEPS: SURFACES OF DISCONTINUITY

The intermediate steps are rather arbitrary, and it requires skill to choose suitable modifications of u_ν fit for the needs and conditions of a given case. We have to keep this freedom of the intermediate steps in order to obtain the best possible service from our method. This means that our approximation method does not generally converge or diverge; if we perform the intermediate steps shrewdly enough we can ensure convergence (e.g. by just guessing the correct wave function); if on the other hand we choose u_ν' unwisely, we can, of course, prevent convergence.

The most important way of proceeding is to restrict the modifications of u_ν to surface discontinuities. That means: we follow our free propagating wave u_ν till it meets the surface of the first obstacle, here we stop and consider from equation (4) how to continue the path of the radiation. We take, so to speak, a pair of scissors and clip our radiation field along the critical surfaces—these 'cuts' according to equation (3) represent a surface density of radiation sources, exactly as Huyghens' principle demands. For illustration we see in Figure 1 a reflecting screen with an aperture. The arrows indicate the direction of propagation of the wave, and the broken lines show where the scissors have to work: we clip along the opening, and also along the back surface of the screen immediately after reflection (the 'reflection zones' of Figure 1 are meant to be infinitely narrow). Let us now calculate the secondary radiation $\delta u_{\nu+1}$. Of course the derivatives which we want for equation (3) are not defined for our discontinuous functions, but we may approximate these by continuous ones and proceed to the limit after integrating equation (4). In that way we get by Gauss' generalized theorem in the electromagnetic case

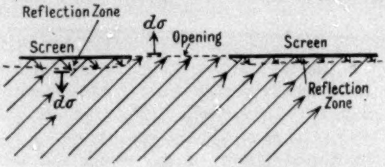

Figure 1. Reflecting screen with opening.

$$\left.\begin{aligned} \int \mathbf{j}_\nu\, d\tau &= \int d\boldsymbol{\sigma} \times \mathbf{H}_\nu'\,; & \int \rho_\nu\, d\tau &= \epsilon \int d\boldsymbol{\sigma} \,.\, \mathbf{E}_\nu'\,; \\ \int \mathbf{j}_\nu^*\, d\tau &= -\int d\boldsymbol{\sigma} \times \mathbf{E}_\nu'\,; & \int \rho_\nu^*\, d\tau &= \mu \int d\boldsymbol{\sigma} \,.\, \mathbf{H}_\nu'. \end{aligned}\right\} \quad \ldots\ldots(5)$$

The vector surface element $d\boldsymbol{\sigma}$ points, as shown in Figure 1, towards the clipped part of the space. For $\mathbf{E}_\nu'$, $\mathbf{H}_\nu'$ we have to take $\mathbf{E}_\nu$, $\mathbf{H}_\nu$ along the aperture, and the field strength of the reflected wave along the reflection zone. As (5) is valid within infinitely small regions of the surface, where r_{PJ} is constant, we may insert a factor $1/r_{\mathrm{PJ}}$ and retard each single integrand of (5):

$$\left.\begin{aligned} \int \frac{[\mathbf{j}_\nu(\mathrm{J})]}{r_{\mathrm{PJ}}}\, d\tau_{\mathrm{J}} &= \int d\boldsymbol{\sigma}_{\mathrm{J}} \times \frac{[\mathbf{H}_\nu'(\mathrm{J})]}{r_{\mathrm{PJ}}}\,; & \int \frac{[\rho_\nu(\mathrm{J})]}{r_{\mathrm{PJ}}}\, d\tau_{\mathrm{J}} &= \epsilon \int d\boldsymbol{\sigma}_{\mathrm{J}} \times \frac{[\mathbf{E}'(\mathrm{J})]}{r_{\mathrm{PJ}}}\,; \\ \int \frac{[\mathbf{j}_\nu^*(\mathrm{J})]}{r_{\mathrm{PJ}}}\, d\tau_{\mathrm{J}} &= -\int d\boldsymbol{\sigma}_{\mathrm{J}} \times \frac{[\mathbf{E}_\nu'(\mathrm{J})]}{r_{\mathrm{PJ}}}\,; & \int \frac{[\rho_\nu^*(\mathrm{J})]}{r_{\mathrm{PJ}}}\, d\tau_{\mathrm{J}} &= \mu \int d\boldsymbol{\sigma}_{\mathrm{J}} \times \frac{[\mathbf{H}_\nu'(\mathrm{J})]}{r_{\mathrm{PJ}}}\,. \end{aligned}\right\} \quad \ldots\ldots(6)$$

These formulae enable us to apply (4 *a*) to surface discontinuities. In the scalar case we have to be more careful because of the second derivative contained in (3), which makes it wrong just to put $1/r$ and retardation into integrals analogous to (5). We get the correct result by twice applying Gauss' theorem to the exact function (4):

$$\delta u_{\nu+1} = -\frac{1}{4\pi}\operatorname{div}_{\mathrm{P}} \int \frac{[u_\nu'(\mathrm{J})]}{r_{\mathrm{PJ}}}\, d\boldsymbol{\sigma}_{\mathrm{J}} - \frac{1}{4\pi}\int \frac{[\operatorname{grad}_{\mathrm{J}} u_\nu'(\mathrm{J})]}{r_{\mathrm{PJ}}}\, d\boldsymbol{\sigma}_{\mathrm{J}}. \quad \ldots\ldots(7)$$

If we insert (6) into (4 *a*), we obtain the corresponding formula of the electromagnetic theory correctly for closed surfaces. However, we meet with difficulties in the case of surfaces which are not closed surfaces, as here the surface currents demand line charges along the boundaries, which are not considered in (6). The simplest way to overcome these difficulties is to eliminate the ρ's from (4 *a*) and to express everything by the **j**'s, which can easily be done after differentiating with respect to time; since we are sure that (4 *a*) satisfies the Maxwell equations (1 *a*) identically in **j** and **j***, we take from (6) only the first right-hand terms of (4 *a*) and obtain the rest by application of (1 *a*):

$$\left.\begin{aligned}\frac{\partial}{\partial t}\delta\mathbf{E}_{\nu+1} &= \frac{1}{4\pi}\frac{\partial}{\partial t}\operatorname{curl}\int d\boldsymbol{\sigma}\times\frac{[\mathbf{E}_\nu']}{r} + \frac{1}{4\pi\epsilon}\operatorname{curl}\operatorname{curl}\int d\boldsymbol{\sigma}\times\frac{[\mathbf{H}_\nu']}{r}\,;\\ \frac{\partial}{\partial t}\delta\mathbf{H}_{\nu+1} &= \frac{1}{4\pi}\frac{\partial}{\partial t}\operatorname{curl}\int d\boldsymbol{\sigma}\times\frac{[\mathbf{H}_\nu']}{r} - \frac{1}{4\pi\mu}\operatorname{curl}\operatorname{curl}\int d\boldsymbol{\sigma}\times\frac{[\mathbf{E}_\nu']}{r}\,.\end{aligned}\right\} \quad \ldots\ldots(7\,a)$$

(7) as well as (7 *a*) satisfies the field equations (1) and (1 *a*) identically, for arbitrary choice of u_ν', $\operatorname{grad} u_\nu'$, $\mathbf{E}_\nu'$ and $\mathbf{H}_\nu'$ as we see at once: every integrand is a function of $t-r/c$, divided by r, and therefore a solution of (1), consequently curl curl in (7 *a*) can be replaced by $\operatorname{grad}\operatorname{div}-(1/c^2)(\partial^2/\partial t^2)$. (Note that $\operatorname{curl}\operatorname{curl}=\operatorname{grad}\operatorname{div}-\Delta$.)

The equations (7) and (7 *a*) are just the formulae of Kirchhoff's theory. Equation (7 *a*) was not hitherto known in this simple and useful form. Some early attempts to arrive at these formulae were refuted by Kottler (1923), as violating Maxwell's equations. Kottler thought it necessary to introduce a correction by applying equation (7) to each component of **E** and **H** and adding certain line integrals. The formulae (7 *a*) were first derived in 1947 by the author* (Franz 1949) for monochromatic waves, but the above derivation for arbitrary time dependence is much simpler and clearer. Another generalization—arbitrarily variable anisotropic ϵ and μ—is derived in another note (Franz 1948).

If the radiation is monochromatic with time-dependence $\exp(-i\omega t)$, $\partial/\partial t$ means a factor $-i\omega$ and retardation a factor $\exp(ikr_{\mathrm{PJ}})$, where $k=\omega/c$, so we get instead of (7) and (7 *a*)

$$\delta u_{\nu+1} = \frac{1}{4\pi}\int\left\{u_\nu'(\mathrm{J})\operatorname{grad}_{\mathrm{J}}\left(\frac{\exp ikr_{\mathrm{PJ}}}{r_{\mathrm{PJ}}}\right) - \frac{\exp ikr_{\mathrm{PJ}}}{r_{\mathrm{PJ}}}\operatorname{grad}_{\mathrm{J}} u_\nu'(\mathrm{J})\right\}.\, d\boldsymbol{\sigma}_{\mathrm{J}}, \quad \ldots\ldots(8)$$

$$\left.\begin{aligned}\delta\mathbf{E}_{\nu+1} &= \frac{1}{4\pi}\operatorname{curl}\int d\boldsymbol{\sigma}\times\mathbf{E}_\nu'\,\frac{\exp ikr}{r} - \frac{1}{4\pi i\omega\epsilon}\operatorname{curl}\operatorname{curl}\int d\boldsymbol{\sigma}\times\mathbf{H}_\nu'\,\frac{\exp ikr}{r}\,;\\ \delta\mathbf{H}_{\nu+1} &= \frac{1}{4\pi}\operatorname{curl}\int d\boldsymbol{\sigma}\times\mathbf{H}_\nu'\,\frac{\exp ikr}{r} + \frac{1}{4\pi i\omega\mu}\operatorname{curl}\operatorname{curl}\int d\boldsymbol{\sigma}\times\mathbf{E}_\nu'\,\frac{\exp ikr}{r}\,.\end{aligned}\right\} \quad \ldots\ldots(8\,a)$$

Some obvious suffixes J and P are omitted.

---

* See *note* at end of paper.

Though (8) is identical with the Kirchhoff integral and (8 *a*) is its consistent electromagnetic analogue, our altered conception of the fundamental ideas yields a series of essential improvements. First, of course, we have an infinite sequence of approximations instead of a single not very clearly established approximate formula. But even in the first approximation we get important advantages from our new aspect: we can apply (8) and (8 *a*) as well to the space before as behind the screen, to screens of arbitrary reflectivity or even transparency and to long waves as well as to short ones—which is all outside the scope of Kirchhoff's theory.

§ 4. SMALL PERFECTLY REFLECTING OBJECTS

If the diffracting objects are small compared with the wavelength, the application of formulae (8), (8 *a*) is straightforward. Let us assume perfect reflectivity by postulating the boundary conditions

$$\frac{\partial u}{\partial n}=0; \qquad \mathbf{E}_{\|}=0 \quad \text{at the surface.} \qquad \ldots\ldots(9)$$

n is the direction perpendicular to the surface, and the suffix $\|$ indicates the part of **E** which is parallel to the surface. Now here the example of Figure 1 is not a good model, because the small object does not succeed in building up a shadow or a reflection front, but is completely illuminated by the wave, without distinction between front and back, so that these terms are now meaningless. For the diffracted wave starting from the surface, we first take over the whole surface

$$\frac{\partial u_\nu'}{\partial n}=-\frac{\partial u_\nu}{\partial n}; \qquad \mathbf{E}_{\nu\|}=-\mathbf{E}_{\nu\|} \qquad \ldots\ldots(10)$$

in order to satisfy the boundary condition (9). In order to obtain zero identically when u_ν or $\mathbf{E}_\nu$ satisfies equation (9), we put in addition

$$u_\nu'=0; \qquad \mathbf{H}_\nu'=0 \quad \text{at the surface,} \qquad \ldots\ldots(11)$$

which gives

$$\delta u_{\nu+1}=\frac{1}{4\pi}\int\frac{e^{ikr}}{r}\,\mathrm{grad}\,u_\nu\,.\,d\boldsymbol{\sigma}; \qquad \ldots\ldots(12)$$

$$\delta\mathbf{E}_{\nu+1}=-\frac{1}{4\pi}\,\mathrm{curl}\int d\boldsymbol{\sigma}\times\mathbf{E}_\nu\frac{e^{ikr}}{r}. \qquad \ldots\ldots(12\,a)$$

We disregard *H* in the calculation of the individual steps of approximation—finally it can be derived by Maxwell's second equation.

For a point P, whose distance is large compared with the dimensions of the object, the first order radiation is easily determined. As u_0 and r are regular within the object, we can apply Gauss' theorem and obtain

$$\delta u_1(\mathrm{P})=\frac{1}{4\pi}\int_{\text{object}}\mathrm{div}_{\mathrm{J}}\left(\frac{\exp ikr_{\mathrm{PJ}}}{r_{\mathrm{PJ}}}\,\mathrm{grad}_{\mathrm{J}}\,u_0(\mathrm{J})\right)d\tau_{\mathrm{J}}$$

$$=-\frac{1}{4\pi}\int_{\text{object}}\left(k^2\frac{\exp ikr_{\mathrm{PJ}}}{r_{\mathrm{PJ}}}\,u_0(\mathrm{J})+\mathrm{grad}_{\mathrm{P}}\left(\frac{\exp ikr_{\mathrm{PJ}}}{r_{\mathrm{PJ}}}\right).\,\mathrm{grad}_{\mathrm{J}}\,u_0(\mathrm{J})\right)d\tau_{\mathrm{J}} \qquad \ldots\ldots(13)$$

$$\delta\mathbf{E}_1(\mathrm{P})=-\frac{1}{4\pi}\,\mathrm{curl}_{\mathrm{P}}\int_{\text{object}}\mathrm{curl}_{\mathrm{J}}\left(\frac{\exp ikr_{\mathrm{PJ}}}{r_{\mathrm{PJ}}}\,\mathbf{E}_0(\mathrm{J})\right)d\tau_{\mathrm{J}}$$

$$=\frac{1}{4\pi}\int_{\text{object}}\left(i\omega\mu\mathbf{H}_0(\mathrm{J})\times\mathrm{grad}_{\mathrm{P}}\frac{\exp(ikr_{\mathrm{PJ}})}{r_{\mathrm{PJ}}}-\mathrm{curl}_{\mathrm{P}}\,\mathbf{E}_0(\mathrm{J})\times\mathrm{grad}\,\frac{\exp ikr_{\mathrm{PJ}}}{r_{\mathrm{PJ}}}\right)d\tau_{\mathrm{J}}. \qquad \ldots\ldots(13\,a)$$

The integrands and their derivatives are practically constant inside the object, consequently the integration yields just a factor V equal to the volume of the object, and the result is:

$$\delta u_1(\mathrm{P}) = -\frac{V}{4\pi}\left\{k^2 \frac{\exp ikr_{\mathrm{P}}}{r_{\mathrm{P}}} u_0 + \operatorname{grad}_{\mathrm{P}} \frac{\exp ikr_{\mathrm{P}}}{r_{\mathrm{P}}} . \operatorname{grad} u_0\right\}, \qquad \ldots\ldots(14)$$

$$\delta \mathbf{E}_1(\mathrm{P}) = \frac{V}{4\pi}\left\{i\omega\mu \mathbf{H}_0 \times \operatorname{grad}_{\mathrm{P}} \frac{\exp ikr_{\mathrm{P}}}{r_{\mathrm{P}}} - \operatorname{curl}_{\mathrm{P}}\left(\mathbf{E}_0 \times \operatorname{grad}_{\mathrm{P}} \frac{\exp ikr_{\mathrm{P}}}{r_{\mathrm{P}}}\right)\right\}. \qquad \ldots\ldots(14a)$$

By omitting the suffix J we take every argument not marked by P at the place of the object, which is almost just a point. In this approximation the object enters only by its volume, and its shape has no effect. This is different in the second and higher orders, where the shape of the object is of decisive importance. In the case of a spherical object the result of the νth approximation is

$$u_\nu(\mathrm{P}) - u_0(\mathrm{P}) = -\frac{k^2 V}{4\pi} \frac{\exp(ikr_{\mathrm{P}})}{r_{\mathrm{P}}}\left\{1 - \frac{3}{2}\left(1 - \frac{1}{3^\nu}\right) \cos\Theta\right\} u_0 \qquad \ldots\ldots(15)$$

$$\mathbf{E}_\nu(\mathrm{P}) - \mathbf{E}_0(\mathrm{P}) = \frac{3V}{4\pi} \frac{\exp(ikr_{\mathrm{P}})}{r_{\mathrm{P}}} \mathbf{k} \times \left\{\mathbf{E}_0 \times \left(\left(1 - \left(\frac{2}{3}\right)^\nu\right)\mathbf{k} - \frac{1}{2}\left(1 - \frac{1}{3^\nu}\right)\mathbf{k}_0\right)\right\}. \qquad \ldots\ldots(15a)$$

Here **k** is the vector wave-number of the diffracted wave in P, $\mathbf{k}_0$ the vector wave-number of the primary wave at the object, Θ the angle they include (for the calculation see Franz 1949, §§ 4 and 8). Equations (15) and (15 *a*) show good convergence towards the well-known exact solution of the problem. The parameters of approximation are pure numbers; this somewhat surprising fact might have been expected since our successive corrections have to amend the violation of the boundary condition, and must therefore be of the same order of magnitude as the starting function, even if numerically smaller. Another puzzling point is why the first step does not itself produce the exact result, seeing that the correction has just the correct discontinuities in $\partial u/\partial n$ and in $\mathbf{E}_{\parallel}$ to cancel the errors in the surface values of the primary wave. The solution of this paradox is, of course, that $\partial \delta u_1/\partial n$ and $\delta \mathbf{E}_{1\parallel}$ are not zero inside the object, so that there is a residual error outside it.

§ 5. PERFECTLY REFLECTING HALF-PLANE

An instructive example is the diffraction of a plane wave by a perfectly reflecting half-plane. This emphasizes the most characteristic features of the new method. Each step of approximation can conveniently be compared with the well-known exact solution of Sommerfeld.

For simplicity we assume cylindrical symmetry, choosing as primary radiation a plane wave incident at right angles to the edge of the half-plane. We describe the points of space by cylindrical coordinates z, ρ, ϕ, with the axis in the edge, $\phi = 0$ in the open half of the diffracting plane (see Figure 2), and $|\phi|$ always less than or equal to π. We have to consider only the scalar wave equation, since for cylindrical symmetry the electromagnetic field can be reduced to a scalar one (with $u = \mathbf{E}$ if **E** is parallel to the edge, and $u = \mathbf{H}$ if **H** is parallel to the edge).

Let us first assume as boundary condition

$$u=0 \quad \text{at both sides of the screen.} \qquad \ldots\ldots(16)$$

The primary plane wave may proceed into the direction ϕ_0, and its wave function may be written

$$u_0(\rho,\phi)=\exp\{ik\rho\cos(\phi-\phi_0)\}; \qquad \ldots\ldots(17)$$

time dependence, as mentioned above, is as $\exp(-i\omega t)$.

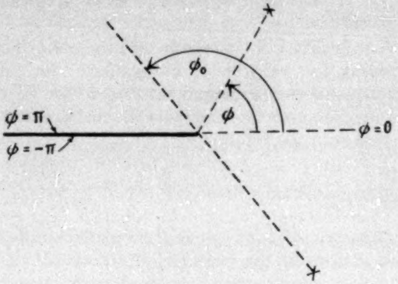

Figure 2. Diffracting half-plane.

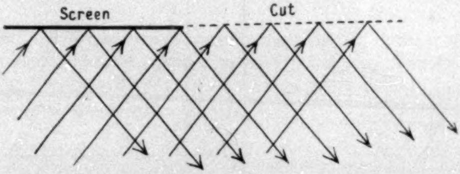

Figure 3. Zero approximation for half-plane.

In the first intermediate step we add a reflected wave at the near side of the screen, and use our scissors to cut away everything beyond the plane of the screen (Figure 3). This gives

$$u_0'=0; \qquad \operatorname{grad} u_0'=0 \quad \text{for} \quad \phi>0$$

$$\left.\begin{aligned} u_0'(\rho,\phi)&=u_0(\rho,\phi)-u_0(\rho,-\phi)\\ \operatorname{grad} u_0'(\rho,\phi)&=\operatorname{grad} u_0(\rho,\phi)+\operatorname{grad} u_0(\rho,-\phi)\end{aligned}\right\} \text{for } \phi<0. \qquad \ldots\ldots(18)$$

(The condition $\phi_0>0$ is essential only for Figure 3 and formula (18), but can be dropped for the rest of the calculation.)

To get the first order correction δu_1 we have to apply (8), integrated along the surface of discontinuity $\phi=0$, and insert the discontinuity of u_0', which is zero for u_0' and $2\operatorname{grad} u_0(\rho,0)$ for $\operatorname{grad} u_0'$. This gives

$$\delta u_1(\rho,\phi)=\frac{k}{2\pi i}\int_{-\infty}^{+\infty} dz_J \int_0^{\infty} d\rho_J \frac{\exp ikr}{r}\sin\phi_0 . \exp(ik\rho_J\cos\phi_0). \qquad \ldots\ldots(19)$$

Integrating dz_J brings in the first Hankel function, which we represent by Sommerfeld's integral

$$\int_{-\infty}^{+\infty} dz_J \frac{e^{ikr}}{r} = i\pi\mathscr{H}_0^{(1)}\{k(\rho^2+\rho_J^2-2\rho\rho_J\cos\phi)^{1/2}\}$$

$$= i\int_C d\phi_1 \exp\{ik(\rho^2+\rho_J^2-2\rho\rho_J\cos\phi)^{1/2}\cos\phi_1\}$$

$$= i\int_{C+(\pi+|\phi|)/2} d\phi_1 \exp\{-ik\rho_J\cos\phi_1+ik\rho\cos(|\phi|-\phi_1)\}. \quad \ldots\ldots(20)$$

The complex path of integration C is shown in Figure 4. The last form of (20) results from changing the variable of integration; the path is shifted into $C+(\pi+|\phi|)/2$, which makes the integral convergent for all values of ρ and ρ_J. If we now deform the path once more to cross the real axis at $\phi_1=\pi$, we can carry out the ρ_J integration with the result

$$\delta u_1(\rho,\phi)=\frac{1}{2\pi i}\int_{C+|\phi|} d\phi_1 \exp\{ik\rho\cos(|\phi|-\phi_1)\}\frac{\sin\phi_0}{\cos\phi_1-\cos\phi_0}, \quad \ldots\ldots(21)$$

crossing at π. After integrating we can shift the path completely into $C+|\phi|$, if we respect the rule of crossing the real axis. Formula (21) is a very convenient integral representation, which can easily be worked out for large as well as for small ρ.

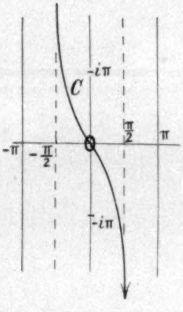

Figure 4. Integration path.

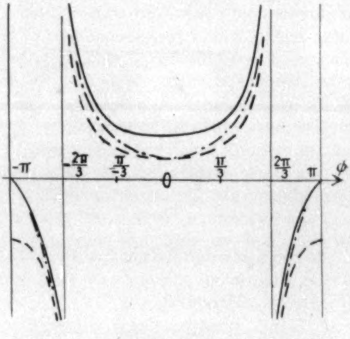

Figure 5. Half-plane, boundary condition $u=0$.
Exact solution ————
First approximation – – – – – – – –
Second approximation –·–·–·–·–·–

Next we have to calculate the second approximation. The situation is that $u_1=u_0'+\delta u_1$ satisfies the field equations everywhere, u_0' also satisfies the boundary condition (16), but δu_1 does not, which makes a second approximation necessary. We have to form a reflection zone according to Figure 1, and to take for u_1' there, of course, $-\delta u_1$. We need not bother with grad u_1', as grad δu_1 is zero for $\phi=\pm\pi$. But the screen is not only reflecting, it also throws a shadow, and this contributes, as δu_1 is penetrating the screen (it does not 'know' anything about the screen), another $-\delta u_1$ at the surface of the cut at $\phi = \pi$. So we get first for $\phi > 0$:

$$\delta u_2(\rho, \phi) = -\frac{1}{2\pi}\int_{(\phi_J=\pi)} d\boldsymbol{\sigma}_J \,.\, \mathrm{grad}_J \left(\frac{e^{ikr}}{r}\right) \delta u_1(\rho_J, \pi) = \frac{1}{2\pi}\,\mathrm{div} \int d\boldsymbol{\sigma}_J \frac{e^{ikr}}{r} \delta u_1(\rho_J, \pi). \qquad \ldots\ldots(22)$$

This formula accounts for the boundary condition at the screen, since the discontinuity is now found to be $-2\delta u_1$, which gives by reasons of symmetry just half the amount, i.e. $-\delta u_1$, at $\pi + 0$, and $+\delta u_1$ at $\pi - 0$. (If we calculate for the region $\phi = -\pi$, we have the opposite sign of n, and so there also the correct surface value.) We carry out the dz_J-integration as in (20):

$$\begin{aligned}\int_{-\infty}^{+\infty} \frac{e^{ikr}}{r}\, dz_J &= i\pi \mathscr{H}_0^{(1)}\{k(\rho^2 + \rho_J^2 + 2\rho\rho_J \cos\phi)^{1/2}\} \\ &= i \int_{C+|\phi|/2} d\phi_2 \,.\, \exp\{ik\rho_J \cos\phi_2 + ik\rho \cos(|\phi| - \phi_2)\}. \qquad \ldots\ldots(23)\end{aligned}$$

The path C has to be shifted by $|\phi|/2$ to ensure convergence for every ρ and ρ_J. Again we have a pure exponential of ρ_J and can integrate if we cross the real axis at $\phi_2 = 0$. The direction of $d\boldsymbol{\sigma}_J$ is towards diminishing ϕ, and therefore div equals $-(\sin\phi(\partial/\partial\rho) + (\cos\phi/\rho)(\partial/\partial\phi))$ of the scalar integral. So we get for $\phi \geqslant 0$:

$$\delta u_2(\rho, \phi) = \frac{1}{2\pi i}\int_C d\phi_1 \frac{\sin\phi_0}{\cos\phi_1 + \cos\phi_0} \int_{C+|\phi|} d\phi_2 \exp\{ik\rho\cos(|\phi| - \phi_1)\} \frac{\sin\phi_2}{\cos\phi_2 + \cos\phi_1}, \qquad \ldots\ldots(24)$$

$d\phi_2$ crossing at zero. Here again we insert the modulus of ϕ in order also to include negative values of ϕ. We can move the path for $d\phi_2$ completely into $C + |\phi|$ without touching a singularity ($\phi_2 = \pm\phi_1 \pm \pi$), as $\phi_1 + \pi$ at C is certainly out of reach. The $d\phi_1$ integration is elementary:

$$\begin{aligned}&\int_C d\phi_1 \frac{\sin\phi_0 \sin\phi_2}{(\cos\phi_0 + \cos\phi_1)(\cos\phi_1 + \cos\phi_2)} \\ &= \left[\frac{\sin\phi_2}{\cos\phi_2 - \cos\phi_0} \ln\frac{e^{i\phi_1} + e^{i\phi_0}}{e^{i\phi_1} + e^{-i\phi_0}} - \frac{\sin\phi_0}{\cos\phi_2 - \cos\phi_0} \ln\frac{e^{i\phi_1} + e^{i\phi_2}}{e^{i\phi_1} + e^{-i\phi_2}}\right]_{+i\infty}^{-i\infty} \\ &= 2i\frac{\phi_0 \sin\phi_2 - \phi_2 \sin\phi_0}{\cos\phi_2 - \cos\phi_0}. \qquad \ldots\ldots(25)\end{aligned}$$

For the evaluation of the last logarithm it is essential that ϕ_2 crosses the axis at zero. We get finally

$$\delta u_2(\rho, \phi) = \frac{1}{2\pi^2 i}\int_{C+|\phi|} d\phi_2 \exp\{ik\rho\cos(|\phi| - \phi_2)\} \frac{\phi_0 \sin\phi_2 - \phi_2 \sin\phi_0}{\cos\phi_2 - \cos\phi_0}. \qquad \ldots\ldots(26)$$

Now no longer does it matter where we cross the axis as the integrand has no singularity except at infinity; the numerator vanishes at $\phi_2 = \pm\phi_0$ as well as the denominator.

To illustrate the result let us calculate u_1 and u_2 for large ρ and compare with the exact solution. In this case only the very neighbourhood of the saddles $\phi_1 = |\phi|$ and $\phi_2 = |\phi|$ contributes to the integrals in (21) and (26) (in (21) we pass a pole of the integrand when $|\phi_0|>|\phi|$ but this contributes only the geometrical wave in which we are not interested). This gives

$$\delta u_1(\infty,\phi)=-\frac{\exp\{i(k\rho+\pi/4)\}}{(2\pi k\rho)^{1/2}}\,\frac{\sin\phi_0}{\cos\phi-\cos\phi_0} \qquad \ldots\ldots(27)$$

$$\delta u_2(\infty,\phi)=-\frac{\exp\{i(k\rho+\pi/4)\}}{(2\pi k\rho)^{1/2}}\,\frac{1}{\pi}\,\frac{\phi_0\sin|\phi|-|\phi|\sin\phi_0}{\cos\phi-\cos\phi_0}. \qquad \ldots\ldots(28)$$

The exact Sommerfeld solution is

$$u_S(\infty,\phi)=-\frac{e^{i(k\rho+\pi/4)}}{(2\pi k\rho)^{1/2}}\,\frac{2\cos\frac{1}{2}\phi\,\sin\frac{1}{2}\phi_0}{\cos\phi-\cos\phi_0}. \qquad \ldots\ldots(29)$$

Figure 5 shows the angular factors of u_1, u_2, u_S, Figure 6 the errors of the first and second approximation. Near the screen the improvement gained by the second approximation is very appreciable. Near the opening the improvement is small; on the contrary we pay for the improvement at the screen by a discontinuity of the normal derivative in the opening, which is the reason that we need a third approximation.

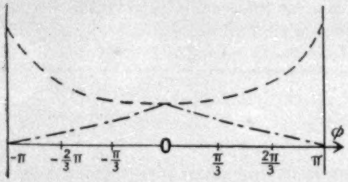

Figure 6. Errors of the first (– – – – – –) and second (– · – · – · – · –) approximation.

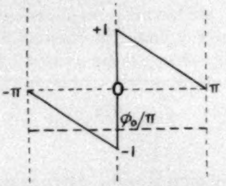

Figure 7. First approximation for half-plane at the edge, boundary condition $u=0$- - - - boundary condition $\frac{\partial u}{\partial n}=0$——

Now if we proceed to the third approximation we meet with a characteristic difficulty: at the edge the function δu_2 is finite, but not continuous—its value depends on the angle. So its tangential gradient is infinite there, and it is just this gradient which we need for δu_3 according to (8), and its singularity makes the integral diverge logarithmically for every ρ_P, ϕ_P. As this difficulty already appears in the second approximation, if we take the boundary condition $\partial u/\partial n=0$, we will now consider this case.

§ 6. THE DILEMMA OF THE EDGES

For the boundary condition

$$\frac{\partial u}{\partial n}=0 \quad \text{at the screen} \qquad \ldots\ldots(30)$$

we modify the incident wave (17) again according to Figure 3, only we take for the reflected wave the opposite sign of (18) in order to satisfy the altered boundary condition. That gives

$$u_0'=0; \qquad \operatorname{grad} u_0'=0 \qquad \text{for } \phi>0$$

$$\left.\begin{aligned} u_0'(\rho,\phi)&=u_0(\rho,\phi)+u_0(\rho,-\phi)\\ \operatorname{grad} u_0'(\rho,\phi)&=\operatorname{grad} u_0(\rho,\phi)-\operatorname{grad} u_0(\rho,-\phi)\end{aligned}\right\}\text{for } \phi<0. \qquad \ldots\ldots(31)$$

Here grad u_0' has no discontinuity, but the discontinuity of u_0' equals $2u_0$. Therefore we get according to (8)

$$\delta u_1(\rho, \phi) = \frac{1}{2\pi} \int_{(\phi_J=0)} d\boldsymbol{\sigma}_J \,.\, \mathrm{grad}_J \left(\frac{e^{ikr}}{r}\right) u_0(\rho_J, 0)$$

$$= -\frac{1}{2\pi} \mathrm{div} \int d\boldsymbol{\sigma}_J \frac{\exp(ikr + ik\rho_J \cos\phi_0)}{r}. \qquad \ldots\ldots(32)$$

The dz_J integration is carried out as in (20), div this time equals $\sin\phi(\partial/\partial\rho) + (\cos\phi/\rho)(\partial/\partial\phi)$ of the scalar integral, so we get

$$\delta u_1(\rho, \phi) = \frac{1}{2\pi i} \, \frac{\phi}{|\phi|} \int_{C+|\phi|} d\phi_1 \exp\{ik\rho\cos(|\phi| - \phi_1)\} \frac{\sin\phi_1}{\cos\phi_1 - \cos\phi_0}, \qquad \ldots\ldots(33)$$

crossing at π.

Now let us consider the behaviour of (33) as well as (21) at the edge. In (21) for $\rho = 0$ we can put 1 for the exponential and the integral becomes

$$\frac{1}{2\pi i} \int_{C+\pi} d\phi_1 \frac{\sin\phi_0}{\cos\phi_1 - \cos\phi_0} = -\frac{1}{2\pi i} \int_C d\phi_1 \frac{\sin\phi_0}{\cos\phi_1 + \cos\phi_0}$$

$$= \frac{1}{2\pi i} \left[\ln \frac{e^{i\phi_1} + e^{i\phi_0}}{e^{i\phi_1} + e^{-i\phi_0}}\right]_{+i\infty}^{-i\infty} = -\frac{\phi_0}{\pi}. \qquad \ldots\ldots(34)$$

In (33) we cannot simply put $\rho = 0$ under the integral as the integrand would not then vanish at infinity. We have first to transform the integral slightly. We shift the crossing point for π to $|\phi|$, which makes an extra contribution of $(\phi/|\phi|)\exp\{ik\rho\cos(|\phi| - |\phi_0|)\}$ if $|\phi| < |\phi_0|$. Then we transform the variable ϕ_1 by subtracting $|\phi|$, after which the path of integration is C. As this path is symmetrical, we can replace ϕ_1 by $-\phi_1$ in the integrand and take the average between this integral and the original one. Now we can put $\rho = 0$ and get

$$\frac{1}{4\pi i} \frac{\phi}{|\phi|} \left[\ln \frac{\cos(\phi_1 - |\phi|) - \cos\phi_0}{\cos(\phi_1 + |\phi|) - \cos\phi_0}\right]_{+i\infty}^{-i\infty} + \begin{cases} \phi/|\phi| & \text{for} \quad |\phi_0| > |\phi| \\ 0 & \text{for} \quad |\phi_0| < |\phi| \end{cases}$$

$$= \frac{\phi}{|\phi|} - \frac{\phi}{\pi}. \qquad \ldots\ldots(35)$$

Figure 7 shows the functions (34) and (35) of the angle ϕ. Inspecting it we must admit that our functions for the boundary condition $\partial u/\partial n = 0$ cannot but behave in this way, because it is just what we demanded: an unambiguous function with a jump of $2u_0$ at $\phi = 0$ and regular everywhere else. To compensate the discontinuous increase and to join regularly at $\phi = \pm\pi$, δu_1 must decrease continually, so this troublesome singularity of the tangential derivative of our function is essential and necessary. For the other boundary condition $u = 0$ such a thing does not happen as there is no discontinuity of u_0' at $\phi = 0$, only of the gradient, which gives no difficulties in the next approximation.

Now the infinity of the gradient at $\rho = 0$ not only frustrates the next approximation, but is a very serious fact in itself, as it makes the energy of the field infinite—there is in the expression of the energy density a term proportional to $(\mathrm{grad}\, u)^2$, and as this behaves along the edge like $1/\rho^2$, the integral diverges logarithmically. This must be, of course, excluded,* therefore we must subtract something from (33) which removes the singularity without adding a singularity anywhere else. In our example of the half-plane, this may be easily done in different ways; we have only to replace the fraction of the integrand (33) by another, which has the same residua for $\phi_1 = \pm\phi_0$, and vanishes in an integrable manner at the boundaries of C. Such a substitution is for instance

---

* The necessity of such a condition was first pointed out by Meixner (1948), who also proved that this edge condition is sufficient to determine the diffraction by an edge unambiguously.

$$\frac{\sin\phi_1}{\cos\phi_1 - \cos\phi_0} \longrightarrow \frac{\sin\phi_0}{\phi_0}\,\frac{\phi_1}{\cos\phi_1 - \cos\phi_0}. \qquad \ldots\ldots(36)$$

Another possibility is the substitution

$$\frac{\sin\phi_1}{\cos\phi_1 - \cos\phi_0} \longrightarrow \frac{\sin\phi_0}{\sin\frac{1}{2}\phi_0}\cdot\frac{\sin\frac{1}{2}\phi_1}{\cos\phi_1 - \cos\phi_0}. \qquad \ldots\ldots(37)$$

This yields the exact solution of Sommerfeld.

For a general kind of screen a regularized solution cannot be found in such a simple way. But in any case we must insert a third kind of step into our approximation method, if we are dealing with diffraction at edges, as in this case we have three conditions to fulfil--wave equation, boundary condition, edge condition. If we ignore the edge condition, there is another method of carrying out the second approximation, by a limiting process, which will be shown in the following section. This process can be transferred to arbitrary edges.

§ 7. IRREGULAR SECOND APPROXIMATION

Though δu_1 in equation (33) displays at $\rho = 0$ the singular behaviour (35), there is, surprisingly, a way of making the integrals of the next approximation converge without really altering δu_1. We note that $\phi\mathscr{H}_0^{(1)}(k\rho)$ is a solution of (1), which is regular everywhere except at the edge (and at infinity of course) and may be suitable to compensate the singularity of δu_1 without violating the conditions of the problem. But for very small ρ the Hankel function tends to infinity, thus any finite multiple of $\phi\mathscr{H}_0^{(1)}(k\rho)$ is far too large to compensate the singularity (35). But we can carry out the second approximation by the following limiting process: we choose a length ϵ which is extremely small compared with the ρ of the observer and the wavelength, and replace δu_1 by

$$\delta u_1 + \frac{2\phi}{\pi}\,\frac{\mathscr{H}_0^{(1)}(k\rho)}{\mathscr{H}_0^{(1)}(k\epsilon)}. \qquad \ldots\ldots(38)$$

The addition is twice the amount required to cancel the singularity of (35) for $\rho = \epsilon$, it satisfies the wave equation everywhere and produces no additional discontinuity at $\phi = 0$; thus our new function is suitable in every respect, and alters δu_1 at the place of the observer only by a negligible amount. Inserting (38) into (8) we get the second approximation for the boundary condition (30):

$$\delta u_2(\rho,\phi) = \frac{1}{2\pi}\int_{\epsilon}^{\infty} d\rho_J \int_{-\infty}^{+\infty} dz_J\,\frac{e^{ikr}}{r}\,\frac{\partial}{\partial n_J}\left(\delta u_1(\rho_J,\phi_J) + \frac{2\phi_J}{\pi}\cdot\frac{\mathscr{H}_0^{(1)}(k\rho_J)}{\mathscr{H}_0^{(1)}(k\epsilon)}\right)\bigg|_{\phi_J=\pi}. \qquad \ldots\ldots(39)$$

At $\rho = \epsilon$ we cut off the surface of integration; in consequence δu_2 added to (38) will satisfy the boundary condition (30) everywhere, if ρ is greater than the chosen ϵ.

If we calculate the normal gradient ($=-(1/\rho_J)(\partial/\partial\phi_J)$) for (33) at $\phi_J=\pi$, we obtain an integral which we transform in the following way:

$$\int_{C+\phi_J} d\phi_1 \frac{\sin\phi_1}{\cos\phi_1-\cos\phi_0}\frac{\partial}{\partial\phi_J}\exp\{ik\rho_J\cos(\phi_J-\phi_1)\,\Big|_{\phi_J=\pi}$$
$$=-\int_{C+\pi} d\phi_1 \frac{\sin\phi_1}{\cos\phi_1-\cos\phi_0}\frac{\partial}{\partial\phi_1}\exp(-ik\rho_J\cos\phi_1)$$
$$=\int_{C+\pi} d\phi_1 \exp(-ik\rho_J\cos\phi_1)\frac{\partial}{\partial\phi_1}\frac{\sin\phi_1}{\cos\phi_1-\cos\phi_0}. \qquad \ldots\ldots(40)$$

Equation (39) now becomes, using (23) for $\phi>0$:

$$\delta u_2(\rho,\phi)=\int_\epsilon^\infty \frac{d\rho_J}{\rho_J}\frac{1}{2\pi i}\int_{C+\phi/2} d\phi_2 \exp\{ik\rho_J\cos\phi_2+ik\rho\cos(\phi-\phi_2)\}.$$
$$\times\left\{\frac{1}{2\pi i}\int_{C+\pi} d\phi_1\exp(-ik\rho_J\cos\phi_1)\frac{\partial}{\partial\phi_1}\frac{\sin\phi_1}{\cos\phi_1-\cos\phi_0}+\frac{2}{\pi}\frac{\mathscr{H}_0^{(1)}(k\rho_J)}{\mathscr{H}_0^{(1)}(k\epsilon)}\right\}. \qquad \ldots\ldots(41)$$

We may neglect some terms which can be made arbitrarily small if we choose ϵ small enough compared with the wavelength. We have first *

$$\lim_{k\epsilon\to 0}\int_\epsilon^\infty \frac{d\rho_J}{\rho_J}\left\{\exp\{ik\rho_J(\cos\phi_2-\cos\phi_1)\}-\frac{1}{1-ik\rho_J(\cos\phi_2-\cos\phi_1)}\right.=-C=-\ln\gamma, \qquad \ldots\ldots(42)$$

where C is the Euler constant 0·577 and $\gamma=\exp C$. Note also that

$$\lim_{k\epsilon\to 0}\frac{1}{\mathscr{H}_0^{(1)}(k\epsilon)}\int_\epsilon^\infty \frac{d\rho_J}{\rho_J}\exp(ik\rho_J\cos\phi_2)\left\{\mathscr{H}_0^{(1)}(k\rho_J)-\frac{2i}{\pi}\ln\frac{\gamma k\rho_J}{2i}\right\}=0, \qquad \ldots\ldots(43)$$

as the integral has for $\epsilon\to 0$ a finite value (Magnus and Oberhettinger 1943, chap. 3, § 1). This transforms (41) into

$$\delta u_2(\rho,\phi)=\frac{1}{2\pi i}\int_{C+\phi/2} d\phi_2\exp\{ik\rho\cos(\phi-\phi_2)\}$$
$$\text{(cross at 0)}$$
$$\left\{\frac{1}{2\pi i}\int_{C+\pi} d\phi_1\frac{\partial}{\partial\phi_1}\frac{\sin\phi_1}{\cos\phi_1-\cos\phi_0}\left(\int_0^\infty\frac{d\rho_J}{\rho_J(1-ik\rho_J(\cos\phi_2-\cos\phi_1))}-\ln\gamma\right)\right.$$
$$\left.+\frac{4i}{\pi^2}\int_\epsilon^\infty\frac{d\rho_J}{\rho_J}\frac{\ln(\gamma k\rho_J/2i)}{\mathscr{H}_0^{(1)}(k\epsilon)}\exp(ik\rho_J\cos\phi_2)\right\}. \qquad \ldots\ldots(44)$$

Integrating the last term by parts and neglecting again terms small for small $k\epsilon$, we get

$$\frac{4i}{\pi^2\mathscr{H}_0^{(1)}(k\epsilon)}\int_\epsilon^\infty\frac{d\rho_J}{\rho_J}\ln\left(\frac{\gamma k\rho_J}{2i}\right)\exp(ik\rho_J\cos\phi_2)$$
$$=\frac{4i}{\pi^2\mathscr{H}_0^{(1)}(k\epsilon)}\left\{\frac{1}{2}\left[\left(\ln\frac{\gamma k\rho_J}{2i}\right)^2\exp(ik\rho_J\cos\phi_2)\right]_\epsilon^\infty\right.$$
$$\left.-ik\cos\phi_2\int_\epsilon^\infty\left(\ln\frac{\gamma k\rho_J}{2i}\right)^2\exp(ik\rho_J\cos\phi_2)\,d\rho_J\right\}$$
$$\longrightarrow-\frac{1}{\pi}\ln\frac{\gamma k\epsilon}{2i}. \qquad \ldots\ldots(45)$$

---

* e.g. Magnus and Oberhettinger (1943, end of Chapter 1).

The remaining $d\rho_3$ integration in (44) is elementary:

$$\int_\epsilon^\infty \frac{d\rho_3}{\rho_3\{1-ik\rho_3(\cos\phi_2-\cos\phi_1)\}} = \ln\left(1+\frac{i}{k\epsilon(\cos\phi_2-\cos\phi_1)}\right)$$

$$\longrightarrow -\ln\frac{\gamma k\epsilon}{2i}+\ln\gamma-\ln 2(\cos\phi_2-\cos\phi_1). \qquad \ldots\ldots(46)$$

In the last line again we have omitted terms small for small $k\epsilon$ and split the result in a useful way. Inserting (45) and (46) into (44) yields:

$$\delta u_2(\rho,\phi) = -\frac{1}{2\pi i}\,\frac{\phi}{|\phi|}\int_C d\phi_1\frac{\partial}{\partial\phi_1}\left(\frac{\sin\phi_1}{\cos\phi_1+\cos\phi_0}\right)$$

$$\times\frac{1}{2\pi i}\int_{C+|\phi|} d\phi_2 \ln 2(\cos\phi_1+\cos\phi_2)\exp\{ik\rho\cos(|\phi|-\phi_2)\}. \qquad \ldots\ldots(47)$$

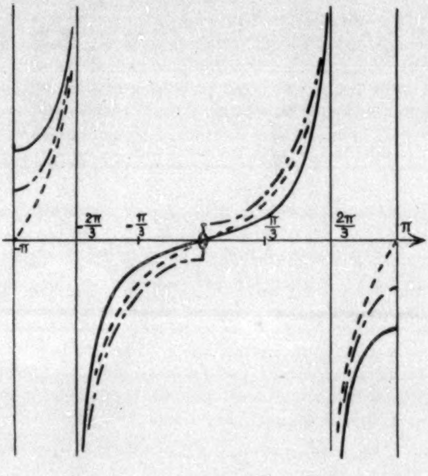

Figure 8. Half-plane, boundary condition $\frac{\partial u}{\partial n}=0$. Exact solution ———. First approximation - - - - - - - -. Second approximation - · - · - · - · -.

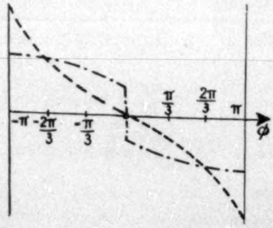

Figure 9. Errors of the first (– – – – – –) and second (– · – · – · –) approximation.

By inserting the modulus of ϕ at the proper places we make the formulae valid also for negative ϕ. The ϕ_1-integration can be carried out with the result

$$\delta u_2(\rho,\phi)=\frac{1}{2\pi^2 i}\,\frac{\phi}{|\phi|}\int_{C+|\phi|} d\phi_2\,\frac{\phi_2\sin\phi_2-\phi_0\sin\phi_0}{\cos\phi_0-\cos\phi_2},\exp\{ik\rho\cos(|\phi|-\phi_2)\}. \quad \ldots\ldots(48)$$

This is now independent of ϵ, thus our limiting process works. As only the immediate neighbourhood of the edge is concerned with this process, it can be applied also to arbitrary screens, at least if the curvature of the edge is continuous.

To illustrate the result (48) we calculate the value of the wave function for a distant observer, from (33) and (48):

$$\delta u_1(\infty,\phi)=-\frac{\exp\{i(k\rho+\pi/4)\}}{(2\pi k\rho)^{1/2}}\,\frac{\sin\phi}{\cos\phi-\cos\phi_0}. \quad \ldots\ldots(49)$$

$$\delta u_2(\infty,\phi)=-\frac{\exp\{i(k\rho+\pi/4)\}}{(2\pi k\rho)^{1/2}}\,\frac{\phi}{|\phi|}\,\frac{1}{\pi}\,\frac{\phi_0\sin\phi_0-\phi\sin\phi}{\cos\phi-\cos\phi_0}. \quad \ldots\ldots(50)$$

The exact Sommerfeld solution is

$$u_S(\infty,\phi)=-\frac{\exp\{i(k\rho+\pi/4)\}}{(2\pi k\rho)^{1/2}}\,\frac{2\sin\frac{1}{2}\phi\,\cos\frac{1}{2}\phi_0}{\cos\phi-\cos\phi_0}. \quad \ldots\ldots(51)$$

Figures 8 and 9 show the values and defects of the first and second approximation. By the second approximation we gain a reasonable improvement near the screen (mainly with respect to the boundary condition (30), which we tried to improve by this step), but we have to pay for it by a discontinuity of the function in the opening, which makes the third approximation necessary.

Note added in proof (see p. 928). This statement is not quite correct. As I have learned in the meantime, L. de Broglie in ***Problèmes de propagations guidées des ondes électromagnétiques*** (Paris, 1941) arrived at an equation equivalent to (8*a*) as a preliminary form of Kottler's formulae. Obviously he did not realize the importance of this formula, and it remained generally unknown until the present author stressed its usefulness (Franz 1948).

REFERENCES

Franz, W., 1948, *Z. Naturforsch.*, **3a,** 500; 1949, *Z. Phys.*, **125,** 563.
Kottler, F., 1923, *Ann. Phys., Lpz.*, **71,** 457.
Magnus, W., and Oberhettinger, F., 1943, *Formeln und Sätze für die speziellen Funktionen der mathematischen Physik* (Berlin : Springer).
Meixner, J., 1948, *Z. Naturforsch.*, **3a,** 506.

Intensity Distribution in Band-systems of O_2 and O_2^+

By M. E. PILLOW
Imperial College, London, and Northern Polytechnic, London

MS. received 13*th December* 1949

ABSTRACT. The intensity distributions for three oxygen band-systems, the Schumann–Runge and Herzberg systems of O_2 and the second negative system of O_2^+, are calculated, and compared where possible with experimental results. Some suggested identifications of bands observed in emission from the night sky are checked by comparison with the calculations.

---

§ 1. INTRODUCTION

In an earlier paper (Pillow 1949) an attempt was made to estimate, by comparison of calculated results with experimental observations, the accuracy with which the distribution of intensity among the bands of a system for a diatomic molecule could be predicted by an approximate theoretical method. The calculations were there carried out on the γ-system of MgH^+, and were taken only as far as the $v=8$ vibrational levels. Within these limits, observation and calculation were found to be in close agreement.

It has been suggested that in view of the probable existence of oxygen band-systems, both in emission in the night-sky spectrum and in absorption in the sun's atmosphere, a theoretical estimate of the intensity distributions to be expected in these spectra might be of some use as a guide to the identification of suspected bands. Accordingly, the intensity distribution schemes have been worked out for the Schumann–Runge and Herzberg systems of the O_2 molecule, and for the second negative system of O_2^+. For the potential energy curves the Morse function has been used, and the wave functions for the vibrational levels are obtained as before by graphical distortion from those for a harmonic oscillator. For this purpose, the wave functions corresponding to a quadratic potential function have been calculated for vibrational levels up to $v=16$. Table 1 is therefore complementary to the table of wave functions previously published.

The intensity in emission of the (v', v'') band is taken in the first place to be proportional to

$$\nu^4\left(\int \psi'_{v'}\psi''_{v''}\,dr\right)^2$$

and the intensity in absorption to

$$\nu\left(\int \psi'_{v'}\psi''_{v''}\,dr\right)^2,$$

ν being in each case the wave number of the origin of the band considered. This neglects the effect of vibration on the electric moment of the molecule, regarding this as constant. The general agreement of the results with those of experiment suggests that this is permissible. Also, the formula as it stands assumes that the vibrational levels in the initial state are all equally populated—that is, it assumes infinitely high temperature and the absence of any other factors causing preferential distribution. Where it seems likely that thermal motion is the main factor affecting the distribution this has been introduced in the Boltzmann factor

$$\exp[-\boldsymbol{h}\boldsymbol{c}\omega_e'(v'+\tfrac{1}{2})/\boldsymbol{k}\theta]$$

for emission, or $\exp[-\boldsymbol{h}\boldsymbol{c}\omega_e''(v''+\frac{1}{2})/k\theta]$ for absorption.

It is realized that at the higher levels the effect on the calculated intensity values of the departure from normalization caused by distorting the wave functions may be appreciable, and the effect of this has been considered when dealing with the Schumann–Runge system.

Table 1. Wave Functions for a Simple Harmonic Oscillator
i.e. $(2^n n!\sqrt{\pi})^{-1/2}\exp\{-\frac{1}{2}s^2\}H_n(s)$

s	$n=8$	9	10	11	12	13	14	15	16
0	0·393	0	−0·373	0	0·357	0	−0·344	0	0·333
$\frac{1}{4}$	0·128	0·339	−0·154	−0·332	0·112	0·341	−0·077	−0·368	0·042
$\frac{1}{2}$	−0·184	0·315	0·246	−0·248	−0·285	0·184	0·294	−0·122	−0·307
$\frac{3}{4}$	−0·395	−0·044	0·357	0·157	−0·297	−0·241	0·218	0·290	−0·135
1	−0·234	−0·358	0·061	0·368	0·091	−0·321	−0·208	0·231	0·283
$1\frac{1}{4}$	0·144	−0·307	−0·315	0·129	0·361	0·054	−0·331	−0·202	0·230
$1\frac{1}{2}$	0·397	0·051	−0·342	−0·267	0·164	0·357	0·042	−0·318	−0·209
$1\frac{3}{4}$	0·310	0·353	−0·018	−0·356	−0·239	0·203	0·368	0·078	0·331
2	−0·028	0·344	0·334	−0·043	−0·355	−0·254	0·155	0·356	0·102
$2\frac{1}{4}$	−0·349	0·026	0·359	0·320	−0·093	−0·394	−0·241	0·177	0·375
$2\frac{1}{2}$	−0·428	−0·318	0·051	0·357	0·316	−0·034	−0·327	−0·267	0·082
$2\frac{3}{4}$	−0·235	−0·427	−0·303	0·053	0·349	0·330	0·002	−0·312	−0·301
3	0·094	−0·249	−0·424	−0·304	0·027	0·328	0·341	0·061	−0·266
$3\frac{1}{4}$	0·366	0·081	−0·246	−0·418	−0·319	−0·005	0·301	0·352	0·113
$3\frac{1}{2}$	0·526	0·375	0·087	−0·226	−0·399	−0·347	−0·104	0·198	0·346
$3\frac{3}{4}$	0·520	0·522	0·382	0·114	−0·192	−0·397	−0·373	−0·132	0·187
4	0·418	0·513	0·522	0·400	0·154	−0·144	−0·364	−0·394	−0·204
$4\frac{1}{4}$		0·400	0·493	0·512	0·416	0·204	−0·077	−0·315	−0·398
$4\frac{1}{2}$	0·174	0·277	0·392	0·487	0·521	0·456	0·265	0	−0·257
$4\frac{3}{4}$		0·160	0·254	0·369	0·457	0·511	0·466	0·320	0·087
5	0·045	0·087	0·151	0·238	0·342	0·447	0·506	0·497	0·389
$5\frac{1}{4}$									
$5\frac{1}{2}$	0·008	0·018	0·036	0·063	0·110	0·178	0·207	0·353	0·434
$5\frac{3}{4}$									
6	0·001	0·003	0·006	0·012	0·024	0·046	0·064	0·131	0·201
$6\frac{1}{4}$									
$6\frac{1}{2}$									
$6\frac{3}{4}$									
7	0	0	0	0	0	0·001	0·001	0·003	0·007

Of the systems considered, the Schumann–Runge has been observed in the laboratory both in emission and in absorption, the Herzberg system, so far, in absorption only, and the O_2^+ system, naturally, in emission only. The experimental results in each case have been compared with those obtained from the calculations made on the corrected wave functions, and the agreement is, on the whole, good. This seems to indicate that the method of calculation is, with certain limitations to be discussed later, still sound even at fairly high energy levels, and that the estimated distribution of intensity under appropriately chosen conditions can be taken as a fairly reliable guide to the identification of bands suspected of belonging to one of these systems.

§ 2. THE SCHUMANN–RUNGE SYSTEM FOR O_2

This system of bands has been photographed in emission by several workers. The results were analysed, and further measurements made, by Lochte-Holtgreven and Dieke (1929). The system has been further studied in emission by Feast (1949), who has analysed a number of new bands. (Millon and Herman (1944) and Lal (1948 a, b) suggest further bands, but in neither of these cases is an analysis published. These are discussed by Feast.)

The most reliable observations on the same system in absorption in cold gas are those of Knauss and Ballard (1935). Füchtbauer and Holm (1925) photographed and measured bands appearing in absorption in heated gas up to temperatures of about 1,050° c.

The constants for the two electronic states involved are taken from the measurements of Lochte-Holtgreven and Dieke and of Knauss and Ballard. These give, with the usual notation: (i) for the excited state, $\omega_e'=700{\cdot}36$, $\omega_e'x'=8{\cdot}002$, $\omega_e'y'=0{\cdot}375$ (neglected in this calculation), $B_e'=0{\cdot}801$; (ii) for the ground state, $\omega_e''=1{,}584{\cdot}9$, $\omega_e''x''=11{\cdot}645$, $B_e''=1{\cdot}46$.

The absorption bands in the $v''=0$ progression converge to a limit at about 56,877 cm^{-1}, and the (0, 0) band of the system is calculated to have its origin at 49,363 cm^{-1}. For the excited state, therefore, the value of D' in the Morse function is 7,862 cm^{-1}.

The value of D'' for the ground state can be calculated from the limit of the $v''=0$ progression of the Herzberg system, which has the same ground-state as the Schumann–Runge system, and whose two potential curves approach the same limit. It may also be found by considering the two atomic states into which the molecule can dissociate. This is discussed fully by Gaydon (1947). The value adopted here for D'' is 42,070 cm^{-1}.

The intensities in emission for the bands of the Schumann–Runge system, calculated as described above for infinite temperature and for 3,000° K., are set out in Tables 2 and 3. The bands recorded by Lochte-Holtgreven and Dieke and by Feast are shown in the tables. In these cases the emission occurred in some form of gas discharge, so that any assumption of thermal equilibrium is invalid, and for comparison with the experimental results it is probably useful to consider mainly the table corresponding to infinite temperature.

As has been mentioned, it seemed advisable to try to estimate, at least approximately, how far the distorted wave functions used here depart from normalization. This was done by making a numerical computation of the quantity $\int\psi_v^2\,dr$ for each of a number of wave functions, and comparing the values with those for the undistorted functions. The results for the wave functions of the ground state showed a gradual, almost linear, increase of the ratio from 1 to 1·5 as the vibrational level rose from 0 to 16. This means that the intensities in any v' progression should be divided by the factor, between 1 and 1·5, appropriate to that value of v''. This has been done for the first few progressions in emission, and the results are shown in Table 4.

For the excited state, the correction is much more difficult to estimate, since the wave function curves are very greatly distorted for high r-values, and the quantity $\int\psi_v^2\,dr$ tends to very large values when calculated from the graphs. But this great distortion occurs only in those parts of the wave function curves that are not in fact used, since they do not overlap the curves for the ground state. It seems wise, therefore, to attempt no correction for the intensity values in the v'' progressions, but to bear in mind that the intensities calculated for high values of v' are probably slightly too great. This is of importance only when considering absorption at very high temperatures.

It is seen that of the bands analysed the great majority are those to which calculation attributes a high intensity. There are a few exceptions, the most

Table 2. Schumann–Runge System
Calculated intensities in emission at infinite temperature

$v'\backslash v''$	0	1	2	3	4	5	6	7	8	9	10	11	12	13	14	15	16
0							2	6	14	32^{F}	60^{F}	83^{F}	$100^{F,L}$	$99^{F,L}$	$68^{F,L}$	$39^{F,L}$	$15^{F,L}$
1						1	5	10	18^{F}	25^{F}	27^{F}	16^{F}	2^{F}	4	23	63	$80^{F,L}$
2					2	3	9^{F}	15^{F}	22^{F}	22^{F}	13^{F}	4	0	3	8	0	9^{L}
3				1	3	7	13^{F}	22^{F}	24	16	5	0	4	9	6	2	1
4				2	6	13	22	29	24	8	1						
5			1	3	5	14^{F}	31^{F}	31	18	2	2						
6			1	6	18	31	39	26	8	0	8						
7			2	9	24	39	39	17	1	5	13						
8		1	4	12	27	36	28	6	2	19	18						
9		2	5	14	28	28	16	1	6	16	7						
10		2	5	13	21	24	1	4	8	5	0						

L = bands recorded by Lochte-Holtgreven and Dieke.

F = bands recorded by Feast.

Table 3. Schumann–Runge System
Calculated intensities in emission at 3,000° K.

$v'\backslash v''$	0	1	2	3	4	5	6	7	8	9	10	11	12	13	14	15	16
0							2	6	14	32	60	83	100	99	68	39	15
1						1	4	7	13	18	19	12	1	3	16	45	57
2					1	2	5	8	11	11	7	2		2	4		5
3					1	3	5	8	9	6	2		1	3	2	1	
4				1	2	3	6	7	6	2							
5				1	1	3	6	6	3								
6				1	2	4	5	4	1		1						
7				1	2	4	4	2			1						
8				1	2	2	2			1	1						
9				1	1	1	1			1							
10					1	1											

Table 4. Schumann–Runge System
Calculated intensities in emission at infinite temperature, corrected for failure of normalization

$v'\backslash v''$	0	1	2	3	4	5	6	7	8	9	10	11	12	13	14	15	16
0							3	7	16	35^{F}	63^{F}	86^{F}	$100^{F,L}$	$98^{F,L}$	$66^{F,L}$	$37^{F,L}$	$14^{F,L}$
1						1	6	11	21^{F}	27^{F}	28^{F}	17^{F}	2^{F}	4	22	59	$73^{F,L}$
2					3	4	11^{F}	17^{F}	24^{F}	24^{F}	14^{F}	4		3	7		8
3				1	4	8	15^{F}	25^{F}	27	17	6		4	8	6	1	1

L = bands recorded by Lochte-Holtgreven and Dieke.
F = bands recorded by Feast.

obvious being the (1, 12) band claimed by Feast and the (2, 15) of Lochte-Holtgreven and Dieke. Feast considers the (1, 12) band to be definitely present, though it is very weak, and exists in a region of many blended lines so that he has been able to measure fewer lines of this band than of others. He does not find the (2, 15) band at all with the exposures he has used, and it is noteworthy that Lochte-Holtgreven and Dieke have recorded only lines corresponding to high rotational levels in this band. This suggests a possible explanation of the appearance of some bands which lie near the main Franck–Condon parabola in the vibration table, but whose calculated intensity is low. The method of calculation used here takes no account of rotation, and the intensities given are therefore those corresponding to the lines near the band-origin. If rotational energy is taken into account, the potential curve is slightly displaced, and this could produce appreciable changes in band intensities. It seems safe, then, to say that if a band has a high calculated intensity some part of it should certainly be observed, but that a band of low calculated intensity, particularly if near the main parabola, may yet have some lines visible. If this is the true explanation, no such discrepancy should exist in a band system where measurements are made mainly on or near band heads, as in the Herzberg and O_2^+ systems.

Flory's suggestion, discussed by Feast, that among other bands the (3, 15) and (3, 16) bands should appear, is not supported by the calculated intensities. The (1, 15) band, on the other hand, should according to calculation be readily observed, but apparently it has not been recorded by any workers.

In considering absorption, the effect of temperature is very much greater than in emission for two reasons; the temperatures involved are, as a rule, low compared with those in emission, and the constant ω_e'' is generally greater than ω_e'. On the other hand, provided that the temperature is known with reasonable precision, the effect can be predicted fairly certainly, since there is little likelihood of the distribution of molecules among levels in the ground state being affected by anything other than thermal disturbance under laboratory conditions. (In the sun's atmosphere this assumption is not justified.) The intensities in absorption for the Schumann–Runge system have been calculated for 300° K., showing, as expected, only the $v''=0$ progression, for 1,300° K., this being about the highest temperature used by Füchtbauer and Holm, for 2,300° K., which can reasonably be expected in a laboratory furnace, and for infinite temperature, which should give some guidance in examining the solar spectrum. These intensities are shown in Table 5–8.

The slightly irregular variation of intensity in the $v''=0$ progression is of no significance, since the fundamental quantity

$$\left[\int \psi'_{v'} \psi_0'' \, dr\right]^2$$

is very small for all the terms in this progression, and the errors involved in reading from the graphs are enough to account for the irregularity.

§ 3. THE HERZBERG SYSTEM FOR O_2

These bands have so far been observed only in absorption in the laboratory. Herzberg (1932) observed seven absorption bands in oxygen at atmospheric pressure, and for six of these he made rotational analyses. He considered that besides the seventh band there was yet another, too faint for any kind of measurement. Chalonge and Vassy (1934) obtained the same series of bands in absorption

Table 5. Schumann–Runge System
Calculated intensities in absorption
at 300° K.

$v' \backslash v''$	0
0	
1	
2	
3	
4	
5	1^{K}
6	5^{K}
7	20^{K}
8	29^{K}
9	51^{K}
10	50^{K}
11	78^{K}
12	100^{K}
13	90^{K}
14	95^{K}

K = bands observed in absorption in cold gas by Knauss and Ballard.

Table 6. Schumann–Runge System
Calculated intensities in absorption
at 1,350° K.

$v' \backslash v''$	0	1	2	3	4	5	6
0							
1							
2				1	1		
3			1	1	2	1	
4		1	3	4	3	1	
5	1	3^{H}	6	6^{H}	2^{H}	1^{H}	
6	2	8^{H}	14	12^{H}	8^{H}	3^{H}	1
7	8	16^{H}	24	19^{H}	8^{H}	3^{H}	1
8	12	27^{H}	35	23^{H}	11^{H}	3^{H}	
9	21	34	43	24	10	2	
10	20	43	45	24	8	1	
11	31	70	62	31	8	1	
12	40	88	67	30	7		
13	36	100	59	23	5		
14	38	77	55	19	3		

H = bands observed in absorption in heated gas by Füchtbauer and Holm.

Table 7. Schumann–Runge System
Calculated intensities in absorption at 2,300° K.

$v' \backslash v''$	0	1	2	3	4	5	6	7	8	9
0						1	1	1	1	1
1					1	2	2	2	2	1
2				2	5	3	4	3	2	1
3			1	4	9	8	6	4	2	1
4		1	4	11	16	15	10	5	2	
5		3	9	19	11	15	14	6	1	
6	1	6	20	36	46	32	16	5	1	
7	3	12	36	56	47	38	16	3		
8	4	19	52	70	65	35	11	2		
9	8	25	64	72	61	27	6			
10	8	33	67	73	51	17	1			
11	12	49	92	91	49	13				
12	15	63	100	89	40	8				
13	13	72	87	70	28	3				
14	14	56	81	57	20	2				

Table 8. Schumann–Runge System
Calculated intensities in absorption at infinite temperature

$v' \backslash v''$	0	1	2	3	4	5	6	7	8	9	10	11	12	13	14	15	16
0							1	3	7	19	40	62	87	94	72	48	21
1						1	2	4	9	14	17	11	1	4	23	72	100
2						1	3	6	10	12	7	2		2	6		11
3					1	2	5	7	11	8	3		3	6	5	2	1
4					2	4	8	12	10	4							
5					1	4	10	12	7	1	1						
6				1	5	9	13	10	3		4						
7			1	2	5	11	12	6		2	6						
8			1	2	7	10	9	4	1	6	8						
9			1	3	6	8	4		2	6	3						
10			1	3	5	5			3	2							

in the atmosphere, and their microphotometer trace shows clearly the eighth band which Herzberg presumed to exist, and gives a definite indication of one more. Their measurements did not extend to rotational structure. Herman (1939) made a large number of observations on absorption in oxygen at various pressures, and found that as the pressure increased the Herzberg system gave place to a triplet system of longer wavelength, the range covered by one system being apparently contiguous to that covered by the other. Herman observed and measured fully all the bands recorded by Chalonge and Vassy, and considered that there might be two further bands, of still longer wavelength, the rotational constants for which he obtained by extrapolation. Morguleff and Vassy (1939) also made measurements on the system in absorption in the atmosphere. Their record is very similar to that of Chalonge and Vassy. They have made rotational measurements, which, however, give more erratic values for the rotational constants B' of the upper electronic state than do those of Herman, or even the original values of Herzberg. Stopes-Roe (1948) photographed the system in oxygen in the laboratory, and he has kindly allowed the writer the use of his plates to make yet again a rotational analysis. The comparison spectrum used is that of a copper arc. All the values for band-head wavelengths and for B' are shown in Table 9.

Table 9

Herzberg			Chalonge and Vassy			Herman			Morguleff and Vassy			Values now obtained from Stopes-Roe's plates		
v'	λ_0	B'	v'	λ_0	B'	v'	λ_0	B'	v'	λ_0	B'	v'	λ_0	B'
						0	2795·2 ?	(1·05)						
						1	2737·6 ?	(1·02)						
			0	2689		2	2685·0	0·98					?	
0	?	(0·84)	1	2639		3	2637·7	0·92		2638·3	0·82		†	
1	2595	(0·81)	2	2595		4	2594·0	0·86		2593·1	0·79		2593·2*	0·82*
2	2554	0·77	3	2556		5	2554·6	0·81		2553·8	0·78		2554·2	0·80
3	2519·1	0·75	4	2521		6	2519·1	0·75		2519·1	0·74		2519·1	0·75
4	2488·5	0·70	5	2491		7	2489·1	0·69		2488·1	0·72		2488·7	0·69
5	2463·0	0·65	6	2465		8	2463·4	0·65		2462·5	0·63		2463·2	0·65
6	2442·8	0·59	7	2445		9	2443	0·56		2442·0	0·57		2442·8	0·57
7	2429·0	0·53	8	2431		10	2429	0·50		2428·3	0·51		2429·1	0·49
			9	2423										
				+continuum									source too faint here	

Numbers in brackets are extrapolated values.
? indicates a band considered to exist, but not measured.
† lines present, but too faint for useful measurement.
* measurements doubtful near band origin.

It can be seen that there is room for considerable doubt as to the wavelength of the (0, 0) band, and the constant B_e' to be used in drawing the potential curve for the upper state of the system. Herman's B' values are very much the most regular in their variation with v'. The values deduced by the writer from Stopes-Roe's plates agree better with these than with those of either Herzberg or Morguleff and Vassy, and Herman's values have been adopted here as far as the 2685 A. band—that is, as far as his actual measurements go. For the two doubtful bands of longer wavelength, Herman gives extrapolated values of B'. In view of the almost exactly linear variation with v' of his measured values it is difficult to see why he has adopted these two values, which are well off the linear relation, and changes in the extrapolated values can so alter the calculated values of B_e' that, if the two long-wave bands are accepted, the equilibrium distance apart of the nuclei, r_e', can be anything from 1·30 to 1·40.

The ground-state of the system, since the absorption takes place in cold gas, is the same as for the Schumann–Runge system. Since the bands consist of a Q-series of lines only, with alternate lines missing, the value of B_0'' for the ground-state has to be used in finding B' each time.

Herzberg considered that there should be an absorption continuum at the short-wave end of the system, though his plates did not show it. Chalonge and Vassy (1934) and Gotz (1934) state that it certainly is there, beginning at about 41,300 cm^{-1} (λ=2420 A.), though Gotz concedes that it may not be wholly due to oxygen. Stopes-Roe's plates leave the existence of this continuum uncertain, as his source was weak in this region.

Calculations have here been made on the intensities of the absorption bands in cold gas, using various assumptions as to the origin of the system, and the results compared with visual estimates of the intensities in the photographs available (plates of Stopes-Roe and print of Morguleff and Vassy), in order to give some guidance in deciding between the various suggested positions for the origin. The photographs show a rapid increase of intensity from the long-wave end of the system to the 2489 A. band, and then nearly equal intensities, perhaps falling off slightly at the 2429 A. band. Table 10 shows how very sensitive are the calculated intensities to change of r_e' and also to change of numbering of the bands. It appears from this table that the numbering of Chalonge and Vassy, which includes all the bands actually measured by any observers, taken with Herman's rotational figures, gives calculated intensities whose order is in very close agreement with that observed, while the assumption of the existence of two further bands makes the long-wave bands more intense in theory than they actually appear to be, and it is difficult to see why, if the two bands exist, they do not appear clearly. Hence the numbering has been adopted here which makes

Table 10. Herzberg System

Calculated intensities in absorption in cold gas, for various systems of numbering of bands

v' according to:	Herzberg		Chalonge and Vassy		Herman					
λ_0 (A.)	r_e=1·58		r_e=1·44		r_e=1·30		r_e=1·38		r_e=1·40	
	v'	I	v'	I	v'	I	v'	I	v'	I
2795·2					0	64	0	12	0	5
2737·6					1	100	1	39	1	17
2685·0			0	1	2	83	2	69	2	35
2637·7	0	1	1	5	3	42	3	48	3	57
2594·0	1	3	2	12	4	17	4	92	4	71
2554·6	2	7	3	26	5	18	5	91	5	82
2519·1	3	15	4	58	6	9	6	79	6	79
2489·1	4	28	5	74	7	3	7	77	7	73
2463·4	5	50	6	95	8	—	8	100	8	80
2443	6	83	7	99	9	—	9	41	9	63
2429	7	100	8	100	10	—	10	40	10	100
2423			9	89						

the (0,0) band of the system that with $\lambda_0 = 2685$ A. and $B_e' = 1{\cdot}01$, so that $r_e' = 1{\cdot}44 \times 10^{-8}$ cm. The formula for the band-origins is taken as

$$\nu = 36{,}791 + 787{\cdot}2(v' + \tfrac{1}{2}) - 31{\cdot}9(v' + \tfrac{1}{2})^2,$$

and with the band-limit at about 41,280 cm^{-1} this gives $D_e' = 4{,}433$ for use in the Morse potential function. With these assumptions, the intensities in emission at infinitely high temperature have been calculated, and are shown in Table 11.

Table 11. Herzberg System

Calculated intensities in emission at infinite temperature

v' \ v''	0	1	2	3	4	5	6	7	8	9
0	 (2665)	2 (2862)	8 (2928)	24 (3063)	50 (3209)	75 (3368)	100 (3539)	67 (3726)	41 (3931)	19 (4155)
1	1 (2638)	6 (2751)	20 (2872)	39 (3002)	40 (3142)	22 (3294)	1 (3458)	9 (3636)	40 (3831)	61 (4043)
2	2 (2594)	12 (2703)	28 (2820)	29 (2945)	22 (3081)	13 (3225)	9 (3383)	18 (3554)	8 (3739)	 (3941)
3	5 (2555)	21 (2660)	32 (2773)	16 (2895)	2 (3025)	6 (3165)	8 (3316)	2 (3480)	3 (3658)	13 (3851)
4	11 (2519)	30 (2622)	31 (2732)	5 (2849)	3 (2975)	9 (3111)	4 (3256)	1 (3414)	3 (3585)	2 (3771)
5	15 (2489)	34 (2589)	19 (2696)	 (2811)	11 (2933)	9 (3065)				
6	20 (2463)	35 (2562)	9 (2666)	5 (2778)	12 (2898)	3 (3026)				
7	21 (2443)	23 (2540)	1 (2642)	10 (2752)	11 (2870)					
8	22 (2429)	18 (2524)	 (2626)	12 (2734)	3 (2850)					
9	19 (2423)									

(For purposes of comparison with measurements, the wavelengths of the band heads are given.)

Now a number of bands appearing in the night-sky spectrum have been tentatively attributed to the Herzberg system. In particular, Barbier (1947) made a number of exposures in the region 3100 – 4600 A., and estimated the variation of intensity with wavelength, showing this graphically. Many of his peaks correspond to wavelengths appropriate to Herzberg bands, and in most of these cases he considers also that the profile of the band is of the right form for this system. Table 12 shows those of Barbier's bands which can be identified thus, and beside each is given the intensity as calculated here, if this is sufficient to allow the band to be visible. It can be seen that there is good correspondence. Moreover, the bands which, according to calculated intensities, might be expected to appear, can, at least within the range 3100–4100 A., all be identified with one of Barbier's bands. (The calculations have not been carried to longer wavelengths.) This is shown in the Figure, where the heights of the vertical lines represent the intensities of the corresponding bands. Above each band, or close pair of bands, is written one of Barbier's wavelengths. It can be seen that there is an observed band to correspond with each of the calculated bands of appreciable intensity.

In identifying night-sky bands, recourse has been had in some cases (Dufay and Déjardin 1946, Déjardin 1948) to the two further progressions, which are here rejected, and even to others beyond them. The identifications are, however, very doubtful, for the photographs are all taken on very small dispersion, and in the $v'=0$, $v'=1$ progressions as used here there are band origins of wavelengths sufficiently close to those in the two suggested progressions to be distinguished from them only very uncertainly. It seems, then, satisfactory to adopt this system of numbering, at least until further evidence is available, and if this is done the intensities as calculated here give some indication of the bands to be expected in emission.

Table 12.

Bands in Barbier's Plates of Night-sky Spectrum which have Heads of Wavelength appropriate to Herzberg Bands

λ_0	Suggested (v', v'')	Calc. I	Log I (Barbier)	λ_0	Suggested (v', v'')	Calc. I	Log I (Barbier)
3084	(2, 4)	22	0·5	3546*	(0, 6)	100	1·5
3144*	(1, 4)	40	1·0	3552	(2, 7)	18	
3164	(3, 5)	6	0·6	3634*	(1, 7)	9	1·4
3213*	(0, 4)	50	1·1	3653	(5, 8) ?		1·3 ?
3228	(2, 5)	13	0·9	3736*	(0, 7)	67	1·5
3295*	(1, 5)	22	1·2		(2, 8)	8	
3372*	(0, 5)	75	1·4	3832	(1, 8)	40	1·5
3386	(2, 6)	9	1·1	3946*	(0, 8)	41	1·5
3453	(1, 6) ?		1·2		(2, 9)	0	
3483	(3, 7)		1·3	4045	(1, 9)	61	1·7

Bands marked * are those considered by Barbier to have the correct profile for Herzberg bands.

Values in columns 4 and 8 are read from graph published by Barbier, and give an indication of relative intensities.

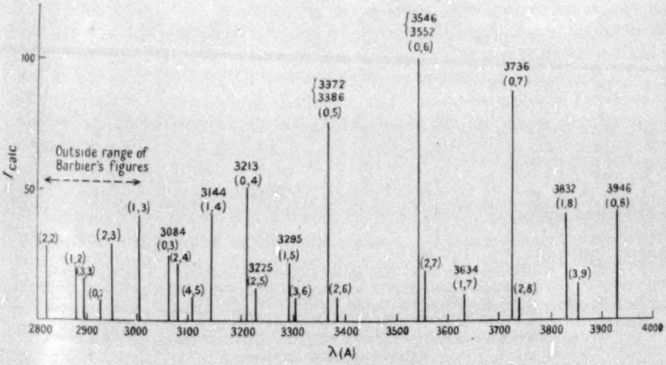

§ 4. THE SECOND NEGATIVE SYSTEM OF O_2^+

The second negative system of O_2^+ consists of a large number of double-headed bands, the uniform interval between the heads being 200 cm^{-1}. These have been observed by Johnson (1924), Ellsworth and Hopfield 1927), Stevens (1931), Mulliken and Stevens (1933), Lal (1948 a, b) and recently by Feast. Mulliken and Stevens measured the lines of some of the bands and obtained the molecular constants for the two electronic states $\mathrm{A}\,^2\Pi_u \rightarrow \mathrm{X}\,^2\Pi_g$, and discussed the dissociation energies, as Gaydon has also done (1947). In plotting the potential curves and wave functions for these calculations, the following values have been adopted for the various constants :

(1) upper state: $\omega_e' = 898{\cdot}9$, $x_e'\omega_e' = 13{\cdot}7$, $D' = 14{,}622\,\mathrm{cm}^{-1}$, $a = 2{\cdot}78 \times 10^8$, $r_e' = 1{\cdot}41 \times 10^{-8}\,\mathrm{cm}^{-1}$;

(2) lower state: $\omega_e'' = 1{,}876{\cdot}4$, $x_e''\omega_e'' = 16{\cdot}53$, $D'' = 53{,}218\,\mathrm{cm}^{-1}$, $a = 2{\cdot}81 \times 10^8$, $r_e'' = 1{\cdot}145 \times 10^{-8}\,\mathrm{cm}^{-1}$.

Working with these in the same way as before, the intensities to be expected in emission have been calculated on the assumption of equal population in all the vibrational levels of the excited state. For the wave numbers of the band origins the component of longer wavelength has in each case been used. The small difference between the components will make no appreciable difference to the calculated intensity of a band.

Table 13. Second Negative System of O_2^+

Calculated and observed intensities

v' \ v''	0	1	2	3	4	5	6	7	8	9	10	11	12	13	14
0				**1**	**2**	**5** 8^J 8^F	**7** 8^J 7^F	**8** 8^J 8^F	**8** 8^J 8^F	**7** 4^J 6^F	**4** 5^F	**2** 3^F	**1** 1^F		
1			**1**	**3** 3^F	**6** 5^J 5^F	**7** 6^J 6^F	**6** 7^J 7^F	**2** 8^J 8^F		**1** 1^J	**4**	**5** 3^F	**4**	**3** 4^F	**1** 2
2		**1** 1^F	**3** 2^F	**6** 6^J 7^F	**8** 8^J 8^F	**6** 8^J 8^F	**2** 8^J 4^F	2^J 2^F	**1**	**2**	**1**		**1**		
3		**2** 1^F	**5** 2^F	**8** 9^J 8^F	**5** 8^J 7^F	**1** 6^F	a^F	**2**	**2** 8^J a^F	**2** a^F		**1**			
4	**1**	**4** 3^F	**7** 6^J 6^F	**6** 7^J 7^F	**2** 8^J 7^F	3^F	**2**	**2**	**1**		**2**	**1**			
5	**1**	**6** 3^J 2^F	**8** 8^J 8^F	**4** 7^J 7^F		**2**	**3**	**1** a^F		**1**	**1** a^F		**1**		
6	**2** a^F	**8** 2^J 2^F	**7** 6^J 6^F	**1** 4^J 4^F	**1**	**3** 4^F	**1** 5^F		**1**	**1**		**1**	**1**		
7	**4** a^F	**10** 3^J 3^F	**6** 6^J 6^F	1^F	**2**	**2** 4^J 3^F	2^F	**2** a^F	**1** 3^F		**1**	**1**			
8	**7** a^F	**11** 1^J 1^F	**3** 1^J 1^F	**1**	**4** 1^F	**1**	**1**	**2** 2^F	3^F	**1**	**1** 2^F		**1**		
9	**9** a^F	**11** a^F	**1**	**1**	**3**		**1**			**1**	4^F		**1**		
10	**17** a^F	**9** a^F		**5**	**2** 4^F	**1**	**2**		**1**	**1**	1^F	**1**			
11	**13** a^F	**6** a^F													
12	**14** a^F	**4**													

Numbers in heavy type show calculated intensities.
J = intensities observed by Johnson.
F = intensities observed by Feast.
a = bands observed by Feast, but no estimate of intensity made.

[All the bands reported by Lal are included among those measured by Feast. Lal does not quote intensities.]

Now Johnson estimated the intensities of the bands he observed, on a scale which made $I = 9$ for his strongest band. Feast has made visual estimates of the intensities of the same bands and of a number of others, expressing them as nearly as possible on the same scale. The calculated intensities have therefore in this case been reduced to a scale which gives the observed values for a few of the strongest bands, so that comparison can readily be made. Table 13 shows the calculated intensities, those observed by Johnson and those observed by Feast.

It can be seen that there is very good agreement between theory and observation over the progressions involving low vibrational levels—that is, over most of the main Franck–Condon parabola. Even here, however, to a slight extent, and more noticeably over the subsidiary parabolae, the observed bands correspond to slightly higher vibrational levels in the excited state than do the calculated maxima, indicating a denser population in the higher vibrational levels than even infinite temperature would give under a thermal distribution. Feast has pointed out, however, that this is a likely result of the production of excited O_2^+ ions from molecules in the ground state of O_2.

A number of bands in the lower left-hand corner of the vibration scheme, with high calculated intensities, have been observed by Mulliken and Stevens, and by Ellsworth and Hopfield. These are in the vacuum region of wavelengths, and the fact that they are reported as being faint does not constitute a serious disagreement with calculation.

Lal's suggestion that some of the observed bands would fit better a narrow Franck–Condon parabola receives no support from the calculated intensity scheme.

§ 5. CONCLUSIONS

This method of calculating intensities appears to involve many approximations, so that it might be thought that the results obtained by it would be unreliable. It has now been tested, however, by comparison with observation on several band systems and over a wide range of vibrational levels, and it seems to be justified by the very good agreement found. The results may therefore fairly be used as a guide in looking for new bands, or in identifying bands suspected of belonging to one of the systems discussed, and this should prove of some use in the investigation of spectra such as that of the night sky, the aurora, and the sun's atmosphere.

ACKNOWLEDGMENTS

The writer's thanks are due to Dr. R. W. B. Pearse for his suggestions, and for help in obtaining material for these calculations and comparisons, to Dr. M. W. Feast for the opportunity of comparing his experimental results with theory while his work was still in progress, to Professor L. Herman for references to work on the Herzberg system, and to Mr. H. V. Stopes-Roe for the use of his plates of the Herzberg system for rotational measurements.

REFERENCES

Barbier, D., 1947, *Ann. Astrophys.*, **10**, 141.
Chalonge, D., and Vassy, E., 1934, *Revue d'Optique*, **13**, 113.
Déjardin, G., 1948, *The Emission Spectra of the Night Sky and Aurorae* (London : The Physical Society).
Dufay, J., and Déjardin, G., 1946, *Ann. Geophys.*, **2**, 249.
Ellsworth, V. M., and Hopfield, J. J., 1927, *Phys. Rev.*, **29**, 79.
Feast, M. W., 1949, *Proc. Phys. Soc.* A, **62**, 114; 1950, *Ibid.*, **63**, 549, 557.

Füchtbauer, C., and **Holm**, E., 1925, *Phys. Z.*, **26**, 345.
Gaydon, A. G., 1947, *Dissociation Energies and Spectra of Diatomic Molecules* (London Chapman and Hall).
Gotz, F. W., 1934, *Arch. Sc. Phys. Nat.*, **16**, 266.
Herman, L., 1939, *Ann. Phys., Paris*, **11**, 548.
Herzberg, G., 1932, *Naturwissenschaften*, **20**, 577.
Johnson, R. C., 1924, *Proc. Roy. Soc.* A, **105**, 583.
Knauss, H. P., and **Ballard**, S. S., 1935, *Phys. Rev.*, **48**, 796.
Lal, L., 1948 a, *Nature, Lond.*, **161**, 477; 1948 b, *Phys. Rev.*, **73**, 255.
Lochte-Holtgreven, W., and **Dieke**, G. H., 1929, *Ann. Phys., Lpz.*, **3**, 937.
Millon, J., and **Herman**, L., 1944, *C. R. Acad. Sci., Paris*, **218**, 154.
Morguleff, N., and **Vassy**, A., 1939, *Ann. d'Astrophys.*, **1**, 427.
Mulliken, R. S., and **Stevens**, D. S., 1933, *Phys. Rev.*, **44**, 721.
Pillow, M. E., 1949, *Proc. Phys. Soc.* A, **62**, 237.
Stevens, D. S., 1931, *Phys. Rev.*, **38**, 1292.
Stopes-Roe, H. V., 1948, *Thesis*, University of London.

Ultra-Violet Bands of K_2

By S. P. SINHA
Science College, Patna, India

Communicated by R. W. B. Pearse; MS. received 24th March 1950

ABSTRACT. Bands of K_2 have been photographed in absorption in the region λ 3924–λ 3420 A. on a Hilger E1 quartz spectrograph. The bands lie in two groups, one between λ 3924 and λ 3686 A. and the other between λ 3640 and λ 3420 A., and appear to belong to two different systems.

The bands in the first group have been analysed. They can be represented by the equation :

$$\nu=26493{\cdot}0+60{\cdot}6u'-0{\cdot}15u'^2-92{\cdot}64u''+0{\cdot}354u''^2,$$

where $u=v+\frac{1}{2}$.

The upper state of this system is considered to dissociate into 4^2S+5^2P atoms of potassium.

No analysis for the bands lying between λ 3640 and λ 3420 A. has been possible.

§ 1. INTRODUCTION

POTASSIUM has several systems of bands in the infra-red, the visible and the ultra-violet regions. Although the study of the infra-red and the visible bands is fairly complete as far as their vibrational structure is concerned, the position with regard to the ultra-violet bands is still far from satisfactory (Sinha 1947, 1948).

The ultra-violet bands of K_2 have been reported in previous work (Chakraborty 1936, Yoshinaga 1937, and Sinha 1945 a, b) to extend to wavelengths as low as λ2900 A. The analysis of these bands provided by the various authors does not appear satisfactory and more work was therefore considered necessary. Consequently the K_2 bands between λ4510 and λ3940 A. were photographed in the first order of a 21-ft. concave grating with a dispersion of 1·28 A/mm. These bands were found to belong to two systems, one lying between λ4510 and λ4220 A. (the blue system) and the other between λ4160 and λ3940 A. (Sinha 1948). In the present investigation the lower wavelength limit has been extended to about λ3680 A.

§ 2. EXPERIMENTAL

The bands have been studied in absorption. The details of the absorption tube used and the method employed for purifying the metal and heating it are essentially the same as previously described (Sinha 1948). An ordinary 6-volt motor headlamp was found to give a satisfactory continuum up to about λ 3400 A. which was fairly strong when the current through the lamp was slightly higher than the rated value. To prevent rapid distillation of the metal to the cooler parts of the tube, nitrogen from a gas cylinder was introduced inside the absorption tube and maintained at suitable pressures. A Hilger E1 quartz spectrograph was used to photograph the bands.

With a column of the hot potassium vapour about 20 cm. long, the bands in the region λ 3900 to λ 3700 A. appeared most satisfactorily at temperatures between 700 and 800° C., when the pressure of nitrogen inside the absorption chamber was about 15 cm.Hg.

§ 3. APPEARANCE OF THE BANDS AND THEIR MEASUREMENTS

The bands appear in two distinct regions: λ 3924 – λ 3686 A. and λ 3640 – λ 3420 A. In general they are weakly developed although in the former region they appear somewhat stronger than in the latter. The bands are all degraded to the red.

Measurements of the band heads in the two regions are given in Tables 1 and 2. Intensities given are visual estimates on a scale of 1–10. The asterisks in Table 2 indicate that these bands were in the region covered by the principal series line at λ 3447 A. which had broadened to cover a region of about 60 A. between λ 3430 and λ 3490 A. under the conditions of the experiment.

Table 1. K_2 Bands: λ 3924 – λ 3686 A.

λ_{air} (A.)	Int.	v', v''	$\nu_{obs} - \nu_{calc}$ (cm^{-1})	λ_{air} (A.)	Int.	v', v''	$\nu_{obs} - \nu_{calc}$ (cm^{-1})
3923·6	1	—	—	3784·4	7	2, 2	2·6
3906·5	3	0, 10	1·2	3776·0	7	3, 2	1·7
3894·0	3	0, 9	−2·1	3771·5	8	2, 1	1·7
3880·8	5	0, 8	−1·1	3767·0	6	—	—
3867·6	5	0, 7	−0·1	3762·8	7	3, 1	3·3
3854·9	5	0, 6	−2·5	3759·1	5	—	—
3841·3	3	0, 5	0·9	3754·7	6	4, 1	1·2
3832·6	5	1, 5	−0·3	3748·8	4	—	—
3828·1	5	0, 4	1·5	3746·6	7	5, 1	−0·3
3819·4	5	1, 4	−0·7	3738·1	7	6, 1	1·6
3813·9	3	—	—	3733·8	7	5, 0	−0·7
3806·2	7	1, 3	1·8	3725·3	6	6, 0	1·6
3801·7	5	—	—	3722·8	5	—	—
3797·6	10	2, 3	1·3	3717·2	6	7, 0	1·5
3793·7	10	1, 2	−2·2	3708·9	4	8, 0	3·5
3789·2	7	3, 3	−0·1	3701·1	?	—	—
				3686·1	?	—	—

§ 4. VIBRATIONAL ANALYSIS AND MOLECULAR CONSTANTS

The bands between λ 3924 and λ 3686 A. have been found to belong to a single system. The assignment of their vibrational quantum numbers is given in Table 1. It has not, however, been possible to propose any satisfactory analysis for the bands in the region λ 3640–λ 3420 A.

Table 3. Deslandres' Scheme for the Second Ultra-Violet System of K_2 Bands

v' \ v''	0	1	2	3	4	5	6	7	8	9	10	Mean diff.
0					26115·2	26025·5	25933·7	25848·5	25760·6	25673·3	25591·1	59·3
1			26352·0	26265·5	26174·7	26084·6						62·2
2		26507·1	26416·8	26325·0								59·5
3		26568·4	26475·6	26384·3								57·3
4		26625·7										57·6
5	26774·8	26683·3										60·9
6	26835·9	26744·0										58·4
7	26894·3											60·2
8	26954·5											
Mean diff.	91·7	91·6	90·2	90·8	89·9	91·8	85·2	87·9	87·3	82·2		

Table 3 gives the $(v'-v'')$ scheme for the bands in the region λ3924–λ3686 A. In conformity with the name proposed for the K_2 bands between λ4160 and λ3940 A. as the first ultra-violet system of K_2 bands (Sinha 1948), the bands between λ3924 and λ3686 A. will be named the second ultra-violet system of K_2 bands.

Table 2. K_2 Bands: λ3640–λ3430 A.

λ_{air} (A.)	Int.	λ_{air} (A.)	Int.	λ_{air} (A.)	Int.
3640·3 ?	2	3568·4	4	3503·3	*
3632·2 ?	1	3560·9	3	3501·1	*
3612·7 ?	2	3557·0 ?	1	3491·0	*
3603·5	2	3552·5	1	3483·6	*
3600·0	2	3545·4	2	3474·6	*
3594·8	3	3537·5	1	3461·8	*
3590·7	5	3529·9 ?	1	3451·6	*
3586·4	5	3520·0	1	3441·5	*
3583·5	4	3511·7 ?	1	3434·3	*
3575·8	4	3505·0 ?	1	3429·9	*

* See text.

The bands measured in the present investigation between λ3924 and λ3686 A. can be represented by the equation

$$\nu = 26493{\cdot}0 + 60{\cdot}6u' - 0{\cdot}15u'^2 - 92{\cdot}64u'' + 0{\cdot}354u''^2 \qquad \ldots\ldots(1)$$

where $u = v + \frac{1}{2}$. The terms in u'' are those from the work of Loomis and Nusbaum (1932). The values of $\nu_{\text{obs}} - \nu_{\text{calc}}$ given in Table 1 indicate that the agreement between the observed values of ν and those calculated from equation (1) is fairly satisfactory.

The constants of the six states of K_2 now known have been summarized in Table 4. The constants ν_e, ω_e, $\omega_e x_e$, $\omega_e y_e$, $\omega_e z_e$ are those in equation (2), and are given in cm⁻¹:

$$\nu = \nu_e + \omega_e u - \omega_e x_e u^2 + \omega_e y_e u^3 - \omega_e z_e u^4. \qquad \ldots\ldots(2)$$

Table 4. Vibrational Constants for the Ground and the Excited States of K_2

States	ν_e	ω_e	$\omega_e x_e$	$\omega_e y_e$	$\omega_e z_e$	D	Dissociation products
$^1\Sigma_g{}^+$	—	92·64	0·354	—	—	4135	$4\,^2S + 4\,^2S$
$^1\Sigma_u{}^+$	11683·6	69·09	0·153	—	—	5510	$4\,^2S + 4\,^2P$
$^1\Pi_u$	15378·0	75·00	0·388	0·00437	0·00018	1780	$4\,^2S + 4\,^2P$
$^1\Sigma_u{}^+$?	22970·0	60·60	0·20	—	—	4560	$4\,^2S + 5\,^2P$
—	26427·7	61·60	0·90	0·0010	0·00030	980	$4\,^2S + 3\,^2D$
$^1\Pi_u$?	26493·0	60·6	0·15 ?	—	—	2365 ?	$4\,^2S + 5\,^2P$?

§ 5. DISSOCIATION PRODUCTS

The energy of the dissociated atom is calculated from $\nu_{\text{atom}} = \nu_{0,0} + D' - D''$, where the terms used have the usual significance. In order, therefore, to calculate ν_{atom} one should be able to obtain a value of D' from equation (1), the value of D'' being already known from previous work to be equal to 4135 cm⁻¹ (Loomis and Nusbaum 1932). D' may be determined by applying Birge and Sponer's extrapolation rule. The value thus obtained is approximately 6000 cm⁻¹. Such a determination may be altogether out of order, first because only a few levels have been observed and consequently the range of extrapolation is too large, and secondly because the values of mean differences given for the excited state in the last column of Table 3 are so irregular that it is not possible to judge from them whether the separation between the excited state vibrational levels actually decreases linearly, even over the short range observed, a condition which is essential for the application of Birge and Sponer's extrapolation rule.

With such a doubtful evaluation of D' an attempt to determine the states of the atoms into which the molecule in the excited state dissociates may not seem justifiable, especially in view of the fact that the atomic states in this region are rather crowded. However, one may try to obtain the probable dissociation products from other considerations.

It has been shown earlier (Sinha 1948) that, of the four systems of bands, the infra-red and the red systems are due to transitions from the ground state to the excited states dissociating into $4\,^2S$ and $4\,^2P$ atoms. The upper state of the blue system dissociates into $4\,^2S$ and $5\,^2P$ atoms and that of the first ultra-violet system ($\lambda 4165$–$\lambda 3940$ A.) into $4\,^2S$ and $3\,^2D$(?) atoms. Theoretical considerations indicate that there should be one more system of bands whose upper state would dissociate into $4\,^2S$ and $5\,^2P$ atoms, another whose upper state would dissociate into $4\,^2S$ and $3\,^2D$ atoms and yet another whose upper state would dissociate into $4\,^2S$ and $5\,^2S$ atoms, in addition to several other systems whose upper states would involve potassium atoms in still higher excited states. We have now to decide which of the above sets of dissociation products would be probable for the system of bands investigated in the present work. Now from the line spectra data for potassium we have $4\,^2S-5\,^2S=21{,}025$ cm^{-1}, $4\,^2S-3\,^2D=21{,}540$ cm^{-1} and $4\,^2S-5\,^2P=24{,}710$ cm^{-1}. In the equation $\nu_{\text{atom}}=\nu_{0,0}+D'-D''$, assuming the value of $\nu_{0,0}$ to be 26,480 cm^{-1} approximately (see equation (1)) and $D''=4135$ cm^{-1} (Loomis and Nusbaum 1932), we can calculate the values of D' necessary in order that the dissociation products may be one of the sets of atoms for which the line spectra data are as quoted above. These values are found to be -1320, -805, or 2365 cm^{-1} for dissociation products $4\,^2S+5\,^2S$, $4\,^2S+3\,^2D$ and $4\,^2S+5\,^2P$ atoms respectively. The first two sets are thus automatically ruled out as D' cannot be negative, and hence the only probable dissociation products are the atoms of potassium in the $4\,^2S$ and $5\,^2P$ state. The corresponding value of D', viz. 2365 cm^{-1}, is low compared with the value obtained from Birge and Sponer's extrapolation rule. However, this is not very unusual, as the extrapolation rule often gives a higher value (Gaydon 1946). A comparison with the values of the heat of dissociation for the $^1\Sigma_u^+$ and $^1\Pi_u$ states of the molecule resulting from the $4\,^2S$ and $4\,^2P$ atoms of potassium, given in Table 4, also indicates that the value 2365 cm^{-1} for D' is not unlikely.

ACKNOWLEDGMENT

The author wishes to express his thanks to the authorities of the Patna Science College for granting facilities for the work.

REFERENCES

Chakraborty, B. K., 1936, *Ind. J. Phys.*, **10,** 155.
Gaydon, A. G., 1946, *Proc. Phys. Soc.*, **58,** 525.
Loomis, F. W., and Nusbaum, R. E., 1932, *Phys. Rev.*, **39,** 89.
Sinha, S. P., 1945 a, *Curr. Sci.*, **14,** 230; 1945 *b*, *Thesis*, University of Patna, India; 1947, *Thesis*, University of London; 1948, *Proc. Phys. Soc.*, **60,** 436.
Yoshinaga, H., 1937, *Proc. Phys.-Math. Soc., Japan*, **19,** 847.

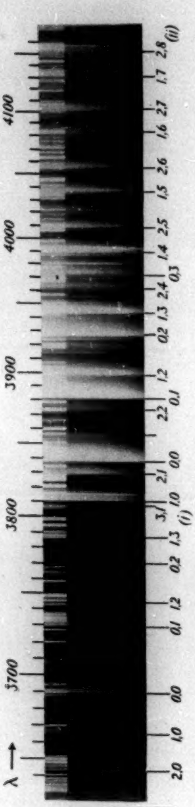

The near ultra-violet band system of GeBr: quartz Littrow spectrogram. Fe arc comparison spectrum.

To face page 957

A New Ultra-Violet Band-System of GeBr

BY E. B. ANDREWS AND R. F. BARROW
Physical Chemistry Laboratory, Oxford University

MS. received 12*th April* 1950

ABSTRACT. The vibrational analysis of a new system of GeBr has been made. The constants derived in cm^{-1} are :

	ν_e	ω_e	$x_e\omega_e$
$^2\Delta$ or $^2\Pi$	27252	$197{\cdot}_3$	$7{\cdot}_{18}$
	27156	$190{\cdot}_1$	$7{\cdot}_{25}$
$^2\Pi_{3/2}$	1150	$295{\cdot}_4$	$0{\cdot}7_2$
$^2\Pi_{1/2}$	0		

The upper state, probably $^2\Delta$ or $^2\Pi$, appears to converge rather rapidly to a limit at about 3·5 ev. above $v''=0$ of $^2\Pi_{1/2}$.

The band-spectrum of GeBr was first studied by Jevons, Bashford and Briscoe (1937). They photographed a system, probably $^2\Sigma-{}^2\Pi$ (ground state), lying in the region 2950-3260 A., and gave a vibrational analysis. By analogy with GeCl, for which two ultra-violet systems are known (Jevons, Bashford and Briscoe 1937, Barrow and Lagerqvist 1949) it was expected that a second system of GeBr should exist at somewhat longer wavelengths than the $^2\Sigma-{}^2\Pi$ system. Spectrograms of this system have now been obtained, and the vibrational analysis is given below.

The spectrum was excited in a stream of $GeBr_4$ vapour by an oscillator dissipating about 400 watts at a wavelength of about 30 metres. This gave a very pure spectrum, consisting of GeBr bands, weak emission at shorter wavelengths from GeO, and Ge and Br lines. It was photographed on a Hilger quartz Littrow spectrograph (E.478) on Ilford Process plates. Exposure times were about 30 minutes. The band-heads were measured against Fe arc lines whose wavelengths were taken from the M.I.T. tables (1939).

A reproduction of a spectrogram is given in the Plate. The system splits obviously into two sub-systems, of which the longer wavelength component appears to be somewhat the more intense. The vibrational analysis is straightforward, and the results are given in Table 1.

Little can be said of the structure of the bands. The 0, 0(i) band certainly possesses two heads, at 27107·9 and 27102·1 cm^{-1}, but the 0, 0(ii) head appears single under the present resolving power. Away from the origins, the vibrational isotope effect becomes marked, and on the long-wavelength side, four heads are often measurable. Comparison with the calculated shifts showed that the heads observed here were due to ^{74}Ge^{81}Br, ^{74}Ge^{79}Br, a blend of ^{72}Ge^{79}Br and ^{70}Ge^{81}Br, and ^{70}Ge^{79}Br, in order of increasing wavelength. The measurements given in Table 1 are considered to relate to ^{74}Ge^{79}Br ($\mu=63{\cdot}38\times10^{-24}$ gm.), which is close to the average GeBr molecule for which $\mu=63{\cdot}16\times10^{-24}$.

Table 1. Band-head Data for Near Ultra-violet System of GeBr

(Figures in parentheses are visual relative intensities)

v'	$v'' \to$ 0		1		2		3		4		5		6		7		8
							Sub-system (ii)										
3			26258·6 (2) *3807·20*														
			150·1														
2			26108·5 (6) *3829·09*	292·9	25815·6 (3) *3872·53*				25234·2 (3) *3961·76*	289·4	24944·8 3 *4007·72*	286·8	24658·0 (3) *4054·34*	287·7	24370·3 (2) *4102·20*	290·$_3$	24080 (1) *4151·6*
			168·$_5$		168·8				169·1		168·5		168·$_0$		164·$_3$		
1	26236·2 (7) *3810·45*	296·$_2$	25940 (2) *3854·0*	293·$_2$	25646·8 (6) *3898·02*	292·2	25354·6 (8) *3942·94*	289·5	25065·1 (3) *3988·48*	288·8	24776·3 (3) *4034·98*	286·$_3$	24490 (2) *4082·1*	284	24206 (0) *4130·1*		
	184·7		181·$_8$		182·7		182·4										
0 ↑ v'	26051·5 (10) *3837·47*	293·3	25758·2 (10) *3881·16*	294·1	25463·1 (8) *3926·15*	291·9	25172·2 (4) *3971·52*										
							Sub-system (i)										
2	27437 (1) *3643·7*	292·$_0$	27145·0 (2) *3682·87*	291·$_0$	26854 (1) *3722·8*												
	159·$_2$		162·$_0$		162·$_1$												
1	27277·8 (4) *3664·94*	294·$_8$	26983 (0) *3705·0*	291·$_1$	26691·9 (3) *3745·40*	287·$_8$	26404·1 (4) *3786·22*										
	175·7		173·$_4$		176·5												
↑ v'	27102·1 (6) *3688·71*	292·5	26809·6 (5) *3728·95*	294·2	26515·4 (4) *3770·33*												

The derived constants are given in Table 2. Those given for the ground state have been obtained by treating mean $\Delta G''$ values from Jevons, Bashford and Briscoe and from the present work. Figures for the $^2\Sigma$ state are included. The $^2\Pi_{3/2} - {}^2\Pi_{1/2}$ separation, from the analysis of the $^2\Sigma - {}^2\Pi$ system, is 1150 cm^{-1} : using this value, the multiplet separation in the new upper level is 96 cm^{-1} as compared with 62 cm^{-1} for what appears to be the corresponding state in GeCl. The figures are compatible with these states being either $^2\Delta$ or $^2\Pi$.

Table 2. Summary of Constants for GeBr

State	ν_e	ω_e	$x_e\omega_e$
$^2\Sigma$	33413	$383\cdot_7$	0·7
? $^2\Delta$, $^2\Pi$	25252	$197\cdot_3$	$7\cdot_{18}$
	25156	$190\cdot_1$	$7\cdot_{25}$
$^2\Pi_{3/2}$	1150	$295\cdot_4$	$0\cdot7_2$
$^2\Pi_{1/2}$	0		

The vibrational levels of the upper state appear to converge rather rapidly : a linear Birge–Sponer extrapolation gives $D_e(\text{i}) = 1250$, $D_e(\text{ii}) = 1360$ cm^{-1}, but it is probable that both estimates are a little high, for the fairly well identified position of the 3, 1 (ii) band suggests that $y'_e\omega'_e$ is not negligible. If we assume $D_e(\text{i}) = 1100$, $D_e(\text{ii}) = 1200$, we get dissociation limits at 28,110 and 28,300 cm^{-1} above $v'' = 0$ of $^2\Pi_{1/2}$. The difference between these values is too small for it to be regarded as certain, but we can be fairly confident that there is at least one dissociation limit at about 28,200 cm^{-1} or 3·5 ev. The energies and products of dissociation in this group of molecules will be considered in a later paper.

REFERENCES

Barrow, R. F., and Lagerqvist, A., 1949, *Ark. Fys.*, **1,** No. 8.

Jevons, W., Bashford, L. A., and Briscoe, H. V. A., 1937, *Proc. Phys. Soc.*, **49,** 532.

Massachusetts Institute of Technology, 1939, *M.I.T. Wavelength Tables* (London: Chapman and Hall).

A Large β-Spectrometer with Two-Directional Focusing for Precise Measurements of Nuclear Radiation

By A. HEDGRAN, K. SIEGBAHN and N. SVARTHOLM
Nobel Institute for Physics, Stockholm, Sweden

Communicated by J. D. Cockcroft; MS. received 14*th December* 1949

ABSTRACT. In the present paper a large double focusing spectrometer is described, which is convenient for precise measurements of β- and γ-radiation. The magnetic field form is discussed and also the arrangement to measure the value of the field continuously with an accuracy appropriate to investigations of this kind. The difficulties due to electron straggling in the β-source or converter are emphasized, and this effect is for the moment the factor which prevents the full utilization of the high resolving power of the apparatus. A number of typical spectra are given to illustrate the applicability of the instrument to different cases.

INTRODUCTION

It has long been recognized that one great disadvantage of the ordinary semicircular focusing principle, formerly extensively used in β-ray spectroscopy, was the inability of focusing electrons in more than one plane, i.e. that perpendicular to the lines of force. For this reason the semicircular method has been almost abandoned in favour of the magnetic lens method, which has the important property of space focusing.

For very precise measurements, however, the ordinary lens method may no longer compete so favourably with the semicircular one, since at higher resolving powers the use of ' central rays ' in the electron-optical image formation becomes of increasing importance. These rays have, as is well known, to be screened off by a central shutter in the lens case, but will always constitute the most valuable part of the beam in the semicircular case. It has been shown in earlier papers by two of us (Svartholm and Siegbahn 1946) that it is possible to combine the advantages of space focusing (high transmission) with that of using central rays (high resolving power). The basic idea was to use an inhomogeneous field of axial symmetry and of such shape that there is axial focusing as strong as the radial focusing. In the present paper we shall give, in § 1, a short review of the characteristic properties of this focusing method including some alternative subsidiary cases with reference to the special demands of the β-spectroscopic technique. The aberration effect is treated in some detail in §2. In §3 the electron-optical arguments of the first section are faced by the specific problems of magnet construction. §4 gives a general description of the apparatus, while §5 deals with the equipment for the magnetic field measurement to which some attention has been paid. A record of some of the adjustments and calibrations made is given in §6. Finally some results some of which have been published in other contexts, are reproduced in §7 in order to show some of the facilities of the instrument.

§ 1. THE ELECTRON-OPTICAL PROPERTIES OF THE TWO-DIRECTIONAL FOCUSING MAGNETIC FIELD

According to the theory of the focusing properties of an inhomogeneous magnetic field of cylindrical symmetry, there is, in every field, an axial focusing action which decreases outwards from the axis of symmetry, and a radial focusing action provided that it does not decrease more rapidly than the reciprocal of the distance from the axis. Consequently there is a two-directional focusing in every field or region of a field, which fulfils both these conditions. Or, more precisely, with a view to the application of this principle in a β-spectrometer, if the magnetic field has a symmetry plane perpendicular to its axis and if the axial component of the field in this plane at the distance r from the axis is denoted by $H(r)$ and its derivative with respect to r by $H'(r)$, then an electron leaving a point on the circle $r=r_0$ in the above-mentioned plane with a velocity v_0 corresponding to a momentum $mv_0=er_0H(r_0)$ and at a small angle to the circle, will first strike the cylindrical surface $r=r_0$ after an angle ϕ_r, the radial focusing angle, and the symmetry plane after an angle ϕ_z, the axial focusing angle. These focusing angles are determined by the equations :

$$\phi_r=\pi\left[1+\frac{r_0H'(r_0)}{H(r_0)}\right]^{-1/2}, \qquad \ldots\ldots(1)$$

$$\phi_z=\pi\left[-\frac{r_0H'(r_0)}{H(r_0)}\right]^{-1/2}, \qquad \ldots\ldots(2)$$

with the obvious relationship

$$\frac{1}{\phi_r{}^2}+\frac{1}{\phi_z{}^2}=\frac{1}{\pi^2}.$$

Generally this focusing system is astigmatic, but putting $\phi_r=\phi_z$, which gives

$$H'(r_0)=-\frac{1}{2r_0}H(r_0), \qquad \ldots\ldots(3)$$

makes the radial and axial focusing equal in strength and gives the focusing system all the characteristic properties of a Gaussian imaging system, the only difference being that the optical axis is a circle with a definite radius. Therefore, an extended object gives an inverted but true image in natural size after the angular distance $\pi\sqrt{2}\simeq 255°$ from the object.

In so far as only central rays are considered the focusing conditions (1) and (2) are identical with the stability conditions in the theory of the betatron by Kerst and Serber (1941), cf. also Kurie, Osoba and Slack (1948). The condition (3) is then equivalent to the requirement of a field varying approximately as $1/\sqrt{r}$. As in our case, however, non-central rays must also be taken into account, we have to define the field shape more closely, for example, by means of a series expansion of the axial field component in the vicinity of the optical axis

$$H(r)=H_0\left[1+\alpha_1\left(\frac{r-r_0}{r_0}\right)+\alpha_2\left(\frac{r-r_0}{r_0}\right)^2+\ldots\right], \qquad \ldots\ldots(4)$$

where the coefficient α_1 according to equation (3) has to be chosen equal to $-\frac{1}{2}$ while the other coefficients, such as α_2, are at our disposal. It was shown by one of the present authors (Svartholm 1946) and independently by McMillan (1946, private communication) and Shull and Dennison (1947) that the coefficient α_2 is the factor determining the aberration properties of the system and, consequently, the resolving power of the spectrometer. Though the requirements of β-spectroscopy must not be identified *a priori* with those of faithful image formation, we may state that the spherical aberration is the most important factor, while other factors, which must be taken into consideration, are the sizes of the radioactive sample and of the slit of the G-M tube, astigmatism of the field, disturbances, and so on.

Furthermore, the accessible resolving power of a β-spectrometer must always be considered in relation to its transmission power, a fact which must be remembered when different types of spectrometers are compared. It is also advisable for full utilization of any apparatus to balance some of the factors contributing to the resolving power, such as the spherical aberration, the size of the sample and the slit width of the G-M tube, in such a way that the transmission power, or more precisely, the counting rate in a definite momentum (or energy) range, will be as high as possible. Now the transmission power is usually defined as the solid angle in which the radiation from the sample is utilized in the apparatus, a definition which is adequate only in so far as the influence of the size of the sample upon the resolving power can be neglected. As this condition is not fulfilled in most applications, especially in investigations of primary β-spectra where the specimen must be made very thin and, therefore, large, it seems preferable to introduce a quantity defined as the solid angle multiplied by the area of the sample, and in accordance with a recent paper by Geoffrion (1949) on optimum conditions in the semicircular β-spectrometer we shall call this quantity the *luminosity* of the apparatus.

The resolving power of a β-spectrometer is defined empirically as the relative half-width of a β-line. The possible contributions to the line width can be referred either to electron-optical imperfections, such as aberrations, or to effects inherent in the sample, such as the straggling effect. In a broad sense the latter effects constitute the natural line width of the sample. Since the latter may be highly different in different investigations it is desirable that the electron-optical line width (or the proper line width of the apparatus) be known for different arrangements of the shutters, slits and so on. This can be done either experimentally (by using samples with a negligible natural line width) or theoretically. There are at least two reasons for making a careful study of this question. On the one hand, knowing the electron-optical line shape promotes greater accuracy in the energy determination of a β-line. On the other hand it is possible on the same basis to determine the natural line shape in order to investigate the influence of straggling and similar effects upon the primary radiation.

As the electron-optical line shape may be very different in different cases it seems to be more practicable in a theoretical discussion to use the total relative line width instead of the former. The total relative line width is determined by the total image width δ (in which the width of the G-M slit may be included in an incorrect sense) and the dispersion. The length of the G-M slit is assumed to be so large that no radiation is lost. The dispersion d is expressed (Svartholm and Siegbahn 1946) by

$$d = 4r_0 \Delta v / v,$$

which is twice as large as the corresponding quantity for a homogeneous field. This means that the total line width expressed for example by $\Delta H/H$ is expressed as

$$\Delta H/H = \delta/4r_0.$$

The proper image width δ is composed of two terms at least, the object or sample width δ_0 and the aberration width δ_{ab}. When the double focusing condition is not exactly fulfilled on the optical axis a third term must be included, namely the astigmatic line width δ_{as}. The aberration width δ_{ab} comes only from the spherical aberration. It is a characteristic property of the apparatus as a dispersive instrument with geometrical focusing that the object width enters the total line width to the first power while the aperture angles appear as the second power.

The aberration width may be expressed (cf. Svartholm 1946) by

$$\delta_{ab} = (p\gamma_1^2 + q\gamma_2^2)r_0, \qquad \ldots\ldots(5)$$

where γ_1 and γ_2 are the radial and axial aperture angle, respectively. The numerical coefficients p and q are both related to the second derivative of the magnetic field according to the formulae

$$p = \tfrac{2}{3}(8\alpha_2 - 1), \qquad \ldots\ldots(6)$$

$$q = \tfrac{2}{3}(3 - 8\alpha_2). \qquad \ldots\ldots(7)$$

In the region $\frac{1}{8} < \alpha_2 < \frac{3}{8}$ both p and q are positive. In the case of a square aperture $\gamma_1 = \gamma_2 = \gamma$; we then obtain from equation (5)

$$\delta_{ab} = (p+q)\gamma^2 r_0 = \tfrac{4}{3}\gamma^2 r_0,$$

which is *independent* of the value of α_2. For this reason it is impossible to diminish the aberration line width by a suitable choice of α_2 when the radial and axial aperture angles are of the same order of magnitude. A considerable reduction of the aberration can be achieved, however, by a radially *or* axially extended aperture choosing α_2 in these cases equal to $\frac{1}{8}$ or $\frac{3}{8}$ respectively. This question will be discussed in more detail later.

The astigmatic line width δ_{as} derives from an incident deviation of the gradient of the field from its prescribed value. According to equation (3) the quantity α_1, defined by

$$\alpha_1 = r_0 H'(r_0)/H(r_0),$$

should have the value $-\frac{1}{2}$. If the relative deviation of α_1 from this value is ϵ, so that $\alpha_1 = -\frac{1}{2}(1+\epsilon)$, then the path of a paraxial ray in the symmetry plane of the field is determined (Svartholm 1949) by

$$r - r_0 = r_0\gamma_1\left(\frac{1+\epsilon}{2}\right)^{-1/2} \sin\phi\left(\frac{1+\epsilon}{2}\right)^{1/2},$$

where ϕ is the angular distance from the object. In the image plane $\phi = \pi\sqrt{2}$ we obtain in the first approximation

$$r - r_0 = -r_0\gamma_1\epsilon\pi/\sqrt{2},$$

which means that the astigmatic line width is

$$\delta_{as} = r_0\gamma_1\epsilon\pi\sqrt{2}$$

and that the intensity distribution within the line is the same as that within a line from an object of the same radial width. As a rule the astigmatism should be negligible, but in all cases where iron is used it is unavoidable that α_1 depends upon H in the region of weak fields. Moreover, if the sample and the G-M slit are situated on a circle of a radius r_1, which differs by Δr from the radius r_0 of the optical axis, then there is an astigmatism of the first order expressed by

$$\epsilon = (3 - 8\alpha_2)\Delta r / 2r_0 ,$$

which vanishes if $\alpha_2 = \frac{3}{8}$. The meaning of this result is simply that there is only one field form, which gives double focusing for every value of r, namely that varying as $1/\sqrt{r}$. In all other cases the double focusing condition is satisfied only for a special value of r (in the general case, however, for *two* different values of r).

While the question of the greatest utilizable aperture angle is intimately connected with the problem of magnet construction, which will be treated in §3, it is useful to study to what extent the resolving power can be increased by means of shutters at the least possible cost of the aperture angle. In the cases $\alpha_2 = \frac{3}{8}$ and $\frac{1}{8}$ where the aberration line width depends upon only one of the angles γ_1 and γ_2, it is evidently possible *and* advisable to diminish only the angle in question. In this way the solid aperture angle is varied linearly, while the line width is varied according to a square law. In our case where $\alpha_2 = \frac{3}{8}$ and the maximum values of γ_1 and γ_2 are equal ($= 0{\cdot}2$ radians), the relation between the relative line width δ and the solid angle Ω is, for radial shutters,

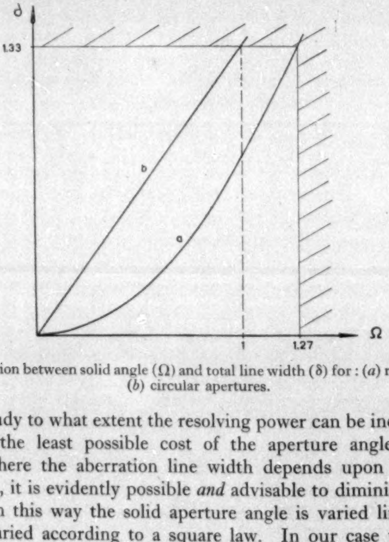

Figure 1. The relation between solid angle (Ω) and total line width (δ) for: (*a*) rectangular apertures, (*b*) circular apertures.

$$\delta = \pi^2\Omega^2 / 3\gamma_2^{\,2}$$

where Ω is expressed in fractions of 4π (Figure 1). According to this formulae the line width is $\frac{4}{3}$ per cent for the solid angle $4/\pi$ per cent, but only $\frac{1}{3}$ per cent for the angle $2/\pi$ per cent. A similar result is obtained in the case $\alpha_2 = \frac{1}{8}$ if axial shutters are used. For other values of α_2 one needs both radial and axial shutters to obtain a solely linear dependence between δ and Ω.

§ 2. THE THEORETICAL LINE SHAPE

The electron-optical line shape, which will be discussed now, is defined as the number of electrons of a definite energy entering the slit of the G-M tube as a function of the magnetic field strength. Among the different contributions to the line shape only one has to be discussed in some detail, namely that due to aberration.

When the line width is caused by more than one factor a composition of these is accomplished mathematically by the well-known 'Faltung' process. If for example a finite object width gives in itself the intensity distribution $I_0(H)$ and if similarly the spherical aberration gives $I_{\mathrm{ab}}(H)$ then the resulting intensity distribution is expressed by

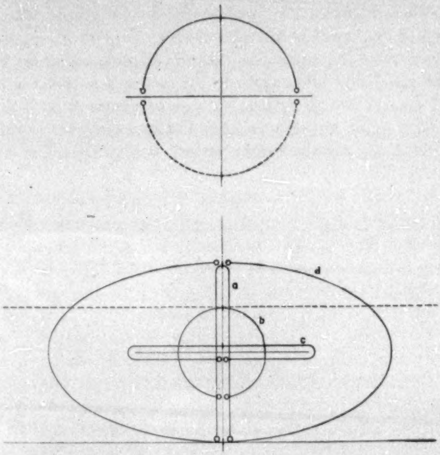

Figure 2. The aberration pattern of a point object and circular aperture in the cases: (*a*) $\alpha_2=3/8$, (*b*) 5/16, (*c*) 1/7, (*d*) 1/8.

$$I(H)=\int I_0(H-H')I_{\mathrm{ab}}(H')dH'.$$

If the number of electrons emitted per unit area of the sample is constant so that

$$I_0(H)=I_0 \qquad \text{for } H_0<H<H_0+\Delta H_0$$

and

$$I_0(H)=0 \text{ elsewhere,}$$

then

$$I(H)=I_0\int_{H_0}^{H_0+\Delta H_0} I_{\mathrm{ab}}(H-H'')dH''.$$

The function $I_{\mathrm{ab}}(H)$ is calculated from the intensity distribution in the image plane of a point object emitting radiation isotropically. Since every primary direction determined by the aperture angles γ_1 and γ_2 is represented by a point of the image in the image plane according to the formulae

$$r - r_0 = -(p\gamma_1^2 + q\gamma_2^2)r_0, \qquad \ldots\ldots(8)$$

$$z = -2q\gamma_1\gamma_2 r_0, \qquad \ldots\ldots(9)$$

it is possible to calculate the shape of the aberration pattern as a function of the aperture shape. The representation is visualized schematically in Figure 2 for four different values of the coefficient α_2. The marginal rays of a circular aperture γ are indicated by two semicircles in the upper part of the Figure, one corresponding to rays inside, the other to rays outside the cylinder $r = r_0$. In the general case both semicircles are represented by an ellipse with its centre in the point $r = r_0 - \frac{2}{3}\gamma^2 r_0$, $z = 0$ and the semi-axes $a = \frac{1}{2}|p - q|\gamma^2 r_0$ and $b = |q|\gamma^2 r_0$. The ellipse degenerates (cf. equations (6) and (7)) into a straight line in the two cases $\alpha_2 = \frac{3}{8}$ and $\alpha_2 = \frac{1}{4}$ and into a circle in the case $\alpha_2 = 5/16$. For all values of α_2 in the region $\frac{1}{8} < \alpha_2 < \frac{3}{8}$ the aberration pattern corresponding to the full circular aperture is limited by an arc of an ellipse and two tangents through the centre $r = r_0$, $z = 0$. For $\alpha_2 = \frac{3}{8}$ the aberration pattern is a straight line of length $\frac{4}{3}\gamma_1^2 r_0$ for any aperture shape with a maximum radial aperture angle γ_1. For $\alpha_2 = \frac{1}{8}$ the aberration pattern for a circular aperture is the ellipse itself while a rectangular aperture gives a pattern limited by an arc of the parabola $r - r_0 = -3z^2/16\gamma_1^2 r_0$ and the straight line $r - r_0 = -4\gamma_2^2 r_0/3$. The pattern is plotted for four different values of γ_1 and γ_2 in Figure 3. For a square aperture $\gamma_1 = \gamma_2 = \gamma$ the largest extent of the image in the axial direction is $16\gamma^2 r_0/3$, which is twice that for a circular aperture with the angular radius γ and four times the radial extent of the image. For reasonable values of r_0 and for example $r_0 = 50$ cm., $\gamma = 0{\cdot}2$, this figure is as large as 11cm. ; this is the stronger argument against the case $\alpha_2 = \frac{1}{8}$ since the axial extent is a function of both angles γ_1 and γ_2.

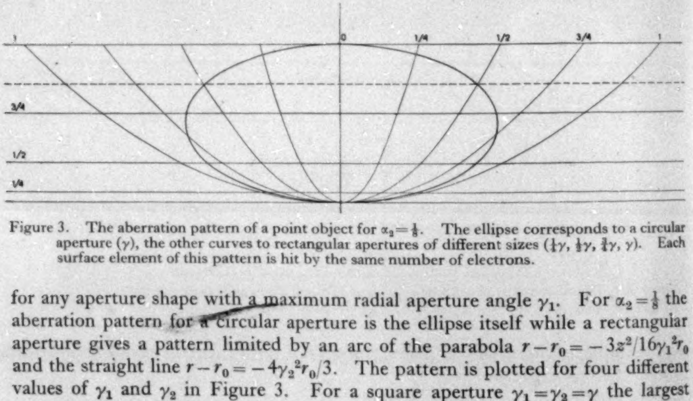

Figure 3. The aberration pattern of a point object for $\alpha_2 = \frac{1}{8}$. The ellipse corresponds to a circular aperture (γ), the other curves to rectangular apertures of different sizes ($\frac{1}{4}\gamma$, $\frac{1}{2}\gamma$, $\frac{3}{4}\gamma$, γ). Each surface element of this pattern is hit by the same number of electrons.

Now we calculate from equations (8) and (9) a relation between the small solid angle $d\gamma_1 d\gamma_2$ and a surface element $drdz$ of the image

$$d\gamma_1 d\gamma_2 = \frac{1}{4r_0}[q^2(r - r_0)^2 - pqz^2]^{-1/2}\, drdz\,. \qquad \ldots\ldots(10)$$

As the number of electrons emitted within the angle $d\gamma_1 d\gamma_2$ is proportional to this angle the right-hand side of equation (10) gives the intensity distribution of the image. By integrating the expression (10) with respect to z between the margins of the pattern we obtain the number of electrons hitting a narrow slit of radial extent dr. This number, being a function of r, represents the intensity distribution of a β-line measured by means of a G-M tube the slit of which is infinitely narrow in the radial direction but sufficiently long in the axial direction. The result of the integration will be reproduced only in some especially important cases. Thus in the case $\alpha_2 = \frac{3}{8}$ the intensity distribution, when a rectangular aperture is used, is proportional to $(r_0 - r)^{-1/2}$ within the range $r_0 > r > r_0 - 4\gamma_1^2 r_0/3$ and zero elsewhere, while in the case $\alpha_2 = \frac{1}{8}$ the distribution has the same shape within the range $r_0 > r > r_0 - 4\gamma_2^2 r_0/3$. If a circular aperture of the radius γ is used, the distribution is

$$\left[\frac{1}{r_0 - r} - \frac{3}{4\gamma^2 r_0}\right]^{1/2}$$

within the range $r_0 > r > r_0 - 4\gamma^2 r_0/3$ and zero elsewhere. It is noteworthy that the distribution function for rectangular shutters is the same in the cases $\alpha_2 = \frac{3}{8}$ and $\frac{1}{8}$ as for the semicircular focusing system. Consequently the well-known theory of the composition of object width and aberration width can be transferred in full detail.

§3. PRINCIPLES OF MAGNET CONSTRUCTION

It is no doubt possible to realize a magnetic field possessing the required properties of inhomogeneity in a number of ways. Some general points can be stated, however, if one tries to reconcile the electron-optical demands defined in the preceding sections with the practical possibilities of magnet construction. As the dispersion is a linear function of the mean radius r_0 it is desirable to choose the latter as large as possible. Now, measuring β-ray energies of 5·5 MeV. requires a value of $H\rho$ equal to 20,000 gauss cm. Putting $r_0 = 50$ cm. this gives $H_0 = 400$ gauss, which is a reasonable value for a magnet having a large pole gap. For a value of $H\rho$ 40 times smaller, corresponding to a β-energy of about 20 kev., the magnetic field strength is only 10 gauss. This is a just tolerable lower limit partly because of the remanence effect of the iron and partly because of the influence of the earth's magnetism. Consequently a universally serviceable β-spectrometer should not have a mean radius greater than 50 cm., at least if iron is used. After having fixed the radius our next task is concerned with the dimensions of the pole gap. In our first small apparatus, which was used solely for demonstration of the double focusing principle, the magnetic field was realized by means of a ring magnet with a central cylindrical yoke surrounded by the coil. Though it is possible by using other designs for the yoke to utilize the space taken up by the coil for the effective pole gap, the ring magnet type was found to have some important advantages, especially the easy accessibility of the pole gap. As this arrangement prevents the use of a considerably large width of the pole gap, and consequently a large radial aperture angle γ_1, we preferred the case $\alpha_2 = \frac{3}{8}$ instead of $\alpha_2 = \frac{1}{8}$. In that case the largest line width is determined only by γ_1, and equal to 4/3% for $\gamma_1 = 0{\cdot}2$, which corresponds to an effective width of the pole gap $2a = 28$ cm., which is computed from the formula $a = r_0\gamma_1\sqrt{2}$. The choice of the height of the pole gap $2b$, connected with the axial aperture angle γ_2 by means of the relation $b = r_0\gamma_2\sqrt{2}$ is then mainly a question of power consumption. In other words, the solid aperture angle and the transmission power can be increased, the resolving power being fixed, by an increase of power. For larger pole distances, however, the fringing fields become more troublesome and require the use of an impracticably large amount of iron. For this reason we took $\gamma_2 = 0{\cdot}2$, which corresponds to a mean distance between the pole faces equal to 28 cm. so that the pole gap profile is approximately a square. It should be admitted that resolution twice as good as ours can be obtained with a pole gap of the same size by choosing $\alpha_2 = \frac{1}{4}$ and using circular shutters, but in that case we lose the possibility of improving the resolving power according to a square law by diminishing the radial aperture, as was expounded in § 1. This possibility was considered advantageous for precise energy measurements.

§ 4. GENERAL DESIGN

The large spectrometer to be described in this paper has, compared with the first model, about ten times greater solid angle, this being about or somewhat more than 1% of 4π. Furthermore the mean radius of curvature has been increased to 50 cm. We believe that a further increase in radius and dimensions would be impracticable since the amount of iron which has to be put into such an apparatus rapidly limits these possibilities.

Generally the resolution of a spectrometer is given by a sum of two terms, one depending on the solid angle used and the other on the sizes of the sample and the G-M slit compared with the radius of curvature. Thus by making the spectrometer large the important advantage is obtained that more extended sources can be used at a given resolution. When working at very good resolution ($\lesssim 1\%$), for which the new spectrometer is intended, this condition must be regarded as rather essential since in a great number of cases the maximum obtainable resolution is limited by the *thickness* of the radioactive sample itself due to straggling. This is especially obvious when investigations of secondary photo electrons expelled from a lead converter are made. The number of photo electrons increases when the amount of lead is increased. On the other hand the photo lines soon get broader than approximately 1% when the thickness of the converter exceeds a few mg/cm^2 of lead. It is therefore important to spread out the lead on a large, thin surface (by evaporation) which in turn requires a big spectrometer if the geometrical resolution due to the large surface is not to be decreased too much. Furthermore, when the dimensions of the spectrometer are increased, the G-M counter can be more effectively shielded from stray radiation and γ-radiation from the source.

The Magnet

If the iron permeability is put equal to infinity the surfaces of the pole shoes are equipotentials. In this first approximation the airgap is very nearly a parabola $Z = C\sqrt{r}$, i.e. with the vertex at the centre of the magnet. One has to take into account the effects of finite iron permeability and also the outer and inner fringing fluxes. The magnitudes of these corrections are largely dependent on the type of magnet chosen. As was mentioned in the preceding section we preferred an alternative shown in the lower part of Figure 4, where the airgap surrounds the coil as well as the iron yoke.* Another alternative shown in the upper part of Figure 4 proposed to us by Dr. L. Dreyfus at ASEA has the advantage that the fringing fluxes are more easy to handle. This alternative requires, however, more copper and power, but seems to have definite advantages, for example in the case of smaller magnets.

---

* We are indebted to Dr. Dreyfus for the design of the magnet.

If $H\rho = 20{,}000$ is put as an upper limit for any β-spectrum to be investigated, it is immediately realized that the magnetic fields employed at $\rho = 50$ cm. are rather small (less than 400 gauss, usually of the order of 50–100 gauss or still smaller). The problems of remanence and of changing permeability at the lower part of the magnetization curve have also to be considered. It is therefore impossible to base $H\rho$ determinations on any approximate linear relationship between current and magnetic field since the departure from this linearity is far too great, at least in the lower energy region. It is therefore necessary to be able to measure the magnetic field directly and for convenience this can be done continuously in the present apparatus. The system adopted for this purpose will be described later on in this paper.

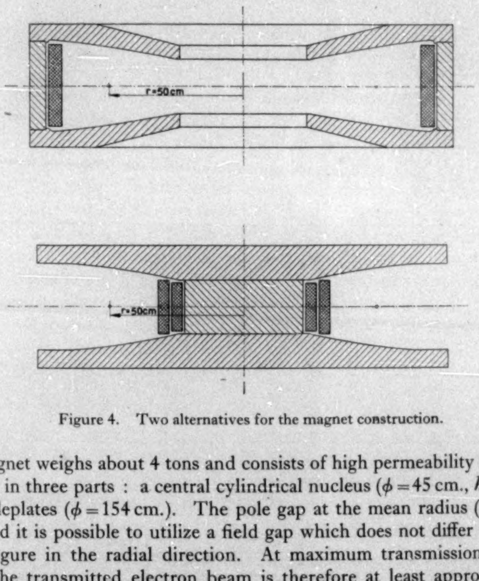

Figure 4. Two alternatives for the magnet construction.

The magnet weighs about 4 tons and consists of high permeability iron. It is constructed in three parts : a central cylindrical nucleus ($\phi = 45$ cm., $h = 20$cm.), and two poleplates ($\phi = 154$ cm.). The pole gap at the mean radius ($\rho = 50$ cm.) is 28 cm. and it is possible to utilize a field gap which does not differ very much from this figure in the radial direction. At maximum transmission the cross section of the transmitted electron beam is therefore at least approximately a square. Since the type of field chosen in this apparatus has the property of focusing electrons in the axial direction to a higher order of approximation than in the radial direction, the cross section of the transmitted beam at better resolution is made rectangular by keeping the height constant and decreasing the radial aperture. Thus, at good resolution a departure from the required exact field form in the outer parts of the field is comparatively unimportant. The magnet is excited by four coils in series having a total resistance of 16 Ω. The number of turns is 2,000 and the copper wire has a cross section of 2 × 4 mm.

As the shape of the pole shoes was computed for a maximum field of 400 gauss the field form must be expected to deviate from the computed one at very much lower fields, but this deviation can to a great extent be compensated for by a suitable premagnetization. A deviation in the field gradient from the correct one at lower fields causes only a very small shift of the top of the lines, but the intensities can be affected more seriously. If good intensity measurements are to be performed, especially at low energies, the behaviour of the field gradient must be carefully controlled.

The measured magnetic field distribution is shown in Figure 5. These measurements were performed with a fluxmeter and search coil at fields 400, 128 and 36 gauss. The fields corresponding to $\alpha_2 = \frac{1}{8}$ and $\frac{3}{8}$ are drawn in the Figure for comparison. The two field distributions at 400, 128 and 36 gauss are, as can be seen almost identical and come very close to the $\frac{3}{8}$ case, especially for $r < 60$ cm. where the deviation is generally less than 0·2%, considered a reasonable tolerance.

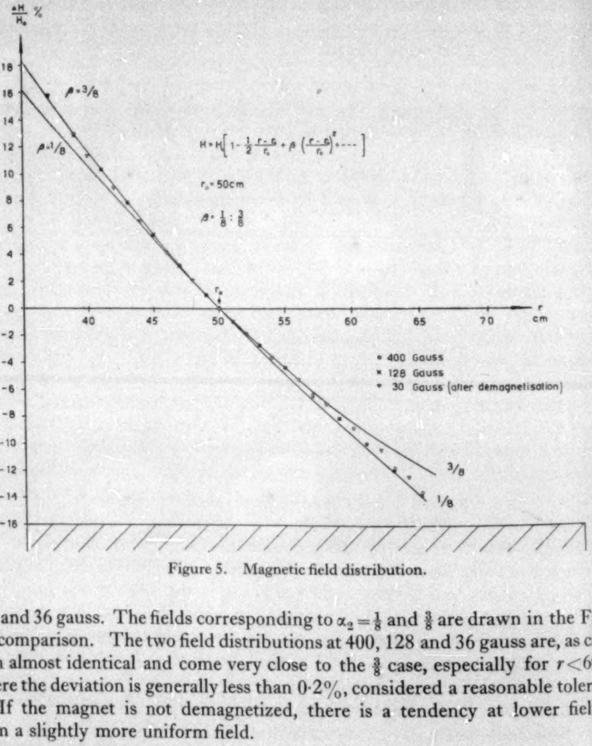

Figure 5. Magnetic field distribution.

If the magnet is not demagnetized, there is a tendency at lower fields to form a slightly more uniform field.

Design of the Spectrometer

The interior of the spectrometer can be seen in Figure 6 (Plate). Two 15 mm. thick brass cylinders form the outer and inner walls of the vacuum tank. The pole shoes of the magnet constitute the roof and bottom of it and are pressed against rubber gaskets (cross section 4 mm. × 6 mm.) running in grooves along the edges of the brass cylinders.

The sample holder can be seen to the right in the figure. The sample is introduced into the vacuum chamber by means of a vacuum lock device.

There are three shutters. The first of these is permanently set for a little more than the intended maximum transmission of the spectrometer. The other two shutters are adjustable from outside by means of Wilson sealing arrangements and the position of their two vertical defining slits can be read on a millimetre scale. Since the focusing in the axial direction, as mentioned before, is attained to a higher approximation than in the radial direction, the upwards and downwards defining slits for our field can be set for maximum transmission in that direction (defined by the pole distance), and need not be adjusted when better resolving power is wanted (at least to a certain limit).

The G-M counter (of bell type) is mounted on an adjustable brass holder and different sized G-M slits can be moved in front of the counter (width = 3, 6, 12, 24 mm.).

Large lead blocks (not shown in the figure) are placed between the source and the G-M counter, and because of the large distance between these units even very strong sources can be used without increasing the background (about 20 impulses/minute) of the counter to any noticeable amount.

The vacuum chamber (approximately 300 litres) is evacuated by means of a big molecular disc pump (200 l/sec.) combined with a Cenco rough vacuum pump, and the pressure ($\sim 15 \times 10^{-5}$ mm.) can be controlled by an ordinary ionization vacuum gauge, stabilized for constant emission. The lock device for the sample can be separately connected to the rough pump, so that the high vacuum is not destroyed when the sample is introduced into the spectrometer.

The magnetic field measuring equipment, which will be described below, contains a rotating coil system on a long rod. This rod enters the spectrometer through a brass tube, closed at the inner end and screwed on to the spectrometer wall. (It is rendered vacuum-tight by means of rubber gaskets.) This tube can be seen in the front of Figure 6.

Figure 7 (Plate) shows a photograph of the total apparatus.

§ 5. MAGNETIC FIELD-MEASURING EQUIPMENT

The large dimensions of the spectrometer with the correspondingly great dispersion make the instrument well suited for precise energy measurements of β-lines and photo electron lines. The resolution or relative half-width of the lines is in most cases limited to about 1% or a little less. This limit is not set because of the focusing properties of the instrument itself, but is due to β-source thickness and converter thickness in practical cases. Though it doubtlessly may be possible in many cases to decrease the ‘ natural ’ line widths caused by straggling in the source and converter respectively, the experience hitherto gained clearly demonstrates that a number of difficulties arise in connection with a full utilization of still smaller line widths. Some of these will be discussed later.

If the relative line width (measured at half maximum height of the line) is 1% it ought to be possible to locate the position of the line within about 0·1%. This means that the magnetic field has to be measured with the same accuracy. Furthermore the field has to be measured for each setting and controlled continuously. This, of course, necessitates that the measuring system should be easy to handle. Ordinary ballistic methods are therefore unsuitable. Various of other methods already in existence which allow continuous readings are either definitely not accurate enough or else too uncertain to be relied upon for longer and repeated runs. We have finally adopted a balance system (null method) making use of a reference field produced in a Helmholtz coil, placed at a distance from the spectrometer.

Two coils, one in the spectrometer and the other in the reference field, rotate on the same axis. The magnetic field in the spectrometer is adjusted until the E.M.F. induced in the rotating coil in the spectrometer is equal to that induced in the corresponding coil in the Helmholtz field. By carefully adjusting the rotating coils relative to the two fields once and for all the phases of the E.M.F. induced in the two coils can be made very nearly opposite. When the spectrometer field is changed until minimum alternating current flows in the rotating system, the current through the Helmholtz coil is a measure of the magnetic field in the spectrometer. The calibration of the arrangement is most conveniently made by means of a strong β-line of known energy (e.g. ThB F line etc.).

The actual arrangement is shown schematically in Figure 8. The two rotating coils (A and B) are situated on a stainless steel rod 2 metres long which has been accurately straightened. A third coil (C_1) on the steel rod rotates around its own axis and is connected to an amplifier and a microammeter. The coils A and B ($\phi = 30$ mm.) contain each 1,000 turns 0·2 mm. copper wire, the coils C_1 ($\phi = 44$ mm.) 2,000 turns 0·2 mm., and C_2 ($\phi = 55$ mm.) 4,000 turns 0·1 mm. respectively. The rod rotates at a speed of about 30 revolutions per second and is driven by means of a motor. The arrangement does not require a particularly constant speed of rotation.

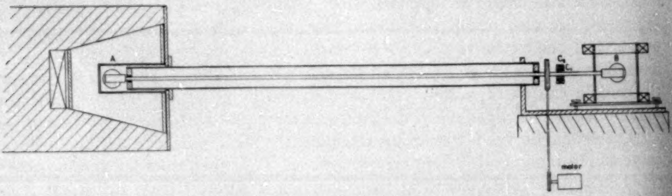

Figure 8. Arrangement for measuring the magnetic field.

In order to obtain sharp minima for the field determinations the rotating system has to be very carefully balanced mechanically so that no extra vibrations etc. occur. The rotating coils should be adjusted to rotate around a diameter. The sharpness of the minimum is also critically dependent on the adjustment of the relative phases of the two induced E.M.F's. The final adjustments in this respect are perfected by means of screws supporting the Helmholtz coils on the rigid foundation.

Figure 9 shows the amplified current through the pick-up coil system on the microammeter, viz. current through the Helmholtz coil, the spectrometer field being kept constant (25 gauss). According to this curve the position of the minimum can be defined with an accuracy within about ±0·1%.

ROC. PHYS. SOC. VOL. 63, PT. 9—A (A. HEDGRAN, K. SIEGBAHN AND N. SVARTHOLM)

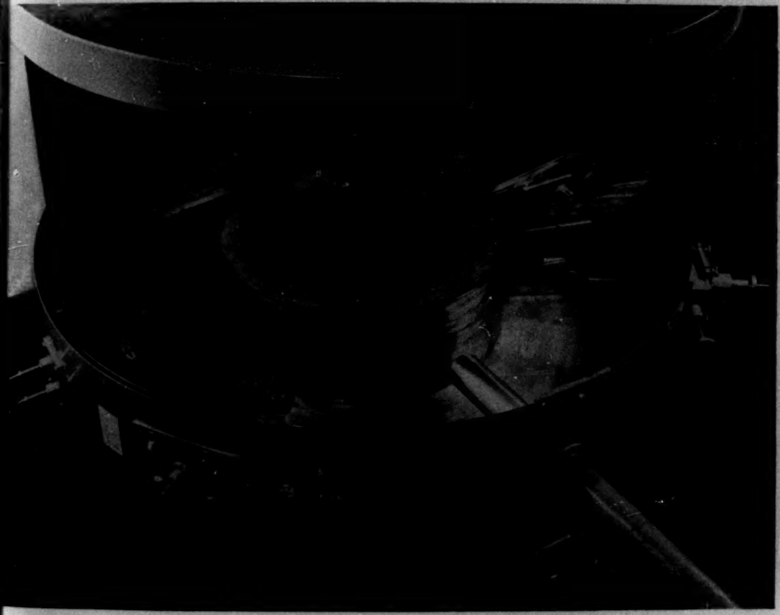

Figure 6. The interior of the spectrometer.

To face page 972

PROC. PHYS. SOC. VOL. 63, PT. 9—A (A. HEDGRAN, K. SIEGBAHN AND N. SVARTHOLM)

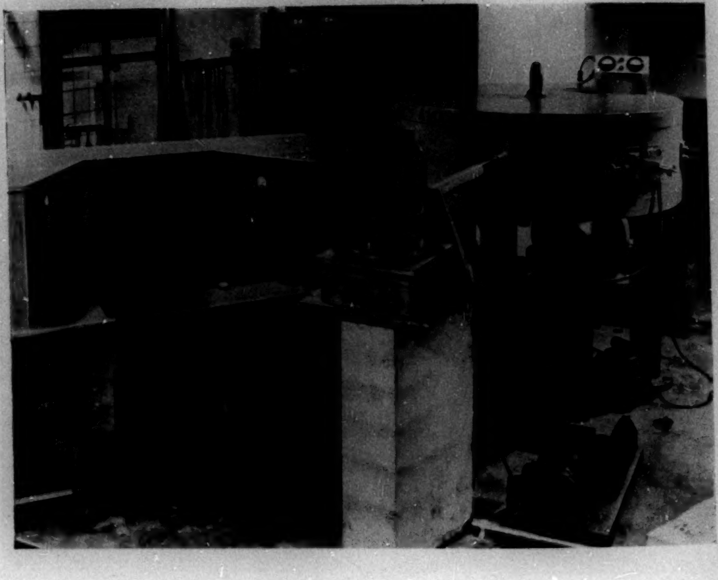

Figure 7. Photograph of the spectrometer.

Most of the experiments so far made with the spectrometer have been performed with the system described above. It should be mentioned here, however, that recently this system has been rebuilt. The mechanical stability is increased and the definition of the minimum is now around 0·01%. The description of this improved system will soon be published, when more experience has been gained with it.

The rotating rod is situated in the north–south direction and the earth's magnetic field then contributes by its vertical component (H_{vert}) to the E.M.F. produced by the field in the Helmholtz coil. The magnitude of this component has been measured and must be considered when evaluating the $H\rho$ values for different values of I through the Helmholtz coil. The relation ($H\rho$, I) (amps through Helmholtz coil) is then expressed by

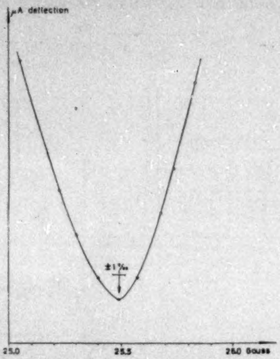

Figure 9. The minimum of the induced E.M.F. in the rotating system, showing the value of the magnetic field.

$$H\rho \text{ (gauss cm.)} = \text{constant} \times I + \rho H_{\text{vert}}$$

($\sim 50 \times 0{\cdot}4$). The last term is, however, always very small compared with the first one.

It is important that the coil rotating in the spectrometer is actually placed at the same distance from the centre of the magnet as the sample and detector (optical axis of the spectrometer). Small changes in the magnetic gradient which, as stated above, by themselves cause no noticeable shifts of the line peak, will of course introduce errors in the relative field determinations if the coil is not placed on the mean radius used ($\rho = 50$ cm.).

Since the electric power required to focus even high energy β-particles with the spectrometer is quite low (for instance 2 MeV. corresponds to about 200 watts) one can very conveniently use batteries as current supply. Thus no extra current-stabilizing system is needed.

The current and magnetic field regulating system is shown schematically in Figure 10. The principle of the arrangement is the following. A certain current through the Helmholtz coil is first chosen (regulated by means of the resistance R_1)

corresponding to the desired field in the spectrometer. This current branches into two, one branch exciting the magnet. The Helmholtz coil is so designed that it will produce a field equivalent to half that in the spectrometer at the same current. By means of the small resistance R_2 the ratio between the two currents in the bridge can be varied, until the magnetic field in the spectrometer just balances the Helmholtz field (as indicated by the rotating system). This adjustment will not affect the total current through the Helmholtz coil in the first approximation, provided the resistances of the two branches are approximately equal, and R_2 is small compared with R_3. These conditions are always satisfied in our case for high fields. At low fields, when the deviation from linear relationship between current and magnetic field is relatively greater, the bridge has to be side-balanced more than the small resistance R_2 would allow. This is accomplished by the multipole switch system, shown in the Figure. By means of this the current through the spectrometer can be changed in bigger jumps simultaneously with the introduction of new resistances into the main line, so that the total current is kept constant. When this switch is far from its zero position the first of the above conditions is violated. However, as mentioned before, this only happens for low fields, where the resistance R_1 is very high compared with the resistance in the bridge. In that case the final balancing adjustments by the resistance R_2 will not affect the main current either. The practical experience gained with the system here described has shown that one never needs to readjust the main current (giving the desired field) after balancing the bridge, which simplifies the field setting very much. It should also be remarked that within smaller field intervals, such as that occupied by a single line etc., the balancing does not need to be changed.

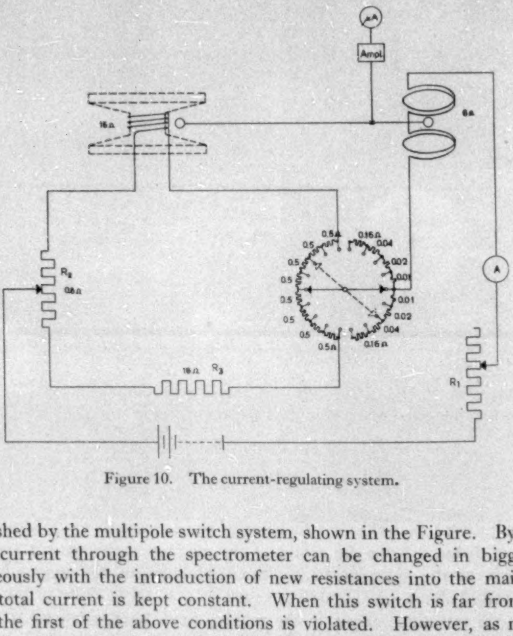

Figure 10. The current-regulating system.

§6. ADJUSTMENTS AND CALIBRATION OF THE SPECTROMETER

After the magnetic gradient has been measured and a convenient mean radius (radius of the optical axis) chosen, the positions of the sample and detector must be experimentally adjusted relative to each other. This is most easily accomplished by means of the photographic method. The exposure of a strong β-line (the source being deposited on an aluminium cross) will immediately tell if the image falls on the correct height relative to the G-M slit. Simultaneously the axial focusing properties are especially well demonstrated on such plates.

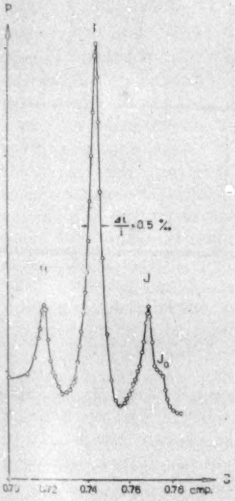

Figure 11. The H, I, J and J_a-lines of ThB. Width of sample = 5 mm. Shutter widths = 10·5cm. G-M slit = 6 mm.

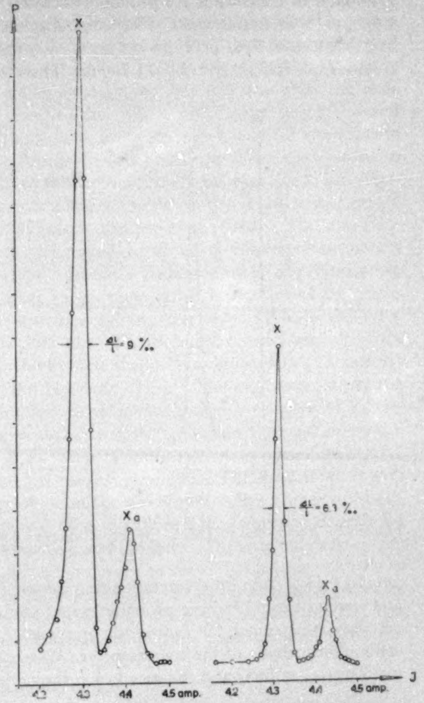

Figure 12. The X and X_a-lines of ThC″ (E_γ = 2·62 MeV.) Width of sample = 3 mm., shutter width, left 10·5 cm, right 6·5 cm. G-M slit, left 12 mm., right 6 mm.

The choice of shutters and width of the G-M slit has to be investigated for different widths of the samples and the resulting resolving powers, as obtained from the half-widths of lines, registered. These investigations must be performed by means of weightless samples such as ThB + products since otherwise the line widths may be strongly dependent on the weight of samples used, energy of β-lines etc., due to straggling in the source itself. Figures 11, 12 and 13 show a number of β-lines obtained by the spectrometer with different shutters, G-M slit width and sample width. The height of the sample and G-M slit was kept constant (20 mm.). Decreasing the line width below 0·35% was not tried since the field measuring equipment used in these experiments limited such possibilities.

The spectrometer was calibrated using seven different β-lines in the spectrum of ThB + products, namely (according to Ellis' notation) : F, H, I, J, Ja, X, Xa lines. These lines cover an energy range from 150 kev. to 2·6 Mev. The relative $H\rho$ values of these lines are probably accurate within about 0·1% according to Ellis' (1934) measurements. The latest absolute determination (Siegbahn 1944) of $H\rho$ values in this spectrum concerns only the F and I lines and provides the values $H\rho_F = 1{,}383{\cdot}8$ and $H\rho_I = 1{,}749{\cdot}6$. These values (based on x-ray data) differ only by 0·15% from Ellis' corresponding values ($H\rho_F = 1{,}385{\cdot}8$ and $H\rho_I = 1{,}751{\cdot}0$) and were estimated to have probable errors around 0·03%. This β-spectrum is certainly well suited for calibration purposes. The constant before I in the calibration formula of the spectrometer ($H\rho = \text{constant} \times I + 20$) was determined for these seven lines and the results are shown in Table 1.

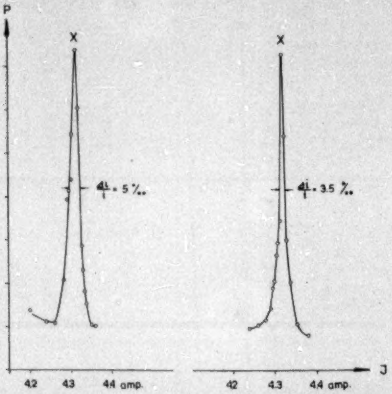

Figure 13. The X-line of ThC″. Width of sample = 3 mm., G-M slit = 3 mm., shutter width, left 10·5 cm., right 6·5 cm.

Table 1. Calibration : $H\rho = \text{constant} \times I + 20$

Line	I (amp. at peak)	Constant	Line	I (amp. at peak)	Constant
F	0·590(0)	2313	J_a	0·774(0)	2323
H	0·719(0)	2320	X	4·31(0)	2312
I	0·745(5)	2315	X_a	4·42(0)	2317
J	0·769(5)	2319		Mean :	2317

The maximum deviation in any line measurement from the mean value is about 0·2%. Furthermore there is no sign of any systematic change in the value of the constant as a function of the β-energy. The maximum deviation of 0·2% must be expected since the ammeter used in these experiments (Western Electric Instr. Corp. Model 5, No. 1695) to measure the current through the Helmholtz coil has a precision of within ±0·1% (calibrated recently at our Institute) and the field balancing system was able to give the same accuracy. With the new balancing system and a compensation arrangement to measure the current there are good possibilities of increasing the precision still more in the future.

On this point it should be stressed, however, that in ordinary cases, i.e. when the weight of the sample is not negligible, there are great difficulties which prevent full use being made of much better accuracy than that already obtained (within 0·1 – 0·2%). The electron straggling in the sample which is energy dependent will not only cause a line broadening, but will also shift the lines towards lower energies. To handle this effect and make accurate, well established corrections for it is an intricate problem, which calls for a systematic experimental investigation in the future, in order to bring down the systematic errors in β-energy determinations to the region of 0·1% or less. Such investigations are in progress in this laboratory and valuable contributions have recently been supplied by Jensen *et al.* (1949) and Lauritsen *et al.* (1949). The straggling effect is perhaps most obviously recognized when using converters to obtain external photo lines from the γ-rays. In these cases one must of necessity use radiators of finite thickness in order to get measurable intensities of the photo lines. It is found that line shifts due to straggling may very well be of the order of 1% even if the radiator is less than 10μ. Furthermore the relative line shifts are not only dependent on the γ-energy, but also on the actual choice of spectrometer resolution etc. (Lauritsen and Hornyak 1949). The most straightforward procedure to investigate this problem is to measure first a number of β-lines from ThB + products (weightless sample) and then measure the position of the corresponding external photo lines from a converter in a given geometry. Another valuable method, which has been suggested by DuMond *et al.* (1948) would be to determine the energy of a number of different γ-rays from wavelength measurements by X-ray methods and then to calibrate the converter directly by observing the position of the corresponding photo lines. Hitherto only a few γ-ray wavelengths are known with sufficient accuracy to serve this purpose and there are some difficulties in measuring hard γ-rays (i.e. >1 MeV.) accurately with this method. The half-widths hitherto obtained by DuMond are around 1%, but the wavelengths are estimated to be considerably more precisely known (for the annihilation radiation to approximately 1 part in 10^4).

Before these questions are completely mastered the uncertainty in the energy determinations from photo lines or from β-lines of non-weightless samples generally have to be given with larger errors than those set by the half-widths of the lines and the field measuring system themselves.

In those cases where the energy of the photo line comes very close to the energy of the photo lines of the annihilation radiation the energy dependence of the line shift may be disregarded and a direct comparison can be made between the unknown γ-line and the energy of annihilation radiation. If the same converter is used in both cases or, better, if the two samples are simultaneously put in the same converter, one can measure a close 'doublet' of photo lines, one of which is very well known ($E_{\text{annih. rad.}} = 510{\cdot}8$ kev.). This procedure was tried by Siegbahn and Hedgran (1949) with the spectrometer in the case of ^{198}Au, where the K photo line of the annihilation radiation and the L photo line of the gold γ-radiation form a doublet consisting of two lines only 28 kev. apart from each other, when using lead converter (the doublet would be still closer if uranium instead of lead had been used). In this way the γ-radiation was determined to be $411{\cdot}0 \pm 1{\cdot}0$ kev., in good agreement with DuMond's corresponding crystal value (411·2 kev.). It is of course possible to extend this procedure to other energies by comparing the K photo line of gold against an L photo line of some other γ-ray using the same converter etc. The doublet method can certainly be made more accurate in future with the new field-measuring system.

§ 7. SOME RESULTS

The spectrometer has been used for some time to study different radioactive disintegration problems. Some of these investigations have already been published or will appear elsewhere. In most cases the spectrometer has been adjusted to give a resolving power of about 1% or slightly less. To make full use of this resolving power it has been found necessary to restrict the thickness of the lead converter in γ-ray investigations in most cases to be less than 5μ (evaporated on an aluminium foil). The heights of the photo lines compared with the inevitable Compton electron distributions are then not particularly

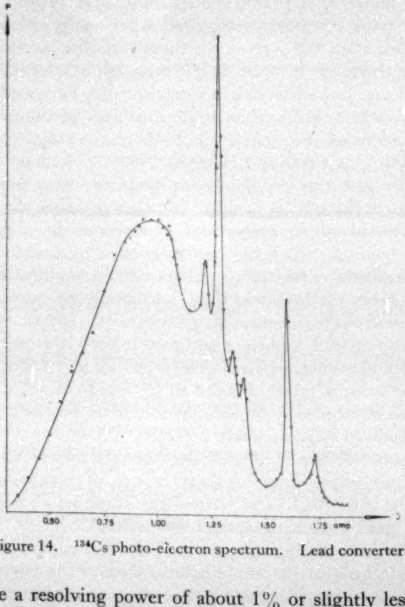

Figure 14. ^{134}Cs photo-electron spectrum. Lead converter 9 μ.

[Continued on p. 984

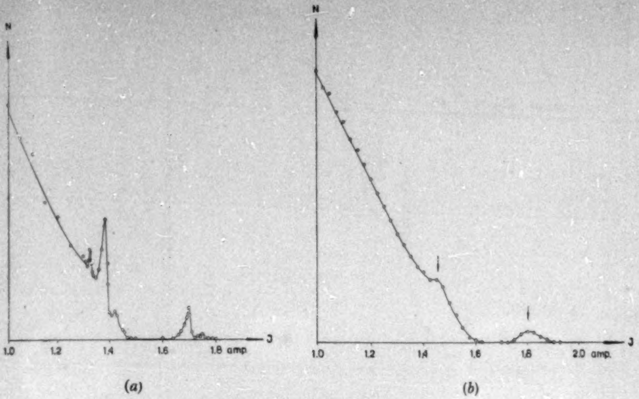

(*a*) (*b*)

Figure 15. ^{134}Cs β-spectrum.

(*a*) With 1% resolution in the spectrometer.
(*b*) With 4·5% resolution taken with another spectrometer.

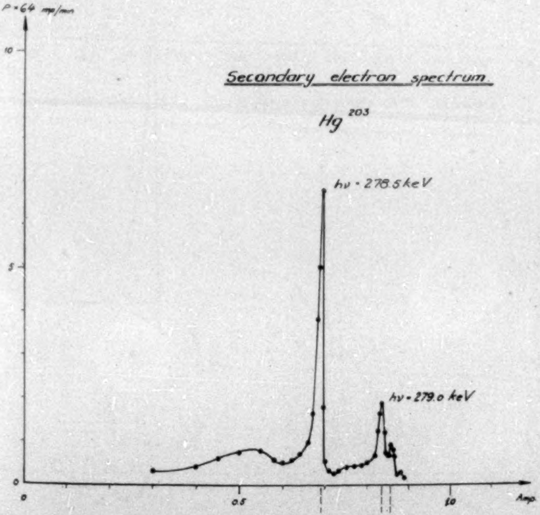

Figure 16. ^{203}Hg photo-electron spectrum. Lead converter 3·7 μ.

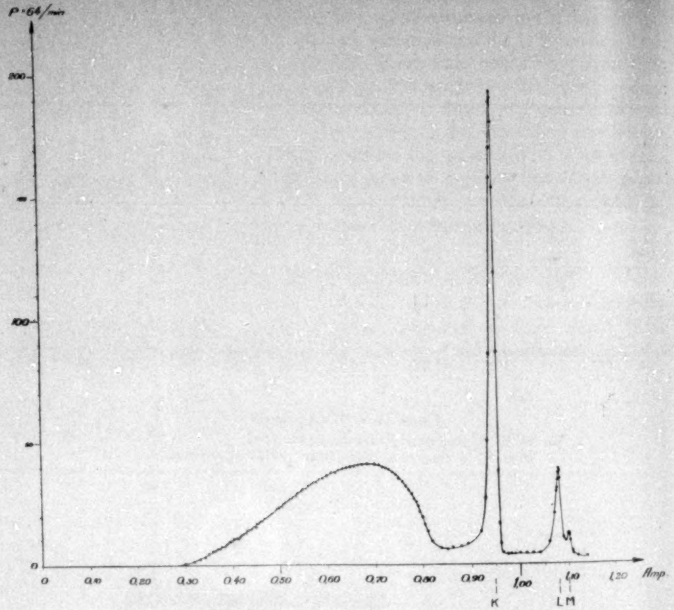

Figure 17. ^{198}Au photo-electron spectrum. Lead converter 3·7 μ.

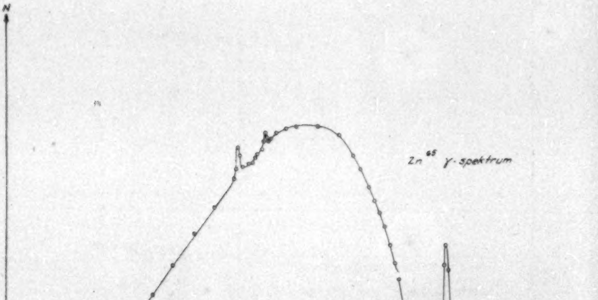

Figure 18. ^{65}Zn photo-electron spectrum. Lead converter 9 μ.

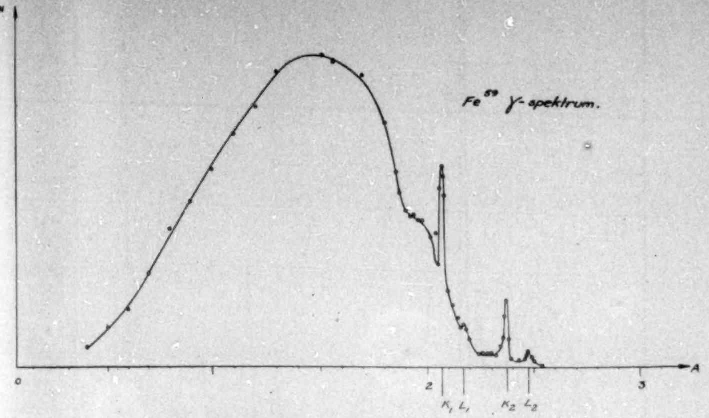

Figure 19. ^{59}Fe photo-electron spectrum. Lead converter 9 μ.

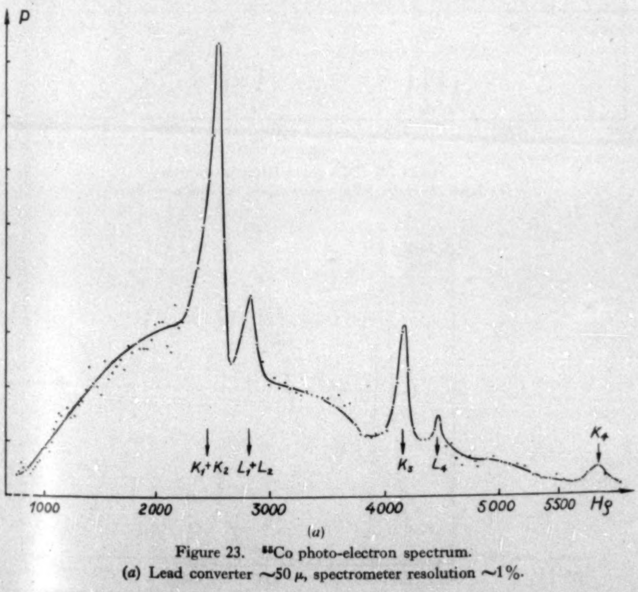

Figure 23. ^{56}Co photo-electron spectrum.
(*a*) Lead converter ~50 μ, spectrometer resolution ~1%.

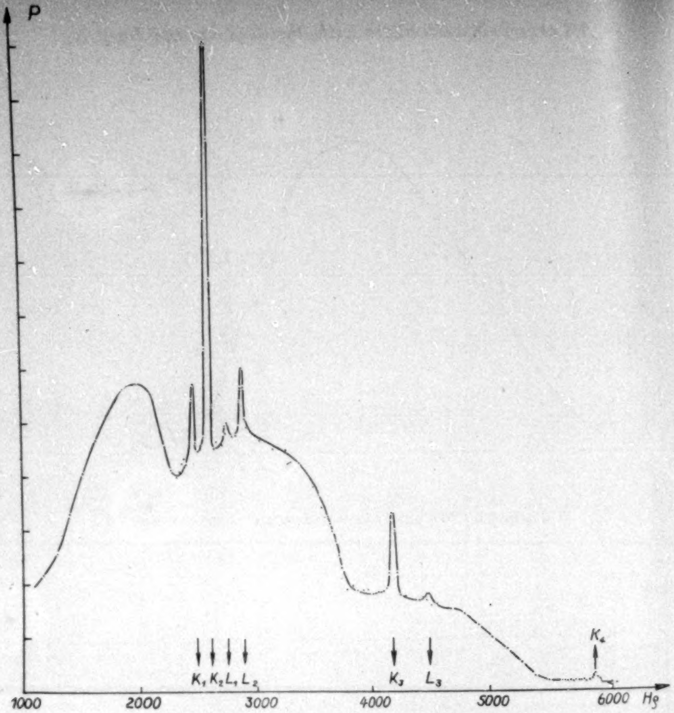

(*b*)

Figure 20. ^{56}Co photo-electron spectrum.
(*b*) Lead converter $3{\cdot}7\,\mu$, spectrometer resolution $\sim 1\%$.

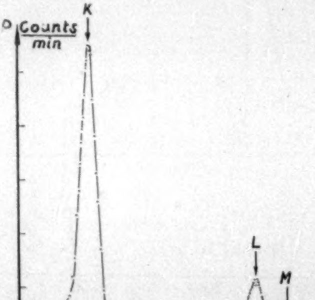

Figure 21. K, L and M photo lines from the annihilation radiation ($E_{\gamma} = 510{\cdot}8$ kev.).

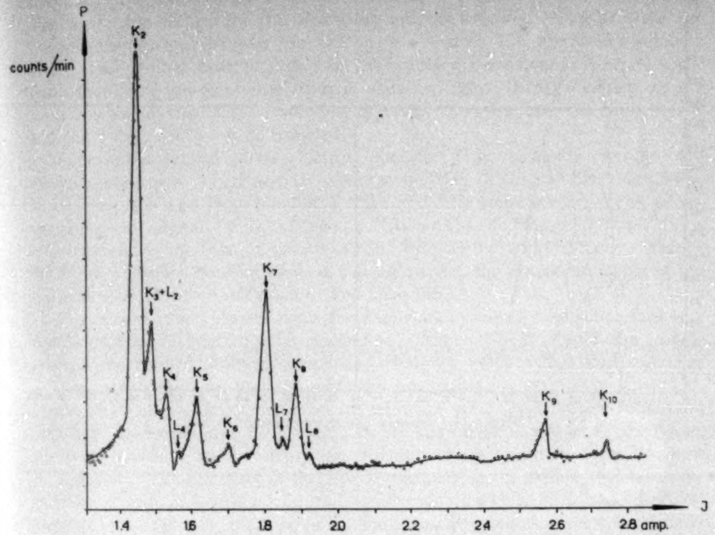

Figure 22. Part of the β-spectrum of ^{110}Ag.

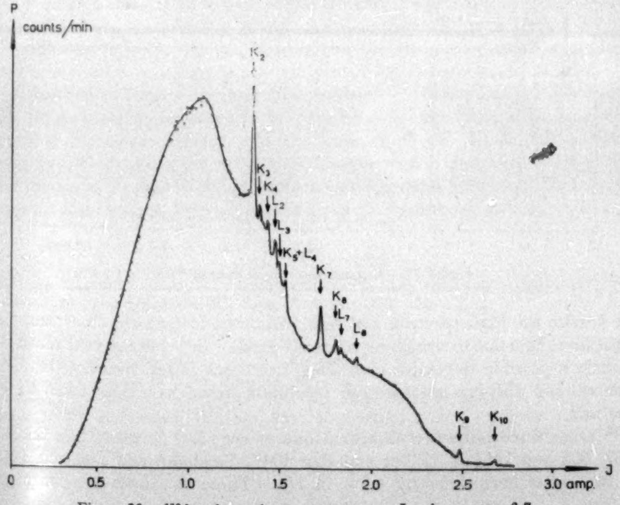

Figure 23. ^{110}Ag photo-electron spectrum. Lead converter 3·7 μ.

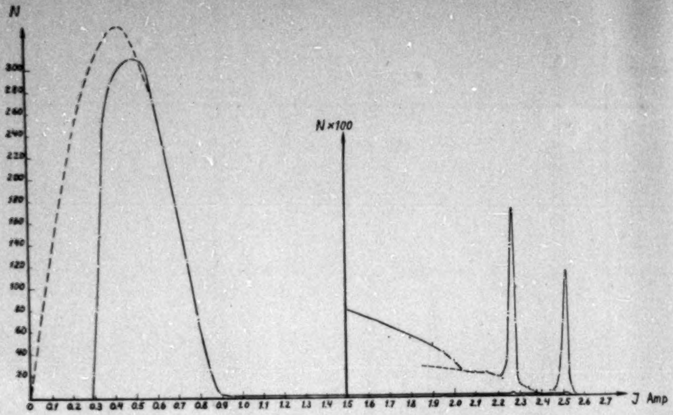

Figure 24. Internal conversion lines of ^{60}Co.

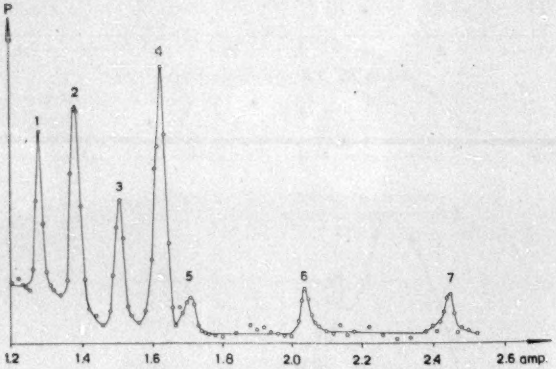

Figure 25. Internal conversion lines of ^{82}Br.

great despite the high spectrometer resolution, but instead the lines are sharp and the line shifts due to straggling relatively small. In some cases the resolution has made it possible to resolve close lines from each other, which with thicker converters and with less spectrometer resolution would have been taken to be a single line.

^{134}Cs has three γ-lines (plus a hard one of very low intensity at 1·35 MEV.) at 567, 603 and 796 kev. (Elliot and Bell 1947, Siegbahn and Deutsch 1948). The two softer lines differ by 4·5% in $H\rho$. These two lines are completely resolved in the photo-electron spectrum shown in Figure 14 (Pb converter 9μ). The conversion factors for the γ-rays are low, as expected ($4{\cdot}4\times10^{-3}$) for the two softer γ-rays and $2{\cdot}4\times10^{-3}$ for the one at 796 kev. The increased resolution makes these β-lines easy to detect in the primary β-spectrum (Figure 15 (*a*)). For comparison the same spectrum is shown (Figure 15 (*b*)) obtained with a spectrometer adjusted for a resolution of 4·5%. (In that case the two softer β and photo lines could not be resolved.)

Some other typical photo-electron spectra (with increasing energies) are shown in Figures 16, 17, 18 and 19 (γ-rays from ^{203}Hg (Slätis and Siegbahn 1949), ^{198}Au (Siegbahn and Hedgran 1949), ^{65}Zn and ^{59}Fe respectively). The corresponding γ-energies are $^{203}\mathrm{Hg}=279$ kev., $^{198}\mathrm{Au}=411$ kev., $^{65}\mathrm{Zn}=1{\cdot}125$ Mev. (plus a few presenting annihilation radiation[*] and $^{59}\mathrm{Fe}=1{\cdot}097$ and 1·295 Mev. Except for ^{198}Au, where the doublet method has been used, the maximum errors of the γ-energies should not yet be set at less than 0·5%.

Figure 20 is a good illustration of the importance of using a converter thickness suitable for good spectrometer resolution. Figure 20 (*a*) shows the photo-electron spectrum of ^{55}Co (Deutsch and Hedgran 1949) with a lead converter approximately 50μ thick and the spectrometer set for a resolution of about 1%. Figure 20 (*b*) shows the same spectrum with the same spectrometer resolution, but with a lead converter $3{\cdot}7\mu$ thick. In the last case a K and an L photo line, previously masked by the strong annihilation radiation photo lines, can now be observed. The existence of this line is essential for the disintegration scheme of ^{55}Co. Figure 21 (with a $3{\cdot}7\mu$ lead converter) shows the K, L and M photo-electron lines from the annihilation radiation used to calibrate the spectrometer for photo-electron spectra around these energies. The calibration factors obtained from the three different lines differ among themselves by less than 0·2%.

Figures 22 and 23 show part of the primary β-spectrum of ^{110}Ag (Siegbahn 1949) and the corresponding photo and Compton electrons from a $3{\cdot}7\mu$ lead converter respectively. As can be seen this spectrum is unusually complex and good resolution is necessary if any analysis of the radiation is to be tried.

According to theory the internal conversion coefficients at low Z values and hard γ-rays must be expected to be very low. Comparison with theory in this region is therefore difficult. In the case where the β-lines fall outside the continuous β-spectrum the situation is however much simplified. This happens for instance in the case of ^{60}Co (Deutsch and Siegbahn 1950) and ^{82}Br (Siegbahn, Hedgran and Deutsch 1949). These two spectra are shown in Figures 24 and 25.

REFERENCES

Deutsch, M., and Hedgran, A., 1949, *Phys. Rev.*, **75**, 1443 (a full paper is under preparation);

Deutsch, M., and Siegbahn, K., 1950, *Phys. Rev.*, **77**, 680.

DuMond, J., Lind, D., and Watson, B., 1948, *Phys. Rev.*, **73**, 1392.

Elliot, L. G., and Bell, R. E., 1947, *Phys. Rev.*, **72**, 979.

Ellis, C. D., 1934, *Proc. Roy. Soc.* A, **143**, 350.

Geoffrion, C., 1949, *Rev. Sci. Instrum.*, **20**, 638.

Jensen, E., Laslett, L., and Pratt, W., 1949, *Phys. Rev.*, **75**, 458.

Kerst, D. W., and Serber, R., 1941, *Phys. Rev.*, **60**, 53.

Kurie, F. N. D., Osoba, J. S., and Slack, L., 1948, *Rev. Sci. Instrum.*, **19**, 771.

---

[*] In this case the very small internal conversion line, corresponding to the line at 1·125 Mev., was also found and measured.

Lauritsen, T., and Hornyak, W. F., 1949, *Bull. Amer. Phys.. Soc.*, **24**, No. 2, 10.
Shull, F., and Dennison, D., 1947 *Phys. Rev.*, **71**, 681, **72**, 256.
Siegbahn, K., 1944, *Ark. Mat. Astr. Fys.*, **30A**, No. 20; 1949, *Phys. Rev.*, **75**, 1277 (a full paper is under preparation).
Siegbahn, K., and Deutsch, M., 1948, *Phys. Rev.*, **73**, 410.
Siegbahn, K., and Hedgran, A., 1949, *Phys. Rev.*, **75**, 523.
Siegbahn, K., Hedgran, A., and Deutsch, M., 1949, *Phys. Rev.*, **76**, 1263.
Siegbahn, K., and Svartholm, N., 1946, *Nature, Lond.*, **157**, 872.
Slätis, H., and Siegbahn, K., 1949, *Ark. Mat. Astr. Fys.*, **36A**, No. 21.
Svartholm, N., 1946, *Ark. Mat. Astr. Fys.*, **33A**, No. 24; 1949, *Ibid.*
Svartholm, N., and Siegbahn, K., 1946, *Ark. Mat. Astr. Fys.*, **33A**, No. 21.

Experiments with a Magnetic Lens Spectrometer, employing Post-focusing Acceleration: the L-Auger Lines of Thorium-active Deposit

By D. K. BUTT
Department of Natural Philosophy, University of Edinburgh

Communicated by N. Feather; MS. received 25th January 1950; *in amended form 18th March* 1950

ABSTRACT. A post-focusing electron accelerator has been developed to reduce the absorption of low-energy electrons by the Geiger counter window of a β-ray lens spectrometer. Its useful range is for β-rays having energies between 0 and 30 kev., and although, in general, for a portion of this range only partial transmission will be obtained, correction curves for the absorption can be accurately determined.

In order to test the spectrometer, an investigation of the L-Auger lines of thorium-active deposit has been made. An identification of the lines has been attempted.

§ 1. INTRODUCTION

To improve the transmission of a magnetic lens spectrometer* for low energy electrons a post-focusing accelerator has been fitted to the spectrometer tube. An account of a similar apparatus has already been published by Langer and Cook (1948); construction of the present apparatus was, however, carried out quite independently of this publication, and the tests to which it has been subjected are possibly more severe than those applied by Langer and Cook to their apparatus.

The function of the accelerator is merely to accelerate the electrons, after they have been focused, to give them additional energy so that they may penetrate the Geiger counter window. A diagram of the apparatus is shown in Figure 1.

The electrons are focused through a hole A, just over 2 mm. in diameter. After passing through this hole, they are accelerated towards the Geiger counter window B. In the present case the window consists of collodion foil, approximately 0·4 mg/cm^2 in thickness, mounted on a brass grid. As will be described in more detail later, the accelerating potential normally used is about 18 kv.

Since the Geiger counter is, of necessity, at this high positive potential, it has been found most convenient to raise the counter scaling circuit and power pack to the same potential. The general layout of the necessary apparatus is shown in

---

* Details of the constants of this spectrometer have been given in an earlier paper (Butt 1949).

Figure 2. The scaler circuit and power pack are housed in a bin lying horizontally on four insulators. The A.C. supply to these units is insulated from the A.C. mains by means of a 1 : 1 ratio transformer, the primary of which is insulated from the secondary to a potential of 100 kv. The dials of the scaler are observed through windows in the side of the bin, and the controls are operated by means of ebonite rods protruding from the side of the bin.

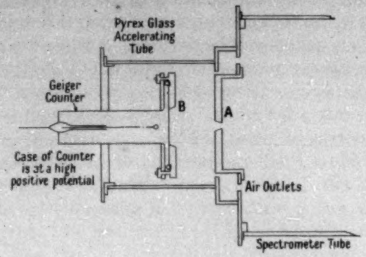
Pyrex Glass Accelerating Tube
Geiger Counter
B
A
Case of Counter is at a high positive potential
Air Outlets
Spectrometer Tube

Figure 1.

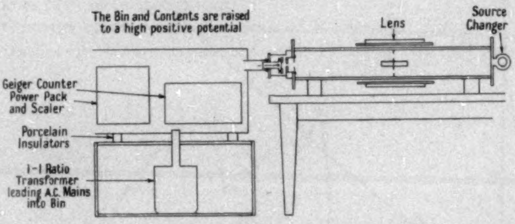
The Bin and Contents are raised to a high positive potential
Lens
Source Changer
Geiger Counter Power Pack and Scaler
Porcelain Insulators
1-1 Ratio Transformer leading A.C. Mains into Bin

Figure 2.

The accelerating voltage is supplied by a 100 kv. X-ray transformer, the output of which can be continuously controlled over the whole of its range. This voltage is rectified by means of a half-wave valve rectifier and smoothed by a 0·02 mF. condenser.

During operation, the pressure in the accelerating tube is kept below 10^{-5} mm. Hg.

§ 2. PERFORMANCE OF THE ACCELERATOR

When preliminary tests of the accelerator were made, the following characteristics were recorded. Initially, with no source in the spectrometer, the spectrometer was evacuated to a pressure of less that 10^{-5} mm. Hg and the Geiger counter was filled. The accelerating voltage was gradually raised from zero. No spurious counts were observed until the accelerating potential was approximately 19 kv. Above this voltage, however, the number of such counts increased very rapidly until, at about 20 kv., the scaling circuit was completely blocked.

To determine whether these spurious counts were due to radiation actually entering the counter, a 20 mg/cm² copper foil was placed in front of the counter window. On the application of the acceleration voltage no spurious counts were recorded. This points to the fact that these spurious counts are caused by electrons or ultra-violet radiation.

That the spurious counts are due to electrons was finally verified by deflecting them away from the counter by means of a magnetic field. These spurious counts are presumably due to the formation of positive ions in the accelerating chamber which bombard the cathode and cause it to eject electrons; these in turn are accelerated to the Geiger counter window. From this theory it is to be expected that spurious counts will begin to occur when the ejected electrons are accelerated through the Geiger counter window. The fact that, in the present case, spurious counts begin to occur at 18 kv. roughly supports this idea, because it is to be expected that a 0·4 mg/cm^2 window will begin to transmit when the electrons reach an energy of about 18 kev.

An attempt to reduce these spurious counts by using an aluminium cathode and then coating it with 'Aquadag', in order to raise the work function of the cathode surface and lower the stopping power to the positive ions, made very little difference. A natural limitation of the useful accelerating voltage (at about 18 kv.) was therefore accepted. Since the collodion windows can transmit electrons with energies as low as 18 kv., with the aid of the accelerator, a small percentage of electrons having energies of only 1 or 2 kev. can be detected.

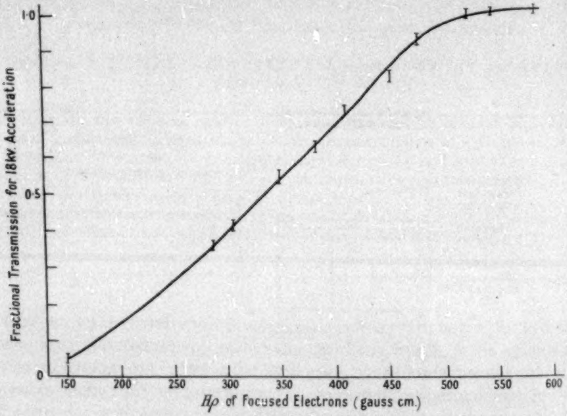

Figure 3.

An advantage of the method of acceleration is that the transmission curve for any window can be quickly and accurately determined. A source is put into the apparatus, and the lens is made to focus electrons of a certain momentum. The accelerating voltage is then applied and is increased in steps of 1 kv., counting being continued until a saturation counting rate is reached. At this stage all the electrons incident on the window are transmitted. From one such curve the transmission of the film for electrons of any energy may obviously be determined. Such a curve is shown in Figure 3 for one of the windows used in the present work.

§3. INVESTIGATIONS WITH THORIUM-ACTIVE DEPOSIT

In order to test the behaviour of the apparatus, the low-energy line spectrum of Th(B + C + C′ + C″) was investigated. The active deposit was carried on a thick platinum button just under 2 mm. in diameter. Back-scattering from the thick button, of course, made the continuous spectrum in the low-energy range almost entirely 'instrumental', but it was thought that the relative intensities of the lines in the same region should not have been greatly affected.

To test the possibility of the electric field leaking through the hole A (Figure 1) into the spectrometer chamber, and so vitiating the calculation of line energies, the low-energy spectrum was observed with an accelerating potential of 10 kv. and then with an accelerating potential of 18 kv. Calculated line energies were the same within acceptable limits.

There is a further effect which might lead to the distortion of the line energies, at very low energies. This arises from the fact that the axis of the spectrometer is horizontal and only the vertical component of the earth's magnetic field is compensated. The axial focusing field, therefore, is not strictly proportional to the focusing current. To test whether this was affecting the calibration of the spectrometer in any way, the line energies were observed with the focusing current passing first in one direction and then in the other. The energies agreed to within 1% within the energy range 6–12 kev., which is about the limit of accuracy with which the energies can be determined.

The low-energy spectrum finally obtained is shown in Figure 4. As will be explained, the lines in this spectrum are L-Auger lines of ThC(83) and ThC″(81).

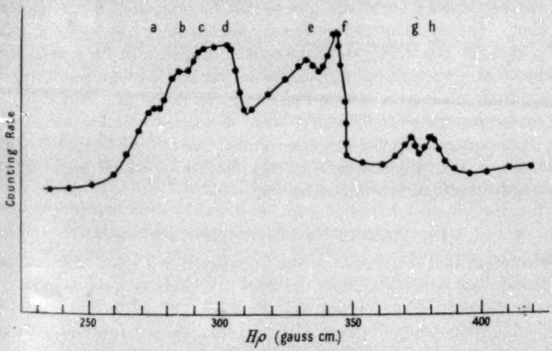

Figure 4.

Flammersfeld (1939) published some low energy lines in the Th(B + C + C′ + C″) spectrum that he presumed to be new. He reported four lines of $H\rho$ values 284, 314, 333 and 368 gauss cm. Flammersfeld hinted that these lines were possibly due to Auger electrons, but he made no effort to identify the transitions concerned.

These lines of Flammersfeld are presumably the same as those investigated photographically by Black (1925). Strangely enough, Flammersfeld's energies do not appear to agree very well with those of Black; for instance, his most intense line is that of $H\rho = 284$, whilst Black's strongest line is of $H\rho = 303{\cdot}4$. Flammersfeld found no line near $H\rho = 303{\cdot}4$.

The general shape of the spectrum obtained in Figure 4 closely resembles that obtained by Flammersfeld, though there is considerably more detail present in Figure 4 than there is in Flammersfeld's spectrum. Black's spectrum also has more lines than Flammersfeld's and, as the following table shows, our energies agree with Black's in nearly every case. Flammersfeld's energies are included for comparison. All values are in kev.

Table 1

Flammersfeld	Black	Author	Flammersfeld	Black	Author
	6·46	6·71 a*	8·7	9·82	9·82 e
	7·06	7·10 b	9·7	10·45	10·39 f
	7·53	$7·55 \pm 0·05$ c	10·45	12·44	12·26 g
7·00	8·11	$8·10 \pm 0·05$ d		12·69	12·62 h
	8·47				

* The lettering here given to the lines is the author's own nomenclature.

Relative intensities are omitted, since Black's are merely visual estimates, and it is obvious from Figure 4 that ours cannot be determined with any high degree of accuracy. In respect of energies, our lines a and g diverge slightly from Black's values, and line c is one that he suspected as being present but was unable to confirm. Black also queried the genuineness of the 310·1 $H\rho$ line (8·47 kev.), and Figure 4 shows no sign of it.

In view of the general agreement between the last two columns of Table 1, Flammersfeld's energy values are rather difficult to explain. One possible reason why he obtained lower energies is that he deposited his source on a thin Zapon film. The resultant charge lost by such a source is negative, and Zapon film in a vacuum is a very good insulator. Braden and his colleagues (1948) have shown that in such circumstances the source may become positively charged, so that electrons leaving the source lose energy in doing so. The fact that both Black's source and the author's source were deposited on a conductive platinum backing is perhaps significant in this connection. On the other hand Flammersfeld's spectrum is not uniformly lower in energy than ours, which might be expected from a simple explanation along these lines.

§4. IDENTIFICATION OF THE LINES

In attempting an identification of the lines listed in Table 1, it is first necessary to determine from which elements the lines are likely to have originated. The elements in equilibrium on the source have $Z = 81$, 82, 83 and 84. Clearly, only those giving strong groups of secondary internal conversion electrons need be considered as sources of tertiary Auger electrons.

From Flammersfeld's tables it can be seen that by far the most intense internal conversion occurs in the K and L levels of element 83 and in the L levels of element 81. For the present purpose the contributions of elements 82 and 84 can be neglected. We shall therefore proceed to estimate the ultimate intensity of L shell ionization in $Z = 83$, 81 and its distribution amongst L_{I}, L_{II} and L_{III} as a basis for our discussion.

$Z = 83$.

It is well known that strong internal conversion takes place in the K and L shells of this element due to the Dg, E, F, Fa and H γ-rays (nomenclature of Ellis).

These γ-rays produce the K internal conversion lines D, A′*, F and H, which give a total K ionization of 33·12 per 100 disintegrations.

Again, according to Flammersfeld, the total L shell ionization (for all three shells) due to the complex lines E, I and Jc is 5·94 per cent.

A photographic determination, by Surugue (1937), of the relative intensities of internal conversion corresponding to the three components of the I line gave $L_{\rm I}=1$, $L_{\rm II}=0{\cdot}06$, $L_{\rm III}=0{\cdot}004$. If similar ratios hold in the other two cases we have $L_{\rm I}=5{\cdot}58\%$, $L_{\rm II}=0{\cdot}33\%$, $L_{\rm III}=0{\cdot}02\%$ for the total intensities of primary L ionization due to the three lines concerned.

Secondary L ionization will result from the transference of most of the K ionization, either by Auger transitions, or x-ray emission, to the L shells.

From Flammersfeld's figures the total intensity of the K-Auger lines is 0·89 per cent. This leaves an intensity of 32·23 per cent to be transferred to the L and higher shells by x-ray emission.

From Massey and Burhop's (1936) tables 53% of the 32·23 goes to the $L_{\rm III}$ shell on the emission of the $K\alpha_1$ x-ray, and another 26% goes to the $L_{\rm II}$ shell by the $K\alpha_2$ emission. The rest of the K ionization goes to the M and N shells and does not concern us here ($L_{\rm I}\rightarrow K$ is a forbidden transition).

Hence the ionization of the three L shells resulting from the primary K ionization that gives rise to x-rays is, per 100 disintegrations, $L_{\rm I}=0$, $L_{\rm II}=8{\cdot}38$, $L_{\rm III}=17{\cdot}1$.

The small contribution of the K-Auger lines to L ionization can be estimated from the work of Ellis (1933). From the relative intensities of the K-Auger lines the L ionizations are obtained as follows: $L_{\rm I}=0{\cdot}59\%$, $L_{\rm II}=0{\cdot}38\%$, $L_{\rm III}=0{\cdot}55\%$.

Taking the three calculated contributions together, the total intensities of L ionization are, therefore, $L_{\rm I}=6{\cdot}17$, $L_{\rm II}=9{\cdot}09$, $L_{\rm III}=17{\cdot}67$ per 100 disintegrations.

$Z=81$.

The primary ionization in element 81 is due to the two γ-rays A and Ga, which have energies of 39·8 and 286·9 kev. respectively.

The intensity of the K internal conversion line of Ga is 0·11 per cent and the L internal conversion lines are so weak that Flammersfeld did not detect them. In the following calculations therefore the effects of this γ-ray will be neglected.

$\gamma_{\rm A}$, having an energy of only 39·8 kev., produces no K internal conversion line, but is strongly converted in the L shells. Flammersfeld was unable to resolve the lines due to the three shells, but determined their total intensity as 20·9 per 100 disintegrations. Included in this figure, it must be remembered, is the intensity of 3·5 per cent due to the A′ line mentioned previously. Thus an intensity of ionization of 17·4 per cent remains to be divided between the three shells.

Surugue's (1937) relative intensities for the three L-lines are $L_{\rm I}=1$, $L_{\rm II}=0{\cdot}1$, $L_{\rm III}=0{\cdot}01$. Since he did not resolve the A′ line these values are somewhat in doubt. For our purposes, however, they are probably accurate enough. We therefore divide the 17·4 per cent according to the above ratios and obtain for the primary ionizations: $L_{\rm I}=15{\cdot}67\%$, $L_{\rm II}=1{\cdot}57\%$, $L_{\rm III}=0{\cdot}16\%$.

The relative intensities of L ionization for elements 83 and 81, calculated above, are further considerably modified by two very intense Auger transitions that were first identified by Coster and Kronig (1935). Coster and Kronig were concerned in explaining the anomalous intensity distribution of the x-ray emission lines and their satellites, and explained the anomalies on the basis of the high probabilities of the two transitions $L_I \rightarrow L_{III}M_{IV}$ and $L_I \rightarrow L_{III}M_V$. The Coster–Kronig phenomenon was first taken account of in relation to the Auger effect in radioactive decay by Kinsey (1948).

---

* The A′ line is almost coincidental with the A line, and its intensity is calculated from a knowledge of the intensity of the E line (the L conversion of the same γ-ray) (Kinsey 1948).

Obviously Coster–Kronig transitions can take place only when

$$E_{L_I} > E_{L_{III}} + E_{M_{IV,V}}.$$

It is interesting to note that energetically this condition holds only for elements of atomic number less than 53 and greater than 74. For $Z=81$, 83 this condition most certainly obtains.

Coster and Kronig estimated that as much as 80% of the initial L_I ionization is transferred to the L_{III} shell by the transitions at present in question. Although the precise figure is rather uncertain, we take this value to obtain ultimate intensities of ionization per 100 disintegrations in the three L shells as follows.

Table 2

Z	L_I	L_{II}	L_{III}
83	1·23	9·09	22·61
81	3·13	1·57	12·69

It may be remarked here that the Coster–Kronig transitions should give rise to very strong Auger lines in the region under 1 kev. So far, due to the difficulty of accurate neutralization of the earth's magnetic field for these low energy electrons, this energy region of the spectrum has not been investigated.

Using the ionization figures of Table 2 as a guide, an attempt may now be made to fit the observed L-Auger lines (Table 1) into a scheme. For this purpose, values of the L, M and N ionization energies used were taken fron Lindh's (1927) table.

As indicated by Ellis (1933), the energy of the Auger lines cannot be obtained accurately from such x-ray data, for it must be remembered that the atom left by an Auger electron is ionized doubly, not singly as in the case of the x-ray ionization, and no systematic information regarding x-ray levels in deeply ionized atoms is available. For the K-Auger lines of ThB Ellis estimated the additional binding energy for the second L ionization between 100 and 300 ev. In the present case, in some disintegrations, the second ionization occurs either in an M or an N level, and consequently the additional binding energy will be considerably less (probably well under 100 ev.), but in others the atom is already doubly ionized, after a Coster–Kronig transition, and becomes triply ionized after the Auger transition which is observed. In these disintegrations obviously a slightly greater additional binding energy will apply.

From Table 2 we naturally attempt to explain the observed lines as originating in transitions from the most frequently ionized states, namely 83 L_{III}, 81 L_{III} and 83 L_{II}. Table 3 gives possible transitions on this basis.

It is satisfactory that on this basis we find, for any strong line originating from the L_{III} shell of element 83, a corresponding line for element 81. Such pairs are ab, cd and ef. Since the strongest x-ray originating from the L_{III} shell is the $L_{III}M_V(L\alpha_1)$, it is further satisfactory that the most prominent Auger lines involve the same transition.

Lines g and h, on energetic grounds, are not likely to originate from the L_{III} shell of either element. They probably originate from the L_{II} shell of element 83. The main X-ray originating from this shell is the $L_{II}M_{IV}(L\beta_1)$, and they have therefore been attributed to the internal conversion of this X-ray. It is satisfactory that the relative intensities roughly deducible from Figure 4 give general support to these identifications on the basis of the ionizations given in Table 2.

Table 3

	Line (kev.)	Element 83	Energy (kev.)	Element 81	Energy (kev.)
h	12·62	$L_{II}M_{IV}N_{VI}$	12·58		
g	12·26	$L_{II}M_{IV}N_{II}$	12·21		
f	10·39	$L_{III}M_VN_V$	10·36		
e	9·82			$L_{III}M_VN_V$	9·86
d	8·10 ± 0·05	$L_{III}M_VN_{IV}$	8·12		
c	7·55 ± 0·05			$L_{III}M_VN_{IV}$	7·74
b	7·10	$L_{III}M_VM_{II}$	7·11		
a	6·71			$L_{III}M_VM_{II}$	6·81

ACKNOWLEDGMENTS

The author's thanks are due to Professor N. Feather, who has given his continued support throughout the work, and with whom many helpful discussions have taken place on the subject of the L-Auger lines. Thanks are also due to Mr. R. E. Siday, under whose guidance the work was initiated, and who gave most helpful advice in the development of the electron accelerator.

REFERENCES

Black, D. H., 1925, *Proc. Camb. Phil. Soc.*, **22,** 838.
Braden, C. H., Owen, G. E., Townsend, J., Cook, C. S., and Shall, F. B., 1948, *Phys. Rev.*, **74,** 1539.
Butt, D. K., 1949, *Proc. Phys. Soc.* B, **62,** 551.
Coster, D., and Kronig, R. De L., 1935, *Physica,* **2,** 13.
Ellis, C. D., 1933, *Proc. Roy. Soc.* A, **139,** 336.
Flammersfeld, A., 1939, *Z. Phys.*, **114,** 227.
Kinsey, B. B., 1948, *Canad. J. Res.*, **26,** 404.
Langer, L. M., and Cook, C. S., 1948, *Rev. Sci. Instrum.*, **19,** 257.
Lindh, A. E., 1927, *Phys. Z.*, **28,** 93.
Massey, H. S. W., and Burhop, E. H. S., 1936, *Proc. Camb. Phil. Soc.*, **32,** 461.
Surugue, J., 1936–7, *Ann. Phys., Paris,* **8,** 484.

Photoelectric Dissociation of the Deuteron

By C. H. COLLIE, H. HALBAN and R. WILSON
Clarendon Laboratory, Oxford

MS. received 5th December 1949

ABSTRACT. The cross section for the photo-disintegration of the deuteron has been measured by detecting the photo-protons formed in a high pressure ionization chamber. The values obtained are $13{\cdot}91 \pm 1 \times 10^{-28}$ cm^2 for 2·62 Mev. γ-rays from radio-thorium and $15{\cdot}6 \pm 1 \times 10^{-28}$ cm^2 for the 2·76 Mev. γ-rays from radio-sodium.

---

§ 1. INTRODUCTION

For the investigation of nuclear forces two-body problems are of primary interest. This is as much due to the possibility of solving the wave equation exactly as to the relative simplicity of the experiments involved.

It is well known that the assumption of a strong nuclear attraction (about 20 Mev.) acting over a short range ($2{\cdot}8 \times 10^{-13}$ cm.) is adequate to reproduce the main properties of the deuteron and the interaction of slow neutrons and protons. The direct production of π-mesons by the interaction of high energy nuclear particles leaves little doubt that nuclear forces are due to a meson field whose nature is to be determined by a combined appeal to direct experiment and the restricted principle of relativity. The latter is of course an appeal to imaginary experiments of which one is not supposed to doubt the issue. As is well known (Bethe 1940), the latter principle severely restricts the interaction potentials which come into consideration to terms of the type $e^{-\kappa r}/r$, in which the range of the forces is unambiguously given in terms of the π-meson mass μ by $\kappa = \mu \mathbf{c}/\hbar$. Thus on a strict meson theory the range of the nuclear forces is not a disposable constant unless one imagines that mesons other than π-mesons play a part.

Once the nature of the interaction between the two nucleons has been determined, the wave functions of the deuteron can be obtained by solution, usually numerical, of the wave equation. A knowledge of the wave equation enables the interaction of the deuteron with an electromagnetic wave to be calculated by conventional methods and thus a direct comparison to be made between theory and experiment. The experimental quantities which can be measured are : (*a*) the absolute value of the cross section at a given value of incident quantum energy ; (*b*) the relative variation of cross section with energy ; (*c*) the angular distribution of the emitted particles, which is in effect a measure of the relative proportions of the disintegration due to the electric and magnetic vectors of the incident wave.

The present measurements are concerned with the first two of these possibilities.

§2 PREVIOUS WORK

Although many measurements of these quantities have been made previously, owing to the technical difficulties of the measurement and the exigencies of the times they have lacked the precision necessary to distinguish between the competing theories which have been put forward, and have done little more than lend support to the general wave mechanical treatment of the deuteron. The most important measurements which have been made in this field are tabulated in Table 1. The more precise of them had not been made when our work was started.

Table 1

Cross Section

Author	Date	Method	γ-ray energy (Mev.)	$\sigma \times 10^{28}$ cm^2
Chadwick and Goldhaber	1935	Ionization chamber	2·620	6±6
Halban	1938	Neutron standard	2·620	10±1
Richardson and Emo	1938	Cloud chamber	2·758	11±11
van Allen and Smith	1941	Ionization chamber	6·13	11·6±1·5
Lassen	1948	Proportional counter	2·758	25±8
Russell	1948	Neutron standard	2·758	16±4
Snell, Barker and Sternberg	1949	Neutron standard	2·758	14·5±1·5
			2·51	10·7±1
Wilson, Collie and Halban	1948 1949	Ionization chamber	2·620	13·9±1
			2·758	15·6±1
Wäffler and Younis	1949	Photographic plate	17·6	8±3
Barnes, Stafford and Wilkinson	1950	Ionization chamber	6·13	21·5±1·2
			17·6	8·5±1·2

Angular Distribution

Author	Date	Method	γ-ray energy (Mev.)	H = counts at 90°/counts at 0°
Chadwick, Feather and Bretscher	1938	Cloud chamber	2·620	0·25
Halban	1938	Activation detector	2·620	0·07±0·06
Myers and van Atta	1942	BF_3 counter	x-rays to 2·43	0·87±0·07
Graham and Halban	1945	BF_3 counter	2·620	0·20±0·05
Lassen	1948	Proportional counter for protons	2·758	0·15±0·03
Woodward and Halpern	1949	Proportional counter for protons	2·46	0·33±0·1
			2·90	0·15±0·03
Hamermesh and Wattenberg	1949	BF_3 counter	2·758	0·19
Gibson, Green and Livesey	1947	Photographic plate	6·13	0·2
Meiners, Smith and Slack	1949	BF_3 counter	2·758	0·16±0·02

§3 METHOD OF MEASUREMENT

The measurement of the absolute cross section of the photo-distintegration of deuterium,

$$ {}^2_1\mathrm{H} + h\nu = {}^1_1\mathrm{H} + {}^1_0\mathrm{n} + \mathrm{Q}, $$

is in principle simple, all that is required being a known source of γ-rays, a specimen of a deuterium compound whose deuterium content is known, and a detector capable of detecting either the proton or the neutron. In practice, however, it is found that there is some difficulty in evolving an experimental technique capable of the overall accuracy to within 5% which was aimed at as being the least which could be of use in a comparison between theory and experiment. After careful consideration it was decided to detect the proton rather than the neutron emitted in the disintegration. It is true that the great penetrating power of neutrons, together with the ease with which they can be detected, enables the difficulties due to the small value of the photo cross section ($\sim 10^{-27}$ cm^2) to be in part off-set by the use of a large amount of deuterium in the target. However, none of the devices (e.g. BF_3 chamber) for detecting neutrons are absolute and the lack of a reliable neutron standard* as yet prevents satisfactory absolute measurements being made in this way. This objection does not apply with equal force to measurements of the variation in the relative cross section with incident quantum energy. A further disadvantage of methods of measurement based upon the detection of the neutron, when using the very convenient γ-rays from ThC, lies in the relatively large neutron background of this source. The unwanted neutrons are produced by the intense α-particle bombardment of the light elements unavoidably included in the carrier used in the chemical separation of the radio-thorium from the mesothorium parent.

§ 4. THE IONIZATION CHAMBER

The protons were detected in a spherical ionization chamber, filled with deuterium under pressure, connected to a linear amplifier. A cylindrical chamber was used in some preliminary experiments. The design of both chamber and amplifier are dictated by the experimental difficulties which have to be overcome, and are as near the optimum as was possible by simple means. Details of the ionization chambers are shown in Figure 1.

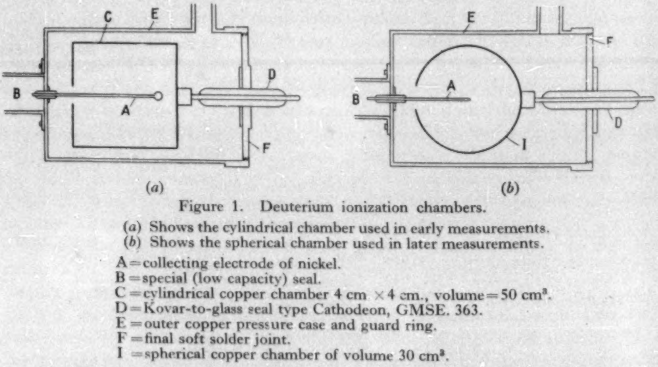

(*a*) (*b*)

Figure 1. Deuterium ionization chambers.

(*a*) Shows the cylindrical chamber used in early measurements.
(*b*) Shows the spherical chamber used in later measurements.

A = collecting electrode of nickel.
B = special (low capacity) seal.
C = cylindrical copper chamber 4 cm × 4 cm., volume = 50 cm^3.
D = Kovar-to-glass seal type Cathodeon, GMSE. 363.
E = outer copper pressure case and guard ring.
F = final soft solder joint.
I = spherical copper chamber of volume 30 cm^3.

The metal-glass seals are soldered with silver tin solder softening at 300° c.

Using the γ-rays of ThC (2·62 MEV.), the energy of the photo-proton is 210 KV., so that its range will be 1·0 cm. in deuterium at N.T.P., and it will produce about 6,000 ion pairs. This small ionization, even under the most favourable circumstances, will not produce a change of potential of the first grid of the amplifier greater than 70 microvolts. The pulses due to the protons can be distinguished from random noise and other pulses by their uniform size, and advantage must be taken of this fact to obtain sufficient discrimination for absolute measurements in the presence of recoil protons from unavoidable neutrons and random fluctuations in the ionization current produced by the γ-rays traversing the chamber.

---

* The position in this respect has recently improved, but no standard reliable to better than 5% is known, and the neutron flux is spread over a very large energy range which makes comparison difficult.

The pulses from the photo-proton are not quite uniform in size owing to the momentum of the incident quantum which must appear in the combined momentum of the proton and neutron. This effect amounts to a spread of ± 26 kev. in the energy of the recoil protons. Recombination and shielding of the inner electrode by the positive ions will also cause a spread in the measured pulse height. The detection and measurement of this spread affords a satisfactory indication of the correct functioning of the whole system.

Some of the photo-protons will arrive at the walls before they have expended all their energy in producing ions in the gas, and this ' wall effect ' will be an additional cause of variation in the recorded ionization produced by the photo-disintegration. The magnitude of this effect, which can be fairly simply calculated provided the range–energy relationship is known, will become proportionally less as the gas pressure in the ionization chamber is increased, and will be least and most easily evaluated for a spherical chamber. Another advantage of a spherical chamber is that it has no corners in which the field driving the ions to the central electrode is very weak, thus increasing the time available for recombination. These considerations determined the design of the chamber : a pressure of about 6 atmospheres in a 4 cm. diameter sphere reduces the wall effect to manageable proportions, but brings other difficulties in its train.

Owing to the small absolute value of the photo cross section, the ionization in the gas due to γ-rays greatly exceeds that due to the protons and increases with the pressure. The statistical fluctuations in this constant ionization current ultimately approach, and even exceed, the pulse of ionization due to the proton, and this sets an upper limit to the gas pressure which can usefully be used. If the collection time of the ions is a few milliseconds, as is the case for molecular ions, this ' piling up ' of the γ-ray pulses in the time required for complete collection makes measurements at 6 atmospheres impossible, but if the negative ions remain as free electrons, so that the collection time is a fraction of a microsecond, the statistical fluctuation in this short time is reduced sufficiently for one to be able to choose a deuterium pressure (about 6 atmospheres) at which the wall effect is small and the γ-ray noise sufficiently low to make measurements possible.

The achievement of electron conduction can only be attained if the gas is extremely pure and free from molecules such as oxygen, which have large electron attachment coefficients. It was widely believed that even in pure hydrogen electron conduction ceased at about 3 atmospheres pressure but, as was first shown by Stafford (1948), this is not so, electron conduction being maintained up to 80 atmospheres in hydrogen of extreme purity admitted through a palladium leak. For our work, using pressures below 30 atmospheres, we found that a less rigorous but more convenient system of purification was sufficient. After careful cleaning and final assembly, the chamber was pressure-tested and usually x-rayed to see that the central electrode was symmetrically placed. This avoided wasting time and deuterium on a chamber which would ultimately prove useless. It also provided a record of the exact position of the inner chamber with respect to the outer wall. The chamber was then connected to a vacuum system through an ordinary union rendered vacuum tight with hard Cavendish wax (Everett's No. 3) and baked out at as high a temperature as the last soldered joint allowed. The baking was usually for two days at 160° c. When no more occluded gas was given off the chamber was flushed out with deuterium and then filled under pressure from a cylinder of gas which had been purified by distillation from charcoal cooled with liquid oxygen. The whole of these operations were greatly facilitated by the use of the small diaphragm taps described by two of us (Halban and Wilson 1949) which have the merit of acting both as vacuum and pressure taps. The pressure was indicated by a miniature Bourdon gauge, but the actual pressure in the ionization chamber was determined at the end of a series of measurements by expanding the gas into a known volume and measuring the pressure on a wide-bore mercury manometer. Specimens of the gas were retained for analysis. On occasions chambers which did not show electron conduction immediately after filling developed it in the course of a few days, showing that the clean copper walls of the chamber were capable of absorbing the impurity, presumably oxygen, responsible for the unwanted electron attachment.

§ 5. THE AMPLIFIER

In order to make full use of the small collection time (found experimentally to be about 0·2 μsec.) so desirable from the point of view of reducing γ-ray noise from the ionization chamber, the bandwidth of the amplifier must be increased, thus introducing more noise from the amplifier. The necessary compromises were on the whole found experimentally by measuring the signal/noise ratio with the pulse amplitude (Figure 3, see below) discriminator. The 2-μsec. pulse duration found in this way agreed very well with the value obtained by a careful analysis of the circuit carried out subsequently (Wilson 1950).

The first, or pre-amplifier, stage avoided input circuit noise by using a high value (about 1,000 megohms) of the grid leak so that the current pulse from the photo-proton produces a rapid quasi-permanent increase in the grid potential. Since it is important to avoid the scattering of γ-rays by apparatus near the ionization chamber the first valve was connected to the main amplifier through a transmission line which was matched into a grounded grid triode. The resulting low gain of the first valve, which would in a conventional circuit allow appreciable noise from the second valve, is off-set by the degenerative effect of the high impedance of the first valve in the cathode circuit of the second. This circuit was adapted from circuits used in radar by Wallman, MacNee, and Gadsden (1948). The output from this pre-amplifier stage consists of a sharp voltage rise due to the arrival of the electrons at the collecting electrode, and before passing through a conventional amplifier this was converted into a true voltage pulse by means of the network shown in Figure 2. The advantage of an independent pulse-shaping network is the very much greater control one has over the pulse shape. When working near the noise limit the relatively small improvement in signal/noise ratio obtained by using a delay line as first suggested by Frisch results in a substantial gain in discrimination against unwanted signal. Working in this way, a factor of 1·5 in the signal/noise ratio over that given by a simple differentiating circuit can be obtained. Exact analysis by Wilson (1950) shows that the best shape of pulse occurring at a mean time t_m should be $\exp\{-|(t-t_m)/\tau|\}$, in which the parameter τ is determined from the ratio of the valve noise to the γ-ray noise. In this way one could obtain a further 20% increase in signal/noise ratio, but so far no sufficiently stable circuit for producing this pulse shape has yet been devised. After the pulse is shaped it is further amplified by a wide-band amplifier of conventional design and applied to the discriminator unit shown in Figure 3 (*a*), whose purpose is to enable only counts above a certain threshold, or between two thresholds, to be recorded.

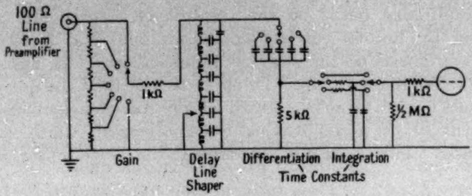
100 Ω
Line
from
Preamplifier
1 kΩ
5 kΩ
1 kΩ
½ MΩ
Gain
Delay
Line
Shaper
Differentiation
Integration
Time Constants

Figure 2. Pulse-shaping circuit.

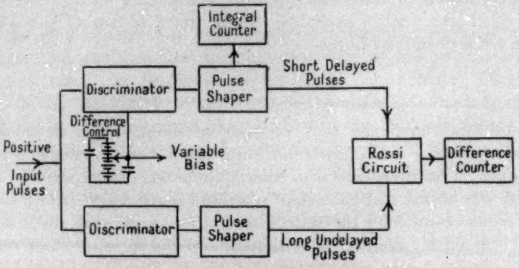
Integral
Counter
Short Delayed
Pulses
Discriminator
Pulse
Shaper
Difference
Control
Positive
Input
Pulses
Variable
Bias
Rossi
Circuit
Difference
Counter
Discriminator
Pulse
Shaper
Long Undelayed
Pulses

Figure 3 (*a*). Single channel kicksorter.

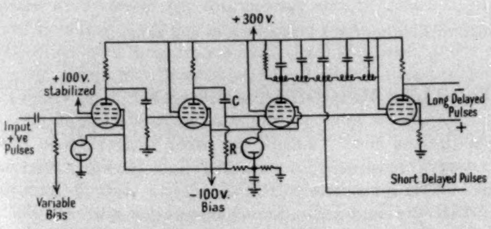
+300 V.
+100 V.
stabilized
C
Input
+ve
Pulses
R
Long Delayed
Pulses
+
−
Short Delayed Pulses
−100 V.
Bias
Variable
Bias

Figure 3 (*b*). Discriminator and pulse shaper.

The whole of the power supplies were stabilized against fluctuations and the overall gain was constant to better than 1%.

§6. THE γ-RAY SOURCE

Since the photo cross section varies rapidly with quantum energy, the monochromatic sources from excited nuclei are the most useful. Three ways of determining the number of γ-rays emitted from such a source are available, namely : (*a*) Direct ionization measurements in which the theoretical cross sections for Compton scattering and pair production are assumed (Gray 1936). (*b*) Absolute calibration based on the coincidence method first proposed in this connection by Rotblat (private communication) and Dunworth (1940). Extensive measurements on the γ-rays of radio-sodium, ^{24}Na, have been made by Putman and Willment (1950). To apply this method the decay scheme of the nucleus must be well established with a β-ray spectrometer (Siegbahn 1946). (*c*) Measurement of an accompanying α-disintegration, which can be made much more easily. This method is applicable to the γ-rays from a radio-thorium source.

The number of radioactive substances of reasonable half-life emitting γ-rays of greater quantum energy than the binding energy of deuterium (2·220 MEV.) is limited, only RdTh (2·62), ^{24}Na (2·758), ^{72}Ga (2·51), ^{140}La (2·56), ^{56}Mn (2·7) and Ra (2·42) being readily available. Only the first two of these have been used in the work described here.

§7. THE RADIO-THORIUM SOURCE

The radio-thorium source used consisted of about 400 MC. of radio-thorium, carefully purified and mixed with platinum black before sealing in a stainless steel cylinder. The preparation of this source was undertaken by Thorium Limited. It was hoped that the use of platinum black might reduce the number of fast neutrons emitted by the source since these were thought to come from the α-particle bombardment of light elements in the thorium oxide carrier used in the separation of the radio-thorium from its parent mesothorium. This device proved unsuccessful and the source emitted approximately 2,000 neutrons per second.

Radio-thorium disintegrates according to the scheme

$$\begin{tikzcd} & & & & & & \mathrm{ThC'} \arrow[dr, "\alpha"] & \\ \mathrm{RdTh} \arrow[r] & \mathrm{ThX} \arrow[r] & \mathrm{ThEm} \arrow[r] & \mathrm{ThA} \arrow[r] & \mathrm{ThB} \arrow[r] & \mathrm{ThC} \arrow[ur, "\beta"] \arrow[dr, "\alpha"'] & & \mathrm{ThD}. \\ & & & & & & \mathrm{ThC''} \arrow[ur, "\beta"'] & \end{tikzcd}$$

The 2·62 MEV. γ-rays are emitted from the ThD nucleus, which is left in an excited state after the ThC″ disintegration. Higher energy γ-rays (3·2 MEV.) were looked for using the high-pressure ionization chamber but were not found. If they exist, their intensity, less than one per thousand disintegrations, is low enough to be neglected in these measurements (Bishop, Wilson and Halban 1950). Thus the absence of any high-energy (5 MEV.) β-rays in the ThC″ β-ray spectrum shows that every ThC″ disintegration is accompanied by one γ-ray, so that the absolute number of γ-rays can be obtained by counting the number of α-particles emitted by a known amount of ThC.

This measurement has been made by Ricoux (1937), who measured the total ionization current produced by the α-particles from a known amount of ThC. To recover Ricoux's calibration a similar ionization chamber (the well-known

Paris pattern first described by Madame Curie (1912) for radium measurements) was constructed and calibrated with a known radium source (249·5 mc., N.P.L. Certificate No. RG.467). Ricoux's measurement is not based upon direct counting of the α-particles, and therefore depends upon a knowledge of the relative ionizations of α-particles of different ranges. He assumed that the energy required to form an ion pair was the same for all α-particles. This assumption is not quite correct, as was shown by Gray (1944), but a recalculation using the new data leaves Ricoux's result unchanged because the weighted mean range of the two α-particles from ThC is the same as that of the α-particles from RaC. The radio-thorium source was also measured with a standard N.P.L. chamber. Each intercomparison could be made to about ¼%, but the calculation of the absolute γ-ray intensity introduces two further uncertainties. Since Ricoux measured the total α-particle ionization of ThC the branching ratio ThC″/ThC′ enters directly into the calculation. This ratio is usually quoted as 35%, based upon the work of Albrecht (1919), but Kovarik and Adams (1938) obtained 33·7%, and we have adopted 34% as a weighted mean. This agrees well with the results of Meitner and Freitag (1926), who used a cloud chamber.

Since the whole method of measurement is based upon comparison with a radium standard, the absolute disintegration rate of radium must be known. This is often taken on Rutherford's authority (Rutherford, Chadwick and Ellis 1932) to be $3{\cdot}70 \times 10^{10}$/sec/curie, but the recent measurements of Kohman, Ames and Sedlet (1947) suggest that $3{\cdot}61 \times 10^{10}$/sec/curie is nearer the truth. Adopting the latter figure, we find the effective disintegration rate of our source (No. RdTh. 139) to be $4{\cdot}54 \times 10^{9}$ quanta/sec. calculated back to 9th June 1948. The greatest uncertainty in this figure is the branching ratio in ThC, which could easily be in error by 3%. The calculations, however, do include a change in the accepted wall and salt absorption correction (Kaye, Aston and Perry 1934) to take into account the different geometries of the N.P.L. and Paris ionization chambers.

The disintegration rate of the source may also be based upon the data of Shenstone and Schlundt (1922), who compared the number of α-particles from a ThC′–ThD source with those from a RaC′–RaD source of equal γ-ray intensity. The result is 4% lower than that based on Ricoux's measurements, a figure which also agrees with an estimate based on ionization chamber measurements made by Gray. On the whole we have given greater weight to the very careful and consistent measurements made by Ricoux. It is unlikely that the value we have adopted is more than 5% in error. A further comparison of radium and radio-thorium sources on the Paris ionization chamber has been made by Winand (1939). In these experiments the total α-particle energy was measured with a micro-calorimeter and the results agree with Ricoux's measurements to within 1%.

§ 8. THE RADIO-SODIUM SOURCE

The radio-sodium source was prepared by exposing 30 grammes of pure sodium carbonate in the A.E.R.E., Harwell, Pile in an aluminium container. After shaking well (to minimize small effects due to non-uniform activation of the sodium carbonate), the main bulk of the material was transferred to a flat tinned steel box ($\frac{1}{4}$ mm. wall thickness) and weighed. An aliquot was reserved and its absolute disintegration rate determined at A.E.R.E., using the coincidence method. This method of calibration depends upon the validity of the decay scheme for radio-sodium given by Siegbahn (1946) and Wiedenbeck (1947). Two γ-rays of quantum energy 2·76 Mev. and 1·38 Mev. are emitted in cascade. The β-ray spectrum is a simple one with maximum energy 1·38 Mev. At least 99% of the disintegrations follow this simple scheme. A further point is that the calculation of the intensity from the observed β–γ coincident rate involves the assumption that there is no angular correlation between the β- and γ-radiation. This point has been checked by Grace *et al.* (1949), who showed experimentally that the departures from a random distribution are less than 1% of the observed β–γ coincidences. This method of calibration has been checked by the absolute ionization method (Gray 1949). The two methods of calibration agree within the experimental error.

The half-life of radio-sodium enters directly into this method of calibration; the value 14·90 ± 0·02 hours found by Wilson and Bishop (1949) in an investigation undertaken for this reason was used in reducing the experimental values. The radio-sodium sources used emitted some 10^9 quanta/second, which enabled the source to be placed about 20 cm. from the counter.

Experimental Results

Typical differential bias curves using radio-thorium and radio-sodium are shown in Figures 4 and 5. The hump due to the photo-protons is clearly defined and measurable, but it is clear that it is only just separated from the γ-ray background when the lower energy protons from radio-thorium are being counted.

In order to determine the true number of photodisintegrations produced in this case one has to decide what the differential bias curve would have been had no photo-protons been produced. This was done in two ways. A radium source was brought up to the counter and its position adjusted until it gave the same γ-ionization current in the counter as had been given by the ThC source. The differential bias curve obtained under these conditions, which represented the noise due to the ionization current from the radium γ-rays, was assumed to be the same as the contribution of the ThC γ-rays to the composite differential bias curve in which the noise due to γ-rays and the tail of the proton peak are superimposed. The true photo-proton count in the region of overlap was obtained by subtraction. The assumption that the shape of the differential bias curve for γ-ray noise depends primarily on the ionization current and not on the γ-ray energy is reasonable since most of the electrons crossing the chamber are Compton electrons produced in the chamber wall. Alternatively the profile of the well-resolved proton peak obtained with radio-sodium γ-rays was carefully measured and corrected for wall effect. This measured photo-proton peak from 2·62 Mev. γ-rays was then used as a basis for extrapolating the tail of the measured proton peak from ThC γ-rays into the region where it overlapped with the γ-ray noise.

The agreement between the two methods was satisfactory and the correction itself was often zero and always less than 2% of the total counts. The total

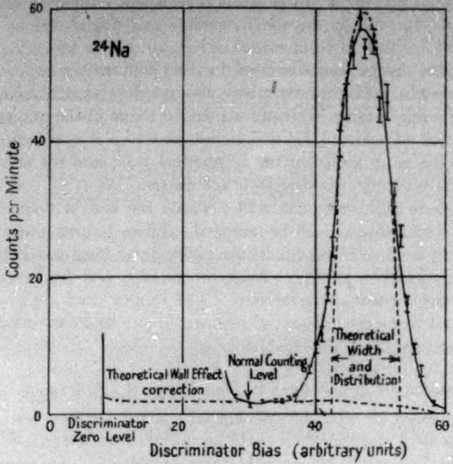

Figure 4. Differential bias curve for photo-protons from radio-sodium γ-rays.

——— observed curve.
– – – – ideal curve with no wall effect.
·–·–·– calculated counts due to wall effect.

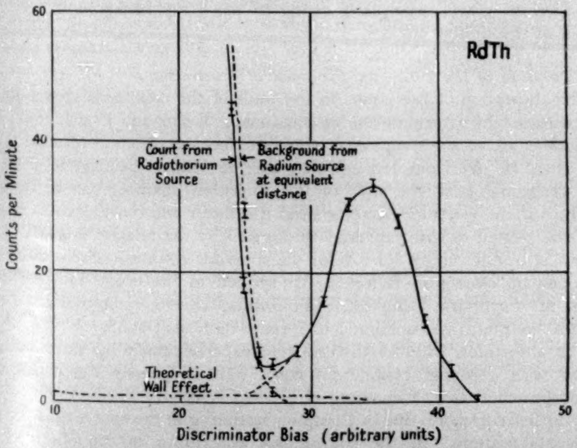

Figure 5. Differential bias curve for photo-protons from radio-thorium γ-rays.

——— observed curve.
– – – – γ-ray background from radium source giving the same ionization current.

observed number of disintegrations obtained in this way still has to be corrected, as follows :

(*a*) *Wall effect.*

Some 8% of the protons liberated in the chamber are not counted because they hit the walls. The number was estimated in the following way. The number of protons of range R produced within range of the wall of the chamber of area A is AR, of which $\frac{1}{4}AR$ will strike the wall if it is plane. This remains true to a second approximation for a spherical wall, and the main difficulty in calculating the wall effect is due to other causes.

Some protons will strike the wall towards the end of their range and will produce sufficient ionization to be counted. Thus, to give a concrete example, if the counting level is 150 kev. and the mean pulse height is 290 kev., the wall effect is approximately $\frac{1}{4}A(R_{290}-R_{140})$, where R_{290} and R_{140} are the ranges of 290 and 140 kev. protons respectively. The ranges used are given below and were calculated from the ranges of protons in air and the stopping power of hydrogen given by Gray (1944).

Estimated Proton Ranges in Deuterium at 760 mm. and 15° c.

Residual energy (kev.)	50	100	150	200	250	300
Range (mm.)	1·92	3·91	6·33	9·21	12·41	16·15

To some extent the correctness of the estimated wall effect can be checked by observing the minimum of the differential bias curve for radio-sodium (Figure 4) in the region where it should have fallen to zero. If the whole of the residual count is attributed to wall effect, the agreement between calculated and observed wall effect is good. A similar check could not be made when radio-thorium γ-rays were used owing to the γ-ray background overlapping the tail of the proton curve.

(*b*) *Absorption of the γ-rays in the walls of the counter.*

The absorption of the γ-rays in the walls of the counter is appreciable and was estimated by extending the calculations of Evans and Evans (1948). The calculations are to a certain extent simplified because quanta scattered through more than 10° by Compton collision can no longer disintegrate deuterium. Thus scattering from the ends of the ionization chamber can be neglected. For the various electrode systems used the mean effective thickness ϖ of the walls was related to the measured thickness t by the relation $\varpi = 1{\cdot}77t$ for the cylindrical counter and $\varpi = 1{\cdot}57t$ for the spherical counter. From these values the following correction factors to be applied to the crude value of σ were calculated : cylindrical counter, radio-sodium 1·0596, radio-thorium 1·0605 ; spherical counter, radio-sodium 1·053, radio-thorium 1·0538.

The absorption was also investigated experimentally by surrounding the counter with a copper cylinder of equal wall thickness. Agreement within the experimental error was obtained.

A further correction due to Compton scattering in the source must be made. Quanta scattered in the source will contribute to the observed γ-ray intensity as observed with an ionization chamber, but nearly all of them will have a quantum energy below the deuterium threshold because of the energy lost to the recoil electron. This effect was estimated roughly at 1·45% for measurements on the Paris chamber and 1·9% for measurements on the N.P.L. chamber. This particular type of correction is not necessary in the case of the radio-sodium source, which was calibrated absolutely through an aliquot: an ordinary correction for absorption in the source must be applied, but was in fact small (1·8%) owing to the shallow container in which it was placed. Because of the low specific intensity of the radio-sodium source the container was rather large and its average distance $\bar{r}$ from the ionization chamber had to be estimated from the formula

$$\frac{1}{\bar{r}^2}=\frac{1}{\rho^2}\left\{1+\frac{a^2}{5\rho^2}-\frac{x^2+y^2}{3\rho^2}\right\},$$

in which ρ is the corrected measured distance to the centre of the counter, a is the counter electrode radius, and $2x$ and $2y$ are the breadth and width of the square source.

(*c*) *Purity of the deuterium.*

The deuterium was made by electrolysing 99·5% heavy water, so that, allowing for an enrichment factor of 6, the gas produced electrolytically could have had up to 3% of ordinary hydrogen in it. After the plant had been running for some time the composition of the gas should have slowly approached that of the water. Since the possibility of exchange with ordinary hydrogen occurring in tap grease, etc., could hardly be avoided, samples of the deuterium gas from the ionization chambers were analysed with a mass spectrograph by Messrs. K. Wood and J. Blears at the Metropolitan-Vickers Research Laboratory, Trafford Park, Manchester. The deuterium concentration did not fall below 98·7% in any of the samples analysed. The measurements were made by assuming that the measured ionization current in the spectrometer was proportional to the concentration of the corresponding nucleus in the gas. The peaks measured were due to D_2^+ and DH^+ under conditions in which it had been verified that the discrimination between mass number 4 and mass number 2 was less than 10%.

(*d*) *Neutron background.*

The radio-thorium source emitted an appreciable number of fast neutrons which produced recoil protons in the ionization chamber. By bringing the source up to the side of the counter a countable number of high energy (up to 500 kv.) recoil protons was observed having a continuous energy distribution. The number to be expected in the energy range of the photo-protons could not be observed directly under these conditions because of the γ-ray fluctuations, but was estimated to be 2·2% by extrapolating the observed distribution into the γ-ray background. The extrapolation could be carried out with some confidence since it was based upon a blank experiment using a counter filled with ordinary hydrogen. No recoil protons were observed when a hydrogen-filled chamber was exposed to the radio-sodium source.

Results

Complete data for a typical run are shown in Table 2, and the collected results in Table 3.

Table 2. Radio-Sodium γ-Rays

Counter B, Run 2, 25th October 1948. Clock time running 0·3% fast.
Observed counts are already corrected for natural background of the ionization chamber.

				Corrected to 0000 G.M.T. 25.10.48.		
(1)	(2)	(3)	(4)	(5)	(6)	(7)
30	16·12	196·7	1·2	416·9	2·5	2%
	20·26	165·1	0·9	425·9	2·3	2%
	22·14	139·5	0·4	396·5	1·1	2%
	22·59	153·7	0·75	446·2	2·2	2%
	23·35	133·0	0·77	397·1	2·3	2%
32	16·58	188·3	0·8	413·5	1·7	½%
	16·21	188·7	1·3	412·8	2·8	3%
34	20·11	161·7	0·9	412·3	2·3	2%
	Mean counting rate at bias of 30 is 417·0					1%

(1) Discriminator bias; (2) mean time; (3) integral counting rate per minute; (4) differential counting rate per minute; (5) integral counting rate; (6) differential counting rate; (7) statistical accuracy in integral count.

The above table shows the experimental data from which was constructed the approximately horizontal portion of the differential bias curve shown in Figure 4. The remainder of the curve showing the pronounced peak at a bias of 47 is obtained in a separate experiment and is only used for calculating the subsequent corrections.

The total number of photo-protons, 417 per minute, is given by the integral counting rate at a bias 30, i.e. all those particles whose amplitude exceeds the threshold bias of 30. The choice of 30 is arbitrary, any point on the flat part of the differential bias curve could have been chosen. If a lower voltage had been chosen, a higher integral count would have been obtained, but the correction added for wall effect would have been less; if a higher bias voltage had been chosen, the integral count would have been smaller but the wall-effect correction to be added would have been greater.

If C is the mean counting rate at a bias of 30 (=417/minute), N the source strength at zero time $=1{\cdot}632\times10^{11}$ disintegrations/minute, ρ the distance between the centre of the sodium source and the centre of the counter $=21{\cdot}91$ cm., $\bar{r}$ the distance when corrected for the finite size of the source and counter $=22{\cdot}03$ cm., p the counter pressure $=6{\cdot}865$ atmospheres at 0° c. or 7·23 atmospheres at 15° c. (for use in calculating the wall-effect correction), V the volume of the counter $=30{\cdot}14$ cm^3, L Loschmidt's number $=2{\cdot}687\times10^{19}$, then the uncorrected value of the cross section σ is given by

$$\sigma=\frac{4\pi C\bar{r}^2}{2LVpN}=13{\cdot}94\times10^{-28}\text{ cm}^2.$$

The further corrections which have to be applied are given in Table 3, which also gives the results of other runs.

Discussion

Theoretical values of the cross section have been given by many authors, but those of Hansson and Hulthén (1949) correspond well with the conditions of our experiment. These authors have based their calculations upon the Møller-Rosenfeld theory and its variants, in which the static interaction in various states is of the form given below.

		State		
Type of theory	^{1}S	^{3}S	^{3}P	
Møller-Rosenfeld (MR)	$-A$	$-B$	$+B/3$	$\frac{e^{-\kappa r}}{r}$
Symmetrical (O)	$-A$	$-B$	O	
Neutral (S)	$-A$	$-B$	$-B$	

Table 3. Consolidated Results

	σ (uncorrected)	Wall absorption	Source absorption	Wall effect (%)	D_2+H_2/D_2	σ	$\sigma_{2\cdot 76}/\sigma_{2\cdot 62}$
A_1 Na	13·60	1·0596	1·015	7·72	1·00835	15·98	
RdTh	12·01	1·0605	1·015	4·7		13·68	1·17
B_1 Na	13·07	1·053	1·018	5·88	1·0082	15·01	
RdTh	12·33	1·0538	1·013	4·1		13·84	1·085
A_2 Na	12·97	1·0596	1·018	6·58	1·0161	15·22	
RdTh	12·19	1·0605	1·015	4·3		14·27	1·066
B_2 Na	13·94	1·053	1·018	6·87	1·0080	16·17	1·156
RdTh	12·43	1·0538	1·015	4·2		13·99	
A_3* Na	16·33	1·053	1·018	5·88	1·0136	——leak——	
RdTh	12·98	1·0538	1·015	5·78			
B_3* Na	14·39	1·053	1·018	5·67	1·0087	15·59	1·119
RdTh	12·38	1·0538	1·015	4·18		13·94	
					Mean Na	15·6	1·12
					Mean RdTh	13·9	

* The counters had both begun to leak after these fillings. With filling B_3 two radiothorium counts were taken which showed that the leak was small. The pressure was measured immediately after one of the counts so that there is less than ½% error introduced in the cross section quoted.

The estimated accuracy of these measurements is about 6% for the radio-thorium measurements and 5% for those using radio-sodium γ-rays. Since both measurements are made under very similar conditions, the observed ratio

$$\sigma_{2\cdot 76}/\sigma_{2\cdot 62}=1\cdot 12\pm 0\cdot 08$$

should be fairly immune from the effect of unsuspected systematic errors. The radiothorium cross section is different from the value $(14\cdot 8\pm 1)\times 10^{-28}$ cm^2 given in a preliminary note (Wilson 1948). The latter figure is an error owing to the inadvertent use of a wrong estimate of the effective number of quanta emitted from the radio-thorium source.

The values of A and B are adjusted to fit the observed neutron–proton scattering cross section and the known binding energy of the deuteron. The absolute cross section obtained is sensitive both to the binding energy of the deuteron and to the meson mass assumed.

As pointed out by Hansson and Hulthén, a good general fit with our results is obtained for a meson mass of 300 electron masses and a high (2·237 MeV.) value of the deuteron binding energy in agreement with the work of Bell and Elliot (1948). The degree of agreement obtained is shown by the results given below, taken from Hansson and Hulthén's calculations for a 2·237 MeV. binding energy.

	Meson mass = 200			Meson mass = 300		
$h\nu$	MR	O	N	MR	O	N
2·62	13·3	13·6	14·6	11·8	11·9	12·1
2·76	16·5	16·9	18·5	14·3	14·4	14·8
6·20	25·0	25·6	28·0	21·2	21·5	22·9

There still remains a substantial discrepancy with the measurements of van Allen and Smith, who found $\sigma = (11 \cdot 6 \pm 1 \cdot 5) \times 10^{-28}$ cm^2 for 6·2 Mev. quanta, and it is in this experimentally difficult energy range that the discrepancy between the cross section calculated from a Yukawa potential and the simple short range theory of Bethe and Peierls (1935) is greatest. Recent measurements (Barnes *et al.* 1950) are, however, in much better agreement with the calculated cross sections for a Yukawa potential. A certain discrepancy still remains between our results and the theoretical cross sections. This can well be expressed in terms of the ratio $\sigma_{2\cdot 76}/\sigma_{2\cdot 62}$, which we find to be 1·12 ± 0·08. The value derived from the theory is not very dependent upon meson mass or binding energy, and has a value of about 1·22. At this stage it is not possible to say that this discrepancy is well established. Owing to the very involved nature of the calibration of the radio-thorium source we are inclined to attach greater weight to the radio-sodium results, which are in fair agreement with the theoretical cross section based upon a high meson mass.

Further experimental work is being undertaken in collaboration with Dr. Siegbahn to establish the relative γ-ray intensities of the available sources upon a sounder basis.

ACKNOWLEDGMENTS

We have to thank Messrs. J. L. Putman and J. Willment for calibrating the radio-sodium sources by the coincidence method, Professor Hulthén for allowing us to see the results of his calculations before publication, and Professor Lord Cherwell for his continued interest and support of the work. Our thanks are also due to Messrs. K. Wood and J. Blears for the analysis of deuterium samples, to the Department of Scientific and Industrial Research for financial assistance to one of us (R.W.), and to Messrs. Thorium Ltd. who made up the radio-thorium sources according to our wishes.

REFERENCES

ALBRECHT, E., 1919, *S.B. Akad. Wiss. Wien*, IIa, 128, 925.

ALLEN, J. A., and SMITH, N. M., Jr., 1941, *Phys. Rev.*, **59,** 618.

BARNES, C. A., STAFFORD, G. H., and WILKINSON, D. H., 1950, *Nature, Lond.*, **165,** 69.

BELL, R. E., and ELLIOT, L. G., 1948, *Phys. Rev.*, **74,** 1552.

BETHE, H., 1940, *Phys. Rev.*, **57,** 260.

BETHE, H., and PEIERLS, R. E., 1935, *Proc. Roy. Soc.* A, **148,** 146.

BISHOP, G. R., WILSON, R., and HALBAN, H., 1950, *Phys. Rev.*, **77,** 416.

CHADWICK, J., FEATHER, N., and BRETSCHER, E., 1937, *Proc. Roy. Soc.* A, **163,** 366.

CHADWICK, J., and GOLDHABER, M., 1935, *Proc. Roy. Soc.* A, **151,** 479.

CURIE, M., 1912, *J. Phys. Radium*, (5), **2,** 795.

DUNWORTH, J. V., 1940, *Rev. Sci. Instrum.*, **11,** 167.

EVANS, R. D., and EVANS, R. O., 1948, *Rev. Mod. Phys.*, **20,** 305.

GIBSON, W. M., GREEN, L. L., and LIVESEY, D. L., 1947, *Nature, Lond.*, **160,** 534.

GRACE, M. A., ALLEN, R. A., and HALBAN, H., 1949, *Nature, Lond.*, **164,** 538.

GRAHAM, G. A. R., and HALBAN, H., 1945, *Rev. Mod. Phys.*, **17,** 297.

GRAY, L. H., 1936, *Proc. Roy. Soc.* A, **156,** 578; 1937, *Ibid.*, **159,** 263; 1944, *Proc. Camb. Phil, Soc.*, **40,** 72; 1949, *Brit. J. Radiol.*, **22,** 677.

HALBAN, H., 1938, *Nature, Lond.*, **141,** 644; 1938, *C. R. Acad. Sci., Paris*, **206,** 11, 90.

HALBAN, H., and WILSON, R., 1949, *J. Sci. Instrum.*, **26,** 424.

HAMERMESH, B., and WATTENBERG, A., 1949, *Phys. Rev.*, **75,** 1290.

HANSSON, I. F. E., and HULTHÉN, L., 1949, *Phys. Rev.*, **76,** 1163.

KAYE, G. W. C., ASTON, C. H., and PERRY, W. E., 1934, *Brit. J. Radiol.*, **7,** 540.

KOHMAN, T. R., AMES, D. P., and SEDLET, J., 1947, *Report MDDC.*, 852.

KOVARIK, A. F., and ADAMS, N. J., Jr., 1938, *Phys. Rev.*, **54,** 413.

LASSEN, N. O., 1948, *Phys. Rev.*, **74,** 1533.

Meiners, E. P., Jr., Smith, D. R., and Slack, L., 1949, *Phys. Rev.*, **75**, 1632.
Meitner, L., and Freitag, K., 1926, *Z. Phys.*, **37**, 481.
Myers, F. E., and van Atta, L. C., 1942, *Phys. Rev.*, **61**, 19.
Putman, J. L., 1950, *Brit. J. Radiol.*, **23**, 265.
Richardson, J. R., and Emo, L., 1938, *Phys. Rev.*, **53**, 234.
Ricoux, J., 1937, *J. Phys. Radium*, **8**, 388.
Russell, B., Sachs, D., Wattenberg, A., and Fields, R., 1948, *Phys. Rev.*, **73**, 545.
Rutherford, E., Chadwick, J., and Ellis, C. D., 1932, *Radiation from Radioactive Substances* (Cambridge : University Press).
Shenstone, A. G., and Schlundt, H., 1922, *Phil. Mag.*, **43**, 1038.
Siegbahn, K., 1946, *Phys. Rev.*, **70**, 127.
Snell, A. H., Barker, E. C., and Sternberg, R. L., 1949, *Phys. Rev.*, **75**, 1290.
Stafford, G. H., 1948, *Nature, Lond.*, **162**, 771.
Wäffler, H., and Younis, G., 1949, *Helv. Phys. Acta*, **22**, 414.
Wallmann, H., MacNee, A. B., and Gadsden, C. B., 1948, *Proc. Inst. Radio Engrs.*, **36**, 700.
Wiedenbeck, N. L., 1947, *Phys. Rev.*, **72**, 429.
Wilson, R., 1950, *Phil. Mag.*, **41**, 66.
Wilson, R., and Bishop, G. R., 1949, *Proc. Phys. Soc.* A, **62**, 457.
Wilson, R., Collie, C. H., and Halban, H., 1948, *Nature, Lond.*, **162**, 185; 1949, *Ibid.*, **163**, 245.
Winand, L., 1939, *J. Phys. Radium*, **10**, 361.
Woodward, W. M., and Halpern, I., 1949, *Phys. Rev.*, **76**, 107.

On the Lateral Spread of Extensive Air Showers

By L. JÁNOSSY
Dublin Institute for Advanced Studies

MS. received 6*th March* 1950

ABSTRACT. The lateral and angular spread of extensive showers is calculated in an approximation where ionization loss and incomplete screening are neglected (approximation A). The atmosphere is taken to be homogeneous. It is shown that the spread at the cascade maximum is equal to the average spread, but the spread increases considerably throughout the shower; the above results are in qualitative agreement with results given by Borsellino. The quantitative discrepancy between the results of Borsellino and other authors is commented on.

§ 1

In a recent paper Borsellino (1949) has calculated the lateral extension of air showers. His results differ from those obtained by other authors, see for example Nordheim and Roberg (1948); they also differ from results previously given by the author (1948). I wish to take this opportunity to elaborate my previous calculations and also to show how the discrepancy with Borsellino's results arises.

§ 2.

Considering a cascade in a homogeneous medium, the mean square angle of scatter or the lateral spread can be expressed according to Nordheim as follows:

$$\langle \vartheta^2 \rangle = A_0^2 \left(\frac{w_0}{w}\right)^2 \qquad \langle r^2 \rangle = A_1^2 \left(\frac{w_0}{w}\right)^2, \qquad \ldots\ldots(1)$$

where

$$A_k^2 = \int_0^\zeta d\zeta \int_0^{w_0} q(w_0, w', \zeta-\zeta') q(w', w, \zeta') \zeta'^{2k} \left(\frac{w}{w'}\right)^2 dw' / q(w_0, w, \zeta),$$
$$k=0, 1. \qquad \ldots\ldots(2)$$

Here $q(w_0, w, \zeta)\,dw$ is the average number of electrons with energies in an interval $w, w+dw$ at a depth ζ produced by a primary of energy w_0.

The integral (2) can be evaluated analytically provided we use the 'approximation A', i.e. neglect ionization loss and incomplete screening. In this approximation we have (e.g. Jánossy 1948, § 379)

$$q(w_0, w, \zeta) = \frac{1}{2\pi i w_0} \int_{y_0 - i\infty}^{y_0 + i\infty} \left(\frac{w_0}{w}\right)^y K(y, \zeta)\, dy, \qquad \ldots\ldots(3)$$

$$K(y, \zeta) = \frac{D - a_1}{a_2 - a_1} \exp(-a_1\zeta) + \frac{a_2 - D}{a_2 - a_1} \exp(-a_2\zeta), \qquad \ldots\ldots(4)$$

where a_1, a_2 stands for $a_1(y), a_2(y)$. Inserting (3) into (2) we find

$$A_k{}^2 q(w_0 w, \zeta) = \frac{w^2}{(2\pi i)^2 w_0} \int_0^\zeta d\zeta \int_0^\infty \frac{dw'}{w'^3} \int_{y_0' - i\infty}^{y_0' + i\infty} \left(\frac{w_0}{w'}\right)^{y'} K(y', \zeta - \zeta')\, dy'$$

$$\times \int_{y_0'' - i\infty}^{y_0'' + i\infty} \left(\frac{w'}{w}\right)^{y''} K(y'', \zeta')\zeta'^2\, dy''. \qquad \ldots\ldots(5)$$

Interchanging the order of integrations we can carry out first the integration over w'. Collecting the factors containing energies we have

$$w_0{}^{y'-1} w^{2-y''} \int_0^{w_0} w'^{\,y''-y'-3}\, dw' = \frac{1}{w_0}\left(\frac{w_0}{w}\right)^{y''-2} \frac{1}{y'' - y' - 2} \qquad \ldots\ldots(6)$$

provided $\mathrm{Re}(y'' - y') > 2$. We introduce (6) into (5); this is legitimate for $y_0'' > y_0' + 2$. The path of integration into y' can now be deformed into a loop round the singularity at $y' = y_0'' - 2$ and can be evaluated by the method of residua. This gives

$$A_k{}^2 q(w_0, w, \zeta) = \frac{1}{2\pi i w_0} \int_0^\zeta d\zeta \int_{y_0 - i\infty}^{y_0 + i\infty} \left(\frac{w_0}{w}\right)^y K(y, \zeta - \zeta') K(y+2, \zeta')\zeta'^{2k}\, dy, \qquad \ldots\ldots(7)$$

where we have written y for $y'' - 2$. Taking the Laplace transform of (7) with respect to ζ we find

$$\int_0^\infty e^{-\lambda\zeta} A_k{}^2 q(w_0, w, \zeta)\, d\zeta = \frac{1}{2\pi i w_0} \int_{y_0 - i\infty}^{y_0 + i\infty} \left(\frac{w_0}{w}\right)^y L_\lambda(y) \frac{\partial^{2k} L_\lambda(y+2)}{\partial\lambda^{2k}}\, dy, \qquad \ldots\ldots(8)$$

where

$$L_\lambda(y) = \int_0^\infty e^{-\lambda\zeta} K(y, \zeta)\, d\zeta \qquad \ldots\ldots(9)$$

and with the help of (4)

$$L_\lambda(y) = \frac{D - \lambda}{(a_1 + \lambda)(a_2 + \lambda)} \qquad \lambda > \mathrm{Re}\, a_1(y). \qquad \ldots\ldots(9a)$$

We evaluate (8) for $\lambda = 0$. We note that $L_0(y)$ has a pole for $y = 2$ as $a_1(2) = 0$ and further poles to the left. If $w_0 \gg w$, then the pole with the largest real part gives the greatest contribution to the integral (8) and we may write approximately

$$\int_0^\infty A_k{}^2 q(w_0, w, \zeta)\, d\zeta \simeq \left(\frac{w_0}{w}\right)^2 L_0(2) \left(\frac{\partial^{2k} L_\lambda(4)}{\partial\lambda^{2k}}\right). \qquad \ldots\ldots(10)$$

In the same approximation one can obtain the well-known formula

$$\int_0^\infty q(w_0, w, \zeta)\, d\zeta = \left(\frac{w_0}{w}\right)^2 L_0(2). \qquad \ldots\ldots(11)$$

Thus, defining an average A_k^2 as

$$\overline{A_k^2} = \int_0^\infty A_k^2 q(w_0, w, \zeta)\, d\zeta \Big/ \int_0^\infty q(w_0, w, \zeta)\, d\zeta \qquad \ldots\ldots(12)$$

we find

$$\overline{A_k^2} = \left(\frac{\partial^{2k} L_\lambda(4)}{\partial \lambda^{2k}}\right)_{\lambda=0}. \qquad \ldots\ldots(13)$$

In particular we have

$$\left.\begin{aligned} \overline{A_0^2} &= \left(\frac{D}{a_1 a_2}\right)_{y=4} = 0{\cdot}570 \\ \overline{A_1^2} &= \left(\frac{2}{a_1^3}\frac{D-a_1}{a_2-a_1} + \frac{2}{a_2^3}\frac{a_2-D}{a_2-a_1}\right)_{y=4} = 0{\cdot}725 \end{aligned}\right\} \qquad \ldots\ldots(14)$$

(Jánossy 1948, §§556–557).

§ 3

The integral (8) can be approximated for arbitrary values of λ in a similar way. The most important singularity in y is attained for $y = y_\lambda$ where y_λ is the largest root of

$$a_1(y) + \lambda = 0. \qquad \ldots\ldots(15)$$

We have thus

$$\int_0^\infty e^{-\lambda\zeta} A_k^2 q(w_0, w, \zeta)\, d\zeta \simeq \frac{1}{w_0}\left(\frac{w_0}{w}\right)^{y_\lambda} \frac{D-a_1}{a_1'(y_\lambda)(a_2-a_1)} \frac{\partial^{2k} L_\lambda(y_\lambda+2)}{\partial \lambda^{2k}}.$$

For simplicity we replace $\simeq$ by the equal sign, and write y instead of y_λ; taking the inverse transform of the above equation we have thus

$$A_k^2 q(w_0, w, \zeta) = \frac{1}{2\pi i w_0} \int_{\lambda_0 - i\infty}^{\lambda_0 + i\infty} e^{\lambda\zeta} \left(\frac{w_0}{w}\right)^y \frac{D-a_1}{a_2-a_1} \frac{\partial^{2k} L_\lambda(y+2)}{\partial \lambda^{2k}} \frac{d\lambda}{a_1'(y)}.$$

We change the integration variable from λ to y with the help of (15) and find

$$A_k^2 q(w_0, w, \zeta) = \frac{1}{2\pi i w_0} \int_{y_0 - i\infty}^{y_0 + i\infty} \exp\{-a_1(y)\zeta\} \left(\frac{w_0}{w}\right)^y \frac{D-a_1}{a_2-a_1} \frac{\partial^{2k} L_\lambda(y+2)}{\partial \lambda^{2k}}\, dy. \qquad \ldots\ldots(16)$$

The above integral can be evaluated by the saddle-point method. We note however, that, apart from the last factor of the integrand, the integral is one which is often used to represent $q(w_0, w, \zeta)$. Regarding therefore the last factor under the integrand as a slowly varying function, we can replace it by its value at the saddle point. In this approximation we can divide both sides of (16) by $q(w_0, w, \zeta)$ and find

$$A_k^2 = \left(\frac{\partial^{2k} L_\lambda(y_0+2)}{\partial \lambda^{2k}}\right)_{\lambda = -a_1(y_0)}. \qquad \ldots\ldots(17)$$

The value of y_0 has to be determined in the usual way from the saddle-point condition, namely

$$-a_1'(y)\zeta + \ln\left(\frac{w_0}{w}\right) + \frac{\partial}{\partial y}\left(\ln \frac{D-a_1}{a_2-a_1}\right) = 0 \qquad \text{for} \quad y = y_0. \qquad \ldots\ldots(18)$$

Equation (17) is written explicitly as

$$\left.\begin{aligned} A_0^2 &= \frac{D-a_1(y)}{[a_1(y+2)-a_1(y)]\,[a_2(y+2)-a_1(y)]}, \\ A_1^2 &= \frac{2}{[a_1(y+2)-a_1(y)]^3}\,\frac{D-a_1(y+2)}{a_2(y+2)-a_1(y+2)} \\ &\quad + \frac{2}{[a_2(y+2)-a_1(y)]^3}\,\frac{a_2(y+2)-D}{a_2(y+2)-a_1(y+2)}. \end{aligned}\right\} \quad \ldots\ldots(19)$$

Equations (18) and (19) give a parameter representation of the lateral spread. Comparing (19) and (14) we see that $(A_k^2)_{y=2}=\overline{A_k^2}$. *Thus the spread of the shower at the maximum is equal to the spread averaged over depth.*

§ 4

In the Table we have collected relevant numerical data. The results are also represented in Figure 1. The abscissa is $\log w_0/w$, ordinate ζ. The straight lines represent regions of constant spread; these are labelled with the corresponding values of A_1. Orbits of constant shower size are also plotted; these

y	$A_0(y)$	$A_1(y)$	$\zeta=\alpha(y)\log(w_0/w)-\beta(y)$		$\log(w_0/w)$	
			$\alpha(y)$	$\beta(y)$	$\zeta=14$	$\zeta=25$
1·1	0·433	0·117	0·092	−0·009	—	—
1·2	0·510	0·195	0·244	−0·005	—	—
1·3	0·563	0·268	0·426	0·012	—	—
1·4	0·604	0·339	0·630	0·042	—	—
1·5	0·638	0·412	0·856	0·084	—	—
1·6	0·668	0·488	1·101	0·140	—	—
1·7	0·694	0·568	1·368	0·213	—	—
1·8	0·717	0·654	1·658	0·305	8·628	—
1·9	0·737	0·748	1·976	0·418	7·297	—
2·0*	0·755	0·851	2·325	0·554	6·260	—
12·	0·771	0·968	2·711	0·718	5·429	9·487
2·2	0·785	1·100	3·141	0·913	4·748	8·250
2·3	0·798	1·250	3·622	1·140	4·180	7·217
2·4	0·809	1·422	4·163	1·403	3·700	6·342
2·5	0·819	1·619	4·772	1·704	3·291	5·596
2·6	0·828	1·846	5·460	2·045	2·939	4·953
2·7	0·836	2·104	6·236	2·428	—	4·398
2·8	0·844	2·399	7·112	2·853	—	3·916
2·9	0·850	2·733	8·099	3·321	—	3·497
3·0	0·856	3·110	9·208	3·833	—	—
3·1	0·861	3·535	10·451	4·389	—	—
3·2	0·866	4·010	11·839	4·989	—	—
3·3	0·870	4·539	13·384	5·632	—	—
3·4	0·874	5·126	15·097	6·319	—	—
3·5	0·878	5·774	16·991	7·048	—	—
3·6	0·881	6·487	19·077	7·821	—	—
3·7	0·885	7·269	21·367	8·637	—	—
3·8	0·888	8·118	23·873	9·495	—	—
3·9	0·891	9·052	26·605	10·394	—	—
4·0	0·895	10·055	29·578	11·337	—	—

* Average.

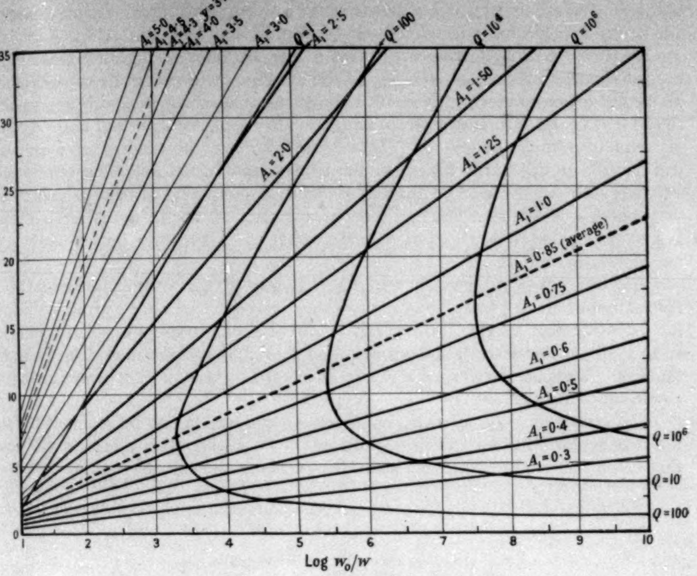

Figure 1.

The lateral spread of air showers.
Straight lines give the location of constant spread in the (log w_0/w, ζ) plane.
Lines of constant shower size ($Q=1$, 100, 10,000, 1,000,000 are also shown).

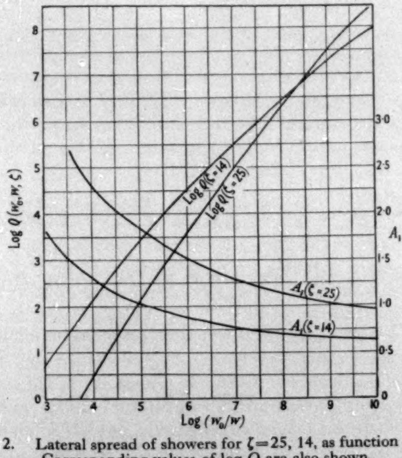

Figure 2. Lateral spread of showers for $\zeta=25$, 14, as function of energy.
Corresponding values of log Q are also shown.

show the average numbers Q of particles with energy above w. Figure 2 shows the lateral spread of showers for $\zeta=25$ (sea level) and also for $\zeta=14$.

As can be seen both from inspection of the Table or of Figure 1 the lateral spread of a shower increases with ζ and the increase continues quite considerably above the average value; this result is in qualitative agreement with the results found by Borsellino. Indeed from equation (19) it can be seen that both A_0 and A_1 tend to infinity for $y\to\infty$. This does not mean, however, that a shower can develop an arbitrarily big spread, as can be seen in the following way. For very large depth ζ the average number of particles $Q(w_0, w, \zeta)$ in a shower becomes very much smaller than unity. This means that at such depths the shower has usually no particle left, but in exceptional cases one may be left and only very rarely more than one.

The one surviving particle can have arrived there only as a result of a fluctuation of energy loss; thus it must have travelled without serious collision for a considerable length. Along this length this one particle may have moved at an angle to the original shower axis and thus it may have moved away from the axis. Thus the large spread is simply caused by the moving away of such a single surviving particle.

The question arises, what is the largest spread which can be reached before the number of particles has been reduced? To answer this question we note that the number of particles in a shower can be represented (Jánossy 1948) as

$$\ln Q(w_0, w, \zeta)=\ln\frac{w_0}{w}\left(y-\frac{a_1}{a_1'}\right)+\text{terms depending only weakly on } w,$$

and

$$\zeta=\frac{1}{a_1'}\ln\frac{w_0}{w}+\text{terms depending on } y.$$

For values of y for which $y-a_1/a_1'>0$, Q can be made large by choosing $\ln(w_0/w)$ sufficiently large. On the other hand for $y-a_1/a_1'<0$, Q is always small. From the tables of a_1 and a_1' we find $y-a_1/a_1'=0$ for $y=3{\cdot}27$. Thus for $y>3{\cdot}27$ all showers are small. Therefore $A_1=4{\cdot}3$ for $y=3{\cdot}27$ is the upper limit for genuine spread, i.e. for spread at a stage where the shower may still contain many particles.

The strong increase of shower spread with depth shows that the spread develops over large distances. This makes it likely that showers developing in the inhomogeneous atmosphere show a spread rather larger than that calculated for a homogeneous medium. We hope to return to this question in the future.

§ 5

In deriving expressions for A_k^2 we have inserted (3) into (2). Instead we might have integrated (2) in ζ thus

$$\int_0^\infty A_k^2 q(w_0, w, \zeta)\,d\zeta=\int_0^{w_0}\left(\frac{w}{w'}\right)^2 dw'\int_0^\infty q(w_0, w', \zeta)\,d\zeta\int_0^\infty q(w', w, \zeta)\zeta^{2k}\,d\zeta. \qquad \ldots\ldots(20)$$

Introducing into (20) the following approximate expression derived from (3) and (8) (see also (11)), viz.

$$\int_0^\infty \zeta^{2k} q(w_0, w', \zeta)\,d\zeta=\frac{w_0}{w'^2}\left(\frac{\partial^{2k}}{\partial\lambda^{2k}}L_0(\lambda)\right)_{\lambda=2} \qquad \ldots\ldots(21)$$

we find

$$\int_0^\infty A_k^2 q(w_0, w, \zeta)\,d\zeta=L_0(2)\left(\frac{\partial^2}{\partial\lambda^2}L_0(\lambda)\right)_{\lambda=2}. \qquad \ldots\ldots(22)$$

The equation (22) is, however, very inaccurate, the inaccuracy arising from the fact that equation (21) is valid only for $w_0 \gg w'$ whereas in inserting (21) into (20) it is used essentially for values $w_0 \sim w'$, as this region gives the most important contribution to the integral in (20). This inaccuracy accounts for the discrepancies mentioned at the beginning of this article.

REFERENCES

Borsellino, A., 1949, *Nuovo Cim.*, Vol. VI, No. 6.
Jánossy, L., 1948, *Cosmic Rays*, see in particular §§ 556–558 (Oxford : University Press).
Nordheim, L. W., and Roberg, J., 1948, *Phys. Rev.*, **75**, 444.

On the Use of β-Formalism of the Meson Field for Nuclear Interactions

By VACHASPATI*
Department of Physics, University of Delhi, Delhi, India

MS. received 14*th December* 1949

ABSTRACT. Following a method due to Harish-Chandra, a correspondence between the Proca and the β-formalisms of the meson field theory is developed. An important feature of the method is that one can at any stage of calculations pass over from one formalism to the other. No explicit representation of the β-matrices is required nor need one know the exact relationship between the elements of the wave function ψ and the Proca field quantities U_μ and $G_{\mu\nu}$. This introduces considerable simplification in the introduction of nuclear interaction as compared with earlier treatments where one has to choose a special explicit representation of the β_μ's and identify the various elements of the matrix ψ with the components of U_μ and $G_{\mu\nu}$. The nuclear interaction is, in fact, here introduced very simply in an elegant way. The quantization is performed for the vector, scalar and pseudoscalar cases assuming in all cases both charge and dipole types of couplings. As an illustration of the method we calculate the scattering of positively charged mesons by protons. The spur calculations, so tedious in the earlier works, are now replaced by simple relations which are easily handled, and the results are obtained with about as much labour as is used in Proca's case with the additional advantage that both the longitudinal and the transverse parts of the meson field can here be treated together.

INTRODUCTION

FOLLOWING a method developed by Harish-Chandra (1947, 1948), we establish here a correspondence between the wave and the particle aspects of the meson theory. One of the important features of this method is that one can at any stage pass over from the β-formalism to Proca's equations or vice versa. No explicit representation of the β matrices is required, nor need one know the exact relation between the components of the wave function ψ and the Proca's field quantities U_μ and $G_{\mu\nu}$. This introduces considerable simplification in the introduction of nuclear interaction as compared with Wilson's (1941) treatment where one has to choose a special representation of the β_μ's and identify the various elements of the matrix ψ with the components of U_μ and $G_{\mu\nu}$. The nuclear interaction can, in fact, be now introduced very simply in an elegant way. The spur calculations also, so tedious in the former calculations, are now replaced

---

[*] All India Research Fellow of the University of Delhi. Present address : Physikalisches Institut eidgenossische Hochschule, Zürich, Switzerland.

by simple relations which are easily handled. These equations are quantized here for vector, scalar and pseudoscalar meson fields. As an illustration of the method, we calculate the scattering of a positively charged meson by a proton. The calculations in this case have already been done by Wilson (1941) and our result agrees completely with his. This method has been applied by the Delhi group of physicists working with Professor R. C. Majumdar to a number of other problems.

§ 1. THE FREE FIELD

(i) *Some Results of Harish-Chandra's*

It is well known that the wave equations of the meson field can be written in the form

$$i\beta^\mu \frac{\partial\psi}{\partial x^\mu} + \chi\psi = 0, \qquad \ldots\ldots(1)$$

where ψ is a column matrix with 5 elements in the case of scalar mesons and 10 in the case of vector mesons; β^μ's are four 5 × 5 or 10 × 10 matrices according as the wave field is scalar or vector. The β_μ's obey the commutation rules

$$\beta^\mu\beta^\nu\beta^\varrho + \beta^\varrho\beta^\nu\beta^\mu = g^{\mu\nu}\beta^\varrho + g^{\nu\varrho}\beta^\mu. \qquad \ldots\ldots(2)$$

We follow here the convention that the Greek suffixes can take the values 0, 1, 2, 3 while the Latin suffix can take only 1, 2, 3. The fundamental metric tensor $g_{\mu\nu}$ is given by

$$g_{00} = -g_{11} = -g_{22} = -g_{33} = 1, \qquad g_{\mu\nu} = 0 \ (\mu \neq \nu).$$

The equivalence of the equation (1) with the wave equations of the Proca field can be shown by taking a suitable representation of the β^μ's. Harish-Chandra (1947, 1948) has, however, shown that the equivalence can be established without making use of any such explicit representation. We first give a summary of his results with slight changes of notation.

The Hermitian conjugate of (2) is

$$\beta^{\mu *}\beta^{\nu *}\beta^{\varrho *} + \beta^{\varrho *}\beta^{\nu *}\beta^{\mu *} = g^{\mu\nu}\beta^{\varrho *} + g^{\nu\varrho}\beta^{\mu *}.$$

$\beta_\mu{}^*$'s thus follow the same commutation rules as the β_μ's. There thus exists a matrix Λ, which can always be chosen to be Hermitian, such that

$$\Lambda\beta^\mu\Lambda^{-1} = \beta^{\mu *}. \qquad \ldots\ldots(3)$$

Writing

$$\psi^\dagger = \psi^*\Lambda, \qquad \ldots\ldots(4)$$

we get the equation conjugate to (1):

$$-i\frac{\partial\psi^\dagger}{\partial x^\mu}\beta^\mu + \chi\psi^\dagger. \qquad \ldots\ldots(5)$$

It can be shown that for spin 0 and 1 there exist one column matrices $\daleth_\mu$ such that $\psi^\dagger\daleth_\mu$ transforms as a vector. Also, we write

$$\Gamma_\mu{}^\dagger \equiv \daleth_\mu{}^*\Lambda, \qquad \ldots\ldots(6)$$

$$\beta \equiv \daleth_\mu\Gamma^{\mu\dagger}. \qquad \ldots\ldots(7)$$

The following relations are then easily established

$$\beta^2=\beta, \tag{I a}$$

$$\beta\beta_\mu+\beta_\mu\beta=\beta_\mu, \tag{I b}$$

$$\Gamma_\mu^\dagger\rceil_\nu=g_{\mu\nu}, \tag{I c}$$

$$\Gamma_\mu^\dagger\beta_\nu\rceil_\varrho=0. \tag{I d}$$

The relations (I) are independent of the commutation rules (2). In the case of spin 1 the following relations hold:

$$\beta_\mu\beta_\nu\beta_\varrho=g_{\mu\nu}\rceil_\varrho+g_{\mu\varrho}\rceil_\nu, \tag{V a}$$

$$\Gamma_\mu^\dagger\beta_\nu\beta_\varrho=\Gamma_\mu^\dagger g_{\nu\varrho}-\Gamma_\nu^\dagger g_{\mu\varrho}, \tag{V b}$$

$$\beta_\mu\rceil_\nu=-\beta_\nu\rceil_\mu, \tag{V c}$$

$$\Gamma_\mu^\dagger\beta_\nu=-\Gamma_\nu^\dagger\beta_\mu, \tag{V d}$$

$$\beta+\tfrac{1}{2}\beta_\mu\beta\beta^\mu=1. \tag{V e}$$

For spin 0 the following relations hold:

$$\beta_\mu\beta_\nu\rceil_\varrho=\rceil_\mu g_{\nu\varrho}, \tag{S a}$$

$$\Gamma_\mu^\dagger\beta_\nu\beta_\varrho=g_{\mu\nu}\Gamma_\varrho^\dagger, \tag{S b}$$

$$\beta_\mu\rceil_\nu=\tfrac{1}{4}g_{\mu\nu}\beta_\varrho\rceil^\varrho, \tag{S c}$$

$$\Gamma_\mu^\dagger\beta_\nu=\tfrac{1}{4}g_{\mu\nu}\Gamma_\varrho^\dagger\beta^\varrho, \tag{S d}$$

$$\beta+\tfrac{1}{4}\beta_\mu\beta\beta^\mu=1, \tag{S e}$$

$$\beta_\mu\beta_\nu\beta_\varrho=g_{\mu\nu}\beta_\varrho\beta+\beta\beta_\mu g_{\mu\nu}. \tag{S f}$$

With the help of $\rceil_\mu$ and $\Gamma_\mu^\dagger$, equations (1) and (5) can be transcribed to Proca's form if we write:

For spin 1

$$\Gamma_\mu^\dagger\psi=\sqrt{\frac{\chi}{\hbar c}}\,U_\mu, \qquad \ldots\ldots(8)$$

$$\Gamma_\mu^\dagger\beta_\nu\psi=\frac{i}{\sqrt{(\hbar c\chi)}}\,G_{\mu\nu} \qquad \ldots\ldots(9)$$

and their complex conjugates. Multiplying (1) by $\Gamma_\nu^\dagger$, we get

$$\frac{\partial G_{\mu\nu}}{\partial x_\nu}+\chi^2U_\nu=0,$$

and, multiplying by $\Gamma_\nu^\dagger\beta_\mu$,

$$G_{\mu\nu}=\frac{\partial U_\nu}{\partial x^\mu}-\frac{\partial U_\mu}{\partial x^\nu}.$$

For spin 0

$$\Gamma_\mu^\dagger\psi=\frac{1}{\sqrt{(\hbar c\chi)}}\,F_\mu, \qquad \ldots\ldots(10)$$

$$\Gamma_\mu^\dagger\beta_\nu\psi=i\sqrt{\frac{\chi}{\hbar c}}\,Ug_{\mu\nu}, \qquad \ldots\ldots(11)$$

giving

$$F_\mu=\frac{\partial U}{\partial x^\mu}$$

and

$$\frac{\partial F^\mu}{\partial x^\mu}+\chi^2U=0.$$

(ii) *Lagrangian, Energy-momentum Tensor, and Current Vector Density*

The wave equations (1) and (5) can be derived by the variation of a Lagrangian

$$\alpha^M = \int L^M \, d^4x,$$

where
$$L^M = \frac{i\hbar c}{8\pi}\left[\psi^\dagger \beta^\mu \frac{\partial\psi}{\partial x^\mu} - \frac{\partial\psi^\dagger}{\partial x^\mu}\beta^\mu\psi\right] + \frac{\hbar c\chi}{4\pi}\psi^\dagger\psi. \qquad \ldots\ldots(12)$$

L^M vanishes if the wave equations are satisfied. For energy-momentum tensor we obtain

$$T_{\mu\nu} = \frac{i\hbar c}{8\pi}\left[\psi^\dagger \beta_\nu \frac{\partial\psi}{\partial x^\mu} - \frac{\partial\psi^\dagger}{\partial x^\mu}\beta_\nu\psi\right] - Lg_{\mu\nu}$$
$$= \frac{\hbar c\chi}{4\pi}\psi^\dagger(g_{\mu\nu} - \beta_\mu\beta_\nu - \beta_\nu\beta_\mu)\psi + \frac{i\hbar c}{8\pi}\frac{\partial}{\partial x^\varrho}[\psi^\dagger(\beta_\varrho\beta_\mu\beta_\nu - \beta_\nu\beta_\mu\beta_\varrho)\psi].$$

$T_{\mu\nu}$ is not symmetrical in μ and ν. We define therefore

$$\theta_{\mu\nu} = T_{\mu\nu} - \frac{i\hbar c}{8\pi}\frac{\partial}{\partial x^\varrho}[\psi^\dagger(\beta_\varrho\beta_\mu\beta_\nu - \beta_\nu\beta_\mu\beta_\varrho)\psi]$$
$$= \frac{\hbar c\chi}{4\pi}\psi^\dagger(g_{\mu\nu} - \beta_\mu\beta_\nu - \beta_\nu\beta_\mu)\psi. \qquad \ldots\ldots(13)$$

We note
$$\int \theta_{\mu 0}\, d^3x = \int T_{\mu 0}\, d^3x.$$

When translated in terms of $G_{\mu\nu}$ and U_μ, (13) agrees completely with the energy-momentum tensor usually employed for Proca's vector meson field. For scalar field, however, one finds that the two expressions differ by a minus sign. This situation can be remedied by taking for the Lagrangian for the scalar meson field an expression (-1) times equation (12). As, however, in actual problems this is not of much importance, we shall retain for the Lagrangian the same expression (12) for both scalar and vector meson fields.

From (13) we get the Hamiltonian density

$$H = \theta_{00} = \frac{\hbar c\chi}{4\pi}\psi^\dagger\eta_0\psi = \frac{\hbar c\chi}{4\pi}\psi^*\Lambda\eta_0\psi. \qquad \ldots\ldots(14)$$

This is positive definite if we choose

$$\Lambda = \eta_0 \qquad \ldots\ldots(15)$$

where
$$\eta_0 \equiv 1 - 2\beta_0{}^2. \qquad \ldots\ldots(16)$$

We notice that $\eta_0{}^2 = 1$ and $\Lambda^{-1} = \eta_0$.

The current density four-vector

$$j_\mu = -\frac{e}{4\pi}\psi^\dagger\beta_\mu\psi, \qquad \ldots\ldots(17)$$

so that, with the help of (15),

$$j_0 = \frac{e}{4\pi}\psi^*\beta_0\psi. \qquad \ldots\ldots(18)$$

The expression (17) also agrees with the corresponding expression in the case of Proca's field, except for a minus sign in the scalar case.

This establishes complete correspondence between the two aspects of the meson field. We proceed next to transform separately the free vector and the scalar meson fields to momentum space. The treatment follows closely that of Booth and Wilson (1940).

(iii) Vector Meson Field in Momentum Space

ψ is easily seen to satisfy the second order wave equation

$$\frac{\partial^2\psi}{\partial x_\nu \partial x^\nu} + \chi^2\psi = 0.$$

We can therefore introduce a plane wave solution

$$\psi_A = u_A \exp(\mp ik_0x_0 + i\mathbf{kx}) \qquad \text{......(19')}$$

$A = 1, 2, \ldots .\ 10,\ k_0 = (k^2 + x^2)^{1/2}$.

For a given $\mathbf{k}$ there exist six independent solutions of (1). We label these by the suffixes $l, m, n, \ldots .$ The most general solution of (1) with a given $\mathbf{k}$ is therefore a linear combination of all these six solutions:

$$\psi_A = \sqrt{(4\pi)} \sum_{l=1}^{6} a_l u_{Al} \exp(-ik_{0l}x_0 + i\mathbf{kx}), \qquad \text{......(19)}$$

where

$$\left.\begin{aligned} k_{01} &= k_{02} = k_{03} = k_0, \\ k_{04} &= k_{05} = k_{06} = -k_0. \end{aligned}\right\} \qquad \text{......(20)}$$

We have here introduced $\sqrt{(4\pi)}$ for reasons of normalization and have supposed the eigenvibrations to be confined in a unit volume.

We postulate the relations

$$\sum_{A=1}^{10} u_{Al}{}^* u_{Am} = \frac{k_0}{\chi}\delta_{lm}, \qquad l, m = 1, 2, \ldots 6 \qquad \text{......(21)}$$

and

$$\sum_{A,B=1}^{10} u_{Al}{}^*(\beta_0)_{AB} u_{Bm} = (\beta_0)_{lm}, \qquad \text{......(22)}$$

so that

$$H = \hbar c x \sum_{A=1}^{10} \sum_{l,m=1}^{6} a_l{}^* a_m u_{Al}{}^* u_{Am} \exp\{i(k_{0l} - k_{0m})x_0\}$$

$$= \hbar c k_0 \sum_{l=1}^{6} a_l{}^* a_l \qquad \text{......(23)}$$

and

$$j_0 = e \sum_{A=1}^{10} \sum_{l,m=1}^{10} a_l{}^* u_{Al}{}^*(\beta_0)_{AB} a_m u_{Bm} \exp\{i(k_{0l} - k_{0m})x_0\}$$

$$= e \sum_{l=1}^{6} a_l{}^*(\beta_0)_{lm} a_m \qquad \text{......(24)}$$

$$= e \sum_{l=1}^{3} a_l{}^* a_l - e \sum_{l=4}^{6} a_l{}^* a_l, \qquad \text{......(25)}$$

where we have taken a representation of the β^μ's in which β_0 is Hermitian and diagonal, the first three diagonal elements having the values 1, the next three -1, and the rest are zero. It then follows that β^k's ($k = 1, 2, 3$) are anti-Hermitian. We may also derive an orthogonality relation inverse to (22):

$$\sum_{B,C=1}^{10} \sum_{l,m=1}^{6} \{(\beta_0{}^2)_{AB} u_{Bl}\}(\beta_0)_{lm}\{u_{lm}{}^*(\beta_0{}^2)_{CD}\} = (\beta_0)_{AD}, \qquad A, D = 1, 2, \ldots 10, \qquad \text{......(26)}$$

which can be written simply as

$$\sum_{l,m=1}^{6} (\beta_0^2 u_l)_A (\beta_0)_{lm} (u_m^* \beta_0^2)_B = (\beta_0)_{AB}. \qquad \ldots\ldots(27)$$

One can easily derive the initial conditions analogous to those employed in Proca's method. Multiplying (1) by $1-\beta_0^2$ from the left and noting that

$$\beta_0^3 = \beta_0, \qquad \beta_0^2\beta_k + \beta_k\beta_0^2 = \beta_k,$$

we get

$$\psi = \beta_0^2\psi - \frac{i}{\chi}\beta_k\beta_0^2\frac{\partial\psi}{\partial\chi_k}. \qquad \ldots\ldots(28)$$

Similarly, from (5),

$$\psi^\dagger = \psi^\dagger\beta_0^2 + \frac{i}{\chi}\frac{\partial\psi^\dagger}{\partial x_k}\beta_0^2\beta_k. \qquad \ldots\ldots(29)$$

(28) and (29) do not involve time and serve as initial conditions.

Applying (28), (29) to (14) and noting that

$$\beta_0\beta_k\beta_0 = 0,$$

we get

$$H = -\frac{\hbar c\chi}{4\pi}\left[\psi^\dagger\beta_0^2\psi - \frac{1}{x^2}\frac{\partial\psi^\dagger}{\partial x_k}\beta_0^2\beta_k\beta_l\beta_0^2\frac{\partial\psi}{\partial x_l}\right]$$

$$= \frac{\hbar c\chi}{4\pi}\psi^*\beta_0^2\left\{1 - \frac{(\mathbf{k\beta})^2}{\chi^2}\right\}\beta_0^2\psi, \qquad \ldots\ldots(30)$$

where

$$(\mathbf{k\beta}) = -k^l\beta_l.$$

(iv) *Scalar Meson Field*

The most general solution corresponding to (19) in the vector case is here

$$\psi_A = \sqrt{(4\pi)}\sum_{l=1,2} a_l u_{Al}\exp(-ik_{0l}x_0 + i\mathbf{kx}), \qquad A = 1, 2, \ldots 5, \qquad \ldots\ldots(31)$$

where

$$k_{01} = k_0, \qquad k_{02} = -k_0. \qquad \ldots\ldots(32)$$

The orthogonality relations corresponding to (21) and (22) are

$$\sum_{A=1}^{5} u_{Al}^* u_{Am} = \frac{k_0}{\chi}\delta_{lm}, \qquad (l, m = 1, 2) \qquad \ldots\ldots(33)$$

and

$$\sum_{A,B=1}^{5} u_{Al}^*(\beta_0)_{AB} u_{Bm} = (\beta_0)_{lm}. \qquad \ldots\ldots(34)$$

The Hamiltonian density

$$H = \hbar c k_0 \sum_{l=1,2} a_l^* a_l \qquad \ldots\ldots(35)$$

and charge density

$$j_0 = e\sum_{l=1,2} a_l^*(\beta_0)_{lm} a_m \qquad \ldots\ldots(36)$$

$$= e(a_1^* a_1 - a_2^* a_2). \qquad \ldots\ldots(37)$$

We have here, too, taken the representation of β^μ's in which β_0 is diagonal, the first element being 1, the next —1, and the remaining three zero.

The inverse orthogonality relation is

$$\sum_{B,C=1}^{5}\sum_{l,m=1,2}\{(\beta_0^2)_{AB}u_{Bl}\}(\beta_0)_{lm}\{u_{lm}^*(\beta_0^2)_{CD}\} = (\beta_0)_{AD}, \qquad A, D = 1, 2, \ldots 5, \qquad \ldots\ldots(38)$$

which can be written simply as

$$\sum_{l,m=1,2} (\beta_0{}^2)u_{lA}(\beta_0)_{lm}(u_m{}^*\beta_0{}^2)_B=(\beta_0)_{AB}. \qquad \ldots\ldots(39)$$

The initial conditions are the same as (28) and (29) and the Hamiltonian density is given by (30).

§ 2. INTERACTION WITH NUCLEAR PARTICLES AND QUANTIZATION

With the help of the matrices ⅂_μ and $\Gamma_\mu{}^\dagger$ introduced in the previous section, we can now introduce nuclear interaction in a simple way. We treat the vector and the scalar cases separately.

(i) *Vector Meson Field*

We assume that in the presence of nuclear particles the Lagrangian density is given by

$$L=\frac{i\hbar c}{8\pi}\left[\psi^\dagger\beta^\mu\frac{\partial\psi}{\partial x^\mu}-\frac{\partial\psi^\dagger}{\partial x^\mu}\beta^\mu\psi\right]+\frac{\hbar c\chi}{4\pi}\psi^\dagger\psi-g_1\sqrt{\left(\frac{\hbar c}{\chi}\right)}[R_\mu{}^*\Gamma^{\mu\dagger}\psi+R_\mu\psi^\dagger\text{⅂}^\mu]$$
$$+\frac{i}{2}g_2\sqrt{(\hbar c\chi)}[P_{\mu\nu}{}^*\Gamma^{\mu\dagger}\beta^\nu\psi-\mathrm{P}_{\mu\nu}\psi^\dagger\beta^\nu\text{⅂}^\mu] \qquad \ldots\ldots(40)$$

(g_1 and g_2 are coupling constants of dimensions of charge e and of a length times e respectively).

$$R_\mu=\phi^\dagger\gamma_\mu\tau_{\mathrm{NP}}\phi, \qquad \mathrm{P}_{\mu\nu}=i\phi^\dagger\gamma_\mu\gamma_\nu\tau_{\mathrm{NP}}\phi.$$

Here ϕ is the compound wave function of the neutron–proton

$$\phi=\begin{pmatrix}\phi_{\mathrm{P}}\\ \phi_{\mathrm{N}}\end{pmatrix} \qquad (\phi^\dagger=\phi^*\gamma_0)$$

obeying the absence of mesons in the wave equation

$$i\gamma^\mu\frac{\partial\phi}{\partial x^\mu}+\frac{1}{\hbar}(M_{\mathrm{P}}\tau_{\mathrm{P}}+M_{\mathrm{N}}\tau_{\mathrm{N}})\phi=0,$$

$$(M_{\mathrm{P}}=\text{mass of proton}; \quad M_{\mathrm{N}}=\text{mass of neutron}).$$

The γ^μ's satisfy the commutation relations $\gamma^\mu\gamma^\nu+\gamma^\nu\gamma^\mu=2g^{\mu\nu}$ and the matrices $\tau_{\mathrm{P}}, \tau_{\mathrm{N}}, \tau_{\mathrm{NP}}, \tau_{\mathrm{PN}}$ are given by

$$\tau_{\mathrm{P}}=\begin{pmatrix}1&0\\0&0\end{pmatrix}, \quad \tau_{\mathrm{N}}=\begin{pmatrix}0&0\\0&1\end{pmatrix}, \quad \tau_{\mathrm{NP}}=\begin{pmatrix}0&0\\1&0\end{pmatrix} \text{ and } \tau_{\mathrm{PN}}=\begin{pmatrix}0&1\\0&0\end{pmatrix}.$$

We shall also write

$$\gamma^k=\gamma_0\alpha^k(k=1,2,3), \qquad (\alpha',\alpha^2,x^3)=\boldsymbol{\alpha}.$$

From (40) we obtain the wave equations

$$i\beta^\mu\frac{\partial\psi}{\partial x^\mu}+x\psi=\frac{4\pi g_1}{\sqrt{(\hbar c\chi)}}R_\mu\text{⅂}^\mu+i2\pi g_2\sqrt{\left(\frac{\chi}{\hbar c}\right)}\mathrm{P}_{\mu\nu}\beta^\nu\text{⅂}^\mu \qquad \ldots\ldots(41)$$

and $$-i\frac{\partial\psi^\dagger}{\partial x^\mu}\beta^\mu+\chi\psi^\dagger=\frac{4\pi g_1}{\sqrt{(\hbar c\chi)}}\Gamma_\mu{}^\dagger R^{\mu*}-i2\pi g_2\sqrt{\left(\frac{\chi}{\hbar c}\right)}\Gamma_\mu{}^\dagger\beta_\nu\mathrm{P}^{\mu\nu*}. \qquad \ldots\ldots(42)$$

Translated to Proca's form these equations reduce to

$$\frac{\partial G^{\mu\nu}}{\partial x^\mu}+\chi^2U^\nu=4\pi g_1R^\nu,$$

and $$G_{\mu\nu}=\frac{\partial U_\nu}{\partial x^\mu}-\frac{\partial U_\mu}{\partial x^\nu}+4\pi g_2\mathrm{P}_{\mu\nu}.$$

From (41) and (42) we can derive the initial conditions corresponding to (28) and (29) for the free field. We obtain

$$\psi=\beta_0{}^2\psi-\frac{i}{\chi}\beta_k\beta_0{}^2\frac{\partial\psi}{\partial x_k}+\frac{4\pi g_1}{\chi\sqrt{(\hbar c\chi)}}R_\mu(1-\beta_0{}^2)\reflectbox{Γ}^\mu+i\frac{2\pi g_2}{\sqrt{(\hbar c\chi)}}\mathrm{P}_{\mu\nu}(1-\beta_0{}^2)\beta^\nu\reflectbox{Γ}^\mu \qquad\ldots\ldots(43)$$

and

$$\psi^\dagger=\psi^\dagger\beta_0{}^2+\frac{i}{\chi}\frac{\partial\psi^\dagger}{\partial x^k}\beta_0{}^2\beta^k+\frac{4\pi g_1}{\chi\sqrt{(\hbar c\chi)}}R_\mu{}^*\Gamma^{\mu\dagger}(1-\beta_0{}^2)-i\frac{2\pi g_2}{\sqrt{(\hbar c\chi)}}\mathrm{P}_{\mu\nu}{}^*\Gamma^{\mu\dagger}\beta^\nu(1-\beta_0{}^2). \qquad\ldots\ldots(44)$$

They will be used to eliminate the non-independent components of ψ.

From (40) we derive the energy-momentum tensor

$$T_{\mu\nu}=\frac{i\hbar c}{8\pi}\left[\psi^\dagger\beta_\nu\frac{\partial\psi}{\partial x^\mu}-\frac{\partial\psi^\dagger}{\partial x_\mu}\beta_\nu\psi\right]-Lg_{\mu\nu}.$$

We define again

$$\theta_{\mu\nu}=T_{\mu\nu}-\frac{i\hbar c}{8\pi}\frac{\partial}{\partial x_\varrho}[\psi^\dagger(\beta_\varrho\beta_\mu\beta_\nu-\beta_\nu\beta_\mu\beta_\varrho)\psi],$$

so that the Hamiltonian density

$$\begin{aligned}H=\theta_{00}=&\frac{\hbar c\chi}{4\pi}\psi^\dagger\eta_0\psi-\tfrac{1}{2}g_1\sqrt{\left(\frac{\hbar c}{\chi}\right)}\psi^\dagger\eta_0\reflectbox{Γ}^\sigma R_\sigma-\tfrac{1}{2}g_1\sqrt{\left(\frac{\hbar c}{\chi}\right)}R_\sigma{}^*\Gamma^{\sigma\dagger}\eta_0\psi\\&-\frac{i}{4}g_2\sqrt{(\hbar c\chi)}\psi^\dagger\eta_0\beta^\sigma\reflectbox{Γ}^\varrho\mathrm{P}_{\varrho\sigma}+\frac{i}{4}g_2\sqrt{(\hbar c\chi)}\mathrm{P}_{\varrho\sigma}{}^*\Gamma^{\varrho\dagger}\beta^\sigma\eta_0\psi\\&+\tfrac{1}{2}g_1\sqrt{\left(\frac{\hbar c}{\chi}\right)}[R_\mu{}^*\Gamma^{\mu\dagger}\psi+R_\mu\psi^\dagger\reflectbox{Γ}^\mu]\\&+\frac{i}{4}g_2\sqrt{(\hbar c\chi)}[\mathrm{P}_{\mu\nu}\psi^\dagger\beta^\nu\reflectbox{Γ}^\mu-\mathrm{P}_{\mu\nu}{}^*\Gamma^{\mu\dagger}\beta^\nu\psi]\\=&\frac{\hbar c\chi}{4\pi}\psi^\dagger\eta_0\psi+g_1\sqrt{\left(\frac{\hbar c}{\chi}\right)}[\psi^\dagger\beta_0{}^2\reflectbox{Γ}^\sigma R_\sigma+R_\sigma{}^*\Gamma^{\sigma\dagger}\beta_0{}^2\psi]\\&+\frac{i}{2}g_2\sqrt{(\hbar c\chi)}[\psi^\dagger\beta_0{}^2\beta^\sigma\reflectbox{Γ}^\varrho\mathrm{P}_{\varrho\sigma}-\mathrm{P}_{\varrho\sigma}{}^*\Gamma^{\varrho\dagger}\beta^\sigma\beta_0{}^2\psi]. \qquad\ldots\ldots(45)\end{aligned}$$

From $\psi^\dagger\eta_0\psi$ we eliminate the non-independent components of ψ and $\psi^\dagger$ by means of the relations (43) and (44). We then get after some simplification in which we use the relations (I), (V) and the commutation rules (2)

$$H=H^{\mathrm{M}}+H^{\mathrm{MN}}, \qquad\ldots\ldots(46)$$

where

$$H^{\mathrm{M}}=-\frac{\hbar c\chi}{4\pi}\left[\psi^\dagger\beta_0{}^2\psi-\frac{1}{\chi^2}\frac{\partial\psi^\dagger}{\partial x_k}\beta_0{}^2\beta_k\beta_l\beta_0{}^2\frac{\partial\psi}{\partial x_l}\right] \qquad\ldots\ldots(46a)$$

and

$$\begin{aligned}H^{\mathrm{MN}}=&g_1\sqrt{\left(\frac{\hbar c}{\chi}\right)}\left[\frac{i}{\chi}\frac{\partial\psi^*}{\partial x_k}\beta_0\reflectbox{Γ}_kR_0+\frac{i}{\chi}R_0{}^*\Gamma_k{}^\dagger\beta_0\frac{\partial\psi}{\partial x_k}-\psi^\dagger\reflectbox{Γ}_kR^k+R_k{}^*\Gamma^{k\dagger}\psi\right]\\&-g_2\sqrt{(\hbar c\chi)}\left[-\frac{1}{\chi}\mathrm{P}_{ik}\frac{\partial\psi^*}{\partial x_k}\reflectbox{Γ}^i+\frac{1}{\chi}P_{ik}{}^*\Gamma^{i\dagger}\frac{\partial\psi}{\partial x_k}-i\psi^*\beta_0\reflectbox{Γ}_k\mathrm{P}^{0k}-i\mathrm{P}_{0k}{}^*\Gamma^{k\dagger}\beta_0\psi\right]. \qquad\ldots\ldots(46b)\end{aligned}$$

We have here replaced $\psi^{\dagger}$ by $\psi^{*}\eta_0$. It is to be noticed that (46) is Hermitian. When translated to Proca's form (46) agrees completely with the usual Hamiltonian.

To pass over to the quantum theory, we postulate the commutation rules

$$[(\beta_0\psi(x)_A,\ (\psi^{*}(x')\beta_0{}^{2})_B] = -4\pi(\beta_0{}^{2})_{AB}\delta(\mathbf{x}-\mathbf{x}') \qquad \ldots\ldots(47)$$

and for the Fourier's expansions of ψ and ψ^{*} we take

$$\psi_A = \sqrt{(4\pi)}\Sigma_k\left\{\sum_{l=1}^{3} a_{kl}{}^{*}u_{Al} + \sum_{l=4}^{6} b_{kl}u_{Al}\right\}e^{i\mathbf{kx}}, \qquad \ldots\ldots(48\,a)$$

$$\psi_A{}^{*} = \sqrt{(4\pi)}\Sigma_k\left\{\sum_{l=1}^{3} a_{kl}u_{Al}{}^{*} + \sum_{l=4}^{6} b_{kl}{}^{*}u_{Al}{}^{*}\right\}e^{-i\mathbf{kx}}. \qquad \ldots\ldots(48\,b)$$

a_{kl} and b_{kl} are q-numbers obeying the commutation rules

$$[a_{kl},\ a_{kl}{}^{*}] = 1, \quad [b_{kl},\ b_{kl}{}^{*}] = 1 \quad \text{(no summation over } k, l\text{)},$$

all other combinations commuting. $a_{kl}{}^{*}$ and a_{kl} are emission and absorption operators for positive mesons, and $b_{kl}{}^{*}$ and b_{kl} for negative mesons.

Making for ϕ the expansion

$$\phi = \Sigma_K C_K V_K e^{i\mathbf{Kx}},$$

we now easily get (bar over H denotes that integration over 3-dimensional volume has been performed)

$$\begin{aligned}
\bar{H}^{\mathrm{MN}} = &-g_1\sqrt{\left(\frac{4\pi\hbar c}{\chi^3}\right)}\sum_{\mathbf{K},\mathbf{K}',\mathbf{k}}\delta(\mathbf{K}-\mathbf{K}'+\mathbf{k})\left\{\sum_{l=1}^{3} a_{kl}u_{kl}{}^{*} + \sum_{l=4}^{6} b_{kl}{}^{*}u_{kl}{}^{*}\right\} \\
&\qquad \times v_{\mathrm{N}}{}^{*}C_K{}^{*}\{\beta_0 k^m + \chi\alpha^m\}\Gamma_m C_{K'}v_{\mathrm{P}}{}' \\
&+g_2\sqrt{\left(\frac{4\pi\hbar c}{\chi}\right)}\sum_{\mathbf{K},\mathbf{K}',\mathbf{k}}\delta(\mathbf{K}-\mathbf{K}'+\mathbf{k})\left\{\sum_{l=1}^{3} a_{kl}u_{kl}{}^{*} + \sum_{l=4}^{6} b_{kl}{}^{*}u_{kl}{}^{*}\right\} \\
&\qquad \times v_{\mathrm{N}}{}^{*}C_K{}^{*}\{\gamma_0(\alpha_n\alpha_m - \alpha_m\alpha_n)k^m - \chi\gamma_0\alpha_n\}\Gamma^n C_{K'}v_{\mathrm{P}}{}' \\
&+g_1\sqrt{\left(\frac{4\pi\hbar c}{\chi^3}\right)}\sum_{\mathbf{K},\mathbf{K}',\mathbf{k}}\delta(\mathbf{K}-\mathbf{K}'-\mathbf{k})v_{\mathrm{P}}{}^{*}C_K{}^{*}\Gamma_m{}^{\dagger}\{\beta_0 k^m + \chi\alpha^m\}C_{K'}v_{\mathrm{N}}{}' \\
&\qquad \times\left\{\sum_{l=1}^{3} a_{kl}{}^{*}u_{kl} + \sum_{l=4}^{6} b_{kl}u_{kl}\right\} \\
&-g_2\sqrt{\left(\frac{4\pi\hbar c}{\chi}\right)}\sum_{\mathbf{K},\mathbf{K}',\mathbf{k}}\delta(\mathbf{K}-\mathbf{K}'-\mathbf{k})v_{\mathrm{P}}{}^{*}C_K{}^{*}\Gamma^{n\dagger}\{\tfrac{1}{2}\gamma_0(\alpha_m\alpha_n - \alpha_n\alpha_m)k^m \\
&\qquad + \chi\gamma_0\alpha_n\}C_{K'}v_{\mathrm{P}}{}'\left\{\sum_{l=1}^{3} a_{kl}n^{*}{}_{kl} + \sum_{l=4}^{6} b_{kl}u_{kl}\right\} \\
&+4\pi\sum_{\mathbf{K},\mathbf{K}',\mathbf{K}'',\mathbf{K}'''}\delta(\mathbf{K}-\mathbf{K}'+\mathbf{K}''-\mathbf{K}''')\Bigg[\frac{g_1{}^2}{\chi^2}(v_{\mathrm{N}}{}^{*}C_K{}^{*}C_{K'}v_{\mathrm{P}}{}') \\
&\qquad \times(v_{\mathrm{N}}{}''^{*}C_{K''}{}^{*}C_{K'''}v_{\mathrm{P}}{}''') + g_2{}^2(v_{\mathrm{N}}{}^{*}C_K{}^{*}(\gamma_0\boldsymbol{\sigma})C_{K'}v_{\mathrm{P}}{}') \\
&\qquad \times(v_{\mathrm{N}}{}''^{*}C_{K''}{}^{*}(\gamma_0\boldsymbol{\sigma})C_{K'''}v_{\mathrm{P}}{}''')\Bigg] \qquad \ldots\ldots(49)
\end{aligned}$$

(ii) *Scalar Meson Field*

For the Lagrangian density in presence of nuclear particles we assume

$$L=\frac{i\hbar c}{8\pi}\left[\psi^\dagger\beta^\mu\frac{\partial\psi}{\partial x^\mu}-\frac{\partial\psi^\dagger}{\partial x^\mu}\beta^\mu\psi\right]+\frac{\hbar c\chi}{4\pi}\psi^\dagger\psi$$
$$+\frac{i}{4}g_1\sqrt{\left(\frac{\hbar c}{\chi}\right)}[R^*\Gamma_\nu{}^\dagger\beta^\nu\psi-R\psi^\dagger\beta^\nu\text{⅂}_\nu]$$
$$+g_2\sqrt{(\hbar c\chi)}[P_\mu{}^*\Gamma^{\mu\dagger}\psi+P_\mu\psi^\dagger\text{⅂}^\mu], \qquad \ldots\ldots(50)$$

where $R=\phi^\dagger\tau_{\mathrm{NP}}\phi,\quad P_\mu=\phi^\dagger\gamma_\mu\tau_{\mathrm{NP}}\phi.$

From (50) one obtains the wave equations

$$i\beta^\mu\frac{\partial\psi}{\partial x^\mu}+\chi\psi=\frac{i\pi g_1}{\sqrt{(\hbar c\chi)}}R\beta_\nu\text{⅂}^\nu-4\pi g_2\sqrt{\left(\frac{\chi}{\hbar c}\right)}P_\mu\text{⅂}^\mu \qquad \ldots\ldots(51)$$

and

$$-i\frac{\partial\psi^\dagger}{\partial x^\mu}\beta^\mu+\chi\psi^\dagger=-\frac{i\pi g_1}{\sqrt{(\hbar c\chi)}}R^*\Gamma_\nu{}^\dagger\beta^\nu-4\pi g_2\sqrt{\left(\frac{\chi}{\hbar c}\right)}\Gamma_\mu{}^\dagger P^\mu. \qquad \ldots\ldots(52)$$

From these equations one can easily pass over to the usual equations of the Proca field.

From (51) and (52) it is easy to derive the initial conditions

$$\psi=\beta_0{}^2\psi-\frac{i}{\chi}\beta_k\beta_0{}^2\frac{\partial\psi}{\partial x_k}+\frac{i\pi g_1}{\chi\sqrt{(\hbar c\chi)}}R(1-\beta_0{}^2)\beta_\nu\text{⅂}^\nu-\frac{4\pi g_2}{\sqrt{(\hbar c\chi)}}P_\mu(1-\beta_0{}^2)\text{⅂}^\mu \qquad \ldots\ldots(53)$$

and

$$\psi^\dagger=\psi^\dagger\beta_0{}^2+\frac{i}{\chi}\frac{\partial\psi^\dagger}{\partial x^k}\beta_0{}^2\beta^k-\frac{i\pi g_1}{\chi\sqrt{(\hbar c\chi)}}\Gamma_\nu{}^\dagger\beta^\nu(1-\beta_0{}^2)R^*-\frac{4\pi g_2}{\sqrt{(\hbar c\chi)}}\Gamma_\mu{}^\dagger(1-\beta_0{}^2)P^{\mu *}. \qquad \ldots\ldots(54)$$

From (50) we get the expression for the energy-momentum tensor

$$T_{\mu\nu}=\frac{i\hbar c}{8\pi}\left[\psi^\dagger\beta_\nu\frac{\partial\psi}{\partial x^\mu}-\frac{\partial\psi^\dagger}{\partial x^\mu}\beta_\nu\psi\right]-Lg_{\mu\nu}.$$

Defining again $\theta_{\mu\nu}=T_{\mu\nu}-\dfrac{i\hbar c}{8\pi}\dfrac{\partial}{\partial x_\varrho}[\psi^\dagger(\beta_\varrho\beta_\mu\beta_\nu-\beta_\nu\beta_\mu\beta_\varrho)\psi],$

we get

$$\theta_{\mu\nu}=\frac{\hbar c\chi}{4\pi}\psi^\dagger(g_{\mu\nu}-\beta_\mu\beta_\nu-\beta_\nu\beta_\mu)\psi+\frac{i}{4}g_1\sqrt{\left(\frac{\hbar c}{\chi}\right)}[R\psi^\dagger\beta_0{}^2\beta_\sigma\text{⅂}^\sigma-R^*\Gamma_\sigma{}^\dagger\beta^\sigma\beta_0{}^2\psi]$$
$$-g_2\sqrt{(\hbar c\chi)}[\psi^\dagger\beta_0{}^2\text{⅂}^\sigma P_\sigma+P_\sigma{}^*\Gamma^{\sigma\dagger}\beta_0{}^2\psi]. \qquad \ldots\ldots(55)$$

Eliminating the non-independent components of ψ and $\psi^\dagger$ by means of (51) and (52), we get

$$H=H^{\mathrm{M}}+H^{\mathrm{MN}}, \qquad \ldots\ldots(56)$$

$$H^{\mathrm{M}}=-\frac{\hbar c\chi}{4\pi}\left[\psi^\dagger\beta_0{}^2\psi-\frac{1}{\chi^2}\frac{\partial\psi^\dagger}{\partial x_k}\beta_0{}^2\beta_k\beta_l\beta_0{}^2\frac{\partial\psi}{\partial x_l}\right] \qquad \ldots\ldots(57\,a)$$

and

$$H^{\mathrm{MN}}=ig_1\sqrt{\left(\frac{\hbar c}{\chi}\right)}[R\psi^\dagger\beta_0\text{⅂}_0-R^*\Gamma_0{}^\dagger\beta_0\psi]-g_2\sqrt{(\hbar c\chi)}[\psi^\dagger\text{⅂}_0\mathrm{P}_0+\mathrm{P}_0{}^*\Gamma_0{}^\dagger\psi]$$
$$-ig_2\sqrt{\left(\frac{\hbar c}{\chi}\right)}\left[P_k\frac{\partial\psi^\dagger}{\partial x_k}\beta_0\text{⅂}_0-\Gamma_0{}^\dagger\beta_0\frac{\partial\psi}{\partial x_k}P_k{}^*\right]. \qquad \ldots\ldots(57\,b)$$

Making now the Fourier expansions

$$\psi = \sqrt{(4\pi)}\Sigma_k(a_k{}^*u_{k1} + b_k u_{k2})e^{i\mathbf{kx}}, \qquad \ldots\ldots(58\,a)$$

$$\psi^* = \sqrt{(4\pi)}\Sigma_k(a_k u_{k1}{}^* + b_k{}^*u_{k2}{}^*)e^{-i\mathbf{kx}}, \qquad \ldots\ldots(58\,b)$$

we easily get

$$\begin{aligned}\overline{H}^{\mathrm{MN}} = &-ig_1\sqrt{\left(\frac{4\pi\hbar c}{\chi}\right)}\sum_{\mathbf{K},\mathbf{K}',\mathbf{k}}[\delta(\mathbf{K}-\mathbf{K}'+\mathbf{k})v_{\mathrm{N}}{}^*C_K{}^*\gamma_0 C_{K'}v_{\mathrm{P}}'(a_k u_{k1}{}^* + b_k{}^*u_{k2})\beta_0\rceil_0\\ &+\delta(\mathbf{K}-\mathbf{K}'-\mathbf{k})\Gamma_0{}^\dagger\beta_0(a_k{}^*u_{k1}+b_k u_{k2})v_{\mathrm{P}}{}^*C_K{}^*\gamma_0 C_{K'}v_{\mathrm{N}}']\\ &+g_2\sqrt{\left(\frac{4\pi\hbar c}{\chi}\right)}\sum_{\mathbf{K},\mathbf{K}',\mathbf{k}}[\delta(\mathbf{K}-\mathbf{K}'+\mathbf{k})(a_k u_{k1}{}^*+b_k{}^*u_{k2}{}^*)\\ &\qquad\times v_{\mathrm{N}}{}^*C_K{}^*(\chi-\beta_0 k^m\alpha_m)\rceil_0 C_{K'}v_{\mathrm{P}}'\\ &-\delta(\mathbf{K}-\mathbf{K}'-\mathbf{k})\Gamma_0{}^\dagger v_{\mathrm{P}}{}^*C_k{}^*(\chi-\beta_0 k^m\alpha_m)\rceil_0 C_{K'}v_{\mathrm{P}}']\\ &+4\pi g_2{}^{s^2}\sum_{\mathbf{K},\mathbf{K}',\mathbf{K}'',\mathbf{K}'''}\delta(\mathbf{K}-\mathbf{K}'+\mathbf{K}''-\mathbf{K}''')(v_{\mathrm{N}}{}^*C_K{}^*\boldsymbol{\alpha}C_{K'}v_{\mathrm{P}}')\\ &\qquad\times(v_{\mathrm{P}''}C_{K''}{}^*\boldsymbol{\alpha}C_{K'''}v_{\mathrm{N}}'''). \qquad \ldots\ldots(59)\end{aligned}$$

(iii) *Pseudoscalar Meson Field*

Proceeding as in the scalar case it is easy to derive the following expression for the interaction Hamiltonian in the case of pseudoscalar mesons:

$$\begin{aligned}\overline{H}^{\mathrm{MN}} = &\,ig_1\sqrt{\left(\frac{4\pi\hbar c}{\chi}\right)}\sum_{\mathbf{K},\mathbf{K}',\mathbf{k}}[\delta(\mathbf{K}-\mathbf{K}'+\mathbf{k})v_{\mathrm{N}}{}^*C_K{}^*\gamma_0\alpha^1\alpha^2\alpha^3 v_{\mathrm{P}}'\\ &\qquad\times(a_k u_{k1}{}^*+b_k{}^*u_{k2}{}^*)\beta_0\rceil_0\\ &+\delta(\mathbf{K}-\mathbf{K}'-\mathbf{k})\Gamma_0{}^\dagger\beta_0(a_k{}^*u_{k1}+b_k u_{k2})v_{\mathrm{P}}{}^*C_K{}^*\gamma_0\alpha^1\alpha^2\alpha^3 C_{K'}v_{\mathrm{N}}']\\ &+g_2\sqrt{\left(\frac{4\pi\hbar c}{\chi}\right)}\sum_{\mathbf{K},\mathbf{K}',\mathbf{k}}[\delta(\mathbf{K}-\mathbf{K}'+\mathbf{k})(a_k u_{k1}{}^*+b_k u_{k2}{}^*)\\ &\qquad\times v_{\mathrm{N}}{}^*C_K{}^*(i\chi\alpha^1\alpha^2\alpha^3-\beta_0\sigma_m k^m)\rceil_0 C_{K'}v_{\mathrm{P}}'\\ &-\delta(\mathbf{K}-\mathbf{K}'-\mathbf{k})\Gamma_0{}^\dagger v_{\mathrm{P}}{}^*C_K{}^*(i\chi\alpha^1\alpha^2\alpha^3-\beta_0\sigma_m k^m)C_{K'}v_{\mathrm{N}}'\\ &\qquad\times(a_k{}^*u_{k1}+b_{k2}u_{k2})]\\ &+4\pi g_2{}^2\sum_{\mathbf{K},\mathbf{K}',\mathbf{K}'',\mathbf{K}'''}\delta(\mathbf{K}-\mathbf{K}'+\mathbf{K}''-\mathbf{K}''')(v_{\mathrm{N}}{}^*C_K{}^*\boldsymbol{\sigma}C_{K'}v_{\mathrm{P}}')\\ &\qquad\times(v_{\mathrm{P}}''C_{K''}\boldsymbol{\sigma}C_{K'''}v_{\mathrm{N}}'''). \qquad \ldots\ldots(60)\end{aligned}$$

§ 3. APPLICATION TO THE SCATTERING OF POSITIVE MESONS BY PROTONS

As an illustration of the method developed above, we shall here calculate the cross section for the scattering of positive vector mesons by protons. The scattering is described by the scheme

$$\mathrm{Y}^+(\mathbf{p}_0)+\mathrm{P}(-\mathbf{p}_0)\rightarrow \mathrm{Y}^+(\mathbf{p}_0)+\mathrm{Y}^+(\mathbf{p})+\mathrm{N}(-\mathbf{p}_0-\mathbf{p})\rightarrow \mathrm{Y}^+(\mathbf{p})+\mathrm{P}(-\mathbf{p}),$$

where by $\mathrm{Y}^+(\mathbf{p})$ we denote a positive meson, by $\mathrm{P}(\mathbf{p})$ we denote a proton and by $\mathrm{N}(\mathbf{p})$ a neutron each with momentum $\mathbf{p}$. We have to make a second order perturbation theory and the interaction matrix elements for the transition are easily seen to be

$$H_{\mathrm{in}}=g_1\sqrt{\left(\frac{4\pi c}{\hbar\chi^3}\right)}\,v^*(-\mathbf{p}_0)\Gamma_m{}^{\dagger}(p^m\beta_0+\mu c\alpha^m)v(-\mathbf{p}_0-\mathbf{p})u_{l'}(\mathbf{p})$$

$$H_{\mathrm{nf}}=-g_1\sqrt{\left(\frac{4\pi c}{\hbar\chi^3}\right)}\,u_l{}^*(\mathbf{p}_0)v^*(-\mathbf{p}_0-\mathbf{p})(\beta_0 p_0{}^m+\mu c\alpha^m)\reflectbox{Γ}_m v(-\mathbf{p})$$

$$(\mathbf{p}_0=\hbar\mathbf{k}_0,\quad \mathbf{p}=\hbar\mathbf{k},\quad \mu=\hbar\chi). \qquad \ldots\ldots(61)$$

Here the suffix i denotes the initial state, f the final, and n intermediate. The suffix *l′* is used to denote the polarization of the initial meson and *l* for that of the final meson. Hence

$$\begin{aligned}H_{\mathrm{if}}&=\sum_{\mathrm{n}}\frac{H_{\mathrm{in}}H_{\mathrm{nf}}}{E_{\mathrm{i}}-E_{\mathrm{n}}}\\&=-\frac{4\pi g_1{}^2c}{\hbar\chi^3}\,\frac{1}{(E_{\mathrm{N}}-E)^2-M^2c^4-c^2(\mathbf{p}_0+\mathbf{p})^2}\,v^*(-\mathbf{p}_0)\Gamma_m{}^{\dagger}(p^m\beta_0+\mu c\alpha^m)\\&\quad\times\{E_{\mathrm{N}}-E-c(\boldsymbol{\alpha},\mathbf{p}_0+\mathbf{p})+Mc^2\gamma_0\}u_{l'}(\mathbf{p}_0)u_l{}^*(\mathbf{p}_0)(p^n\beta_0+\mu c\alpha^n)\reflectbox{Γ}_n v(-\mathbf{p}),\end{aligned} \qquad \ldots\ldots(62)$$

and

$$\begin{aligned}H_{\mathrm{if}}H_{\mathrm{fi}}=\frac{4\pi^2g_1{}^4c^2}{\hbar^2\chi^6E_{\mathrm{N}}Q^2}&v^*(-\mathbf{p}_0)\Gamma_m{}^{\dagger}(p^m\beta_0+\mu c\alpha^m)\{E_{\mathrm{N}}-E-c(\boldsymbol{\alpha},\mathbf{p}_0+\mathbf{p})+Mc^2\gamma_0\}\\&\times u_{l'}(\mathbf{p})u_l{}^*(\mathbf{p}_0)(\beta_0p_0{}^n+\mu c\alpha^n)\reflectbox{Γ}_n v(-\mathbf{p})\\&-v^*(-\mathbf{p})\Gamma_{n'}{}^{\dagger}(\beta_0p_0{}^{n'}+\mu c\alpha^{n'})u_l(\mathbf{p}_0)u_{l'}{}^*(\mathbf{p})\{E_{\mathrm{N}}-E-c(\boldsymbol{\alpha},\mathbf{p}_0+\mathbf{p})+Mc^2\gamma_0\}\\&\times(p^{m'}\beta_0+\mu c\alpha^{m'})\reflectbox{Γ}_{m'}v(-\mathbf{p}_0),\end{aligned}$$

where

$$Q=(E_{\mathrm{N}}-E)^2-M^2c^4-c^2(\mathbf{p}_0+\mathbf{p})^2,\quad E=c(p^2+\mu^2c^2)^{1/2},\quad E_{\mathrm{N}}=c(p^2+M^2c^2)^{1/2}$$

$$|\mathbf{p}|=|\mathbf{p}_0|=p,\quad (\mathbf{p}\mathbf{p}_0)=p^2\cos\theta. \qquad (M=\text{mass of nucleon}).$$

Summing over the final states of the nucleon and averaging over the initial ones, we get (i_{N} denotes initial nucleon states, f_{N} denotes final nucleon states, and by i_{M} and f_{M} we denote the corresponding meson states; sp_{N} denotes spur of the nucleon matrices, i.e. of γ_0, $\boldsymbol{\alpha}$ etc.)

$$\begin{aligned}\sum_{\mathrm{f}_{\mathrm{N}}}\tfrac{1}{2}\sum_{\mathrm{i}_{\mathrm{N}}}H_{\mathrm{if}}H_{\mathrm{fi}}=\frac{2\pi g_1{}^4c^2}{\hbar^2\chi^6E_{\mathrm{N}}{}^2Q^2}&\mathrm{sp}_{\mathrm{N}}[u_l{}^*(\mathbf{p}_0)\{\beta_0p_0{}^n+\mu c\alpha^n\}\reflectbox{Γ}_n\{E_{\mathrm{N}}-c(\boldsymbol{\alpha}\mathbf{p})+Mc^2\gamma_0\}\\&\times\Gamma_{n'}{}^{\dagger}(\beta_0p_0{}^{n'}+\mu c\alpha^{n'})u_l(\mathbf{p}_0)u_{l'}{}^*(\mathbf{p})\{E_{\mathrm{N}}-E-c(\boldsymbol{\alpha},\mathbf{p}_0+\mathbf{p})+Mc^2\gamma_0\}\\&\times(p^m\beta_0+\mu c\alpha^m)\reflectbox{Γ}_m\{E_{\mathrm{N}}-c(\boldsymbol{\alpha}\mathbf{p}_0)+Mc^2\gamma_0\}\\&\times\Gamma_{m'}{}^{\dagger}(p^{m'}\beta_0+\mu c\alpha^{m'})\{E_{\mathrm{N}}-E-c(\boldsymbol{\alpha},\mathbf{p}_0+\mathbf{p})+Mc^2\gamma_0\}u_{l'}(\mathbf{p})].\end{aligned} \qquad \ldots\ldots(63)$$

We now write

$$x=\sum_{l=1}^{3}u_l{}^*(\mathbf{p}_0)\{\beta_0p_0{}^n+\mu c\alpha^n\}\reflectbox{Γ}_n\{E_{\mathrm{N}}-c(\boldsymbol{\alpha}\mathbf{p})+Mc^2\gamma_0\}\Gamma_{n'}{}^{\dagger}\{\beta_0p_0{}^{n'}+\mu c\alpha^{n'}\}u_l(\mathbf{p}_0) \qquad \ldots\ldots(64)$$

and to make this summation over the meson states we use (19′) and the initial conditions (28), (29), so that

$$\sum_{l=1}^{3}\beta_0u_l(\mathbf{p}_0)u_l{}^*(\mathbf{p}_0)\beta_0=\frac{1}{2E}\left\{E\beta_0+\frac{1}{\mu}(p^m\beta_m)^2-\mu c^2\right\}\beta_0{}^2. \qquad \ldots\ldots(65)$$

We then get

$$\begin{aligned} x = {} & p_0{}^m p_0{}^n \frac{1}{2E} \Gamma_m{}^\dagger \left\{ E\beta_0 + \frac{(p_0{}^l \beta_l)^2}{\mu} - \mu c^2 \right\} \beta_0{}^2 \rceil_n \{ E_{\mathrm{N}} - c(\boldsymbol{\alpha}\mathbf{p}) + Mc^2\gamma_0 \} \\ & + \frac{\mu c}{2E} \Gamma_m{}^\dagger \beta_0 \left\{ E\beta_0 + \frac{(p_0{}^l \beta_l)^2}{\mu} - \mu c^2 \right\} \beta_0{}^2 \rceil_n p_0{}^n \{ E_{\mathrm{N}} - c(\boldsymbol{\alpha}\mathbf{p}) + Mc^2\gamma_0 \} \alpha^m \\ & + \frac{\mu c}{2E} p_0{}^m \alpha^n \{ E_{\mathrm{N}} - c(\boldsymbol{\alpha}\mathbf{p}) + Mc^2\gamma_0 \} \Gamma_m{}^\dagger \left\{ E\beta_0 + \frac{(p_0{}^l \beta_l)^2}{\mu} - \mu c^2 \right\} \beta_0 \rceil_n \\ & + \frac{\mu^2 c^2}{2E} \alpha^n \{ E_{\mathrm{N}} - c(\boldsymbol{\alpha}\mathbf{p}) + Mc^2\gamma_0 \} \alpha^m \Gamma_m{}^\dagger \beta_0 \left\{ E\beta_0 + \frac{(p_0{}^l \beta_l)^2}{\mu} - \mu c^2 \right\} \beta_0 \rceil_n . \end{aligned} \qquad \ldots\ldots(66)$$

To simplify further we note the relations

$$\left. \begin{aligned} & \Gamma_m{}^\dagger \beta_0{}^2 = \Gamma_m{}^\dagger, \qquad \beta_0{}^2 \rceil_m = \rceil_m, \\ & \Gamma_m{}^\dagger \beta_0 \rceil_n = \Gamma_m{}^\dagger \beta_0 \beta_r \beta_s \rceil_n = \Gamma_m{}^\dagger \beta_r \beta_s \beta_0 \rceil_n = 0, \\ & \Gamma_m{}^\dagger \rceil_n = g_{mn}, \\ & \Gamma_m{}^\dagger \beta_r \beta_s \rceil_n = g_{mn} g_{rs} - g_{ms} g_{rn}, \\ & \Gamma_m{}^\dagger \beta_0 \beta_r \beta_s \beta_0 \rceil_n = g_{mr} g_{ns}. \end{aligned} \right\} \qquad \ldots\ldots(67)$$

Hence

$$\begin{aligned} x = {} & \frac{\mu}{E} [\{ (c^2 p^2 + \tfrac{3}{2} \mu^2 c^4) E_{\mathrm{N}} + E c^2 (\mathbf{p}_0 \mathbf{p}) \} - \tfrac{3}{2} \mu^2 c^4 M c^2 \gamma_0 - E E_{\mathrm{N}} c (\boldsymbol{\alpha} \mathbf{p}_0) \\ & + \tfrac{1}{2} (\mu^2 c^4 - c^2 p^2) c (\boldsymbol{\alpha}\mathbf{p}) - \tfrac{1}{2} c^3 (\boldsymbol{\alpha}\mathbf{p}_0)(\boldsymbol{\alpha}\mathbf{p})(\boldsymbol{\alpha}\mathbf{p}_0)]. \end{aligned} \qquad \ldots\ldots(68)$$

Denoting by x' the matrix obtained from (68) by interchanging $\mathbf{p}$ and $\mathbf{p}_0$ we get from (63)

$$\begin{aligned} \tfrac{1}{3} \sum_{i_{\mathrm{M}}, f_{\mathrm{M}}} \tfrac{1}{2} \sum_{i_{\mathrm{N}}, f_{\mathrm{N}}} H_{\mathrm{if}} H_{\mathrm{fi}} = {} & \frac{2\pi^2 g_1{}^4 c^2}{3\hbar^2 \chi^6 E_{\mathrm{N}}{}^2 Q^2} \mathrm{sp}_{\mathrm{N}} \{ x [E_{\mathrm{N}} - E - c(\boldsymbol{\alpha}, \mathbf{p}_0 + \mathbf{p}) + Mc^2 \gamma_0] \\ & \times x' [E_{\mathrm{N}} - E - c(\boldsymbol{\alpha}, \mathbf{p}_0 + \mathbf{p}) + Mc^2 \gamma_0] \}, \end{aligned}$$

and we obtain the differential scattering cross section

$$d\phi = \tfrac{1}{6} \left(\frac{g_1{}^2}{E_{\mathrm{N}} + E} \right)^2 \frac{\Lambda \, d\Omega}{\mu^4 c^8 [(E_{\mathrm{N}} - E)^2 - M^2 c^4 - c^2 (\mathbf{p}_0 + \mathbf{p})^2]^2}, \qquad \ldots\ldots(69)$$

where

$$\begin{aligned} \Lambda = {} & 8 E_{\mathrm{N}}{}^4 c^4 p^4 + 8 E E_{\mathrm{N}}{}^3 c^2 p^2 \{ - E^2 \cos\theta + c^2 p^2 (1 + 4\cos\theta) \} \\ & + E_{\mathrm{N}}{}^2 \{ 18 E^6 - 20 E^4 c^2 p^2 (2 + \cos\theta) + 2 E^2 c^4 p^4 (23 + 18\cos\theta + 4\cos^2\theta) \\ & \qquad + c^6 p^6 (-24 + 8\cos\theta + 16\cos^2\theta \} \\ & + E E_{\mathrm{N}} c^2 p^2 \{ E^4 (-10 + 22\cos\theta) + E^2 c^2 p^2 (5 - \cos\theta - 8\cos^2\theta) \\ & \qquad + c^4 p^4 (-10 - 18\cos\theta + 28\cos^2\theta + 4\cos^3\theta) \} \\ & + E^6 c^2 p^2 (-9 + \cos\theta) + E^4 c^4 p^4 (35 - 13\cos\theta + 12\cos^2\theta) \\ & \qquad + E^2 c^6 p^6 (-43 + 23\cos\theta - 4\cos^2\theta - 12\cos^3\theta) \\ & \qquad + c^8 p^8 (17 - 11\cos\theta - 8\cos^2\theta + 20\cos^3\theta). \end{aligned} \qquad \ldots\ldots(70)$$

This agrees with the cross section obtained by Wilson. The great simplification of the procedure must, however, be emphasized.

ACKNOWLEDGMENTS

The author is grateful to Professor R. C. Majumdar for his help throughout the work and many valuable discussions. He also thanks the authorities of the Delhi University for the award of an All India Research Fellowship to enable him to work there.

REFERENCES

BOOTH, F., and WILSON, A. H., 1940, *Proc. Roy. Soc.* A, **175,** 483.
HARISH-CHANDRA, 1946, *Proc. Roy. Soc.* A, **186,** 502; 1947, *Phys. Rev.*, **71,** 793; 1948, *Proc. Roy. Soc.* A, **192,** 195.
KEMMER, N., 1939, *Proc. Roy. Soc.* A, **173,** 91.
WILSON, A. H., 1941, *Proc. Camb. Phil. Soc.*, **37,** 301.

A New Method for Determining the Radial Distribution Function

BY KAI-CHIA CHENG
Department of Mathematical Physics, The University, Edinburgh

Communicated by M. Born; MS. received 23rd January 1950

ABSTRACT. It is shown in this paper that Green's integral equation resulting from the Kirkwood approximation for the radial distribution function can be transformed into a differential equation of infinite order, to which the method of successive approximation can be applied without ambiguity. The solution at moderately high temperatures is discussed. The result is a correction to the usual Boltzmann distribution function; the radial distribution function oscillates with decreasing amplitudes at small distances and tends to unity at large distances. The validity of the approximations is discussed in two appendices.

§ 1. INTRODUCTION

THE present paper proposes a new method of treating Green's integral equation (Green 1947) resulting from the Kirkwood approximation for the radial distribution function of molecules. This method consists in transforming the integral equation into a differential equation of infinite order, which can be solved by successive approximations. However, we only present it as a method, and no numerical solution of the equation is attempted. The solution at moderately high temperatures is discussed. The result is a correction to the ordinary crude approximation $\exp\{-\phi/\boldsymbol{k}T\}$ and shows that at relatively low temperatures and for high densities in the gas region, the curve of the distribution has a minimum, in addition to the usual prominent maximum. This is fully confirmed by experiments on the scattering of x-rays at low temperatures, and is also in agreement with the results obtained by Kirkwood (1942).

The validity of the approximation methods is discussed in two appendices. Some criteria are given. In an example for nitrogen, use is made of these criteria to determine the vapour densities and pressures at several temperatures near saturation. They are in fair agreement with the observed ones even in the first approximation.

§2. TRANSFORMATION OF GREEN'S INTEGRAL EQUATION

Green has shown that the distribution function $n_2(r)$ in equilibrium states is determined by the solution of the following integral equation:

$$\ln \frac{n_2(r)}{n_1{}^2} + \frac{\phi(r)}{\boldsymbol{k}T} = \frac{\pi}{n_1{}^3} \int_0^\infty \int_{-s}^{s} (s^2 - t^2) \frac{t+r}{r} \{n_2(r+t) - n_1{}^2\} n_2(s) \frac{\phi'(s)}{\boldsymbol{k}T} \, dt \, ds, \qquad \ldots\ldots(2.1)$$

where n_1 is the average density of molecules, r is the relative distance between a pair of molecules and $\phi(r)$ is the potential function between them. Equation (2.1) can be transformed into a differential equation and can be solved by the method of successive approximation. Define first

$$g(r) = \frac{n_2(r)}{n_1{}^2}, \qquad \text{and} \qquad f(r) = r\{g(r) - 1\}. \qquad \ldots\ldots(2.2)$$

Then (2.1) becomes

$$\ln g(r) + \frac{\phi(r)}{\boldsymbol{k}T} = \frac{\pi n_1}{r} \int_0^\infty \int_{-s}^{s} (s^2 - t^2) f(r+t) g(s) \frac{\phi'(s)}{\boldsymbol{k}T} \, dt \, ds. \qquad \ldots\ldots(2.3)$$

It can be verified by the expansion of $f(r)$ into power series of r that the following relation holds:

$$e^{tD} f(r) = f(r+t), \qquad \ldots\ldots(2.4)$$

where D stands for $\partial/\partial r$. Hence (2.3) becomes, with the help of (2.4),

$$\ln g(r) \, e^{\varphi(r)/\boldsymbol{k}T} = \frac{\pi n_1}{\boldsymbol{k}Tr} \int_0^\infty \int_{-s}^{s} (s^2 - t^2) e^{tD} f(r) g(s) \phi'(s) \, dt \, ds. \qquad \ldots\ldots(2.5)$$

Treating D as an operator which operates on the variable r and which commutes with the variables s and t, one can perform the integration

$$\int_{-s}^{s} (s^2 - t^2) e^{tD} \, dt = \frac{4}{D^3} (sD \cosh sD - \sinh sD). \qquad \ldots\ldots(2.6)$$

With the help of (2.6), (2.5) can be reduced to

$$\ln g(r) \, e^{\varphi(r)/\boldsymbol{k}T} = \frac{4\pi n_1}{r\boldsymbol{k}T} \int_0^\infty \frac{1}{D^3} (sD \cosh sD - \sinh sD) f(r) \phi'(s) g(s) \, ds. \qquad \ldots\ldots(2.7)$$

Expanding (2.7) in powers of D, one obtains

$$\ln g(r) \, e^{\varphi(r)/\boldsymbol{k}T} = \frac{8\pi n_1}{r\boldsymbol{k}T} \sum_1^\infty M^{(\nu)} D^{2\nu-2} f(r), \qquad \ldots\ldots(2.8)$$

where $M^{(\nu)}$ are the moments defined by the expressions

$$M^{(\nu)} = \frac{\nu}{(2\nu+1)!} \int_0^\infty g(r) \phi'(r)^{2\nu+1} \, dr, \qquad \nu = 1, 2, 3, \ldots. \qquad \ldots\ldots(2.9)$$

In the following section the solution at moderately high temperatures will be discussed. In Appendix 1 the validity of such an expansion will be considered.

§3. SOLUTION AT MODERATELY HIGH TEMPERATURES

We shall approach the solution of the equation by the method of iteration. For the sake of convenience in illustration, assumption will be made that only $M^{(1)}$ and $M^{(2)}$ will be needed, while the remaining terms can be ignored. Then (2.8) becomes

$$\ln g(r)\,e^{\varphi(r)/\boldsymbol{k}T} = \frac{8\pi n_1}{r\boldsymbol{k}T}(M^{(1)} + M^{(2)}D^2)f(r). \qquad \ldots\ldots(3.1)$$

The iteration method consists in the evaluation of the distribution function of the $(\mu+1)$th order $g_{\mu+1}(r)$ from the left-hand side of (3.1) in terms of the μth order quantities $M_\mu^{(1)}$, $M_\mu^{(2)}$ and $f_\mu(r)$ from the right-hand side of (3.1). For instance, let $g_\mu(r)$ be the solution of (3.1) in the μth order, and define

$$\left.\begin{aligned} M_\mu^{(1)} &= \frac{1}{6}\int_0^\infty g(r)\phi'(r)r^3\,dr, \\ M_\mu^{(2)} &= \frac{1}{60}\int_0^\infty g(r)\phi'(r)r^5\,dr, \\ f_\mu(r) &= r[g_\mu(r) - 1]. \end{aligned}\right\} \qquad \ldots\ldots(3.2)$$

Then the $(\mu+1)$th order distribution function $g_{\mu+1}(r)$ is given by

$$\ln g_{\mu+1}(r)\,e^{\varphi(r)/\boldsymbol{k}T} = \frac{8\pi n_1}{r\boldsymbol{k}T}(M_\mu^{(1)} + M_\mu^{(2)}D^2)f_\mu(r), \qquad \ldots\ldots(3.3)$$

or

$$g_{\mu+1}(r) = \exp\left\{\frac{8\pi n_1}{r\boldsymbol{k}T}(M_\mu^{(1)} + M_\mu^{(2)}D^2)f_\mu(r) - \frac{\phi(r)}{\boldsymbol{k}T}\right\}.$$

Taking, as a trial function,

$$g_0(r) = e^{-\varphi(r)/\boldsymbol{k}T}, \qquad \ldots\ldots(3.4)$$

and substituting into (3.2) for $M_0^{(1)}$, $M_0^{(2)}$ and $f_0(r)$, one obtains to the first order of approximation,

$$g_1(r) = \exp\frac{1}{\boldsymbol{k}T}\left\{-\phi(r) + \frac{8\pi n_1}{r}(M_0^{(1)} + M_0^{(2)}D^2)f_0(r)\right\}, \qquad \ldots\ldots(3.5)$$

with

$$\left.\begin{aligned} M_0^{(1)} &= \frac{1}{6}\int_0^\infty e^{-\varphi(r)/\boldsymbol{k}T}\phi'(r)r^3\,dr, \\ M_0^{(2)} &= \frac{1}{60}\int_0^\infty e^{-\varphi(r)/\boldsymbol{k}T}\phi'(r)r^5\,dr, \\ f_0(r) &= r(e^{-\varphi(r)/\boldsymbol{k}T} - 1). \end{aligned}\right\} \qquad \ldots\ldots(3.6)$$

With the help of (3.5) and (3.6), (3.1) can be solved to any desired degree of accuracy.

In Appendix 2 the conditions for the validity of the iteration method will be discussed. An application of this method will be given in the following example. Take the potential function $\phi(r)$ as follows (Lennard-Jones 1924):

$$\phi(r) = \lambda r^{-12} - \mu r^{-6}. \qquad \ldots\ldots(3.7)$$

Retaining $M^{(1)}$ and $M^{(2)}$ in (3.5), one obtains by a straightforward computation:

$$g_1(r)=\exp-\left\{\phi(r)+2n_1\left[B'(e^{-\varphi(r)/\boldsymbol{k}T}-1)-B''\left\{\frac{2\phi'}{\boldsymbol{k}T}+\frac{\phi''}{\boldsymbol{k}T}-\left(\frac{\phi'}{\boldsymbol{k}T}\right)^2\right\}e^{-\varphi(r)/\boldsymbol{k}T}\right]\right\}, \quad \ldots\ldots(3.8)$$

where B' is the usual second virial coefficient, being equal to

$$\left.\begin{aligned} B' &= \frac{2\pi}{3}\left(\frac{\lambda}{\mu}\right)^{1/2} y^{1/2}\left\{\Gamma(\tfrac{3}{4})-\sum_1^\infty \frac{1}{4m!}\Gamma\left(\frac{2m-1}{4}\right)y^m\right\},\\ B'' &= -\frac{\pi}{3}\int_0^\infty (e^{-\varphi(r)/\boldsymbol{k}T}-1)r^4\,dr\\ &= \frac{\pi}{15}\left(\frac{\lambda}{\boldsymbol{k}T}\right)^{5/12}\left\{\Gamma\left(\frac{7}{12}\right)-\frac{5}{12}\sum_1^\infty\frac{1}{m!}\Gamma\left(\frac{1}{2}m-\frac{5}{12}\right)y^m\right\}, \end{aligned}\right\} \quad \ldots\ldots(3.9)$$

and where $y=(\mu^2/\lambda\boldsymbol{k}T)^{1/2}$.

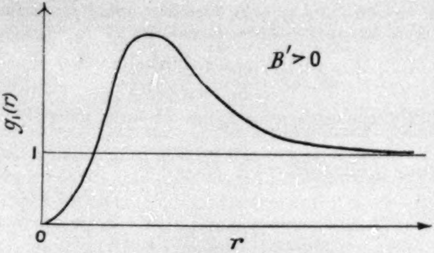

Figure 1. $g_1(r)$ at high temperatures.

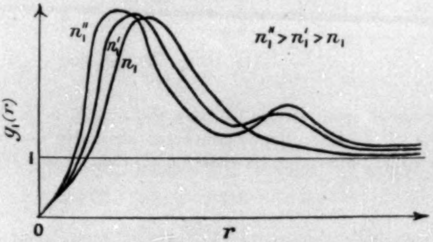

Figure 2. $g_1(r)$ at low temperatures for large values of n_1.

Figures 1 and 2 show the general behaviour of the curve $g_1(r)$ given by (3.8). At high temperatures, it nearly coincides with that of $e^{-\varphi/\boldsymbol{k}T}$. For large values of n_1 and at low temperatures, at which B' and B'' become negative, the curve begins to show another minimum before reaching the maximum. This effect becomes more and more pronounced as the density n_1 becomes larger, in agreement with the experimental evidence of Eisenstein and Gingrich (1940) on liquid argon at 90° K., which shows a similar curve. Our theory here indicates that these phenomena exist quite generally in liquid states.

However, it is expected that at very low temperatures this approximation will not be valid and other methods are required.

APPENDIX 1

THE VALIDITY OF THE EXPANSION (2.8)

In order to discuss the validity of the expansion in (2.8), let us consider the integral,

$$I=\frac{1}{\boldsymbol{k}T}\int_0^\infty \frac{1}{D^3}(sD\cosh sD-\sinh sD)\phi'(s)g(s)f(r)\,ds,$$

which, on integration by parts, is reduced to

$$I=\frac{1}{D}\int_0^\infty s\sinh sD\,G(s)f(r)\,ds, \qquad \ldots\ldots(\mathrm{A}\ 1)$$

where
$$G(s)=-\frac{1}{\boldsymbol{k}T}\int_s^\infty g(t)\phi'(t)\,dt. \qquad \ldots\ldots(\mathrm{A}\ 2)$$

$G(s)$ becomes of the order of $\phi(s)$ when s tends to infinity. Since *

$$\int_{-\infty}^{\infty}|f(r)|\,dr=\int_{-\infty}^{\infty}\mathrm{O}\{r\phi(r)\}\,dr$$

converges absolutely, one can express $f(r)$ as a Fourier integral,

$$f(r)=\int_{-\infty}^{\infty}h(\alpha)\,e^{i\alpha r}\,dr,$$

so that the operator D can be regarded as a purely imaginary quantity $i\alpha$. Let

$$I(\alpha)=\int_0^\infty s^2\frac{\sin\alpha s}{\alpha s}G(s)\,ds. \qquad \ldots\ldots(\mathrm{A}\ 3)$$

Then
$$\int_{s_0}^\infty s^2\left|\frac{\sin\alpha s}{\alpha s}\right||G(s)|\,ds=\mathrm{O}\{s_0{}^2\phi(s_0)\},$$

which can be made as small as one likes by choosing s_0 sufficiently large and independent of α. Therefore (A 3) converges *absolutely and uniformly*. In consequence an upper limit $\bar{s}_0$ can be chosen such that for any small quantity ϵ, independent of α,

$$\left|I(\alpha)-\int_0^{s_0}\frac{\sin\alpha s_0}{\alpha s_0}s^2G(s)\,ds\right|<\epsilon, \qquad s>\bar{s}_0. \qquad \ldots\ldots(\mathrm{A}\ 4)$$

On the other hand one can expand the function

$$I(\alpha_1,s_0)=\int_0^{s_0}\frac{\sin\alpha s}{\alpha s}s^2G(s)\,ds$$

in powers of α:

$$I(\alpha_1,s_0)=\sum_1^\infty M^{(\nu)}(s_0)(-)^{\nu+1}\alpha^{2\nu-2},$$

where
$$M^{(\nu)}(s_0)=\frac{1}{(2\nu+1)!}\int_0^{s_0}G(s)s^{2\nu}ds. \qquad \ldots\ldots(\mathrm{A}\ 5)$$

---

* Here the symbol O is employed to denote ' of the order of ' when r tends to infinity.

Replacing $i\alpha$ by D, one has

$$I(s_0, D) = \sum_1^\infty M^{(\nu)}(s_0) D^{2\nu-2},$$

and with the help of (A 4) one obtains

$$I = \sum_1^\infty M^{(\nu)}(s_0) D^{2\nu-2} f(r) + O(\epsilon) f(r). \qquad \ldots\ldots (\text{A } 6)$$

It is clear from (A5) and from the definition of $G(s)$ in (A2), that the ratio $M^{(\nu+1)}(s_0)D^{2\nu}f(r)/M^{(\nu)}(s_0)D^{2\nu-2}f(r)$ will increase when s_0 increases. Consequently the number of terms of the series in (A 6) which are required to ensure the accuracy one may desire in the sum, will also increase with s_0. One observes that when s_0 tends to infinity the higher moments actually diverge and that the number of terms required is infinite. The expression (2.8) is therefore the limiting form and has to be interpreted in the above sense.

For a given value of s_0, for which the relation (A 4) holds, a practical criterion for the determination of the number of terms N required in (A 6) is that

$$\left| \frac{M^{(\nu+1)}(s_0) D^{2\nu} f(r)}{M^{(\nu)}(s_0) D^{2\nu-2} f(r)} \right| \leqslant \rho < 1, \qquad \ldots\ldots (\text{A } 7)$$

where ρ is a measure of accuracy in the approximation. Equation (A 7) also defines the relative importance of individual terms in the series of expansion.

In the example of (3.7) amd (3.8) etc. the condition that $M^{(2)}$ can be neglected in comparison with $M^{(1)}$ is

$$\tau = \left| \frac{M^{(2)} D^2 f(r)}{M^{(1)} f(r)} \right| \leqslant \rho < 1.$$

By the substitution of B', B'' etc. from (3.8) and (3.9) one has

$$\tau = 0{\cdot}238 y^{7/3} \eta^8 \left| \frac{11 n^6 - 5 - 3\eta^6 y^2 (\eta^6 - 1)^2}{\exp \frac{1}{4}\eta^6 \eta^2 (\eta^6 - 2) - 1} \right| \cdot \left| \frac{F_2(y)}{F_1(y)} \right|, \qquad \ldots\ldots (\text{A } 8)$$

where $$\eta_1 = \frac{r_0}{r}, \qquad y^2 = \frac{T_0}{T} \qquad \ldots\ldots (\text{A } 9)$$

$$\left. \begin{aligned} F_1 &= 1{\cdot}22 - (0{\cdot}906 y + 0{\cdot}153 y^2 + 0{\cdot}0378 y^3 + \ldots), \\ F_2 &= 1{\cdot}53 - (4{\cdot}81 y + 0{\cdot}318 y^2 + 0{\cdot}0667 y^3 + \ldots). \end{aligned} \right\} \qquad \ldots\ldots (\text{A } 10)$$

$r_0 = (2\lambda/\mu)^{1/6}$ is the distance at which $\phi(r)$ assumes a minimum value and

$$T_0 = -\phi(r_0)/\boldsymbol{k}.$$

If either $r_0 \ll r$, or $T_0 \ll T$, then τ will be small and B'' can be neglected. At moderately high temperatures, namely $T \gtrsim T_0$, this condition becomes

$$y^2 \eta^8 \left| \frac{11\eta^6 - 5 - 3y^2\eta^6(\eta^6 - 1)^2}{\exp \frac{1}{4}(\eta^6 - 2) y^2 \eta^6 - 1} \right| \leqslant \left| \frac{5F_1}{F_2} \right| \sim 1, \qquad \ldots\ldots (\text{A } 11)$$

which states that there are regions of r, for instance, at the position $r = r_0$, in which B'' is by no means negligible. On account of the high power of η in the expression (A 11), this condition will be fulfilled at relatively large distances.

APPENDIX 2

THE VALIDITY OF THE ITERATION METHOD

The validity of the iteration method is intimately connected with the choice of the trial function $g_0(r)$, which has to satisfy certain boundary conditions. For instance, if an exact solution of the equation (3.1) is chosen as trial function, then there would be no question of validity at all, provided of course the solution is stable against small perturbations.

First of all, we shall examine the validity of the method at large distances. A necessary condition for validity is that $\lim\limits_{\mu\to\infty} g_\mu(r)$ exists and is equal to $g(r)$, which satisfies the boundary condition $g(r)\to 1$, as $r\to\infty$. From (3.3) one has for $\mu\to\infty$

$$g(r)=\exp-\left\{\frac{8\pi n_1 M^{(1)}}{\boldsymbol{k}T}\{g(r)-1\}+\frac{8\pi n_1 M^{(2)}}{r\boldsymbol{k}T}D^2 r\{g(r)-1\}+\frac{\phi(r)}{\boldsymbol{k}T}\right\} \quad \ldots\ldots(\mathrm{B}\,1)$$

At large distances the terms corresponding to the higher moments

$$\frac{1}{r}M^{(\mu)}D^{2\mu-2}f(r)=\mathrm{O}(\phi(r)r^{2-2\mu})$$

are negligible compared with the first moment $r^{-1}M^{(1)}f(r)=\mathrm{O}\{\phi(r)\}$. Neglecting in the exponent of (B 1) terms of higher order in r^{-1} than $\phi(r)$, one obtains the asymptotic expression of (B 1),

$$g(r)\exp\{2n_1B(g(r)-1)\}=e^{-\varphi(r)/\boldsymbol{k}T}, \quad \ldots\ldots(\mathrm{B}\,2)$$

where B is a function of n_1 and T given by

$$B=-\frac{2\pi}{3\boldsymbol{k}T}\int_0^\infty g(r)\phi'(r)r^3\,dr, \quad \ldots\ldots(\mathrm{B}\,3)$$

which equals approximately the second virial coefficient at high temperatures. Now the solution of (B 2) is simply

$$g(r)=\exp\left\{-\frac{\phi(r)}{\boldsymbol{k}T}(1+2n_1B)^{-1}\right\}. \quad \ldots\ldots(\mathrm{B}\,4)$$

When $B>0$, namely at high temperatures, the factor $(1+2n_1B)^{-1}$ of the exponent (B 4) is always smaller than unity, and it is obvious that if (B 4) is adopted as a trial function, the iteration method is valid.

When $B<0$, namely at lower temperatures, the exponent will become infinitely large if $n_1\simeq n_0$, where n_0 is a solution of the equation

$$2n_0B(n_0,T)=-1. \quad \ldots\ldots(\mathrm{B}\,5)$$

The solution (B 4) is singular when $n=n_0$, in the neighbourhood of which the iteration breaks down. The limiting values n_0 must be in some way connected with the densities of an assembly of molecules undergoing a change of phase.

According to Green (1947), the pressure is equal to

$$p=n_1\boldsymbol{k}T-\frac{n_1^2}{6}\int_0^\infty g(r)\phi'(r)4\pi r^3\,dr=n_1\boldsymbol{k}T(1+n_1B). \quad \ldots\ldots(\mathrm{B}\,6)$$

By the substitution of (B 5) into (B 6) the corresponding limiting pressure is obtained

$$p_0 = \tfrac{1}{2} n_0 \boldsymbol{k} T, \qquad \ldots\ldots \text{(B 7)}$$

which states that the pressure produced by each molecule, e.g. the molecule of a saturated vapour,is about $\frac{1}{2}\boldsymbol{k}T$.

Putting, in the case of nitrogen (Fowler 1936), $\mu = 140 \times 10^{-60}$, $\lambda = 37 \times 10^{-104}$, so that $y^2 = 386{\cdot}7/T$, and assuming that at moderately high temperatures

$$B = B' = \frac{2\pi}{3}\left(\frac{\lambda}{\mu}\right)^{1/2} y^{1/2}\left\{\Gamma\left(\frac{3}{4}\right) - \sum_{1}^{\infty} \frac{1}{4m!}\Gamma\left(\frac{2m-1}{4}\right) y^m\right\} \qquad \ldots\ldots \text{(B 8)}$$

approximately, one obtains from (B 5) the limiting density and the limiting pressure

$$\left.\begin{aligned} n_0 &= 0{\cdot}464 \times 10^{22} y^{1/2}\{1{\cdot}22 - 0{\cdot}906y - 0{\cdot}153y^2 - 0{\cdot}037y^3 - \ldots\}^{-1}, \\ p_0 &= \tfrac{1}{2} n_0 \boldsymbol{k} T. \end{aligned}\right\} \qquad \ldots\ldots \text{(B 9)}$$

It is clear from (3.1) that on letting n_1 tend to zero, one has

$$g \to e^{-\varphi(r)/\boldsymbol{k}T}, \qquad B \to B',$$

so that (B 8) represents the first term in the expansion of B in powers of n_1. The assumption thet $B \simeq B'$ is equivalent to the assertion that terms of higher powers than the zeroth in n_1 in the expansion are small. Hence n_0 in (B 9) is the smallest root of the equation (B 5) expanded in powers of n_1, and represents the limiting value of n_1 in the gas region. Thus n_0 and p_0 given by (B 9) should be near the values of n_1 and p of a saturated vapour. The Table gives the computed values of n_0 and p_0 at several temperatures for nitrogen and also the observed densities and vapour pressure of the same element in saturated vapour states. The agreement between the two sets of values is close enough in this rough approximation.

Saturated Vapour Pressures and Densities of Nitrogen

Temp. (° K.)	n_0 ($\times 10^{-21}$/cm³)	n_0 (gm/cm³)	n_0 (gm/cm³) (obs.)	p_0 (atm.)	Pressure (atm.) (obs.)
108·8	2·39	0·110	—	22·37	13·60
116·8	2·71	0·125	—	27·24	20·47
119·4	2·76	0·128	0·118	—	—
121·5	2·95	0·136	0·164	—	—
123·2	2·98	0·138	—	30·83	26·75
124·9	3·05	0·141	0·200	—	—

Finally, the validity of the approximation method at small distances will be considered. In the following, a tentative criterion will be adopted, as a rigorous treatment is not available in the present stage.

Let $g_\mu(r)$ be varied to $g_\mu(r)(1+\epsilon)$, ϵ being a small quantity; $g_{\mu+1}(r)$ is thereby changed to $g_{\mu+1}(r) + \epsilon W(r)$. According to (3.3) and (3.2) one has

$$\delta \ln g_{\mu+1}(r) = \delta\left\{\frac{8\pi n_1}{r\boldsymbol{k}T}(M^{(1)} + M^{(2)}D^2) r(g(r)-1)\right\},$$

$$\delta M_\mu^{(1)} = \epsilon M_\mu^{(1)}; \qquad \delta M_\mu^{(2)} = \epsilon M_\mu^{(2)},$$

so that

$$W(r) = g_{\mu+1}(r)\left\{\frac{16\pi n_1}{r\boldsymbol{k}T}(M_\mu^{(1)} + M_\mu^{(2)}D^2) r(g(r)-\tfrac{1}{2})\right\}.$$

The ratio

$$\tau_\mu = \frac{\epsilon W(r)}{\epsilon g_\mu(r)} = \frac{g_{\mu+1}(r)}{g_\mu(r)} \left\{ \frac{16\pi n_1}{r\boldsymbol{k}T} (M_\mu^{(1)} + M_\mu^{(2)} D^2) r (g(r) - \tfrac{1}{2}) \right\}$$

gives a measure of the relative deviations of $g_\mu(r)$'s of two consecutive orders produced by such a variation. A small τ_μ means that higher order approximations are not sensitive to small deviations of the lower order approximations and thus ensures great stability and rapid convergence of the sequence $g_\mu(r)$. Then each higher order iteration will bring about closer approximation to the exact solution.

Hence a condition for validity of the iteration is

$$|\tau_\mu| = \frac{g_{\mu+1}}{g_\mu} \left| \left\{ \frac{16\pi n_1}{r\boldsymbol{k}T} (M_\mu^{(1)} + M_\mu^{(2)} D^2) r (g(r) - \tfrac{1}{2}) \right\} \right| < 1. \qquad \ldots\ldots \text{(B 10)}$$

Equation (B 10) also gives an estimation of the closeness of the approximation in the μth order. It is interesting to note that at large distances (B 10) reduces to

$$\left| \frac{8\pi n_1}{\boldsymbol{k}T} M_\mu^{(1)} \right| < 1, \quad \text{or} \quad |2n_1 B| < 1,$$

in agreement with the condition given by (B 5).

ACKNOWLEDGMENTS

The author wishes to thank Professor Born for advice during the investigation, and Dr. Yang for the benefit of discussions. He also wishes to express his indebtedness to the British Imperial Chemical Industries for the tenure of a fellowship which rendered the work possible.

REFERENCES

EISENSTEIN, A., and GINGRICH, N. S., 1940, *Phys. Rev.*, **58,** 307.
FOWLER, R. H., 1936, *Statistical Mechanics* (Cambridge : University Press), p. 306.
GREEN, H. S., 1947, *Proc. Roy. Soc* .A, **189,** 103.
KIRKWOOD, J. G., 1942, *J. Chem. Phys.*, **10,** 344.
(LENNARD-) JONES, J. E., 1924, *Proc. Roy. Soc.* A, **106,** 463.

Statistical Equilibrium and Radiation Damping

BY J. HAMILTON*
University of Manchester

Communicated by L. Rosenfeld; MS. received 6th October 1949, *and in amended form 9th May* 1950

ABSTRACT. The reason why the usual form of radiation damping theory does not satisfy the principle of detailed balancing is discussed. A form of damping theory satisfying statistical equilibrium is developed.

THE damping equations for the scattering, creation or annihilation of mesons during the transition of a system having a continuous energy spectrum from a state q to a state p lead to a transition probability $\rho_p |U_{pq}|^2$ where U_{pq} satisfies

$$U_{pq} = H_{pq} - i\pi \int H_{pr} \rho_r d\Omega_r U_{rq}. \qquad \ldots\ldots (1)$$

---

* Now at Christ's College, Cambridge.

r runs over all final states (i.e. states of the same energy as p and q) and $\rho_r d\Omega_r$ is the density of such states in the solid angle $d\Omega_r$. H_{pr} is the compound matrix element connecting r and p.

The damping equation (1) was derived by Heitler (1941) and Wilson (1941) by assuming an exponential time decay of the occupation amplitude a_q of the initial state q. The usual perturbation theory treatment assumes $a_q=1$ for all time, and gives the well-known expression $\rho_p|H_{pq}|^2$ for the transition probability.

It was shown by the author (Hamilton 1947, to be referred to as I) that an equivalent formulation in terms of approximate eigenfunctions of the coupled system of matter and radiation could be given, and that it led to equation (1). In this treatment the sum of the occupation probabilities of the various states is normalized, so that a decrease in the occupation amplitude of the initial state q accompanies any increase in the total occupation amplitudes of the final states r. (Furthermore, the problem is regarded as being the calculation of the transition probabilities arising from given matrix elements. The latter are to be determined by the methods of Schwinger and Tomonaga.)

U_{pq} is not a Hermetian matrix, and several examples have been given (Hamilton and Peng 1944) of processes involving elementary particles in which $|U_{pq}|^2 \neq |U_{qp}|^2$. Consequently it appears that the principle of detailed balancing is no longer valid when the damping correction is included. However, a closer examination of the damping solutions (according to either of the methods mentioned above) shows that they are, in principle, not compatible with detailed balancing. The transition probability $\rho_p|U_{pq}|^2$ is derived by considering the system initially to be in the state q only, and as time proceeds there will be a finite probability of the system being in any one of a set of final states r, one of which is p. Similarly, $\rho_q|U_{qp}|^2$ is derived by considering the system initially to be in state p only. Thus U_{pq} and U_{qp} do not refer to processes which are in any sense inverse. For detailed balancing to be valid in the usual sense it is necessary that probability for transitions from q to p be independent of the occupation probabilities of other final states r. As it is an essential part of damping theory that these probabilities are related, detailed balancing becomes meaningless in a damping problem.

It is also important to notice that the normalization of the occupation probabilities over the initial and final states means that the process described by U_{pq} is not related to statistical equilibrium. In statistical equilibrium the initial state will be a mixture of states $q_1, q_2, \ldots\ldots$ and the normalization condition has to include their occupation probabilities. It will certainly not be true that a solution, in which the occupation probability of a single state decreases exponentially from unity, while those of the other states increase from zero, can in any way represent statistical equilibrium. It is necessary to choose a solution which satisfies initial conditions more appropriate to equilibrium.

In the remainder of the present paper it is shown that the damping approximation as developed in I can be adapted to give results which do not violate statistical equilibrium. It is necessary to consider an ensemble of systems such that their initial states are consistent with statistical equilibrium. The approximations which have to be made at various stages are of the same types as the approximations which were necessary in I.

The notation and methods of I will be used. Any state Ψ of the system can be expanded in terms of the wave functions ψ_r of the free electrons, photons, mesons, etc.

$$\Psi=\sum_r a_r\psi_r=\sum_r a_r\phi_r \exp(-iE_r t).$$

ϕ_r is the time independent wave function, and E_r is the corresponding energy ($\hbar = 1$ throughout). The amplitudes a_r vary with time according to the equation

$$a_r \exp(-iE_r t) = \sum_\nu c_\nu A_r^\nu \exp(-i\Lambda_\nu t), \qquad \ldots\ldots(2)$$

where the Λ_ν are the energy values of the interacting system, while the A_r^ν are a normal orthogonal set of amplitudes satisfying

$$\Lambda_\nu \,.\, A_r^\nu = \sum_s H_{rs} A_s^\nu. \qquad \ldots\ldots(3)$$

The H_{rs} are the usual (compound) matrix elements connecting the final states s and r. The c_ν are determined from the initial values of the amplitudes $a_r(0)$ by the relation

$$c_\nu = \sum_r \bar{A}_r^\nu a_r(0),$$

where $\bar{A}$ is the complex conjugate of A.

The inital conditions for the ensemble of systems in statistical equilibrium can be written in the general form

$$\overline{\overline{\bar{a}_r(0)\,.\,a_p(0)}} = 0, \text{ if } r \neq p; \qquad \overline{\overline{\bar{a}_r(0)\,.\,a_r(0)}} = |f(E_r)|^2, \qquad \ldots\ldots(4)$$

where $f(E_r)$ is some 'slowly varying' function of E_r (i.e. $f(E_r)$ varies little over the line breadths involved in the problem). The double bar denotes the average over the ensemble of systems. Equation (4) can be written in the form

$$a_r(0) = f(E_r) \exp(i\phi_r),$$

where $$\overline{\overline{\exp\{i(\phi_r - \phi_p)\}}} = 0 \quad \text{if} \quad r \neq p.$$

The roots Λ_ν are repeated in each energy interval ΔE, (cf. I §6), and the roots inside one interval ΔE will be denoted by the index α. The solution of (3) is obtained by substituting $A_s^\mu = d_\alpha V_{s\alpha}/(\Lambda_\mu - E_s)$, and then the $V_{s\alpha}$ satisfy the integral equation

$$V_{s\alpha} = \pi \cot\{(\Lambda_\alpha - E_s)\pi/\Delta E\} \int H_{sr} \rho_r d\Omega_r V_{r\alpha},$$

the integration going over all final states. Normalizing the $V_{r\alpha}$ so that

$$\int \rho_r d\Omega_r \bar{V}_{r\alpha} V_{r\beta} = \delta_{\alpha\beta}, \qquad \ldots\ldots(5)$$

the condition $\sum_s |A_s^\mu|^2 = 1$ gives $|d_\alpha|^2 = (\Delta E/\pi^2) \sin^2\{(\Lambda_\alpha - E_s)\pi/\Delta E\}$.

The variation of the a_r with time is given by

$$a_r = \sum_\mu |d_\alpha|^2 \sum_s U_{rs} f(E_s) \exp(i\phi_s) \bar{V}_{s\alpha} V_{r\alpha}/(\Lambda_\mu - E_s)(\Lambda_\mu - E_r) \,.\, \exp\{i(E_r - \Lambda_\mu)t\} \qquad \ldots\ldots(6)$$

Summing the Λ_μ over the different energy intervals gives

$$a_r = -\underset{E_s}{\Sigma_{(E_r)}} \sum_{[s]} U_{rs} f(E_s) \exp(i\phi_s)[\exp\{i(E_r - E_s)t\} - 1]/(E_r - E_s)$$

$$+ (1/\Delta E) f(E_r) \sum_{[s]} \exp(i\phi_s) \left[\sum_\alpha \bar{V}_{s\alpha} V_{r\alpha} - ixU_{rs}\right], \qquad \ldots\ldots(7)$$

where $\sum_{E_s}{}_{(E_r)}$ denotes the summation over all E_s values except E_r, while $\sum_{[s]}$ denotes the sum over the s values corresponding to the energy value E_s. Also,

$$U_{rs} = \frac{1}{\pi}\sum_{\alpha}\frac{\bar{V}_{s\alpha}V_{r\alpha}}{i+\cot\{(\Lambda_\alpha - E_s)\pi/\Delta E\}}. \qquad \ldots\ldots(8)$$

U_{rs} satisfies the integral equation (1). In (7) $x = t\,\Delta E$. Using the relation

$$\left.\begin{aligned}\overline{\overline{\sum_{[s']}\exp\{i(\phi_s - \phi_{s'})\}}} &= 1, \text{ if } E_s = E_{s'},\\ &= 0 \text{ otherwise}\end{aligned}\right\},$$

it is easy to see that

$$\begin{aligned}\overline{\overline{\bar{a}_r a_p}} = \Bigg[&\sum_{E_s}{}_{(E_r, E_p)}\sum_{[s]}\bar{U}_{rs}U_{ps}[\exp\{i(E_r - E_s)t\} - 1]\\ &\qquad\times[\exp\{i(E_p - E_s)t\} - 1]/(E_r - E_s)(E_p - E_s)\\ &+(1/\Delta E)^2\delta(E_r, E_p)\sum_{[s]}(\sum_{\alpha}\bar{V}_{r\alpha}V_{s\alpha} + ix\bar{U}_{rs})(\sum_{\alpha}V_{p\alpha}\bar{V}_{s\alpha} - ix\,U_{ps})\\ &-(1/\Delta E)\{1 - \delta(E_r, E_p)\}\sum_{[s]}\{U_{ps}(\sum_{\alpha}\bar{V}_{r\alpha}V_{s\alpha} + ix\bar{U}_{rs}) - \bar{U}_{rs}(\sum_{\alpha}V_{p\alpha}\bar{V}_{s\alpha} - ixU_{ps})\}\\ &\qquad\times[\exp\{i(E_p - E_r)t\} - 1]/(E_p - E_r)\Bigg]|f(E_r)|^2. \qquad \ldots\ldots(9)\end{aligned}$$

In deriving (9) and in what follows, it is assumed that it is sufficiently accurate to take the values of U_{rs}, $V_{s\alpha}$ and $f(E_s)$ as those on the energy shell $E_s = E_r$. Also $\delta(E_r, E_p) = 1$, if $E_r = E_p$, and zero otherwise. The summation over E_s splits up into the two cases $E_r = E_p$, $E_r \neq E_p$, giving

$$\begin{aligned}\overline{\overline{\bar{a}_r a_p}} = (1/\Delta E)\{1 - \delta(E_r, E_p)\}\Bigg[&-2i(\pi - x)\sum_{[s]}U_{rs}U_{ps} - 2ix\sum_{[s]}\bar{U}_{rs}U_{ps}\\ &-\Delta E(U_{pr} - \bar{U}_{rp})\Bigg][\exp\{i(E_p - E_r)t\} - 1]|f(E_r)|^2/(E_p - E_r)\\ +(1/\Delta E)^2\delta(E_r, E_p)\Bigg[&(2\pi x - x^2)\sum_{[s]}\bar{U}_{rs}U_{ps} + ix\Delta E(\bar{U}_{rp} - U_{pr})\\ &+ x^2\sum_{[s]}\bar{U}_{rs}U_{ps}\Bigg]|f(E_r)|^2. \qquad \ldots\ldots(10)\end{aligned}$$

Here the orthogonal property of the $V_{s\alpha}$ is used to give

$$\sum_{[s]}(\sum_{\alpha}\bar{V}_{r\alpha}V_{s\alpha})U_{ps} = \Delta E\sum_{\alpha}\bar{V}_{r\alpha}\int\rho_s d\Omega_s V_{s\alpha}U_{ps} = \Delta E\,U_{pr}, \text{ etc.}$$

From (8)

$$U_{pr} - \bar{U}_{rp} = -(2i/\pi)\sum_{\alpha}V_{p\alpha}\bar{V}_{r\alpha}\sin^2\{(\Lambda_\alpha - E_r)\pi/\Delta E\},$$

while the orthogonality relation (5) gives

$$\sum_{[s]}\bar{U}_{rs}U_{ps} = (\Delta E/\pi^2)\sum_{\alpha}\bar{V}_{r\alpha}V_{p\alpha}\sin^2\{(\Lambda_\alpha - E_r)\pi/\Delta E\}.$$

Thus (10) reduces to

$$\overline{\overline{\bar{a}_r a_p}} = \delta(E_r, E_p)(1/\Delta E)\sum_{\alpha}\bar{V}_{r\alpha}V_{p\alpha}|f(E_r)|^2. \qquad \ldots\ldots(11)$$

Taking the s values as a discrete set on the shell E_s, the orthogonality relations (5) can be written

$$(1/\Delta E)\sum_{[s]}\overline{V}_{s\alpha}V_{s\beta}=\delta_{\alpha\beta},$$

so that the other set of orthogonality relations become

$$\left.\begin{aligned}(1/\Delta E)\sum_{\alpha}\overline{V}_{r\alpha}V_{p\alpha}&=0, \quad \text{if } r\neq p;\\ &=1, \quad \text{if } r=p.\end{aligned}\right\}.$$

Hence equation (11) shows that the initial equilibrium conditions (4) are invariant with respect to time.

Although the mutual interaction of the final states, which is necessary for radiation damping, makes it impossible, in general, to use the concept of detailed balancing, it is clear that radiation damping does not lead to any effects which are in contradiction with the general ideas of quantum statistical mechanics.

REFERENCES

HAMILTON, J., 1947, *Proc. Phys. Soc.*, **59,** 917.
HAMILTON, J., and PENG, H. W., 1944, *Proc. R. Irish. Acad.*, **49A,** 197.
HEITLER, W., 1941, *Proc. Camb. Phil. Soc.*, **37,** 291.
WILSON, A. H., 1941, *Proc. Camb. Phil. Soc.*, **37,** 301.

LETTERS TO THE EDITOR

A Photographic Method for determining Half-Lives

This letter describes a photographic method of determining the half-lives of radioactive materials.

The method is similar to that of Zuber (1948), who compared the intensities of blackening produced by placing a radioactive metal on a photographic film at different times during its decay, the exposure times being so chosen from a previous knowledge of the approximate half-life that the images were of roughly the same degree of blackness. The same procedure was adopted for the present experiment; however, owing to the stronger source available, the decay could be observed over a large number of half-lives, and thus greater accuracy obtained.

^{64}Cu was chosen as the isotope whose half-life was to be determined. A copper specimen consisting of 1 cm^2 of spectroscopically pure foil of thickness $1{\cdot}2\times10^{-3}$ cm. was irradiated with slow neutrons in the B.E.P.O. at Harwell, and the experiment was started 36 hours after the foil's removal from the pile. Ilfex x-ray film was used and the first exposure was 8 seconds. During subsequent days, further exposures were made on the same piece of film, the exposure times being increased so as to maintain approximately the same degree of blackening. Thus after 39 hours an exposure of 68 seconds was given, after 120 hours an exposure of about 100 minutes. At the end of the experiment, the film was developed for 10 minutes in ID 19, thorough rocking of the dish being maintained to prevent uneven development.

Another piece of Ilfex film was exposed for 60, 63, 66, 69, 72 and 75 seconds, 39 hours after the start of the main experiment. The intensities thus obtained covered the range of intensities expected during the main exposure experiment, and provided a convenient 'step-wedge' for evaluating these exposures. To compare the various images, positives of these two films were obtained by contact printing on ultra contrasty bromide paper. This showed up differences of intensity well, and intensities could be compared to within about 2%. Thus the activity of the source at various times could be calculated.

The Figure shows the logarithm of the intensity of the source plotted against time, the intensity at $T=0$ being taken as unity. It will be seen that after 120 hours the effect of the background due to other activities in the specimen became noticeable, but, on the assumption that these have half-lives considerably longer than that of ^{64}Cu, this background can be regarded as constant and a simple calculation then enables us to eliminate it. Thus useful observations could be extended over a further two days.

The half-life, calculated by least squares from the readings plotted in the Figure is $12{\cdot}82 \pm 0{\cdot}03$ hours. This value, however, must be corrected for the effect of latent image fading, which causes the earlier images to appear weaker than if they had been developed soon after exposure. The correction was evaluated concurrently with the main experiment using a long half-life isotope (250-day ^{65}Zn), and this leads to an adjustment of the half-life of ^{64}Cu to $12{\cdot}80 \pm 0{\cdot}04$ hours. This value agrees well with that of van Voorhis (1936), $12{\cdot}8 \pm 0{\cdot}1$ hours.

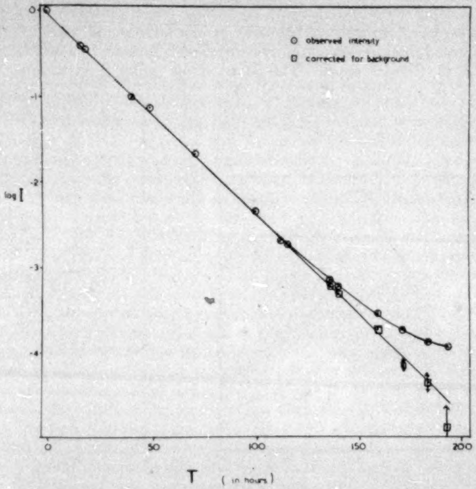

The fact that a straight line was obtained in the Figure indicates that in this case the blackening depended only on the total amount of radiation received (reciprocity law). Since the blackening of the photographic film was mainly due to electrons and positrons, this confirms the view that β-rays do not produce reciprocity failure.

The photographic method of determining half-lives will not in general be more accurate than counting methods. It would, however, appear to be useful for determining half-lives of the order of seconds, since manipulation at the time of the experiment is extremely simple. However, in cases where the blackening is produced entirely or mainly by γ-rays, it may be necessary to apply corrections for reciprocity failure of the photographic film.

Research Laboratory on the Physics and
Chemistry of Rubbing Solids,
Department of Physical Chemistry, Cambridge.
23rd June 1950.

E. Rabinowicz.

van Voorhis, S. N., 1936, *Phys. Rev.*, **50,** 895.
Zuber, K., 1948, *Helv. Phys. Acta*, **21,** 365.

An Order–Disorder Transition Curve in Cobalt Ammonium Sulphate below 0·1° K.

Measurements have been made of the magnetic properties of a spherical single crystal of cobalt ammonium sulphate along its three magnetic axes at temperatures below 0·1° K., using the technique of magnetic cooling. Along the K_1 axis * an interesting new effect was observed.

Measurements were made of the dependence of the differential adiabatic susceptibility (as found by applying a 40 c/s. alternating field of amplitude about 1 gauss) on steady parallel field. Usually such a steady field results in a decrease in differential susceptibility (see, for example, Garrett 1950). This is due partly to the magneto-caloric effect and the related difference between the adiabatic and isothermal susceptibilities—this effect must *always* result in a decrease in differential susceptibility—and partly to ordinary paramagnetic saturation. Along the K_1 axis at temperatures below the Curie point, however, the application of a steady field was found to give an *increase* in the differential susceptibility. Further investigation showed that the susceptibility continued to increase to a fairly sharp maximum and then began to decrease again. The value of the steady field required to reach this maximum increased from zero at the Curie point to about 310 gauss at the lowest temperature reached. The effect is shown in Figure 1. On integration the magnetization M is found as a function of the field H along an isentropic. From these magnetization curves Figure 2 has been drawn, showing lines of constant magnetization and lines of constant entropy on an (H, T) diagram. In constructing this diagram : (i) the entropy S was found from statistical thermodynamics, knowing the principal ionic g-values and the initial field and temperature from which, on demagnetization, each isentropic is reached; (ii) the absolute temperature T in zero field was found as a function of S from relaxation heating measurements (method of de Klerk, Steenland and Gorter 1948) made along the K_3 axis (χ'' was found to be inapplicable at all temperatures when the alternating field was applied along the K_1 axis); and (iii) the magneto-caloric rise or fall in temperatures on applying a steady field was found by evaluating the increase in enthalpy

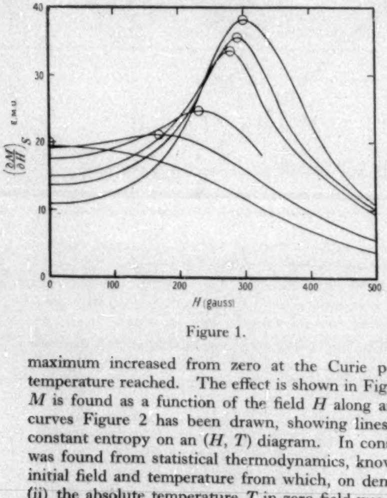

Figure 1.

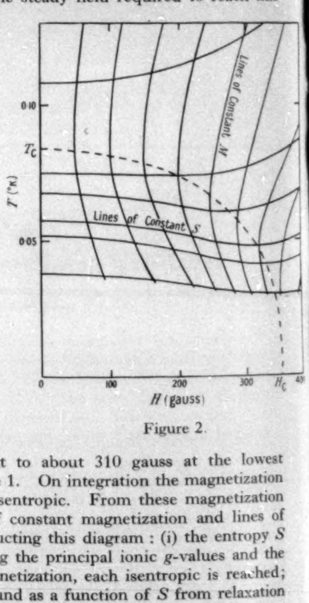

Figure 2.

$$\Delta E = \int_0^H M\,dH_{\text{isentropic}} \quad \text{and deriving} \quad \Delta T = (\partial \Delta E / \partial S)_H.$$

---

* There are two sets of ions in this crystal. At low temperatures the ions behave as though there were only one spin per ion, and are also highly anisotropic. The K_1 axis is inclined at angle of 33° to the strong axis ($g = 6{\cdot}2$) of the ions in both sets.

It will be seen from Figure 2 that the region of anomalous behaviour, where a steady field produces an increase in susceptibility and a fall in temperature, is bounded by a transition curve of crudely parabolic shape. This curve also is shown on Figure 2, being the locus of the minima in the curves of constant magnetization, and must also be the locus of points of lowest temperature on the isentropics, since $(\partial T/\partial H)_S = -(\partial M/\partial S)_H$.

Many features of these experiments are in agreement with the predictions of the model of Sauer and Temperley (1940), designed in the first place to apply to the paramagnetic alums. The authors show that, as a result of dipole–dipole interaction between the ions, the state of lowest energy at the absolute zero and in zero field is that for which alternate rows of ions are aligned in opposite directions. At temperatures other than the absolute zero Sauer and Temperley make use of the Bragg–Williams approximation, and show that the appearance of the ordered phase should be confined to a region on the (H, T) diagram bounded by a transition curve very similar in shape to that shown in Figure 2. This curve meets the temperature axis at right angles at the Curie temperature T_C, and at absolute zero meets the field axis at a field H_C. The values calculated for T_C and H_C hold only for a cubic crystal, so that no quantitative agreement would be expected : but the ratio $\boldsymbol{k}T_C/\mu H_C$ should be 2 irrespective of crystal structure. In cobalt ammonium sulphate the alignment presumably takes place along the strong magnetic axes of the ions in each set, at an angle of 33° to the applied field. Allowing for this, $H_C = 300$ gauss : then, taking $T_C = 0{\cdot}084°$ K. and $\mu = 3{\cdot}1\beta$, the ratio $\boldsymbol{k}T_C/\mu H_C$ is found to be 1·35, in rough agreement with theory. A feature of Sauer and Temperley's model is that the transition should be second-order between T_C and $\frac{2}{3}T_C$ (discontinuity in $(\partial M/\partial H)_T$), whereas below $\frac{2}{3}T_C$ there should be a first-order transition with a discontinuity in M. In practice the transition is found to be smooth throughout the accessible temperature range (T_C to $0{\cdot}4T_C$). This discrepancy, and the departure of the observed $\boldsymbol{k}T_C/\mu H_C$ from the theoretical value 2, are probably due to the fact that Sauer and Temperley assume the Lorentz form for the local field, that is, the average field acting on the ions is taken to be the same (for a spherical specimen) as the externally applied field. In higher approximations this is not so. Both the Onsager and Van Vleck theories indicate that the internal field in a spherical specimen should be less than the applied field by an amount proportional to $(M/H_{\mathrm{ext}})^2$. It can easily be seen that this would prevent any discontinuous change in the magnetization, and would result in the appearance of an intermediate state, where the magnetization might be expected to adjust itself to such a value that the internal field is precisely the critical field at that temperature. Calculation, using either the Onsager or the Van Vleck form of the local field, shows that the width of this intermediate state should be about 100 gauss, which is of the order observed. In this region there should be a marked Barkhausen effect.

From the point of view of Sauer and Temperley's model, a more direct test would be provided by a crystal containing only one ion in unit cell, such as cobalt fluosilicate, since in this case the principal ionic axes must necessarily coincide with the principal magnetic axes of the crystal.

A fuller account of the experiments, giving the results obtained along all three magnetic axes, will appear later.

Royal Society Mond Laboratory,
Cambridge.
12th June 1950.

C. G. B. GARRETT.

GARRETT, C. G. B., 1950, *Proc. Roy. Soc.* A (in the press).
DE KLERK, D., STEENLAND, M. J., and GORTER, C. J., 1948, *Nature, Lond.*, **161**, 678.
SAUER, J. A., and TEMPERLEY, H. N. V., 1940, *Proc. Roy. Soc.* A, **176**, 203.

The Half-Life of the Isomeric State in ^{169}Tm

The half-life of the short-lived ^{169}Tm isomer has been measured using the differential type delayed coincidence recorder described by Bunyan *et al.* (1949). De Benedetti and McGowan (1948) found the half-life of this isomer to be 1·0 microsecond; the present investigation has yielded a value which is considerably lower, namely

$$T_{\frac{1}{2}} = 0{\cdot}658 \pm 0{\cdot}003 \text{ microsecond.}$$

The error given was derived from a least squares analysis of the observations shown in the Figure based on the assumption that all errors are confined to the counting rate values, the pulse delay times being assumed correct. There may, in addition, be an error in the calibration of the delay lines in the recorder. The calibration was carried out both before and after the measurement using a crystal-controlled megacycle oscillator. An independent calibration had also been made by Mr. D. E. Bunyan of this department (cf. footnote to Bunyan *et al.* 1949). Our measurements agreed within 1% and gave values of the pulse delay times within 2% of those computed from the constants of the delay lines.

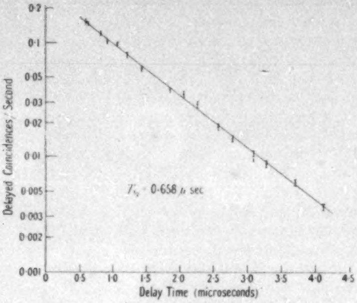

Decay of ^{169}Tm *

Physics Department,
University of Birmingham.
19th June 1950.

E. W. Fuller.

Bunyan, D. E., *et al.*, 1949, *Proc. Phys. Soc.* A, **62**, 253.
De Benedetti, S., and McGowan, F. K., 1948, *Phys. Rev.*, **74**, 728.

Scintillations from Naphthalene–Anthracene Crystals

Anthracene is one of the most suitable organic crystals for the scintillation counting of ionizing radiations. It is transparent to its own fluorescent radiation, and gives large scintillation pulses in the region of 4000–5000 A., which match the spectral response of photo-multipliers with Sb–Cs cathodes. The growth of very large crystals, which are desirable for the absorption and measurement of high energy γ-rays, is however technically difficult with anthracene, due to its relatively high melting-point (216° c.) and the deterioration of the liquid when in contact with oxygen.

Naphthalene (M.P. = 80° c.) can be readily grown in large crystals several inches in diameter, by controlled slow freezing from the liquid state. The scintillation properties of naphthalene—transparency, decay time, energy conversion efficiency—are comparable with those of anthracene, but its fluorescent emission is in the region of 3100–3700 A. This is on the edge of the photo-tube spectral response, and the pulses obtained are only about 20% (dependent on the photo-tube characteristic) of those from anthracene.

Large mixed crystals of naphthalene, containing up to 9% by weight of anthracene (M.P. 77–80° c.) can be grown in a similar manner to those of pure naphthalene. A range of crystals, about 2 cm. diameter × 1 cm. thick, have been prepared, containing various concentrations of anthracene, and the scintillations excited in these by Po α-particles have been investigated. Measurements were made on several small transparent samples cut from each crystal to allow for variations from its mean composition. These gave satisfactorily consistent results, and a mean value was obtained for each concentration. The α-source was mounted 2 mm. in air from the crystal sample, which was placed in direct contact with the face of a 5311 photo-multiplier tube. Integral pulse size distributions were plotted in the usual manner, using a cathode follower, linear amplifier, discriminator and scaler. A broad flat ' plateau ' was obtained in each case, giving the total α-particle flux through the specimen, and the average pulse size was determined from the discriminator setting at which the counting rate was reduced to 50%. The mean pulse sizes for each concentration, expressed relative to those from a pure anthracene crystal, are shown in Figure 1.

The fluorescent emission from the mixed crystals contains two spectral components, N (3100–3700 A.) characteristic of naphthalene, and A (4000–5000 A.) characteristic of anthracene. The intensities of N and A have been measured independently by introducing suitable filters between the crystal and the photo-tube. The average pulse sizes under α-excitation were observed as above, and compared with those from pure naphthalene and pure anthracene under the same conditions. The total intensities obtained by adding the relative proportions of each component measured thus, agreed within 2% with the values obtained from the previous direct observations. This shows the absence of any further fluorescent component within the spectral range of the photo-tube, and also indicates the consistency of the experimental method. The intensities of N and A, relative to the pure crystals, are plotted against composition in Figure 2.

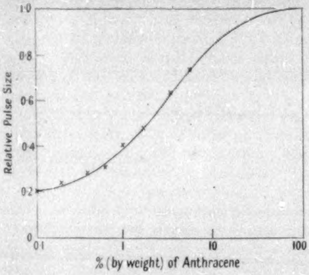

Figure 1.

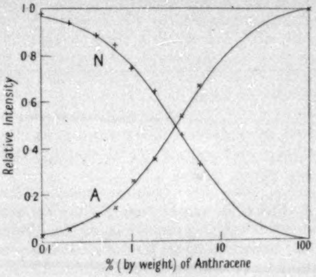

Figure 2.

As the concentration is increased N is progressively suppressed, but *all* the suppressed radiation is emitted as A. This is consistent with the 'exciton' theory proposed by Bowen *et al.* (1949) to account for similar phenomena observed under ultra-violet excitation. The electronic energy excited by the incident radiation is transferred by resonance from molecule to molecule within the crystal, until it is captured by a single molecule, which fluoresces. The probability of capture of the 'exciton' is greater for an anthracene molecule than for a naphthalene molecule because of the lower energy of its excited state. On the simplest model, if k is the ' exciton ' capture probability of the anthracene molecule relative to that of the naphthalene molecule, and x is the anthracene concentration in mols/mol. of naphthalene, then the proportion of N radiation will be

$$n=\frac{1}{1+kx} \qquad \ldots\ldots(1)$$

and the proportion of A radiation will be $1-n$. The solid curves in Figure 2, computed from (1) for $k=43$, are in excellent agreement with the observations.

This value of $k=43$ for Po α-excitation is very much smaller than that of 5×10^4 found by Bowen *et al.* (1949) for naphthalene–anthracene mixtures excited by 2900–3200 A. radiation at 20° c. The difference is significant and is probably related to the low energy-conversion coefficient for α-excitation (>100 ev. per emitted photon) compared with the approximately 100% ultra-violet quantum efficiency of fluorescence.

The 'excitons' produced by the α-particle will be of higher energy (approximately ionization energy) than in the ultra-violet case, i.e. the inter-molecular resonance process may be one of ionization transfer, rather than of excitation transfer. This will considerably reduce the ratio of the differences between the 'exciton' energy and the excited energy levels of the anthracene and naphthalene molecules. The dissipation of the incident α-energy in alternative non-radiative processes may also contribute to the low efficiency and reduction in k.

The dependence of k on the mode of fluorescence excitation in naphthalene–anthracene and other mixed organic crystals is being further investigated, since it represents a new fundamental approach to the study of excitation, ionization and fluorescence in solid crystals.

I am indebted to Mr. F. A. Black, who prepared the crystal specimens.

Department of Natural Philosophy,
The University, Glasgow.
10th June 1950.

J. B. Birks.

Bowen, E. J., Mikiewicz, E., and Smith, F. W., 1949, *Proc. Phys. Soc.* A, **62**, 26.

REVIEWS OF BOOKS

Calcul Opérationel, by É. Labin. Pp. 145. (Paris: Masson et Cie, 1949.) 780 fr.

This work may be regarded as a list of general rules of the operational calculus. These are given without proof, but the conditions under which they apply are stated rigorously. The subject is treated from the viewpoint of Laplace transform and Complex Variable, and there is now no doubt—as experience shows—that for any but simple problems operational procedure must be based upon both of these subjects. There is brief mention of Abelian and Tauberian theorems, while procedure for the solution of linear integral, integro-differential, and differential equations by the operational method is outlined.

There are three lists of Laplace transforms, two inverse and one direct. The first two have the transforms classified as functions of p, i.e. $\phi(p)$, the original $f(t)$ being on the right-hand side. The total number of entries is 114. In the third table, $f(t)$ is on the left of $\phi(p)$, and there are 116 entries. It is very desirable that those who use operational calculus to any extent should have a dual list, i.e. direct and inverse. Unfortunately publishers in this country are averse to issuing lists of formulae of any kind!

Although it contains only one worked example, this book is recommended to those who have an adequate knowledge of the underlying mathematical theory. The printing is clear, and the treatment concise.

N. W. M.

Dynamics of Real Fluids, by E. G. Richardson. Pp. vii+144. 1st Edition. (London: Edward Arnold and Co., 1950.) 21*s*.

Dr. Richardson's book is unique: it has no Preface and the reader is left to guess the purpose for which it was written. The subjects selected for mention range over a very wide field; they include a short introduction to the classical theory of a perfect fluid, the behaviour of fluids of small viscosity, laminar and turbulent boundary-layer flows, experimental and statistical aspects of turbulence, some features of compressible-fluid flow, fluids with a temperature gradient, hot-wire anemometry, surface waves, break-up of liquid jets, liquid drops, the behaviour of particles in suspension, emulsions, some aspects of erosion, elastic liquids, thixotropy.

Clearly, it is not to be expected that a small book of 144 pages could deal comprehensively with these various aspects of fluid dynamics; indeed, the entire space would be needed for adequate treatment of any one of them. It is also doubtful whether the book would fulfil the needs of those who seek an introduction to fluid dynamics, for some previous knowledge on the part of the reader is required. Quite a number of the subjects selected for treatment are those on which the author has made his own contribution to knowledge and, undoubtedly, the attraction of the book is its esoteric appeal, for it gives glimpses of the trend of recent progress in a fascinating subject. A. F.

Ionization Chambers and Counters: *Experimental Techniques*, by B. B. ROSSI and H. H. STAUB. Pp. xviii+243. 1st Edition. (New York, Toronto, London: McGraw-Hill Book Co. Inc., 1949.) 19*s*. 6*d*.

This volume is the second of the National Nuclear Energy Series (Los Alamos Project, Division V) and it has an obviously close association with the first—*Electronics*, by W. C. Elmore and M. L. Sands. The first four chapters deal with the fundamental features of ionization and the general properties of detectors based upon the ionization process. Many readers will find Chapter 1 of special interest since it collects much useful data on the drift velocity and agitation energy of electrons; a good deal of material due to the authors themselves appears here for the first time and it refers closely to counting techniques. Chapters 2 and 3 are concerned with the general design considerations affecting the performance of chambers, and the latter deals in very thorough fashion with the relatively new problem of the measurement of variable ionization. In Chapter 4 the basic ideas of the gas multiplication process are rather briefly presented. A series of curves gives the values of multiplication observed in a variety of gases in typical operating conditions. The studies of pulse shape, end-effect of tubes and multiple-wire arrangements follow. While the allocation of space to the different sections seems somewhat strange in a textbook, all of it is of interest to the specialist in this field.

The last five chapters consider in some detail the design of detectors for beta-, gamma- and X-radiations (Chapter 5), alpha-particles, neutrons and fission products. Chapter 5 is comparatively modest in its scope and rather unbalanced. On the other hand, the compact discussion of α-ray spectroscopy is very meritorious. The two long chapters devoted to the neutron form the core of this section of the book; the whole subject is treated with originality and the authors are to be congratulated on their thorough treatment of the many difficulties encountered in this field. Again, a considerable fraction of the material is original. Finally, Chapter 10 discusses fission detectors.

The book suffers in several directions due to its origin and it is particularly disappointing that there is no bibliography. It is a notable contribution to the very limited number of texts on a subject of major importance in atomic and nuclear physics. The number of engineering drawings is unusually generous. All closely interested in the subject will be grateful to the authors for this excellent book. S. C. CURRAN.

Numerical Analysis of Heat Flow, by G. M. DUSINBERRE. Pp. xiv+227. 1st Edition. (New York and London: McGraw-Hill Book Co. Inc., 1949.) 38*s*. 6*d*.

In discussing the analytical solution of heat conduction problems by setting up the differential equation and solving with specified boundary conditions, the author of this book makes rather too sweeping a statement when he says that ". . . . this direct approach is of little use to the engineer ". Many problems of interest to physicists and engineers have been solved by the methods described in the well-known work of Carslaw and Jaeger. It is true, nevertheless, that occasions arise when it is necessary and desirable to use numerical methods. A formal solution may be impracticable, for instance, because of the complicated shape of a bounding surface. On the other hand, a solution in the form of a slowly converging series can well involve computation far more laborious than that required in the use of a numerical method *ab initio*.

The book starts with a discussion of the fundamental concepts of heat transfer in a somewhat non-fundamental manner. Heat capacity, for instance, is defined by referring to readings on a watt-hour meter. The British system of units is used throughout. Some elementary steady-state problems are solved by simple algebra, and there is a brief account of analytical solutions in simple cases. Then, the method of relaxation, extensively developed by Southwell and his fellow workers, is used for the numerical solution of the heat conduction equation in the steady state, in one and two dimensions. Relaxation, however, is not a suitable method for transient heat flow problems, the equation being of the parabolic type where the boundary conditions are not specified over a closed boundary. There are, of course, other methods available. The one developed in this book is a useful numerical adaptation and extension of the Schmidt graphical method. The book contains some problems involving convection and radiation. There are numerous worked examples to show the details of the numerical technique, and also problems for the reader at the end of each chapter. These problems are of a practical nature, dealing mainly with the heating of rooms, heat transfer through walls and so on.

Anyone whose work entails the consideration of problems of this kind would benefit by reading the book and working through the examples. He would probably be stimulated to learn the full power of the relaxation method by further reading elsewhere. A physicist would be surprised by some curious remarks on the theory of relativity and the quantum theory, which are misleading and not relevant to the main subject-matter. M. R. HOPKINS.

Artificial Radioactivity by P. B. MOON. Pp. vi + 102. Cambridge Monographs on Physics. First Edition. (Cambridge: University Press, 1949). 12*s.* 6*d.*

It is well known that the scientist in the general sense has nowadays nearly become extinct, as there is nobody who masters botany and physics, zoology, chemistry and astronomy equally well. Unfortunately this process of sub-division has not stopped; from the physicist comes the nuclear physicist, and even he has undergone fission into the beta-ray spectroscopist, neutron physicist, cosmic-ray expert and accelerator engineer. But the subconscious urge of the old days to attempt to attain a universal grasp of nature and the burning desire to be up-to-date in neighbouring fields still exists in all of us specialists, and we are therefore grateful if we are helped in this endeavour by the appearance in the series of Cambridge Monographs on Physics of so neat a condensation as the book on *Artificial Radioactivity* by Professor Moon.

Its first 30 pages cover the experimental methods used to measure the energy and intensity of the beta particles and gamma rays emitted by radioactive bodies. The description is very clear but necessarily (and rightly) short, since one could write a whole tome about beta spectrograph design alone. The next 40 pages cover processes in which the atomic number *Z* changes. Here electron and positron energy distributions are discussed and compared with Fermi's calculations. One cannot help admiring Fermi's intuition in constructing at so early a date (1934) so lasting a theory of so elusive a phenomenon as the continuous beta spectrum. A very satisfactory section on *K*-capture and on the experimental evidence, or lack of it, for the existence of the neutrino concludes this part of the book. It is followed by a section of 30 pages about processes which leave the nuclear charge unchanged. Under this paragraph fall such topics as life-times of excited states, gamma-ray selection rules, isomeric transitions, internal conversion and angular correlation between cascade gamma-rays; the experimental facts are generally illustrated by one or more concrete cases. This is followed by a descriptive exposition of the relevant theory unencumbered by actual calculations, but the final formula is as a rule given in a form just usable by the experimentalist. The enormous literature cannot be covered; references to the most important papers will help those who wish to penetrate further into the subject.

The book does not contain a complete list of the radioactive bodies with their emission data and modes of preparation. Such information, together with some additions on the practical side, might have served those readers who will be interested mainly in using beta emitters as tools. The title of the book is therefore slightly misleading as the monograph deals rather with the physics of radioactive decay than with the radioactive material. It is also not quite obvious why the book is restricted to nuclei of light and medium weight only; to include the heavy ones would not have increased its size very much. One serious omission (which may be due to an oversight on the part of the reviewer) seems to exist: the discovery of the effect of the atomic electrons on the decay constant of Be(7) by Segrè and Wiegand (*Phys. Rev.*, 1947, **71**, 274), and by R. Bouchez, P. and R. Daudel, and R. Murart, *J. Phys. Radium*, 1947, **8**, 336). That the rate of *K*-capture of Be(7) depends on the value of the electronic wave function at the nucleus may seem trivial, but the net result is certainly most astonishing and noteworthy, since it is the first time in history that the decay rate of a nucleus has been influenced by external conditions.

One requirement for a book such as the one under review is speed of publication. As the footnote on page 80 indicates, part of the manuscript was written in Spring 1947, the book was presumably completed in 1948, and it carries the date of publication, 1949. As no reference is made to such important recent additions to our collection of nuclear physics tools as the crystal counter (publications started in July 1947, but the method really only became generally used during 1948), it seems that one has to reckon with a delay of one year at least between the completion of the manuscript and the moment of publication. This clearly demonstrates the difficulty of writing anything up-to-date in these days when scientists have to bear such a heavy burden of teaching, and when the time required for book production has been so greatly increased.

E. BRETSCHER.

Cosmic-Ray Physics, by D. J. X. MONTGOMERY. Pp. viii + 370. First Edition. (Princeton: University Press; London: Geoffrey Cumberlege, 1949.) 40*s*.

Although the preface to this book states that it is not supposed to be a laboratory handbook, it nevertheless treats the subject with more detail than is easily digested by the newcomer and contains much information that is of use mainly to the active experimenter in cosmic-ray work. For instance, a valuable appendix is devoted to curves connecting momentum energy and range for electrons, mesons and protons in air, aluminium and lead which are based on more observations than any previously published, and the twenty or so pages on the cloud chamber deal with the instrument in considerably more detail than is usual. On the other hand, the photographic plate method of investigation to which major recent advances are due, receives only four pages, dealing mainly with the capabilities of the method, rather than details of technique.

The book—again despite a disclaimer in the preface—is well provided with references, which are rather unfortunately sandwiched in the text, making reading difficult. Lengthy mathematics is usually avoided, but the Stoermer theory of the motion of a charged particle in a dipole field is included in an appendix. Another appendix is devoted to tables of the results from the statistical theory of showers.

Each topic is brought well up to date, and the features which are still problematical, are made clear. A particularly valuable chapter is included on heavy particles in cosmic radiation, a subject which is receiving much investigation at the present time.

T. E. CRANSHAW.

Radiative Transfer, by S. CHANDRASEKHAR. Pp. xiv + 393. 1st edition. (Oxford: Clarendon Press, 1950.) 35s.

In this book Professor S. Chandrasekhar, F.R.S., who holds the chair of theoretical astrophysics in the University of Chicago, makes an outstanding addition to the systematic treatises on astrophysical problems. Though the book is intended primarily for astronomers it also has great meteorological interest, because the methods of calculation of radiative transfer which it describes are applicable to the very difficult problem of multiple scattering of light in the earth's atmosphere; moreover, essentially similar problems occur in connection with the diffusion of neutrons, hence the book should also attract the attention of theoretical physicists. The main topic, however, is the radiative equilibrium of stellar atmospheres, treated with great breadth and also in much mathematical detail.

The subject goes back at least to Rayleigh's discussion (1871) on the blue light of the sky and its polarization; as far as the earth's atmosphere is concerned, further progress was made by L. V. King, and also by S. Chapman and A. Hammad, but they recoiled from the difficulties of a complete formulation of the problem and its solution;

Chandrasekhar, in recent years, in a long series of papers in the *Astrophysical Journal*, has boldly faced and overcome these difficulties with great mathematical skill; one element in his success is the use and extension of a principle of invariance introduced by the Russian astrophysicist V. A. Ambarzumian (1943). Chandrasekhar, in one of a series of Bibliographical Notes which conclude each chapter (and form a valuable and distinctive feature of the book), points out that some of the basic ideas involved resemble those introduced by Stokes and Rayleigh in the discussion of the reflection and transmission of light by thin plates. Among other authors whose names occur in these Notes are Schuster, Schwarzschild, Sampson, Eddington, Milne, Hopf, van de Hulst and Crum.

The book has a good subject index and index of definitions, but lacks an authors' index.

Radiative transfer is a subject of considerable intrinsic mathematical complexity, but this brilliant and powerful book will smooth the path of knowledge for many readers and thereby give a new impulse to further development of the subject. S. C.

Corrigendum

"The Infra-red Spectrum of Magnesium Oxide", by J. C. WILLMOTT (*Proc. Phys. Soc.* A, 1950, **63**, 389).

The author has asked that the following alteration be noted :

The vertical scale of Figure 5 on page 398 should run from 10^{-4} to 10 instead of from 10^{-5} to 1.

CONTENTS FOR SECTION B

PAGE

Dr. J. B. HIGHAM and Prof. J. M. MEEK. Voltage Gradients in Long Gaseous Spark Channels 633

Dr. J. B. HIGHAM and Prof. J. M. MEEK. The Expansion of Gaseous Spark Channels 649

Dr. C. DODD. The Electrical Resistance of Liquid Gallium in the Neighbourhood of its Melting Point 662

Mr. B. COLLINGE. Hydrogen-filled Geiger Counters 665

Dr. B. E. NOLTINGK and Mr. E. A. NEPPIRAS. Cavitation produced by Ultrasonics. 674

Mr. H. G. W. HARDING. The Colour Temperature of Light Sources. . . . 685

Dr. P. A. LINDSAY. Certain Properties of Electrostatic Fields Encountered in Electron Lenses 699

Mr. U. F. GIANOLA. Reduction of the Spherical Aberration of Magnetic Electron Lenses 703

Mr. W. WEINSTEIN. The Computation of Wave-Front Aberrations of Oblique Pencils in a Symmetrical Optical System 709

Letters to the Editor :

- Mr. E. O. HALL. An Optical Method for Studying the Deformation of Mild Steel 724
- Mr. S. N. DENNO, Mr. H. A. PRIME and Dr. J. D. CRAGGS. The Scattering of 3-cm. Radiation by Ionized Gases 726
- Mr. W. R. LOOSEMORE and Dr. DENIS TAYLOR. Temperature Dependence of Counter Characteristics in Self-Quenching Geiger–Müller Counters . 728

Reviews of Books 730

Contents for Section A 734

Abstracts for Section A 734

ABSTRACTS FOR SECTION B

Voltage Gradients in Long Gaseous Spark Channels, by J. B. HIGHAM and J. M. MEEK.

ABSTRACT. Oscillographic measurements have been made of the variation with time of the voltage drops in long spark channels conducting aperiodic impulse currents rising to a peak in about 1/4 μsec. and decaying to half-value in from 10 to 85 μsec., with peak currents ranging from 60 to 700 amp. The lengths of the spark channels have been measured photographically, and the mean voltage gradients along the channels have been estimated. Results are given for sparks in air, nitrogen, oxygen and hydrogen at atmospheric and reduced pressures. Some preliminary measurements are described for sparks in water and oil, and for sparks in glass tubes. The voltage gradients in the various gases, with the exception of hydrogen, are independent of the peak current, but are influenced by the rate of current decay. The results are correlated with the current densities in spark channels, as recorded in a separate investigation.

The Expansion of Gaseous Spark Channels, by J. B. HIGHAM and J. M. MEEK.

ABSTRACT. A rotating mirror camera with a temporal resolution on the film of 1·5 mm/μsec. has been used to determine the rate of expansion of long gaseous spark channels during their first 10 μsec. of growth. The spark channels conducted aperiodic impulse currents in the range of 60 to 500 amp. peak, which attained their peak values in about 1/4 μsec. and decayed to half-value in 10 or 28 μsec. Sparks have been investigated in air at atmospheric and reduced pressures, and in nitrogen, oxygen and hydrogen at atmospheric pressure. The measured areas of cross section of these spark channels bear a linear relation to the peak currents, except in hydrogen, and are little influenced by the rate of current decay in the range studied. Measurements have also been made with the rotating mirror scanning an image of the spark across a photomultiplier connected to a high speed oscillograph; by this method a direct record is obtained of the radial light distribution across the spark channels. The mechanism of spark channel expansion is discussed, and estimates are made of the average ion densities in spark channels.

The Electrical Resistance of Liquid Gallium in the Neighbourhood of its Melting Point, by C. DODD.

ABSTRACT. In order to determine whether any discontinuous change in electrical properties takes place when a liquid is supercooled, measurements have been made on the resistance of liquid gallium. No such discontinuity has been found, the resistance varying linearly with temperature over the range investigated.

The results yield values for the resistivity and temperature coefficient of resistance of liquid gallium.

Hydrogen-filled Geiger Counters, by B. COLLINGE.

ABSTRACT. Permanent gas counters are discussed and a new quenching circuit is described. Quenching times of about 45 μsec. have been used and plateaux with slopes better than 0·05% per volt obtained. A formula for the correction of counting rates for losses caused by the counter dead-time has been confirmed within wide limits. It has been found possible to measure counting rates as high as 5×10^5 counts per minute with an accuracy closer than 1%.

Cavitation Produced by Ultrasonics, by B. E. Noltingk and E. A. Neppiras.

ABSTRACT. The problem of cavitation produced by ultrasonic vibration is examined theoretically. Equations are developed which describe the motion of a gas-filled cavitation bubble in a liquid medium subjected to alternating pressure; the case of an empty cavity is also considered. Information is obtained concerning the distribution of fluid pressures and velocities in the medium near the bubble surface during the motion. It is suggested that these theoretical conclusions may be used to show how the intensity of the various effects of cavitation will depend on ultrasonic frequency and intensity. In particular, it is predicted that all cavitation phenomena will diminish and finally disappear as the frequency is raised. The important part played by the nuclei from which the cavitation bubbles grow is emphasized.

The Colour Temperature of Light Sources, by H. G. W. Harding.

ABSTRACT. The definition of colour temperature is explained and the approximations of the spectral distributions of energy of lamps to those of black-body radiators are indicated. The value of colour-temperature measurements to the colorimetrist is outlined and difficulties in making the measurements are dealt with. The use of photoelectric devices for colour-temperature measurements are mentioned.

Certain Properties of Electrostatic Fields Encountered in Electron Lenses, by P. A. Lindsay.

ABSTRACT. The equipotential lines in a bipotential electron lens exhibit a fine structure which is revealed by application of the relaxation method to the solution of the Laplace equation in cylindrical coordinates. The asymmetry of the potential field between the two edges of the cylinders is confirmed by the same method and is established to be of the order of 2% in one particular case.

Reduction of the Spherical Aberration of Magnetic Electron Lenses, by U. F. Gianola.

ABSTRACT. The dependence of the resolving power of the asymmetrical bell-shaped magnetic field on the lens parameters is examined for varying degrees of field asymmetry. It is shown that a high asymmetry index favours high resolution, and a preferable value of lens power is specified.

By suitably reinforcing the lens field with that of a small air-cored coil, the theoretical resolving power of the lens is increased. On account of the small size of the coil, the coil current must be pulsed intermittently if an appreciable reinforcing field is to be produced.

The basic factors governing the design and operation of a suitable coil are discussed.

The Computation of Wave-Front Aberrations of Oblique Pencils in a Symmetrical Optical System, by W. Weinstein.

ABSTRACT. Aberration formulae given previously, together with new ones for astigmatism and secondary spherical aberration, are put into forms which are suitable for computation and simplify the treatment of field lenses. A method of comparing the formulae with ray tracing is given, and the results for a triplet objective are discussed.